



Terms and Conditions of Use of Digitised Theses from Trinity College Library Dublin

Copyright statement

All material supplied by Trinity College Library is protected by copyright (under the Copyright and Related Rights Act, 2000 as amended) and other relevant Intellectual Property Rights. By accessing and using a Digitised Thesis from Trinity College Library you acknowledge that all Intellectual Property Rights in any Works supplied are the sole and exclusive property of the copyright and/or other IPR holder. Specific copyright holders may not be explicitly identified. Use of materials from other sources within a thesis should not be construed as a claim over them.

A non-exclusive, non-transferable licence is hereby granted to those using or reproducing, in whole or in part, the material for valid purposes, providing the copyright owners are acknowledged using the normal conventions. Where specific permission to use material is required, this is identified and such permission must be sought from the copyright holder or agency cited.

Liability statement

By using a Digitised Thesis, I accept that Trinity College Dublin bears no legal responsibility for the accuracy, legality or comprehensiveness of materials contained within the thesis, and that Trinity College Dublin accepts no liability for indirect, consequential, or incidental, damages or losses arising from use of the thesis for whatever reason. Information located in a thesis may be subject to specific use constraints, details of which may not be explicitly described. It is the responsibility of potential and actual users to be aware of such constraints and to abide by them. By making use of material from a digitised thesis, you accept these copyright and disclaimer provisions. Where it is brought to the attention of Trinity College Library that there may be a breach of copyright or other restraint, it is the policy to withdraw or take down access to a thesis while the issue is being resolved.

Access Agreement

By using a Digitised Thesis from Trinity College Library you are bound by the following Terms & Conditions. Please read them carefully.

I have read and I understand the following statement: All material supplied via a Digitised Thesis from Trinity College Library is protected by copyright and other intellectual property rights, and duplication or sale of all or part of any of a thesis is not permitted, except that material may be duplicated by you for your research use or for educational purposes in electronic or print form providing the copyright owners are acknowledged using the normal conventions. You must obtain permission for any other use. Electronic or print copies may not be offered, whether for sale or otherwise to anyone. This copy has been supplied on the understanding that it is copyright material and that no quotation from the thesis may be published without proper acknowledgement.

Copyright

by

David P. Hegarty

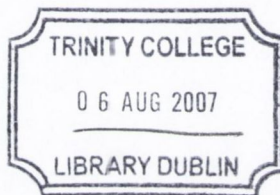
2007

**Analysis of Wheel-Rail Contact Forces Resulting
from Vertical Track Irregularity**

David P. Hegarty

A thesis submitted to the University of Dublin, Trinity College
in partial fulfillment of the requirements for the degree of
Doctor of Philosophy

April 2007



THESIS

8179

Declaration

I, the undersigned, declare that this work has not previously been submitted to this or any other University, and that unless otherwise stated, it is entirely my own work.



David P. Hegarty

Dated: May 6, 2007

Permission to Lend and/or Copy

I, the undersigned, agree that Trinity College Library may lend or copy this thesis upon request.



David P. Hegarty

Dated: May 6, 2007

**Analysis of Wheel-Rail Contact Forces Resulting
from Vertical Track Irregularity**

Approved by
Dissertation Committee:

Dedication

To Gesche

Acknowledgements

I wish to sincerely thank the late Professor Simon Perry, Dr. Roger West, and Professor Margaret O'Mahony, the respective Heads of the Department of Civil, Structural and Environmental Engineering during my time as a postgraduate student at Trinity College, for facilities granted and supporting this research.

A sincere thanks must also go to Dr. Dermot O'Dwyer, my Ph.D. supervisor, primarily for his academic advice, but also for his encouragement and patience over the last few years. Thanks for being a good friend as well as mentor.

I wish to thank Enterprise Ireland and the Department of Civil, Structural and Environmental Engineering at Trinity for their financial support to my postgraduate studies.

A heartfelt thanks to the many friends I have been lucky enough to encounter during my time as a postgraduate student at Trinity College, in particular Cormac, Nora-Áine, Orlaith, Paul, Ronán, Ross, and Una. I will always be grateful for your friendship and support.

I am so grateful to my wonderful family for their support to me over the years. Thanks Paddy, Séamus, Siún and Máire. To my aunt Christine, who has always been a great source of support, many thanks also. I love you all and know that I would not have completed this work without your collective help and encouragement. Special mention must go to my parents, Mary and James. All of the good that we, your children, achieve, is a direct result of the guidance and example you have provided us throughout our childhood and beyond. You truly are unsung heroes

and I am forever grateful.

Finally and most importantly, I would like to thank my wonderful wife, Gesche. The completion of this thesis has been due to your incredible patience and encouragement as much as it has been the result of my own endeavour. I love you.

David P. Hegarty

University of Dublin, Trinity College

April 2007

Summary

The research that is described in this thesis is based upon the formulation and analysis of mathematical models of railway vehicle and track systems. The objective of the research carried out is to compile, and then apply, these models to gain a greater understanding of the nature of the wheel-rail contact forces that are generated due to irregularity of the wheel and track geometry. The response of the vehicle and track system is considered under a number of different types of vehicle wheel and railway track defects. The nature of the different defects require that different types of analysis are used. The modelling of the system response due to random track irregularity lends itself to the use of spectral techniques due to the fact that the dynamic input to the system may be described by spectral functions. Frequency domain analysis is used to calculate the response due random irregularity. The effects of discrete irregularity are more suited to analysis in the time domain. Numerical analysis in the time domain is used to calculate the response due to discrete system defects. Initially, frequency domain analysis was used to examine the effect of random railway track irregularities on the wheel-rail contact forces. Two different types of vehicles were considered, a locomotive and a passenger vehicle. The effects of the various vehicle parameters, and vehicle velocity, were also considered. The random irregularities considered were those that are described by the FRA empirical spectral functions. The effects of these irregularities were found to be small in most cases. However, under some parametric combinations the probability of excessive peak ix forces was observed to increase significantly. A similar model and further

frequency domain analysis was used to observe the different contact force process characteristics at the front and rear wheelsets of a flatbed wagon vehicle model. Similar random irregularities were considered in this model. The analysis of the contact forces in the frequency domain involved the linearisation of the Hertzian contact spring at the wheel-rail interface. The validity of this linearisation is examined by comparing the results obtained using a non-linear and linear spring in a numerical time-domain analysis. It was determined that the linearisation is valid when the random irregularities applied are of low frequency content while at higher frequency, there is greater divergence between the sets of data obtained using the different spring characteristics. The effects of a number of different discrete type irregularities on the wheel-rail contact forces were also considered. A numerical finite element track model was formulated and the effects of a wheel flat, unsupported sleeper and a dipped joint were examined. The results obtained were compared with empirical formulae for the system response. These formulae were found to be of limited value in some of the cases considered. The final study was focussed upon the effect of random track irregularities on the response of railway bridges. Dynamic bridge impact factors were calculated numerically for a range of bridge and vehicle properties. The mean impact factor was generally found to be equal to the equivalent impact factor when no track irregularity was input to the system. However, in some cases, high velocities combined with random irregularities did generate large impact factors. The effect of incorporation of a track model into the system was also investigated. x

Abstract

The modelling and accurate calculation of dynamic wheel-rail contact forces are of critical importance in the field of railway engineering. The nature of these contact forces is a function of both the vehicle and track system properties. The forces are resultant from the dynamic excitation that occurs between the railway vehicle and track systems. This dissertation details the development of a number of mathematical models that are applied for the purpose of calculation of the dynamic response of both the railway vehicle and track. The system response is considered with particular emphasis placed upon the resulting wheel-rail contact forces. Both frequency domain and time domain (transient) analysis techniques are applied.

A parametric analysis of the wheel-rail contact forces generated as a vehicle wheel moves across a track profile with random vertical irregularity is detailed. The frequency domain approach that is applied is dependent upon assumed linearity of the Hertzian contact spring. The spring linearisation is carried out with respect to the static wheel load. The mathematical model and analysis methodology is described and the influence of the vehicle and track parameter values is assessed. A similar mathematical model and technique is then used to investigate the stochastic contact forces that are generated at two wheels of the same bogie.

The validity of the Hertzian spring linearisation is tested by means of a numerical time domain analysis of an interactive vehicle and track system. The finite difference method (FDM) is used to formulate a quasi-infinite beam on elastic foundation model for the railway track. A moving vehicle model similar to that applied in the

frequency domain analysis is applied to the beam and the system equations of motion are solved numerically. Different specifications of random track irregularities and their effect on the wheel-rail contact forces are also investigated using this model.

A number of discrete vertical track irregularities are investigated using a track system model formulated using the finite element method (FEM). This model differs from the previous quasi-infinite beam model in that it is finite in space and is discretely supported by sleepers, which are in turn supported by a discretised ballast medium. The beam on elastic foundation model is not suitable for the analysis of discrete type irregularities due to their high frequency characteristics. Using the FE track model the effect of wheel flats, unsupported sleepers, and dip joints on the system response was calculated.

Finally, the effect of random vertical track irregularity on the dynamic response of railway bridges is considered. FE beam models for a number of different bridge structures are subjected to vehicular loading for different grades of random track profiles. The effect of incorporation of random track irregularities on the dynamic bridge impact factors is calculated using numerical analysis. The effect of the inclusion or otherwise of a track model is also considered.

Contents

Acknowledgements	xiii
Summary	xiv
Abstract	xvi
List of Tables	xxv
List of Figures	xxvii
Chapter 1 Introduction	1
1.1 Preamble	1
1.2 Scope of Work	3
1.3 Thesis Organisation	4
Chapter 2 Review of Vehicle-Track-Bridge Interactive Dynamics	7
2.1 Introduction	7
2.1.1 Background	7
2.1.2 Organisation of Literature Review	10
2.2 Frequency Domain Models	12
2.2.1 Introduction	12
2.2.2 Mechanical Systems Analysis in the Frequency Domain	16
2.3 Dynamic Vehicle-Track Interaction	19
2.3.1 Quasi-Steady State Interaction	19

2.3.2	Interaction with Contact Area Irregularity	25
2.3.3	Contact Mechanism Characteristics and Models	33
2.4	Vehicle-Bridge Interaction	40
2.5	Conclusions	45
 Chapter 3 Parametric Study of Stochastic Wheel-Rail Contact Forces		47
3.1	Introduction	47
3.2	System Model	50
3.2.1	Vehicle Model	50
3.2.2	Railway Track Model	53
3.3	Mathematical Formulation	56
3.3.1	Frequency Response Functions	56
3.3.2	Contact Force Power Spectral Density Function	59
3.3.3	Random Process Statistics	60
3.4	Parametric Study	62
3.4.1	Default System Parameters	62
3.4.2	Parametric Variation	66
3.4.3	Contact Force Process RMS Variations	80
3.4.4	Locomotive Peak Force Probabilities	81
3.4.5	Passenger Vehicle Peak Force Probabilities	87
3.5	Observations and Conclusions	88
3.5.1	Discussion of Results	88
3.5.2	Comment	91
 Chapter 4 Wheelset Coupling Effects on Stochastic Contact Forces		95
4.1	Introduction	95
4.2	Mathematical Formulation	96
4.2.1	Physical Model Description	96
4.2.2	Equation of Motion	99

4.2.3	Contact Force Spectra	100
4.3	Contact Force Spectra Analysis	103
4.3.1	Default Parameter Spectra	103
4.3.2	Velocity variation	109
4.3.3	Comparison of Frequency Response Functions	110
4.4	Observations and Conclusions	111

Chapter 5 Numerical Track Model with Application to Random Track

Irregularity		113
5.1	Introduction	113
5.2	Track Model Formulation	117
5.2.1	Equation of Motion in Convected Coordinates	117
5.2.2	Finite Difference Adaptation	119
5.2.3	Finite Difference Beam Matrices	122
5.3	Model Validation	129
5.4	Effect of Random Vertical Profile Irregularity	137
5.4.1	Introduction	137
5.4.2	Comparison of Empirical PSD Functions	138
5.5	Effect of Non-linear Hertzian Spring	146
5.6	Observations and Conclusions	149

Chapter 6 Finite Element Track Model with Applications to Discrete

Defects		153
6.1	Introduction	153
6.2	Track System Model Formulation	155
6.2.1	Model Assumptions	155
6.2.2	Finite Element Matrices	156
6.2.3	Steady State Response	158
6.3	Wheel Flat	166

6.3.1	Wheel Flat Model	166
6.3.2	Dynamic Response to Wheel Flat	169
6.4	Unsupported Sleeper	175
6.4.1	Unsupported Sleeper Model	175
6.4.2	Dynamic Response to Unsupported Sleeper	175
6.5	Dipped Joint	178
6.5.1	Dipped Joint Model	178
6.5.2	Dynamic Response to Dipped Joint	180
6.6	Ballast Stiffness Effects	182
6.7	Observations and Conclusions	185

Chapter 7 Effect of Random Track Irregularities upon Bridge Impact

Factors		189
7.1	Introduction	189
7.2	Random Profile Irregularity Effect on Dynamic Impact Factors	191
7.2.1	Finite Element Model Validation	191
7.2.2	Effect of Random Irregularities	198
7.3	Case Study	200
7.3.1	Background	200
7.3.2	Profile Irregularity Analysis	204
7.4	Influence of Track Structure	206
7.4.1	Background	206
7.4.2	Analysis Results	207
7.5	Conclusions	210

Chapter 8 Summary and Conclusions **213**

8.1	Summary	213
8.2	Conclusions	215
8.3	Recommendations for Further Research	217

Bibliography	219
Appendix A Order Statistics of Random Process Peaks	231
Appendices	231
Appendix B Four Degree of Freedom Model	233
Appendix C Railway Vehicle Parameters	239
C.1 181 Locomotive Parameters	239
C.2 Mark 3 Coach Parameters	240
Vita	241

List of Tables

3.1	Locomotive and passenger coach default parameters	63
3.2	BEF default model parameters	63
3.3	Individual vehicle and track parameter ranges	65
3.4	Locomotive and passenger coach optimal parameters	93
4.1	Parametric values for vehicle and discretised track model	105
4.2	Contact force process statistics	106
4.3	Numerically calculated contact force RMS values	109
6.1	Track model parameter values	159
7.1	Plate girder bridge models parameters	197
C.1	181 Locomotive model parameters	239
C.2	Mark 3 coach model parameters	240

List of Figures

2.1	Distribution of rail stress and deflection as a function of vehicle velocity	10
2.2	Sample frequency response functions real and imaginary constituent parts	14
2.3	Quasi-stationary contact force and rail displacement time histories at wheel-rail contact point.	26
2.4	Elastic bodies in compressive contact	34
2.5	Contact stress boundary ellipse	35
2.6	Wheel flange forces vertical and lateral forces	37
2.7	Hertzian contact force versus relative wheel-rail displacement for three different values of c_h [$\text{GNm}^{-3/2}$]	39
3.1	Two degree of freedom bogie model on BEF track model with upper profile random irregularity	51
3.2	PSD of random vertical track irregularities (FRA class 4)	55
3.3	Frequency response functions for vehicle model vertical displacements with default parameters	64
3.4	Contact force PSD variation with track class	69
3.5	Contact force PSD variation with velocity	70
3.6	Contact force PSD variation with bogie mass	72
3.7	Contact force PSD variation with wheelset mass	73
3.8	Contact force PSD variation with suspension stiffness	75

3.9	Contact force PSD variation with suspension damping	76
3.10	Contact force PSD variation with track foundation stiffness	78
3.11	Contact force PSD variation with track foundation damping	79
3.12	Contact force probability density functions for vehicle models with default parametric values	80
3.13	Locomotive model contact force RMS parametric variations (A) . . .	82
3.14	Locomotive model contact force RMS parametric variations (B) . . .	83
3.15	Passenger vehicle model contact force RMS parametric variations (A)	84
3.16	Passenger vehicle model contact force RMS parametric variations (B)	85
3.17	Track roughness PSD illustrating deterioration over time	92
4.1	Railway freight vehicle model with discretised mass track model . . .	98
4.2	Frequency response functions for freight vehicle on discretised track masses	104
4.3	Wagon frequency response functions over zero to 10m^{-1} route fre- quency range	106
4.4	Contact force spectra for front and rear wheelsets	107
4.5	Probability density functions for front and rear wheelset contact forces	107
4.6	Ratio of rear contact force process RMS to front equivalent, expressed as a percentage, as a function of vehicle model velocity	110
5.1	Infinite Euler beam on Kelvin elastic foundation	118
5.2	Quasi-infinite beam reactions	121
5.3	Discretisation of infinite beam into nodal masses	122
5.4	Forces at first finite difference node at left-hand extreme	124
5.5	Static beam response to single point force	131
5.6	Quasi-stationary infinite beam response at 60ms^{-1}	133
5.7	Quasi-stationary infinite beam response at 250ms^{-1}	134
5.8	Beam quasi-stationary response to two point forces moving at 60ms^{-1}	136

5.9	Beam on elastic foundation traversed by four-degree of freedom vehicle model	137
5.10	Contact force variation at velocity of 40ms^{-1} for FRA PSD functions	139
5.11	Comparison of FRA and ARS Class 4 PSD functions	140
5.12	Contact force variation at velocity of 40ms^{-1} for ARS PSD functions	140
5.13	Contact force PSD for FRA Class 1 profile irregularity at 40ms^{-1} . .	142
5.14	Contact force PSD for FRA Class 4 profile irregularity at 40ms^{-1} . .	143
5.15	Contact force PSD for ARS Grade 1 profile irregularity at 40ms^{-1} . .	144
5.16	Contact force PSD for ARS Grade 4 profile irregularity at 40ms^{-1} . .	145
5.17	Comparison of frequency and time domain analysis results	148
5.18	Sample vertical track profiles 100m in length	149
5.19	Variation of linearised k_H value with static load	150
6.1	Railway track model	156
6.2	Steady state response of track system model to constant force moving at 40ms^{-1}	163
6.3	Wheel-rail contact forces comparison	164
6.4	Rail pad and ballast forces model comparison at central sleeper . . .	165
6.5	Wheel and rail displacements in steady state	166
6.6	Idealised wheel flat	167
6.7	Rolling of wheel with idealised flat	168
6.8	Typical profile irregularity function for a wheel flat	169
6.9	Contact force resulting from wheel flat at velocity 40ms^{-1}	170
6.10	Wheel and rail displacements at 40ms^{-1}	171
6.11	Contact forces due to wheel flat impacting over sleeper	171
6.12	Contact force variation with distance beyond sleeper	172
6.13	Pad and ballast forces due to wheel flat impact over sleeper for 40ms^{-1} velocity	173

6.14	Pad and ballast forces at 18m located sleeper due to wheel flat impacts 0.3m before and after sleeper at 40 ms ⁻¹	174
6.15	Track model displacement at wheel-rail contact point due to hung sleeper at 21m	176
6.16	Wheel-rail contact forces due to hung sleeper at 21m	177
6.17	Dynamic response to two hung sleepers located at 21m and 21.6m respectively	179
6.18	Wheel-rail contact forces due to 3mm dipped joint in track at vehicle velocity of 40ms ⁻¹	181
6.19	Track bending moments at vehicle velocity of 40ms ⁻¹	182
6.20	Comparison of numerically calculated P ₁ and P ₂ contact forces with their analytical equivalents	183
6.21	Steady state response variation with ballast stiffness (Ballast stiffness expressed as a fraction of the default value)	184
6.22	Track bending moments at fixed points (variation with ballast stiffness)	186
7.1	Impact factors variation with velocity for moving point force (Short span bridge model)	193
7.2	Variation of impact factors with velocity for various beam and vehicle models	196
7.3	Impact factor standard deviations	199
7.4	Quasi-steady response at bridge mid-span	202
7.5	Wheel-bridge contact force variation at leading locomotive axle in quasi-steady state at 40ms ⁻¹	203
7.6	Leading bogie rotation in quasi-steady state at 40ms ⁻¹	204
7.7	Estimate of distribution of dynamic impact factors (assuming normal distribution)	205
7.8	Distribution of maximum front axle contact forces (assuming normal distribution)	206

7.9	Mid-span response of beam models	208
7.10	Contact force variations at leading axle	209
7.11	Sample of contact force histories at leading axle for perfectly smooth, Class 4 and Class 1 track profiles	210
7.12	Lines of best fit for N_r , the ratio of the variance to the quasi-steady state impact factor	212

Chapter 1

Introduction

1.1 Preamble

Railway track systems are essentially comprised of two separate, but dynamically interactive, subsystems; the railway vehicle and the railway track itself. The safe and efficient design of railway vehicle and track systems requires a rigorous understanding of the wheel-rail contact forces that occur at the physical interface between the two dynamic systems. It is these contact forces that constitute the major excitatory inputs to both the vehicle and the track.

Geometrical irregularity of the railway track profile and imperfections of the railway vehicle wheels give rise to peak dynamic contact forces that exceed the quasi-steady state force conditions. The quasi-steady state refers to the dynamic system response when the geometry of both the vehicle wheels and the railway track is perfect. It is referred to as such because, despite the similarity of this response to the static response in that they are both constant at any position along the railway track relative to the wheel, it differs in magnitude due to the Coriolis effect (complementary acceleration) and the effect of path curvature (centripetal acceleration). The extent of both of these effects is dependent only upon the railway vehicle velocity in the quasi-steady state. In practical instances the effects of path

curvature and, in particular, Coriolis effects, are much smaller than the static effects (Frýba 1999).

The quasi-steady state response referred to here is described on the assumption that track foundation is perfectly uniform. In Ireland this is generally not the case and there exists a recognisable periodicity in the response of both the vehicle and track. Both the system displacements and contact forces fluctuate significantly about their respective quasi-steady state conditions. The degree of the response fluctuation in the quasi-steady state is dependent upon both the vehicle and the track parameters. This fluctuation results from the non-uniformity of the track foundation stiffness in the case of discretely supported track, and also from the resulting pitching and bouncing of the vehicle system's inertial components. For ballasted track with sleepers the track is discretely supported upon the sleepers whilst between the sleepers, vertical support to the vehicle is provided only by the moment and shear resisting stiffness of the rail.

Defects in the track and wheels generate dynamic effects that are supplementary to these quasi-steady state effects. However, as will be observed at various points throughout this thesis, track profile and wheel defects can result in system responses that are significantly greater than the equivalent quasi-steady state responses, and in some cases dynamic forces that are multiples of the static. There are many different types of irregularity that can occur in the wheel-rail contact area. The range of defects show vastly different characteristics, both in terms of frequency and magnitude.

The work presented in this thesis is based upon investigation of the dynamic effects of various types of track and wheel defects. For this purpose, it has been found that different types of analytical techniques are suited to different types of problems. In addition to these different techniques, a range of different model formulations are applied to the various problems encountered. The railway vehicle and track systems are highly interactive and complex. The application of frequency domain analysis

can, in some cases, greatly reduce the computation time required to determine the system response. This analysis technique lends itself very conveniently to the analysis of effects occurring due to random track irregularity. Standard spectral techniques, however, require the linearisation of all vehicle and track components. When this is not possible time domain analyses are used. In such cases numerical solutions are obtained by 'time-stepping' through the equations of motion for the time required to obtain an accurate time-history solution. Both approaches are adopted at various points in this thesis.

1.2 Scope of Work

The objective of the work carried out in the research detailed in this thesis is the development of mathematical models of railway vehicle and track systems. These models are then applied for the purpose of calculating the dynamic wheel-rail contact forces that occur as a result of different types of vertical railway track irregularities and defects.

The range of the different types of defects considered required that different types of models and analysis approaches be considered. In the case of perfectly random track irregularity a frequency domain technique was applied to a suitable system model. Using this model the effect of random irregularities on the contact forces generated by different types of railway vehicles was observed. The effect of varying the vehicle parameters on the contact force characteristics is calculated, as are the optimum combination of vehicle parameters for minimising the contact force variance.

Also investigated using a similar frequency domain technique are the different contact force characteristics generated at individual axles of the same railway vehicle model. This effect is investigated for the case of a random vertical track profile.

The linearisation of the Hertzian contact spring that is required for the purpose

of frequency domain analysis is validated by means of applying the vehicle model to a track model formulated using the Finite Difference Method. The equations of motion of the coupled systems are solved numerically and the contact forces calculated. The same model is applied to investigation of the effects of different specifications of random track irregularity Power Spectral Density functions on the wheel-rail contact forces.

The dynamic effects of a number of discrete irregularities are calculated using a finite element track model. Wheel flats, an unsupported sleeper, and a dipped joint are all considered. Particular attention is given to the effect, on the dynamic impact, of the position of occurrence of the wheel flat, and the effect of two consecutive unsupported sleepers.

The effect of random track irregularity on dynamic bridge impact factors is calculated. The bridge impact factors are defined as the ratio of the maximum dynamic bridge response to the maximum static response. Three different bridge models are formulated and analysed, of spans 10m, 35m and 70m respectively, and random track profiles are generated from irregularity PSD functions using trigonometric series. These profiles are then applied at the wheel-bridge or wheel-rail contact interface.

1.3 Thesis Organisation

A review of previous research in the field of railway system dynamics is presented in Chapter 2. A number of different specific research areas are reviewed. Each of these areas are encompassed by the work that is carried out in this thesis. The application of frequency domain techniques in a number of different fields are included, with a specific focus upon application of these techniques to vehicle and beam dynamics. Previous studies of the dynamic vehicle-track interaction and the resultant wheel-rail contact forces are presented. Both the steady-state response and the influence

of track irregularities on the response are considered. This thesis is focussed upon the effects of vertical track irregularities and, for this reason, emphasis is placed upon studies of a similar nature. Research into the dynamic response of railway bridges as a result of moving vehicles is also considered. In all cases the emphasis is upon the effect of various types of wheel and rail defects and irregularities on the dynamic response of vehicle, track and bridge, and the resulting contact forces that are generated in the wheel-rail contact area.

Chapter 3 includes a parametric study of the wheel-rail contact forces generated as a railway vehicle wheel runs along a railway track with a randomly irregular vertical track profile. The equations of motion of a simplified vehicle model are formulated in the time domain, then converted to the frequency domain by applying a Fourier transform. The sole source of dynamic excitation to the vehicle and track system is the random vertical track irregularity which is characterised by one-sided power spectral density (PSD) functions. The frequency domain approach allows for the efficient calculation of contact force spectra under various combinations of parametric values. These spectra contain valuable information about the random processes they represent. One of the assumptions when applying this type of analysis is that the system is linear. The wheel-rail contact spring does not behave linearly but, for the purpose of this study, is linearised about the static wheel load.

In Chapter 4 a frequency domain approach is applied to a vehicle bogie model with two axles. Once again, spectra of the contact force processes are generated; however, in this instance two spectra are generated for each analysis, one for each wheelset. Over a range of different velocities the calculated spectra at each wheelset are found to be non-identical. As a result of this, the mean-square contact force values of the contact forces at each wheelset are also non-identical.

Chapter 5 details the development of a track model for the purpose of calculating wheel-rail contact forces in the time domain. A numerical analysis is applied to the track model equations of motion, which is formulated using the finite difference

method (FDM). Random irregularity of the track is input to the model. This irregularity function is generated using trigonometric series based on various random profile power spectral density functions. The track model is formulated as a quasi-infinite beam. One shortcoming of this type of continuous model is the assumption of the track foundation as a continuously elastic medium. The model is also used to validate the linear Hertzian contact spring model used in Chapters 3 and 4.

Chapter 6 is focussed upon the effect of a number of discrete type irregularities on the wheel-rail contact forces and the resulting track deformation and stresses. The case of a wheel flat impacting the track, the presence of an unsupported sleeper and a dipped joint are investigated. Also observed is the influence on the dynamic response of the track ballast stiffness. The track model is formulated using the finite element method (FEM) with Timoshenko beam elements. This model was used in preference to the model of Chapter 5 due to its ability to model more accurately the high-frequency response that is generally generated by discrete type defects.

Dynamic impact factors for bridges traversed by moving vehicles in the presence of a randomly irregular vertical track profile are calculated in Chapter 7. The bridge models are formulated using the FEM with Euler beam elements. Short, medium and long span bridge models are considered. The effect of including a track model in the analysis is also investigated. As in Chapter 5, the random profiles are generated from trigonometric series derived from empirical one-sided PSD functions.

Finally, the work presented in this dissertation is summarised and conclusions arrived at are presented in Chapter 8. The main findings of the research are discussed and areas of possible further research are suggested.

Chapter 2

Review of Vehicle-Track-Bridge Interactive Dynamics

2.1 Introduction

2.1.1 Background

The essential physical basis of any railway network is formed by two dynamic and interactive subsystems: the mechanical railway vehicle system and the railway track structure, which supports and guides the vehicle. When a vehicle moves on railway track, contact forces are transmitted between the two subsystems via the multiple contact interfaces that are situated at the wheel-rail contact points at intervals along the entire length of the vehicle. In the ideal case, where the vehicle wheel and the track profile are perfectly rounded and smooth respectively, these contact forces approach a condition referred to throughout the literature as the quasi-steady state. The quasi-steady state contact forces are not identical to the static forces. Furthermore, the effect of sleeper spacing and oscillation of the discrete supports generate force fluctuations of approximately 5% above and below the quasi-steady state in the present train velocity range (Dong, Sankar & Dukkipati 1994). However, under idealised track and wheel conditions and at sufficiently low velocities, it

has been shown that the contact forces approach those of the static case (Jenkins, Stephenson, Clayton, Morland & Lyon 1974).

Perfect geometry of the wheel-rail contact area would minimise the contact force oscillation; however, in practice, geometric imperfections in the wheel-rail contact region constitute a major source of dynamic excitation to both the railway vehicle and the railway track systems. Deviations from a geometrically perfect contact area give rise to additional oscillations in the dynamic contact forces that alter both the amplitude and frequency characteristics of the contact forces. The magnitude and frequency of variations in the contact forces dictate the characteristics of the dynamic input to both the vehicle and track systems. Significant deviations in the contact forces from the quasi-steady state condition may result in excessive stresses being imparted to both systems. In addition, the riding comfort of passenger vehicles may be negatively affected (Demic, Lukic & Milic 2002, Karakasis, Skarlatos & Zakinthinos 2005).

The safe and efficient engineering design of both the vehicle system and the track structure requires a comprehensive understanding of the dynamic characteristics of the contact forces. Inherent in this understanding is an appreciation of the many problems that can arise due to the presence of contact area irregularity. These problems include excessive wear of both vehicle and track components, resultant poor ride quality, induction of corrugation and, in the worst case, potential derailment of the vehicle or damage to the track structure to the extent that the track is unusable. Therefore, it is clear that both experimental and theoretical studies of such geometrical irregularity, and its effects, are of great practical interest to railway engineers.

The work presented in this thesis is focussed upon the development of various mathematical models that are used to predict the effects of different types of wheel and track irregularities upon the wheel-rail contact forces. The types of track and wheel irregularities that can distort contact forces from their quasi-steady state are

many and varied. The subsequent dynamic effects are a function of the particular type of irregularity and, as such, vary greatly also. However, all types of irregularities may be broadly categorised as periodic, isolated or random.

Rail corrugations are an example of a periodic excitation source to the vehicle-track system, as are both the sleeper and cross-beam (in the case of bridges) effects. Wheel flats are also periodic given their cyclical characteristics but are modelled as a series of repeating discrete irregularities. In direct contrast, isolated irregularities such as a dipped or poorly welded joint in the track structure may occur at any point over a given section of track, or not at all. Entirely irregular deviations from the ideal railway track profile can be considered random, or stochastic, in nature. Such irregularities are of additional theoretical and mathematical interest due to the fact that they can be described by their statistical characteristics. It is possible to apply frequency domain techniques in the analysis of random track irregularity effects upon the dynamic wheel-rail contact forces.

One particular aspect that is common to each of the aforementioned categories of irregularity is the general increase of the dynamic effect magnitude in line with increasing vehicle velocity (see Figure 2.1 from Eisenmann (1981)). Instances of this general effect are prevalent throughout the literature in various analyses of different types of irregularities at working velocities. Examples include the effects of wheel flats (Fermér & Nielsen 1995, Hou, Kalousek & Dong 2003, Nielsen & Igeland 1995), dipped track joints (Jenkins et al. 1974, Zhai & Cai 1997), random track profile irregularity (Lei & Noda 2002), rail corrugation (Nielsen & Igeland 1995), and local loss of sleeper support (Nielsen & Igeland 1995). Railway administrations allow for this effect by specifying tolerances for track irregularity that are dependent on vehicle velocity. A condensed version of the USA's Federal Railroad Administration (FRA) tolerances is provided by Garg & Dukkipati (1984). The imposition of additional speed limits is far from an ideal solution given the current traffic demands placed upon modern railway services in addition to large projected demand increases into

the foreseeable future (Johnson 2000). It does, however, provide the single most simplistic answer to the problem of excessive dynamic loads. An adequate maintenance and repair regime, that minimises the imposition of such limits, is a much more effective solution (Profillidis 2000).

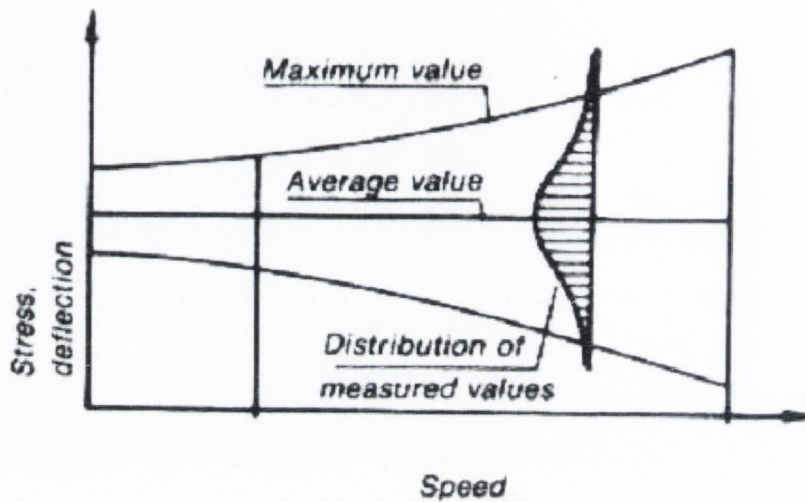


Fig. 2.1: Distribution of rail stress and deflection as a function of vehicle velocity (Eisenmann 1981)

2.1.2 Organisation of Literature Review

The following literature review has been divided into a number of distinct, but fundamentally related aspects, in the general research area of vehicle-track and vehicle-bridge interactive dynamics. The need to address both of these topics, and the vast quantity of literature available in both fields, has required that the review be sub-divided into these two individual sections with emphasis upon these topics. Also included is a section on frequency domain analysis and its applications, a technique which was applied in the research described in this thesis. Therefore, the three topics reviewed are frequency domain systems analysis, the dynamics of the vehicle-track interaction, and the dynamics of the vehicle-bridge interaction.

The application of frequency domain, or spectral, techniques to the analysis of the dynamic vehicle-track interaction forms a very significant portion of this research work. Section 2.2 is focussed upon some of the previous applications of these techniques to the solution of problems of the dynamic response of mechanical systems.

Section 2.3 contains a review of the literature in the specific area of the dynamic interaction between the railway vehicle and the track. This topic includes a review of the literature detailing the individual dynamic responses of vehicle and track. The fluctuating contact forces that arise between the two subsystems are also included. The section is divided into three sub-topics, the first (Section 2.3.1) is based upon studies of the idealised vehicle track interaction, ie. the quasi-steady state response; while the second (Section 2.3.2) concentrates upon literature with an emphasis upon the effect of track and wheel defects upon this interaction. An understanding of the wheel-rail contact mechanism is critical prior to formulating an accurate mathematical model. For this reason, Section 2.3.3 concludes Section 2.3 with a review of some of the research that has been undertaken in studying the behaviour of the interactive wheel-rail contact mechanism. This also comprises a review of some of the mathematical models that have been used to simulate this interaction.

This thesis also includes some work based on studying the effect of wheel-rail contact area irregularity upon the dynamic response of railway bridges. Section 2.4 reviews previous research undertaken in the field of railway bridge dynamics, with particular emphasis placed on the effects of track and wheel irregularities on the bridge dynamic response.

Section 2.5 concludes the review with a brief overview of the reviewed material.

2.2 Frequency Domain Models

2.2.1 Introduction

Irregularity of the wheel-rail contact area geometry, be it in the wheel or track profile, is cited as one of the essential vibration sources to vehicle and track (Dong et al. 1994, Lei & Noda 2002, Mastinu, Gobbi & Pace 2001, Nielsen & Igeland 1995). The analysis of the dynamic response of railway vehicle and track systems as a result of random track profile irregularity can be approached in both the time domain or the frequency domain. Time domain analysis can involve the application of analytical or numerical methods. Cai, Cheung & Chan (1988) and Sun (2001*a*) have detailed exact analytical solutions to different types of beam dynamics problems that are related to railway engineering applications. Cai et al. (1988) detailed an exact method for calculating the dynamic response of a beam resting on discrete roller supports to a moving force while Sun calculated a closed form solution for a continuously supported beam subjected to a moving line load. Note that for both of these solutions, the problem is solved on the basis that the beam excitation force, while moving in space, is of constant magnitude. This is a limitation in applications to railway systems as the wheel-rail forces are not of constant magnitude.

In the event that closed form analytical solutions are not possible, as is the case for the more complex problem of moving sprung masses, numerical integration techniques such as the Runge-Kutta, Newmark β or Wilson θ (Hart & Wong 1999) methods, can be applied to solve the equations of motion of both the vehicle and the track systems. Examples where this approach has been applied to solving for the dynamic response of the interactive systems of railway vehicle and track are common in the literature (Hou et al. 2003, Lei & Noda 2002, Lin & Trethewey 1990, Thambiratnam & Zhuge 1996, Yang, Yau & Hsu 1997).

Non-linearities in the interactive vehicle-track system, such as the force-displacement relationship of the wheel-rail contact indentation, can easily be implemented in such

numerical time domain analyses (Fermér & Nielsen 1995). Non-uniformities, such as the discretely spaced railway sleepers, can also be conveniently incorporated (Fermér & Nielsen 1995, Nielsen & Igeland 1995). However, time domain analysis, though robust and useful, is generally computationally expensive (Hartnett 2000*a*). In addition, the physical system of differential equations of motion, whose solution forms the basis of time-domain analysis, are not easily interpreted in the manner of a frequency domain transfer function.

In contrast to time domain analyses, frequency domain, or spectral, techniques are relatively computationally inexpensive. The dynamic input to the vehicle-track system, in this case the random vertical irregularity of the track profile, can be input to the model, not as a time history, but as a Power Spectral Density (PSD) function that is representative of the random process (Frýba 1996). Frequency domain analysis involves the calculation of system output spectra from the known track displacement input spectra via the system frequency response functions (Newland 1993). Non-linearities in the system are required to be linearised in order that the frequency domain technique can be applied to this particular type of problem (Esveld 1989). There is a large range of texts available that provide broad fundamental explanations of frequency domain techniques (Crandall & Mark 1963, Newland 1993, Piszczek & Nizioł 1986, Robson 1963, Wirsching, Paez & Ortiz 1995).

The most fundamental concept of frequency domain analysis is that, for a linear, single degree of freedom (SDOF) system, given the spectral density function of an input signal to the system as a function of circular frequency ω , $S_i(\omega)$, the spectral density of the output $S_o(\omega)$ may be calculated using the relation

$$S_o(\omega) = |H(\omega)|^2 S_i(\omega) \quad (2.1)$$

$H(\omega)$ is a characteristic of the system parameters and is known as the system frequency response function, or transfer function. The frequency response function is defined such that its magnitude is equal to the amplitude ratio and the ratio of its

imaginary to its real part is equal to the tangent of the phase angle (Newland 1993). The constituent components of the frequency response function for a SDOF system with mass, damping and stiffness parameters 100kg, 500Nsm⁻¹ and 1000Nm⁻¹ respectively are illustrated in Figure 2.2. This fundamental SDOF frequency domain theory can be expanded to the analysis of multi-degree of freedom systems such as the railway vehicle and track system.

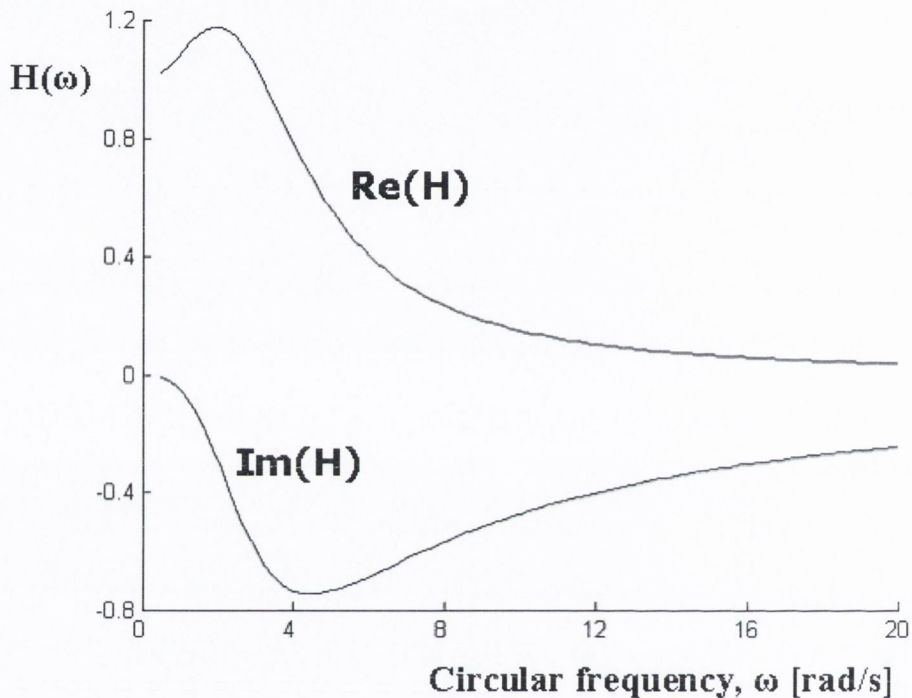


Fig. 2.2: Sample frequency response functions real and imaginary constituent parts

Frequency domain analysis is applicable to a large number of diverse fields of research. Aside from its application to the analysis of mechanical systems, which is reviewed in Section 2.2.2, frequency domain techniques are prevalent in the recent literature in the fields of digital signal processing (Koh & Sarkar 2005), physiology (Bartels, Jelic, Ngai, Gates, Newandee, Reisman, Basner & Meersman 2004) and economics (Pakko 2003), in addition to many others. Some examples of other structural engineering applications include the analysis and subsequent design of off-

shore lattice structures (Hartnett 2000*b*, Hartnett 2000*a*, Kawano & Venkataramana 1999), and earthquake engineering (Bhattacharyya & Chakraborty 2002, Takewaki 2005*b*, Takewaki 2005*a*).

Fourier theory (Newland 1993) forms the basis of spectral analysis; if $x(t)$ is a periodic function of time t , with period T , then $x(t)$ can be expressed as an infinite trigonometric series (a *Fourier series*) of the form:

$$x(t) = a_0 + \sum_{k=1}^{\infty} \left(a_k \cos \frac{2\pi kt}{T} + b_k \sin \frac{2\pi kt}{T} \right) \quad (2.2)$$

While Equation 2.2 assumes that $x(t)$ is periodic, a stationary random process can also be represented by an infinite number of constituent waves of different wavelengths. By manipulating the Fourier series equation for the limiting case when $T \rightarrow \infty$ the random signal $x(t)$ is given by the following equation:

$$x(t) = 2 \int_0^{\infty} A(\omega) \cos(\omega t) d\omega + 2 \int_0^{\infty} B(\omega) \sin(\omega t) d\omega \quad (2.3)$$

This equation is a representation of $x(t)$ by means of a *Fourier integral*. $A(\omega)$ and $B(\omega)$ are the components of the *Fourier transform* of $x(t)$ and are given by:

$$A(\omega) = \frac{1}{2\pi} \int_{-\infty}^{\infty} x(t) \cos(\omega t) dt \quad (2.4a)$$

$$B(\omega) = \frac{1}{2\pi} \int_{-\infty}^{\infty} x(t) \sin(\omega t) dt \quad (2.4b)$$

The study of the effect of random track roughness lends itself to frequency domain analysis due to the fact that irregularity in the vertical track profile can be modelled as a stationary, ergodic, Gaussian random field. A study of data obtained from Indian railways confirmed this characteristic (Iyengar & Jaiswal 1995). As such, these irregularities can be defined in terms of their *Power Spectral Density* (PSD) function, denoted $S(\omega)$. It can be shown (Robson 1963) that the PSD function is

equivalent to $A(\omega)$ from Equation 2.4a, ie.

$$S(\omega) = A(\omega) \quad (2.5)$$

The PSD function can be used to develop track quality standards and to specify the dynamic input imparted to the railway vehicles as a result of these irregularities. In addition, it is possible, with an appropriate mathematical vehicle model, to generate PSD functions defining the vehicle motion (Andersen, Nielsen & Kirkegaard 2001, Sun & Kennedy 2002). If the vehicle system parameters are linear, ie. the displacement and velocity are linearly proportional to the applied force, the dynamic response is also Gaussian (Robson 1963).

Various additional properties of the PSD function allow the calculation of peak vehicle amplitudes and other useful statistical data (Nigam 1983). Iyengar & Jaiswal (1995) apply classical level-crossing and peak statistics theory to calculate the theoretical number of peaks and zeroes of the railway track irregularity process. These numbers, calculated using standard unevenness PSD functions, are then compared with, and found to correspond to, measured data.

The calculation of the Probability Density Function of a Gaussian process requires only that the variance and mean value of the response be known. The process variance is obtained by direct integration of the PSD function for the process (Piszczek & Nizioł 1986), while a zero-mean input process and a linear system model will ensure that the output is zero-mean also.

2.2.2 Mechanical Systems Analysis in the Frequency Domain

In the broad field of mechanical transport system vibrations, spectral analysis has frequently been used to investigate the effects of various vehicle parameters on the spectral density functions of the pavement loads (Sun & Kennedy 2002). These loads

are analogous to the wheel-rail contact forces in railway engineering. A quarter vehicle model of a passenger vehicle is analysed, the results of this analysis are applicable to the optimisation of vehicle suspension systems. The deformation of the underlying pavement was not included in the model. The pavement roughness is described by a double-sided PSD function proposed by the ISO (International Organisation for Standardisation). In Sun (2001*b*), field measurements of the dynamic pavement loads generated by an *IVECO* vehicle are compared with theoretical results obtained using a frequency domain dynamic simulation. The computer simulation results are found to accurately match the field measurements.

The application of frequency domain techniques is prevalent in many studies of wheel-rail contact forces. Lei & Noda (2002) implement a numerical time domain analysis of the vehicle-track interaction using the finite element method (FEM) with Euler beam elements to model the railway track and a 10 degree-of-freedom (DOF) planar vehicle. An Euler beam model is one in which the beam's rotational inertia and shear deformation are disregarded (Esveld 2001). Random vertical track profile irregularity is input to the mathematical model and the simulation results are presented for analysis in both the time and frequency domains. The frequency domain presentation allows easy identification of the critical frequencies. Esveld (1989) and Jenkins et al. (1974) use transfer functions to characterise the nature of the various vehicle displacements and wheel-rail contact forces. A transfer function represents the contribution made by a geometry component to a vehicle reaction in the frequency domain. Jenkins et al. (1974) use the various transfer functions to demonstrate the influence of the different vehicle and track parameters on the wheel-rail contact forces over some broad frequency ranges.

At low frequency excitation (less than 10Hz) suspension force variations are the main source of track loading. In the intermediate frequency range between 20Hz and 100Hz the suspension and track system itself are the main sources of influence. The wheelset masses and the wheel-rail contact stiffness are critical in the high frequency

range of 500Hz to 2000Hz (Jenkins et al. 1974).

The incorporation of the pavement response, or, in the case of railway vehicles, the track response, into the model, greatly increases the complexity of a frequency domain calculation of the contact force (Esveld 1989). Andersen, Nielsen & Iwankiewicz (2002) have formulated a method of calculation of the frequency response function of a SDOF mass moving across a beam with a randomly irregular vertical upper profile supported by a Kelvin elastic foundation. A moving coordinate system is implemented and, initially, the response is calculated for harmonic beam surface irregularities. This model is then extended and the solution is derived for the case of a random beam surface profile. Both the vehicle mass response and that of the underlying beam are determined as a function of the PSD of the random irregularities. For a linear system the solution for any number of uncorrelated single degree of freedom systems may be superposed. It is, however, noted by Andersen et al. in the same study that a more realistic vehicle model would require additional degrees of freedom and multiple beam contact points. An analytical approach to this problem is inconvenient. Indeed, for a moving vehicle with more than two degrees of freedom only a numerical solution may be found (Andersen et al. 2002). As a complete vehicle model requires multiple (greater than two) degrees of freedom and also multiple wheel-rail contact points, a frequency domain approach to the coupled infinite beam and vehicle system is not possible.

Spectral methods have also been applied to the problem of track vibration due to variations of the foundation stiffness (Andersen & Nielsen 2003). The vertical foundation stiffness springs are assumed to be a stochastic field with a small random variation about a mean value. Again, a SDOF vehicle model is considered. Both the moving vehicle and continuous beam responses are shown to increase with both vehicle velocity and the correlation length of the stiffness variation. The correlation length is a measure of the range over which fluctuations in one region of space are correlated with (or influence) those in another region.

The steady state response of a beam on an elastic foundation subject to moving point loads (Sun 2002) and to moving line loads (Sun 2001*c*, Sun 2001*a*) has been solved using frequency domain techniques. Fourier transforms are applied to convert the system equations of motion from the time to the frequency domain.

2.3 Dynamic Vehicle-Track Interaction

2.3.1 Quasi-Steady State Interaction

In the absence of geometrical irregularity of the wheel-rail contact area, the dynamic interaction between railway vehicle and track attains a quasi-steady state condition (Nielsen & Abrahamsson 1992). The dynamics of vehicles and track under such idealised conditions are usually studied separately as two independent dynamic problems. This division within the field may be due in part to the corresponding global engineering divide between the roles of the mechanical and civil/structural engineer. The study of railway vehicle vibration has, historically, been a mechanical engineering topic while civil engineering encompasses the areas of railway track construction and design.

The modelling and simulation of the dynamic response of railway systems with a view to predicting the 'real' system response has been an engineering objective for almost as long as railway vehicle and track systems have existed (Garg & Dukkipati 1984). The importance of railway networks to the global transport infrastructure ensures that this area of research will continue as long as the demand for greater vehicle velocities and capacities remains.

The vehicle system includes wheelsets, car bodies and flexible intermediate structures which are connected by components such as springs and dampers. In many cases, investigation of railway vehicle dynamics is undertaken under the assumption that the underlying track system is rigid or behaves in a similar manner to a beam set upon a continuous elastic foundation (Esveld 1989, Nishimura, Perkins

& Zhang 2004, Stichel 1999). For the beam model, the foundation stiffness and damping are continuously distributed along the length of the beam. Many of the models introduced by Garg & Dukkipati (1984) are based on the assumption of rigid track. The various theoretical assumptions regarding the track system dynamics, such as the assumption of a uniformly continuous foundation of discretely supported track, are discussed by Profillidis (2000). Frequently however, when commercial software such as NUCARS (Blader, Elkins, Wilson & Klauser 1989) or VAMPIRE (Gilbert 2001) are utilised in the analysis of vehicle dynamics, the analysis is performed under one of the two basic assumptions of 'rigid track' or 'continuous elastic foundation'.

The railway track system comprises the rails, rail-pads and sleepers, which are supported by ballast and connected by fastenings. In many cases, the ballast bed lies on a sub-ballast layer which forms the transition layer to the formation. This multi-layered system is often approximated as the simple beam on elastic foundation structure described previously (Hetényi 1946). A common approach throughout the literature has been to model the track system as a theoretically infinite beam on elastic foundation. Engineers solved for the static deflection of an infinite beam on elastic foundation during the 19th century, this has become a landmark solution in the field of railway track design. This type of model was considered representative of a railway track where the sleepers are assumed to be so close together that the track foundation forms a continuous resilient support to the rail. The equations derived are sometimes called the *Zimmerman* equations after one of the pioneering researchers in the field (Hetényi 1946).

The dynamics of the railway track system is generally studied using the simple beam model, supported by an elastic foundation, and traversed by either a single wheel or bogie (Nielsen & Oscarsson 2004, Lee 1998, Thambiratnam & Zhuge 1996). Solutions to dynamics problems involving beams on elastic foundations are of interest to applied mathematicians and engineers involved in a broad spectrum of

practical and theoretical applications. The solutions to these problems have regularly been adopted and developed by researchers of railway track dynamics (Chen & Huang 2003, Frýba 1999, Hetényi 1946, Jenkins et al. 1974, Thambiratnam & Zhuge 1996, Warburton 1976).

The advent of high speed computers and the ensuing development of the finite element method (FEM) has greatly impacted upon the research methods applied in the field of railway track dynamics. The FEM has been applied to such problems by Dong et al. (1994), Lin & Trethewey (1990) and Nielsen & Igeland (1995), amongst many others. The FEM allows additional characteristics of the track system to be easily applied to the simple continuous beam model. An example is the implementation of the periodically spaced sleepers in the track structure model. Closed form solutions for the dynamic response of a beam resting on sleepers to a moving force are possible (Cai et al. 1988, Jezequel 1981, Mead 1970, Mead 1986), but more realistic vehicle models render the solution much more complex and beyond the realm of closed form solutions. In contrast, the corresponding numerical FEM model is increased in terms of both matrix size and computational requirements, but it will always be capable of producing a solution for the system behaviour as a function of time.

The FEM also allows the numerical simulation of more complex beam models that can be developed to include the influence of the track sleepers or ballast on the beam response. Hou et al. (2003), Lei & Noda (2002) and Zhai & Cai (1997) are examples of numerical studies where the sleepers are discretised as a layer of sprung point masses beneath the rails. Interestingly, the sleeper layer itself may also be modelled as a beam (Esveld 1989). In this case the track system is schematised as a double beam where the lower beam, ie. that representing the sleepers, has zero bending stiffness.

While the fundamental simplification of the entire railway track system as a single beam on elastic foundation is a natural progression, modelling the beam end

conditions can be problematic. Hetényi (1946) has presented the derivations of the analytical formulae for the displacement, rotation, bending moment and shear force at any distance from a point force applied to an infinite beam on a continuous elastic foundation. Each equation is given as a function of the distance from the point of application of the force, the beam bending stiffness, and the foundation stiffness parameter. The characteristic length of the beam, $\frac{1}{\lambda}$, is an important factor influencing the deflected shape of such a beam, and is a function of both the flexural rigidity of the beam and elasticity of the supporting medium (see Equation 2.6).

$$\lambda = \sqrt[4]{\frac{k}{4EI}} \quad (2.6)$$

For completeness, Hetényi also details an investigation of the effect of discretising the continuous foundation into a series of periodic supports representing sleepers. In this static application the differences between the beam bending moment due to static vehicle loading with the continuous and discrete foundations are found to be insignificant (less than 2% at the point of load application and less than 7% 2m away from the same point where the deflections are small).

The solution to the dynamic infinite beam problem is much more complex. Closed form solutions are available only under certain, simple, loading conditions. The solution for the quasi-steady state beam response under the action of a moving constant force was first solved by Timoshenko (1926). Frýba (1999) has detailed a solution that includes a study of the effect of varying speeds in addition to different levels of viscous foundation damping. Andersen et al. (2001) applies a convected (moving) coordinate approach to derive a solution for the beam response to moving harmonic excitation. A moving harmonic load case was also considered by Sheng, Jones & Petyt (1999) and Jones, Sheng & Petyt (2000) in a study of ground vibrations induced by railway vehicles travelling at various velocities. The characteristics of harmonic loading enable the analytical solution of the governing beam differential equation. More complicated load cases such as real railway vehicle systems, how-

ever, do not lend themselves to such solutions. These cases are more easily solved using numerical techniques in conjunction with suitable mathematical models for both vehicle and beam (Hou et al. 2003).

The application of suitable transmitting boundary conditions to a quasi-infinite beam system is required in order to solve for problems with greater load complexity than constant moving or harmonically varying forces. An example of such a load case is a more realistic vehicle model with multiple degrees of freedom such as the vehicle models that are applied in analysis by Lei & Noda (2002) and Nielsen & Igeland (1995). Andersen et al. (2001) compared analytically derived results with those obtained using a quasi-infinite FEM formulation of the infinite beam on elastic foundation for the moving harmonic load case. The results generated by means of applying transmitting boundary conditions to the FEM model are shown to agree with the analytical solution for the single frequency excitation tested.

The loading of the track structure at more than one single loading point generates interaction effects. The solutions for static interaction effects are readily derived from static elastic beam theory (Hetényi 1946) and the principle of superposition. The dynamic effects are more complex due to wave propagation and reflection within the track structure. The effect of multiple wheels on the rail is investigated by Wu & Thompson (2001*b*) who determined that when solving for a high frequency excitation, the individual loads and subsequent effects can be treated independently using the superposition principle, provided that the rail vibration is considered as a frequency band average. For the track parameters that were considered it was also found that the wheel-rail interaction effect on the contact force could be neglected at spacing distances of more than 10m. The high frequency wheel response of a passenger wagon will therefore have no effect on the response of other wheels more than 10m away. The same authors also investigate the effect of the presence of multiple wheels on railway rolling noise (Wu & Thompson 2001*a*). It is found that the influence of the wave reflection on track vibration and noise radiation is limited.

Generally, vehicle-track interactive studies have predominantly used numerical models. The vehicle cannot, under normal circumstances, be modelled as a constant moving force or series of forces, due to the presence of the dynamically varying wheel-rail contact forces. The representation of the vehicle as a series of sprung masses is also of limited usefulness as the interaction between vehicle components is not considered. The wheel-rail contact force, in the quasi-steady state, contains two distinct periodic waves (Dukkipati & Dong 1999). The first wave occurs as a result of track stiffness variation due to sleeper spacing. This force wave reaches a maximum when the sleeper passing frequency is equal to the wheel-track resonant frequency or the loaded track frequency. The wheel travelling motion and the oscillation of the discrete supports result in the second contact force wave. As the wheel approaches a support, the loading forces the sleeper downwards. If the sleeper motion is not in phase with the motion of the rail over the sleeper, a support oscillation occurs and results in a fluctuating contact force. It is reported also that, in the conventional train speed range, the steady state is attained after the vehicle has travelled 4 to 5 sleeper spacings. Significantly, the model employed by Dukkipati & Dong showed that, for this idealised vehicle-track interaction, the wheel-track interactive forces caused due to vehicle acceleration, are insignificant.

Previously, Dong et al. (1994) had formulated a simplified, SDOF vehicle model, and applied this model to a similar track model to that of Dukkipati & Dong (1999). The sprung mass is representative of a perfect wheel and, as with Dukkipati & Dong (1999), the track profile is idealised as being perfectly smooth. The time histories of rail and wheel displacements, in addition to that of the dynamic contact force, are obtained from the model. These results are later compared with results from another study of higher model complexity (Sun & Dhanasekar 2002). Sun & Dhanasekar apply a more theoretically advanced track model, where the rail is modelled as an infinitely long continuous Timoshenko beam (Timoshenko 1921). This is in contrast to the more robust truncated beam model that was applied by

Dukkipati & Dong. The vehicle system used by Dukkipati & Dong was modelled as a ten degree of freedom wagon with four wheelsets, two bogies and a wagon body. Initially however, a single degree of freedom moving sprung mass was applied as the loading to the infinite beam model. The period of vibration predicted by both models is identical. This reflects that the dominant period of the contact force time history for discretely supported track is obtained by dividing the sleeper spacing by the vehicle velocity. Difference in the wheel and rail displacement and contact force peak factors, which differ by 5.6% for displacement and 1.95% for contact force, were partly explained by the different methods of calculating the damping coefficients for the pad and ballast. This acceptable agreement was used by Sun & Dhanasekar (2002) to validate their more advanced approach to modelling the track and the multi-body wagon model. This model was then applied in interactive studies involving defects in the wheel and rail geometry (see Section 2.3.2).

The quasi-steady state response of the wheel and rail calculated by Dong et al. (1994) is illustrated in Figure 2.3. Note that the dominating wavelength of the periodicity in the dynamic response is equal to the sleeper spacing. It should be noted once again that the vehicle model in this case was a single DOF sprung mass. More complex vehicle models can impose additional frequencies on the response. However, in the absence of wheel or track defects, the dominating wavelength is always the sleeper spacing distance.

2.3.2 Interaction with Contact Area Irregularity

Previously, in Section (2.3.1), the focus was upon railway engineering studies that did not take into account geometric irregularity of the wheel-rail contact area. The area in which the wheel and rail come into contact was assumed to be perfectly smooth with the result that the variation of the contact forces is minimised. Minimisation of the contact force variation results in minimal track and vehicle system vibration as it is the contact forces that provide the dynamic excitation to both. This section

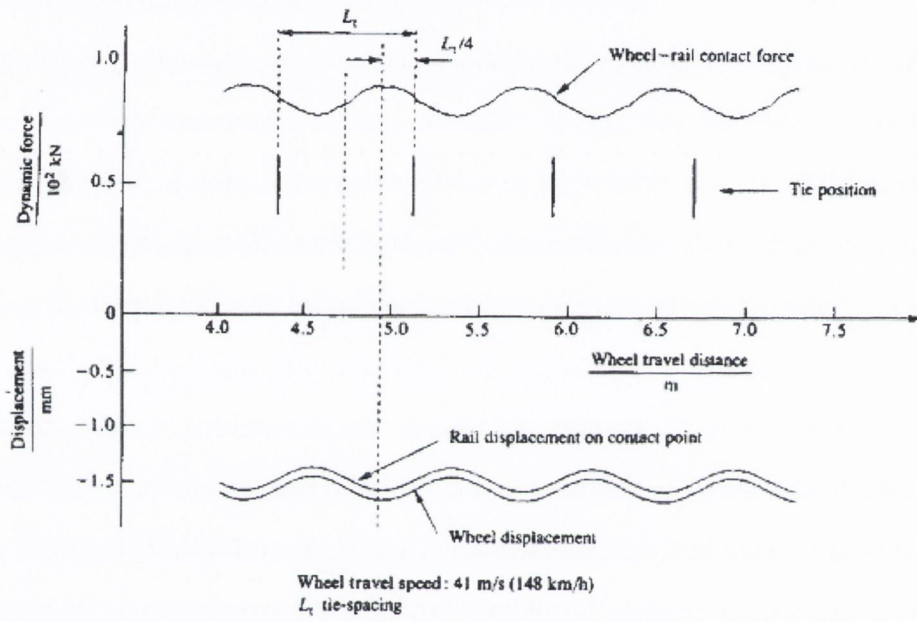


Fig. 2.3: Quasi-stationary contact force and rail displacement time histories at wheel-rail contact point.

(Dong et al. 1994)

concentrates upon studies where irregularity of both the wheel and rail is considered as a source of dynamic excitation to both the vehicle and track systems and these irregularities are incorporated into the mathematical models.

The types of geometric irregularity of the contact area that cause the vehicle-track interaction to deviate from the quasi-steady state vary greatly (Dong et al. 1994, Jenkins et al. 1974, Lei & Noda 2002, Nielsen & Igeland 1995). Track and wheel profile defects give rise to periodic (Hou et al. 2003), isolated (Thompson, Wu & Armstrong 2003, Tanabe, Wakui, Matsumoto, Okuda, Sogabe & Komiya 2003), and random (Kalker & Périard 1996) fluctuations supplementary to the quasi-steady state vehicle-track interaction. The frequency-dependent nature of the vehicle-track interaction is described by Harvey, Gosling & Cope (1993):

“Where two or more mass-spring systems are superimposed on one another, the combined system will possess two or more natural frequencies, and hence if the input (ie., the shape of the wheel-rail interface, seen as a function of time) is a complex periodic one containing many frequencies, resonances may occur at several interfaces within the system. This happens in the vehicle-track system, and several important sets of interactions can be identified.”

Geometric irregularities have the potential to generate sharp peak responses in the interaction (Iyengar & Jaiswal 1995). It is possible to minimise the occurrence of track and wheel defects by imposing a suitable maintenance and repair regime (Harvey et al. 1993). However, the occurrence of geometrical irregularity, of both the vehicle and track systems, is unavoidable. Therefore, the nature of these irregularities and their dynamic effects are a topic of great interest to railway engineers.

Jenkins et al. (1974) outline the fact that it is imperfections in the wheels and rail that supplement contact forces that would, otherwise, be close to the static wheel loads. However, the concept of a perfect contact area is a theoretical assumption that can never be attained in practice. This reality is no different to

many structural engineering applications, where idealistic assumptions are used to simplify theoretical calculation of stresses and deflections.

The major causes of these vertical wheel-rail force increases are identified by Jenkins et al. (1974) as follows:

1. isolated irregularities in the running surface, which occur by default at joints and welds and by design at points and crossings;
2. periodic irregularities, such as corrugation on the rail surface or the repetitive effect of sleeper spacing;
3. random variations of longitudinal profile (track top roughness);
4. defects in the vehicle such as wheel flats and wheel eccentricity;
5. random variations in sleeper support stiffness such as hard spots and voids.

Each of these types of irregularity occurs for a particular reason. While the causes of the occurrence of irregularity at a rail joint or weld are elementary, as is the periodic effect of sleeper spacing, other mechanisms that give rise to irregularity are more complex, an example being rail corrugation.

The different types of irregularities that induce increased wheel-rail contact force magnitudes may alternatively be classified according to their frequency content (Harvey et al. 1993). The various frequency ranges give rise to excitation of different components of the interactive vehicle-track system. Low frequency irregularities, in the 0.5 to 10Hz range, will generally be found to excite only the vehicle body on its primary suspension in addition to the vehicle bogies. The medium frequency range, 20 to 100Hz, of irregularities can excite the unsprung mass to oscillate on the track spring. Track and wheel defects are generally manifest in this frequency band. Higher frequency excitation, at 500Hz and above, is associated with the natural frequency of the track mass on the Hertzian contact spring.

Wheel flats are among the contact area defects that cause periodic contact effects. Flats are created by sliding/skidding of the wheel upon application of the brakes. The effect of sliding causes wearing of the steel wheels at the point of contact and results in a flat spot on the rolling surface of the wheel. Jergéus (1997) has provided an overview of the technical and economical problems caused by wheel flats. The same author has been involved in the testing of railway vehicles with wheel flats (Jergéus 1999). These experimental results were used to verify and calibrate a numerical model for wheel flat prediction. Frýba (1996) includes a brief discussion of the effects of wheel flats on the interactive force between a railway bridge and a vehicle wheel. The largest dynamic effect is found to occur at approximately 30kmhr^{-1} when the wheel loses contact with the rail and on contact recovery generates an impact.

The dynamic effect of a wheel flat can be simulated by modelling an indentation in the rail surface (Sun & Dhanasekar 2002). Alternatively, a modification of the contact spring as an adaptive contact model has also been applied (Dong et al. 1994). At the point in time where the wheel flat comes in contact with the rail the spring is represented as a set of uniformly distributed springs along the length of the wheel flat. The relationship between the total vertical force and the total deformation for the adaptive contact model is equivalent to that of the single Hertzian contact spring model. The two models, applied respectively in the two aforementioned studies, each gave very similar results in terms of the dynamic contact force increments. The general effect on the contact force is a large drop-off followed by a high peak force, the magnitude of the peak being dependent upon the extent of the wheel flat.

The effect of wheel flats on the vehicle-track interaction at varying velocities has also been investigated (Nielsen & Igeland 1995). There is a general increase in the maximum vertical contact force with velocity at higher velocities (greater than 80km/hr). Interestingly however, the calculated maxima are of a similar magnitude between 20 and 80km/hr , this magnitude equates to an increase approximately equal

to the static axle load. The minimum contact force resulting from the wheel flat does decrease with velocity, at velocities greater than 80km/hr there is loss of contact between wheel and rail resulting in zero minima. Hou et al. (2003) considered the effect of a wheel flat on the response of a three dimensional vehicle model. It was reported that a wheel flat on one side of the vehicle significantly affects the wheel-rail interaction at the opposite side where the wheels oscillate on the rail. The wheel without the flat on the same side of the vehicle as the flat wheel displays an impact and subsequent vibration in its contact force history.

The periodic characteristic of the excitation generated by a wheel flat is dependent upon the wheel radius and vehicle velocity. The time between impact is equivalent to the wheel circumference divided by the vehicle velocity. For example, a 1m diameter wheel travelling at 30kmhr^{-1} will give rise to an impact force at a frequency of approximately 2.65Hz.

Sleeper effects can also generate periodic effects in the dynamic response (Frýba 1996). This particular effect was investigated by Fermér & Nielsen (1995) who found that the resulting maximum dynamic response generally increased with increasing vehicle velocity. The dynamic contact forces were found to be largely dependent upon the rail pad stiffness. Soft rail pads yielded smaller contact forces for low vehicle speeds but larger contact forces for higher speeds. However, it is also noted that softer rail pads are favourable to sleeper and ballast loading. The sleeper effect on the dynamic contact force is clearly illustrated by Dong et al. (1994) where the predominant contact force fluctuation is a sinusoid with wavelength equal to the sleeper spacing. The standard sleeper spacing distance of approximately 0.6m gives rise to a harmonic with a frequency of 68Hz for a vehicle velocity of 148kmhr^{-1} (see Figure 2.3).

Random irregularities are imperfections in the track profile that are entirely devoid of periodic content, ie. they are entirely irregular (Frýba 1996). The occurrence of this type of irregularity is inevitable and can be due to wear, subsidence

or insufficient maintenance of the permanent way (Frýba 1996). PSD functions can be used to represent the displacement of such random processes statistically (see Section 2.2). The statistical characteristics of linear dynamic systems subjected to stationary random excitation may be analysed by implementing spectral techniques. Mathematical linearisation of any non-linear vehicle and track components allows analysis of the system response to random irregularity in the frequency domain (Esveld 1989, Jenkins et al. 1974, O'Dwyer, Hegarty & Basu 2002).

Andersen et al. (2002) have derived a solution, using frequency domain techniques, for the system response of an infinite beam with a randomly irregular upper profile being traversed by a moving sprung mass. An analysis of this beam model under a more realistic vehicle model loading is far more complex, and only numerical solutions may be found. Even for the relatively simple case of a two degree of freedom vehicle with two separate contact points, though possible to solve analytically, is more convenient to solve numerically.

The incorporation of random irregularity into numerical vehicle-track analyses is prevalent in the literature (Lei & Noda 2002). The relatively complex vehicle models that are used in these studies prohibit the derivation of an analytical solution using implementations of fundamental random vibration theory techniques that have been presented by Robson (1963) and Newland (1993) among others. Random irregularities are generated numerically from appropriate PSD functions. The track and vehicle systems are modelled using the FEM and numerical solutions are calculated. Lei & Noda (2002) applied a generalised FE Euler beam element to model the track, and included the effect of the sleepers and ballast stiffness. Other studies involving random track roughness have included the effects of the irregularities on the dynamic response of railway bridges (Song, Noh & Choi 2003, Au, Wang & Cheung 2002, Wu & Yang 2003, Wiriyachai, Chu & Garg 1982) (see Section 2.4).

Discrete, or transient, irregularities of the railway track are isolated deviations from the ideal profile. These can occur at any particular point along the railway

track but especially at rail joints, rail switches and bridge approaches, amongst many others. The response of the system to transient type irregularities is most readily suited to calculation by analytical methods (Harvey et al. 1993). However, in many instances, to obtain a more accurate and complete prediction of the dynamic system response it is necessary to use numerical analysis. A summary of the general effects of some discrete track defects is provided by Harvey et al. (1993). In particular, the peak contact forces resulting from a single ramp in the track profile are calculated analytically. This idealised profile irregularity can be used to model a number of different types of discrete irregularity, including a dipped rail joint or a wheel. The ramp gives rise to two readily distinguishable dynamic increments, the first of high frequency acting over a very short time span, and the second of medium frequency. The forces are denoted the P_1 and P_2 forces respectively. The forces are given by the following formulae:

$$P_1 = P_0 + 2\alpha c \sqrt{\frac{hM_{T1}}{1 + M_{T1}/M_u}} \quad (2.7a)$$

$$P_2 = P_0 + 2\alpha c \sqrt{\frac{M_u}{M_u + M_{T2}}} \left(1 - \frac{\pi C_T}{4\sqrt{K_{T2}(M_u + M_{T2})}} \right) \sqrt{k_{T2}M_u} \quad (2.7b)$$

where P_0 is the steady state contact force (in kN), c is vehicle velocity (ms^{-1}), α is the ramp angle (radians), M_{T1} is the effective track mass for the P_1 calculation and M_{T2} the effective track mass for the P_2 calculation (kg). h is the effective Hertzian contact stiffness (MNm^{-1}), C_T is the track damping (kNm^{-1} per sleeper end), M_u is the unsprung mass (kg) and K_{T2} is the track spring stiffness (MNm^{-1}).

Dipped joints are an example of transient type irregularities and can be modelled as a simple ramp with angular deflection equal to the sum of the running on and running off railheads (Harvey et al. 1993, Jenkins et al. 1974, O'Dwyer, Hegarty & Basu 2004). The presence of an unsupported sleeper also constitutes a discrete irregularity and its effect has also been investigated (Nielsen & Igeland 1995, Sun & Dhanasekar 2002). This situation might occur due to erosion of the track ballast

bed. In jointed track in particular, the increased dynamic forces at the joint can cause the ballast to deteriorate. At low vehicle velocities (less than 100kmhr^{-1}) the effect is an additional imposition of load on the neighbouring sleepers. However, higher velocities may lead to cracking of the sleeper as a result of fatigue under abnormally high loading.

2.3.3 Contact Mechanism Characteristics and Models

An understanding of the physical nature of the interactive wheel-rail contact mechanism is critical to all research based upon modelling the dynamic interaction between railway track and vehicles. An understanding of the wheel-rail contact characteristics is therefore vital from a railway engineer's point of view. The points of interaction between the vehicle wheels and the rails provide the sole locations of energy transfer between the two systems, and as such, are the major sources of excitation of both systems. An understanding of the wheel-rail contact characteristics is vital from a railway engineer's point of view. One significant factor that eases the task of understanding the contact mechanism is the fact that the running of a steel wheel on a steel rail is the original feature of all railway systems. This characteristic is a rare constant in a research topic that involves a significant number of variables. In conjunction with this universal feature, also of huge benefit is the fact that the metallurgical properties of the steels used have no appreciable effect on the wheel-rail contact characteristics (Moreau 1992). It should be noted, nonetheless, that while these factors do not affect the dynamic response, the resultant damage to both the wheel and track is highly dependent upon the metallurgical properties (Murakami 2002).

The steel wheel and rail are, in effect, two elastic bodies that are pressed against one another (see Figure 2.4). The shapes of these two steel bodies have been continuously adapted to maximise the dual functions of vehicle guidance and support. The Hertz theory, which was first proposed around 1880, is frequently used to calculate

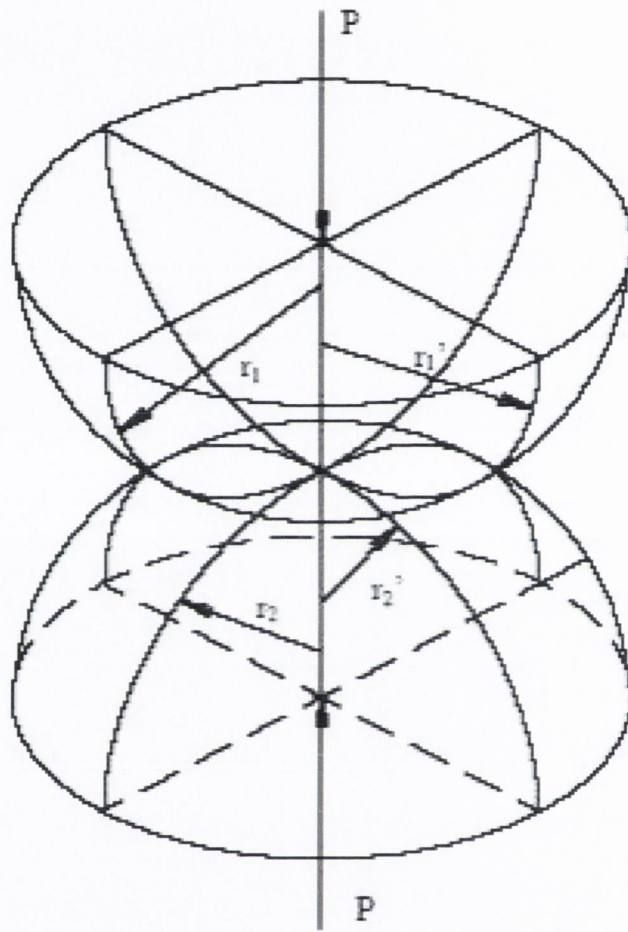


Fig. 2.4: Elastic bodies in compressive contact

the pressures that arise in such contact areas. This theory postulates that the contact area between two curved elastic bodies is generally ellipsoidal, and that the corresponding stress distribution is semi-ellipsoidal. Hertz demonstrated (Moreau 1992) that the intensity of unit stresses, σ was represented by an ellipsoid bounded by the contact ellipse

$$\sigma(x, y) = \frac{3Q}{2\pi ab} \sqrt{1 - \left(\frac{x}{a}\right)^2 - \left(\frac{y}{b}\right)^2} \quad (2.8)$$

The semi-axes of the ellipse, a and b , are determined as functions of the radii of curvature of the contact bodies, the material Young's modulus, and the tracking force of the bodies. Q is the normal load exerted by the wheel on the track.

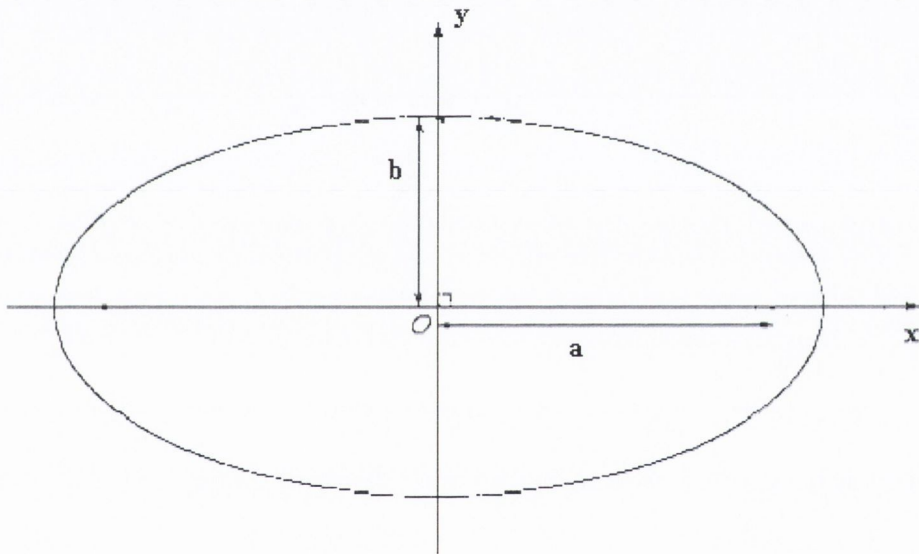


Fig. 2.5: Contact stress boundary ellipse

Esveld (1989) demonstrates a simplified calculation for the wheel-rail contact problem. It has been proven that, for wheel diameters between 0.6m and 1.2m, this two-dimensional calculation of Esveld suffices. It is assumed that all of the curve radii, except for the wheel radius, are infinite, and that the wheel load is evenly distributed over the contact area. The mean contact stress, T , may now be

calculated from

$$T[\sigma] = \sqrt{\frac{\pi E}{64(1 - \nu^2)} \frac{Q}{rl}} \quad (2.9)$$

where r is the wheel radius, l is the half-width of the contact area, E is the Young's modulus, and ν is Poisson's ratio.

The mean stress calculation of Equation 2.9 has been formulated on the basis that wheel-rail contact stresses occur in the vertical direction only. While this assumption is necessary for the purpose of two-dimensional planar analyses, the reality is that the interaction generally possesses both a vertical and horizontal component. Traditionally, Q is used to denote the vertical force and Y the lateral.

Kurek (1981) includes a concise description of the nature of these forces (see Figure 2.6). Under equilibrium conditions their magnitude is dependent upon the total force exerted by the wheel on the rail while their proportion is a function of the slope of the inside wheel flange surface. This slope is defined with respect to the horizontal and is generally denoted by the symbol β . A lateral force imbalance causes the wheel to move laterally until an equilibrium value of the angle β is attained.

The limiting values of the Q and Y forces that can be supported by the railway track system without impairing its serviceability are investigated in a report published by the Office for Research and Experiments of the International Union of Railways (ORE) (1978). While the loading limits of the rail structure are investigated in this report, the ratio of these forces is critical from the point of view of vehicle derailment probability calculations. A summary of derailment criteria is provided by Wickens (2003). It is shown that derailment is most likely when a large lateral Y force occurs simultaneously with a reduced Q force. Nadal's formula (Harvey et al. 1993) states that for derailment to be prevented the following inequality must be satisfied,

$$\frac{Y}{Q} \leq \frac{\tan\beta - \mu}{1 + \mu\tan\beta} \quad (2.10)$$

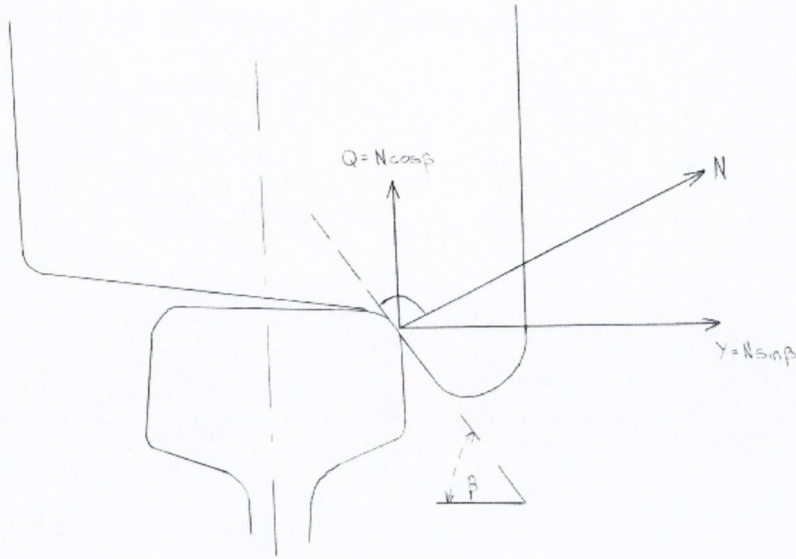


Fig. 2.6: Wheel flange forces vertical and lateral forces
(Kurek 1981)

where μ is the friction coefficient across the contact area. Another mode of failure discussed by Wickens (2003) is the lateral failure of the track due to excessive vehicle forces. An empirical criterion for this particular mode of failure has been given by Prud'homme and is

$$Y = 10 + \frac{W}{3} \quad (2.11)$$

where W is the axle load and all forces are measured in kN.

The means by which the contact mechanism is represented in computational models, in addition to the chosen magnitudes of the Hertzian stiffness parameters, are of great importance in calculating the dynamic wheel-rail contact forces. The Hertzian contact theory described previously is generally used to model the dynamic interaction. The idealised Hertzian contact spring through which wheel-rail forces are transmitted is non-linear in compression and does not store tensile energy. The non-linearity is accounted for by the spherical and cylindrical geometry of the respective contact surfaces. The condition of zero tensile capacity is significant only

in the event of loss of contact between wheel and rail.

Throughout the literature, the modelled element through which the interactive contact forces are transmitted is represented by means of a compressive spring, ie. a mechanical entity that can store compressive energy. Mathematically, the characteristic stiffness of the contact spring, k_h , is expressed by

$$k_h = \begin{cases} c_h(x_w - x_r)^{\frac{1}{2}}, & \text{for } x_w - x_r > 0; \\ 0, & \text{else.} \end{cases} \quad (2.12)$$

where c_h (with units $\text{Nm}^{-3/2}$) is the non-linear Hertzian spring stiffness, and x_w and x_r are the respective wheel and rail displacements (Nielsen & Igeland 1995). It is clear that the spring stores zero energy in the event of loss of contact between wheel and rail. However, compressive energy is stored in the spring due to the indentation of the wheel into the rail surface when the relative displacement is positive.

The application of Equation 2.12 to railway engineering analysis is prevalent in studies throughout the literature. In particular, studies that apply numerical techniques to model the two-dimensional dynamic response of either railway vehicle, track or both, use this relation as the basis of the system interaction (Sun & Dhanasekar 2002, Nielsen & Igeland 1995, Zhai & Cai 1997, Lou 2005, Lei & Noda 2002). The choice for the magnitude of the c_h value varies between the studies, while there is also variation within the study of Sun & Dhanasekar (2002). Nielsen & Igeland apply a value of $93\text{GNm}^{-3/2}$ while Sun & Dhanasekar take values of $100\text{GNm}^{-3/2}$ and $87\text{GNm}^{-3/2}$ respectively. The Hertzian coefficient can be deduced analytically from Equation 2.13 (Johnson 1985). The particular value of $87\text{GNm}^{-3/2}$ was obtained by substitution of the appropriate parameters into this equation.

$$c_h = \frac{4G\sqrt{rR}}{3(1-\nu)} \quad (2.13)$$

where G is the shear modulus, r is the rolling wheel radius, and ν is the Poisson's

ratio. R is obtained from the following equation (2.14) in which r_w and R_t are the wheel profile and rail profile radii respectively.

$$R = \frac{r_w R_t}{r_w - r} \quad (2.14)$$

Figure 2.7 illustrates the compressive contact force that is stored in the Hertzian contact element as a function of the relative wheel-rail displacement for a number of values of c_h . The force values are calculated from the positive condition of Equation 2.12.

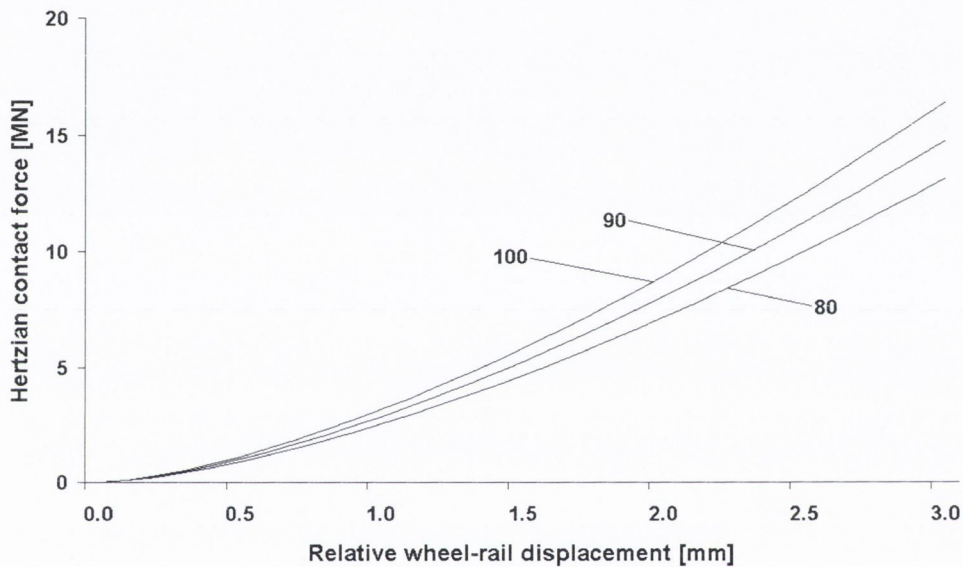


Fig. 2.7: Hertzian contact force versus relative wheel-rail displacement for three different values of c_h [$\text{GNm}^{-3/2}$]

The application of the Hertzian model for the contact area is frequent in a number of other different applications in the literature. Guagliano & Vergani (2005) and Jin, Wen & Wang (2005) analysed the subsurface cracking of railway wheels and the corrugation of rails respectively, in both cases the loading was modelled as a Hertzian type contact force. Ertz & Knothe (2002) compared different analysis methods for the calculation of temperatures in the wheel-rail contact area, again

the system input proposed was based upon the Hertzian contact mechanism.

Frequency domain studies require that the non-linear Hertzian spring be linearised. The compressive relationship between the applied wheel force F and the contact surface indentation y is given by Esveld (1989)

$$F = c_h y^{3/2} \quad (2.15)$$

in which c_h is the Hertzian spring stiffness with dimensions $\text{Nm}^{-3/2}$. The linearised Hertzian spring stiffness is found by examination of the force-displacement relationship around the static wheel load. The linear stiffness k_h is given by the relation:

$$k_h = \frac{dF}{dy} = \frac{3}{2} c_h^{2/3} F^{1/3} \quad (2.16)$$

The c_h value for old and new wheels was determined as a function of wheel diameter by Jenkins et al. (1974). For a static wheel load of 7.5t the k_h values for old and new wheels are 1.6×10^9 and $1.4 \times 10^9 \text{ Nm}^{-1}$ respectively.

2.4 Vehicle-Bridge Interaction

The study of railway bridge dynamics is generally concerned with the calculation and analysis of bridge deflections and stresses. The most important factors influencing the dynamic response of railway bridges are the bridge frequency characteristics, the crossing vehicle's frequency characteristics, the damping parameters of both systems, and the vehicle velocity. These particular parameters have been identified by Frýba (1996), one of the pioneering researchers in the field, who has provided a comprehensive review of the literature in the specific area of railway bridge dynamics. Frýba does however, state that track irregularities also represent an important source of excitation of bridges during the passage of railway vehicles.

As the number of miles of high-speed railway lines increases steadily around the globe, the vehicle-bridge interaction, and its potential effects upon the dynamic

response, has come sharply into focus. The simplest possible model for a railway vehicle is as a series of moving constant forces. Lin & Trethewey (1990) used this type of model to verify a finite element model formulation of a simply supported beam. However, analysis of railway bridge dynamics should not, in general, be simplified by the assumption of a train model comprising a series of moving constant forces. An exception to this generalisation is the case where the bridge self-weight is considerably higher than that of the vehicle weight (Frýba 1996). The moving force model is also limited in that the effect of irregularities in the wheel-rail contact area cannot be modelled. A more realistic vehicle model is required to take account of the dynamic interaction between the vehicle and the bridge itself. These models are generally multiple DOF systems comprising masses supported by springs and dampers representing the vehicle suspension system (Delgado & dos Santos 1997, Tan, Brameld & Thambiratnam 1998). The contact element applied between the vehicle model wheelsets and the track is generally modelled using the Hertzian spring theory described previously in Section 2.3.3 (Tan et al. 1998), or alternatively as an inertial mass element in contact with the track (Biondi, Muscolino & Sofi 2005, Lou 2005, Cheng, Au & Cheung 2001). It is this contact element that determines the dynamic forces imparted to both the vehicle and bridge systems. The complex interaction is affected, to different degrees depending upon their severity, by the presence of imperfections in the railway track and wheel profiles.

The quasi-steady state dynamic response of railway bridges modelled as simple beams, ie. the response when the wheel-rail interface is assumed to be geometrically perfect, is considered by Yang et al. (1997). An interesting observation from this study was that the inertial effects of moving vehicles tends to elongate the period of vibration of the beam, causing the resonant peaks to shift to smaller velocities. Resonant vibration of railway bridges results in passenger comfort deterioration, reduction of traffic safety, and destabilisation of the ballast bed (Frýba 2001). The steady state response of railway bridges is comprehensively reviewed by Frýba

(1996). Steady state in this case refers to the bridge response when the occurrence of track and wheel defects is not considered. The analysis of the characteristics of dynamic bridge response to moving loads is complicated further by the presence of such wheel-rail geometric defects.

Frequently throughout the literature, the effect of random roughness of the track profile has been incorporated into vehicle-bridge interactive models (Wiriyaichai et al. 1982, Au et al. 2002, Wu & Yang 2003, Song et al. 2003, Zhang, Vrouwenvelder & Wardenier 2001, Lou 2005). Smoothed empirical PSD functions representative of different quality track profiles are used to numerically generate random sample profiles with the required statistical properties.

Wiriyaichai et al. (1982) calculated the impact factors in a selection of members from a mathematical model of a single track, open deck, riveted truss bridge of 53.4m span. A Class 6 track roughness spectrum was used to generate track profiles with random irregularities. These profiles were then applied to the rail track in the bridge model. Deviations in alignment, cross-level and gauge, in addition to vertical track roughness, were considered in this particular study. The specified track roughness was found to cause up to 40% of the impact in the members selected for analysis (Wiriyaichai et al. 1982).

Impact factors were also calculated by Au et al. (2002) for a cable-stayed bridge with random vertical track irregularity. Once again, impact factors were calculated for a number of the member stresses, a selection of the cables' tensile stresses, towers' bending moments and also the deck bending moment at various locations. Six different track roughness classes were tested in this study. It was observed that the impact factors for the bending moment at the midspan were minimal. It was also found that the impact factors generated were not proportional to the magnitude of the roughness.

Wu & Yang (2003) also considered random irregularities in an analysis of the various dynamic responses of vehicle, rail and bridge due to a train moving over a series

of simply-supported bridges. Different classes of vertical roughness PSD functions were considered. It was found that the riding comfort of the train was significantly affected by the presence of random irregularity. Song et al. (2003) applied a FEM model to the analysis of high speed vehicle-bridge interaction. A three-dimensional model was formulated that allowed the incorporation of both vertical and lateral track irregularities. It is noted that dynamic impact factors should be evaluated considering not only span length but also the vehicle velocity and the grade of track irregularities. It was also found that, for the bridges evaluated in the study, there were no problems in terms of the bridge serviceability. However, it seemed that in this study only Class 6 roughness, which is the mildest class, was applied.

Zhang et al. (2001) formulated a space model for the bridge-train interaction including the influence of track roughness. The vertical and lateral roughness applied to the track model was found to have an important influence on the wheel motion. However, it is stated that the influence of the rail roughness on bridge deflections is less important when compared with these wheel motions. A planar model was also considered, to which only vertical roughness could be applied. No large difference was found between the response of the space and planar models.

Physically measured track roughness rather than randomly generated series' of vertical coordinates may also be applied to similar models to those that have been described (Xia & Zhang 2005). This approach was taken to verify a mathematical model of a real bridge. The track irregularity input to the model, although deterministic in that it has been physically measured, appears to be random in both the vertical and lateral directions with no obvious discrete features or dominant wavelengths.

Studies of discrete or periodic imperfections and their effect upon railway bridge dynamics are less frequent than those of random irregularities in the literature. In some instances, however, the modelling of both types of imperfections are combined (Wiriyaichai et al. 1982). In this particular case a vehicle wheel flat and its influence

on the bridge impact factors was investigated in addition to the effect of random roughness. Interestingly, the effect on the bridge member impact factors generated by a single, isolated, wheel flat was quite small. However, two wheel flats on the same side of the vehicle were found to approximately double the effect. As one might have expected, increases in the vehicle velocity caused a corresponding increase in the impact factors.

Frýba (1996) graphically illustrates the variation in the wheel-bridge contact force for a wheel with a flat defect over a range of velocities. At low velocities (less than 18kmhr^{-1}) the wheel remains in contact with the rail. The highest dynamic effect occurs between velocities of approximately 30kmhr^{-1} and 48kmhr^{-1} . At these velocities the wheel loses contact with the rail and generates an impact on contact recovery. For greater velocities, an impact is also generated, but the bridge dynamic effects decrease. Frýba (1996) also makes the point that another type of discrete track defect, rail joints, should not occur on bridges because of their potentially large dynamic effects. Most railway administrations have regulations to this effect.

Lou (2005) considered discrete, or local, irregularity of the vertical track profile in a FE vehicle-bridge interaction study with particular emphasis upon the pitching effect of the vehicle system. The irregularity function applied is that proposed by Frýba (1999) was used for this purpose:

$$\xi(x) = \frac{1}{2}a \left(1 - \cos \frac{2\pi x}{L} \right) \quad (2.17)$$

where a is 1mm and L is 1m. While the emphasis of the study was upon the vehicle pitching effect, it was observed that the effect of this pitching on the bridge and track can generally be neglected when the track is assumed to have no irregularities.

2.5 Conclusions

The above sections have detailed some of the research undertaken to date in the field of railway vehicle-track and vehicle-bridge interaction. The research has been carried out in order to calculate a number of different aspects of the dynamic system response, including the response of railway vehicles, railway track and railway bridges under a variety of different conditions. There is considerable scope for further research in each of these three areas.

The frequency domain techniques reviewed in Section 2.2.2 are applied in Chapter 3 to a parametric analysis of the contact forces generated by a railway vehicle wheel moving along a rail with random irregularity of vertical profile. A similar frequency domain analysis is also applied to a railway vehicle bogie model in Chapter 4 in an investigation of the relationship between the dynamic response at the individual axles.

A model with similar characteristics to the track models reviewed in Section 2.3 is developed in Chapter 5. The model is similar to some of the reviewed 'beam on continuous elastic foundation' models that have been discussed above. However, the numerical model developed by the author is adapted as a quasi-infinite beam and is formulated in a convected coordinate system. The validity of the Hertzian contact spring linearisation for the purpose of frequency domain analysis is also examined using this model.

A finite numerical beam model similar to the models of Hou et al. (2003), Lei & Noda (2002) and Zhai & Cai (1997) is applied to the analysis of the effects of a number of discrete wheel-rail interface irregularities in Chapter 6.

Finally, Chapter 7 details an investigation into the effect of random track profile irregularities on bridge dynamic impact factors. This study is similar in objective to some of the material reviewed in Section 2.4. However, in this case three bridge models are considered, one short, one medium and one long span. In addition,

two different classes of track irregularities are considered by the author, one of intermediate quality and one of poor quality.

Chapter 3

Parametric Study of Stochastic Wheel-Rail Contact Forces

3.1 Introduction

This chapter details a parametric study of the stochastic wheel-rail contact forces that result from random irregularity of the vertical railway track profile. The statistical characteristics of these forces are investigated using a frequency domain approach. The overall objective of the study is to investigate the influence of the various railway vehicle and railway track parameters on the Power Spectral Density (PSD) functions of the contact forces. The type of information obtained could be utilised by both railway vehicle and railway track engineers in the design and maintenance of both systems.

Two different types of railway vehicles are considered, a locomotive vehicle and a passenger coach. The contact forces resulting from both vehicle models are included so that a comparison may ultimately be made between the calculated PSD functions for a relatively heavy (locomotive) and a relatively light railway (passenger coach) vehicle. The static load per axle varies greatly over the range of different types of railway vehicles and, in addition to the nominal vehicle weight, is dependent upon

the number of axles supporting the vehicle and the load conditions imposed on the vehicle at any particular time. Other parameters, such as suspension damping and stiffness values, vary from vehicle to vehicle and also change over time due to material wear. This natural variation can be a restriction in a specific theoretical analysis. However, analyses such as this one, where a range of parameter values are considered, are useful in investigating the effect of large parametric variation.

The analysis is undertaken using a frequency domain, or spectral, approach. The irregularity of the vertical track profile is assumed to be the single source of dynamic excitation to the moving railway vehicle system. A perfectly smooth track profile traversed by a perfectly round wheel gives rise to contact forces that approach the steady state case (Jenkins et al. 1974). Random irregularity of the vertical railway track profile gives rise to corresponding random fluctuations in the wheel-rail contact forces at each of the contact points between vehicle and track. These random profile irregularities are one of the essential dynamic vibration sources to both the vehicle and track systems (Lei & Noda 2002).

Frequency domain analysis can be a useful mathematical tool in situations such as this where the dynamic system input is Gaussian random in nature (Iyengar & Jaiswal 1995, Sun & Kennedy 2002). In general, the equivalent time domain analysis would be computationally more expensive because a series of random track profiles would be required. These profiles could be generated numerically from the appropriate track roughness PSD function before being applied as the dynamic input to a mathematical system model in a numerical time-stepping routine (Lei & Noda 2002). A corresponding series of time histories of the dynamic system response, and hence of the wheel-rail contact forces which are a subset of the global system response, could then be calculated. The Gaussian random nature of the track irregularity that is considered here allows us to present the results in a statistical framework. This can be achieved most succinctly in the frequency domain (Hartnett 2000*b*). While the time domain solution produces a series of individual time histories,

the frequency domain approach allows us to calculate important random process characteristics such as the variance of the contact forces and the probabilities of peak values exceeding arbitrary limits.

In addition to the fluctuating dynamic contact forces that are produced by a moving railway vehicle and underlying track structure there is also a constant static force present due to the gravitational force exerted by each of the vehicular components. This static load varies greatly depending upon the vehicle in question and its particular load conditions, ie. tare or fully laden. For the purpose of ease of analysis in the frequency domain it is a prerequisite that all spring and damper components of the system behave linearly. This requires a linearisation of any non-linear components of the physical vehicle and track model, and also of the wheel-rail contact relationship. It should be noted, however, that the linearised Hertzian spring constant is calculated based on an assumed constant axle load, ie. the static axle load. The resulting linearity of the dynamic vehicle system model allows the static load to be neglected during the analysis process. If required, the constant static components of the contact forces may be added to the calculated stochastic dynamic load attributes upon calculation of the random process properties. For example, a zero-mean process variance of x units is calculated and on completion of the analysis is added to the static load component, F_s . The result is a process with variance x but now distributed about a mean value F_s rather than zero.

Resultant contact force PSD functions are calculated for ranges of different values of the various model parameters including velocity and the degree of underlying vertical profile roughness. Prior to commencement of the parametric analysis, a set of default values is applied to each of the model variables. The values are chosen so that their value is representative of the mid-range of the range of parametric values. All subsequent analyses are carried out with respect to these initial default values.

In all, eight different parameters are varied. The initial parametric investigation examines the effect of varying the quality of the railway track profile. The various

quality levels applied are based on a series of empirical PSD functions derived by the FRA (Federal Railroad Administration of the United States) on the basis of extensive measurement of railways in that country (Frýba 1996) (see Section 3.2.2). The effect of varying the vehicle models' velocity, from 10ms^{-1} to 60ms^{-1} (36km/hr to 216km/hr), is subsequently examined. The influence of some of the various physical parameters of the vehicle model itself are then tested. The bogie and wheelset masses, and the suspension stiffness and damping constants, are each varied individually and the effects of these variations upon the resulting contact force PSD functions are observed. The final parametric variation considered is that of the track foundation stiffness and damping parameters.

3.2 System Model

3.2.1 Vehicle Model

The railway vehicle and track models that are formulated for the purpose of this study are illustrated in Figure 3.1. The vehicle model is a simplified representation of a single bogie and wheelset in isolation from a carriage or an engine vehicle. The two degree-of-freedom vehicle model is planar and is simplified such that its degrees of freedom are exclusively translational in the vertical direction, ie. bogie pitching, a real effect that also occurs in the vertical plane, is not considered. In the study of automotive vehicle dynamics, similar vehicle models are often referred to as quarter-vehicle models (Sun & Kennedy 2002). This rigid body model is planar and, therefore, the three dimensional system masses of both the bogie and wheelset are discretised in the vertical plane. The stiffness and damping values of the suspension components from the two sides of a real railway vehicle are also discretised in a single plane. These suspension stiffness and damping parameters are denoted k_b and c_b while the bogie and wheelset masses are denoted m_b and m_w respectively. The linearised Hertzian spring stiffness is denoted k_h as is conventional in the literature.

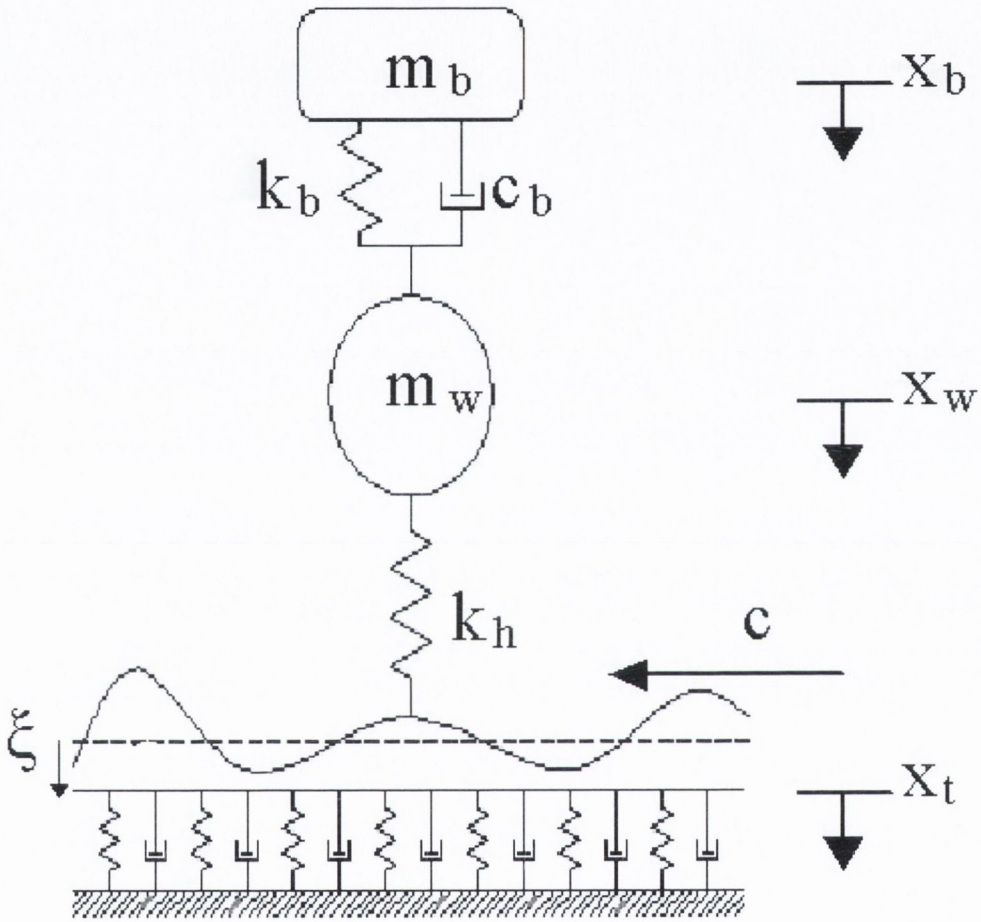


Fig. 3.1: Two degree of freedom bogie model on BEF track model with upper profile random irregularity

The bogie model is dynamically coupled to the track model via the linearised Hertzian wheel-rail contact mechanism (Esveld 1989). The Hertzian spring stiffness is dependent upon the relative wheel-rail displacement and has previously been described by Equation 2.12 in Section 2.3.3.

The railway track system is simplified as a planar beam on a continuous elastic foundation (BEF). The mathematical model is formulated using the standard Euler finite element (FE) beam model with distributed mass. This track model has continuously distributed uniform foundation stiffness, κ_t [Nm^{-2}], and damping, γ_t [Nsm^{-2}]. The beam has a constant Young's modulus E_t , second moment of area I_t , and mass per unit length μ_t . The beam model has an irregular upper surface representative of the vertical railway track irregularity. This profile irregularity function $\xi(t)$ deviates from a mean surface displacement that is assumed to be zero.

A physical railway vehicle would traverse the track at its running velocity c . However, for the purpose of this particular model, the irregular vertical surface profile, and not the vehicle itself, is modelled so that it moves at velocity c , relative to both the vehicle and beam models, at the vehicle-track interface. In doing so, the track profile provides a source of dynamic excitation to both systems. Under this modelling assumption the profile moves in a direction opposite to that of the originally assumed vehicle model motion.

The vertical motion of both the bogie, wheelset, and track are defined by the absolute coordinates x_b , x_w and x_t respectively. All coordinates are defined in the vertical direction with a 'downwards positive' convention adopted. The track surface irregularity is represented by the coordinate $\xi(t)$. An additional relative coordinate, z_w , is introduced to denote the relative displacement between the wheelset and the underlying track surface. This coordinate is convenient in that the wheel motion is now defined relative to the position of the surface of the beam model at the contact point. The wheel-rail contact force may be deduced directly from this relative displacement. Tensile contact spring forces are assumed positive throughout this

analysis. Equation 3.1 defines this relative coordinate.

$$z_w(t) = x_t(t) + \xi(t) - x_w(t) \quad (3.1)$$

It can now be seen, from the following Equation 3.2 that it is upon this relative displacement, and also relative velocity, that the wheel-rail contact force, $P(t)$, depends.

$$P(t) = k_h z_w(t) + c_{k_h} \dot{z}_w(t) \quad (3.2)$$

As this Hertzian contact spring is undamped (ie. $c_{k_h} = 0$) the relative velocity between wheel and rail, $\dot{z}_w(t)$ has no effect on the contact force.

3.2.2 Railway Track Model

Throughout this chapter the vertical railway track profile is assumed to possess different degrees of random irregularity that can be characterised by various PSD functions. This random irregularity, which has been measured and analysed by Iyengar & Jaiswal (1995), is Gaussian, stationary and ergodic in space time and, as such, a one-sided PSD function can correctly be used to describe the irregularity. Many different empirical spectra are available (Frýba 1996). These spectra have been devised by means of the statistical smoothing of measured track data. A result of this smoothing is that these PSD functions yield only averaged information on track quality. However, the smoothed functions remain useful for comparative studies such as this one.

The FRA have devised an empirical formula for random track irregularity based on extensive measurements of the American railway network (Frýba 1996). Six different classes of track have been defined by means of smoothed PSD functions. The classification is based upon the degree of the track irregularities. Class 6 is the profile with the least deviation from an average level while Class 1 is the roughest, ie.

greatest variance from the mean and hence the lowest quality. The one-sided FRA PSD functions for vertical track irregularity are given by the empirical formula,

$$G_{\xi\xi}(\Omega) = \frac{A\Omega_2^2(\Omega^2 + \Omega_1^2)}{\Omega^4(\Omega^2 + \Omega_2^2)} \quad (3.3)$$

where Ω is a parameter known as the route frequency and has units equivalent to m^{-1} . This frequency parameter is directly proportional to the circular frequency of the irregularity function with the vehicle velocity, c , being the constant of proportionality. A is a constant dependent on the track quality. The route frequency is used regularly as an alternative to time-based frequency units in moving vehicle analytical applications as it defines the random process in space rather than in time. This description enables the process PSD function to be represented independently of the vehicle velocity. Were the PSD function to be expressed as a function of circular frequency, a different PSD would be required for each different vehicle velocity considered. The relationship between circular and route frequency is given by,

$$\omega = c\Omega = \frac{2\pi c}{L} \quad (3.4)$$

where L is the irregularity wavelength (in metres). It is the constant A that defines the track class and this parameter ranges from 0.98×10^{-8} (Class 6) to 15.53×10^{-8} (Class 1). Ω_1 and Ω_2 are also constants and are equal to $23.3 \times 10^{-3}m^{-1}$ and $13.1 \times 10^{-2}m^{-1}$ respectively. These constants do not vary in the case of the vertical profile irregularity which is being considered here. For the purpose of this particular study this expression for the PSD function is defined between upper and lower route frequency limits of $0.01m^{-1}$ and $\pi/5m^{-1}$. Other studies in the literature have applied different frequency limits. Au et al. (2002), for example, used the same empirical FRA PSD function but applied an upper limit of $2\pi m^{-1}$. However, at the higher frequencies the magnitude of each of the FRA PSD function is negligible. This does not imply that random track irregularity does not possess high frequency characteristics. High frequency events do occur but their analysis is better suited

to the separate use of time-domain techniques due to the unpredictability of their occurrence.

The PSD function of the vertical track irregularities for Class 4 track is illustrated in Figure 3.2 on a log-log scale. It is this intermediate level track irregularity of Class 4 that is assumed as the default profile irregularity throughout this study.

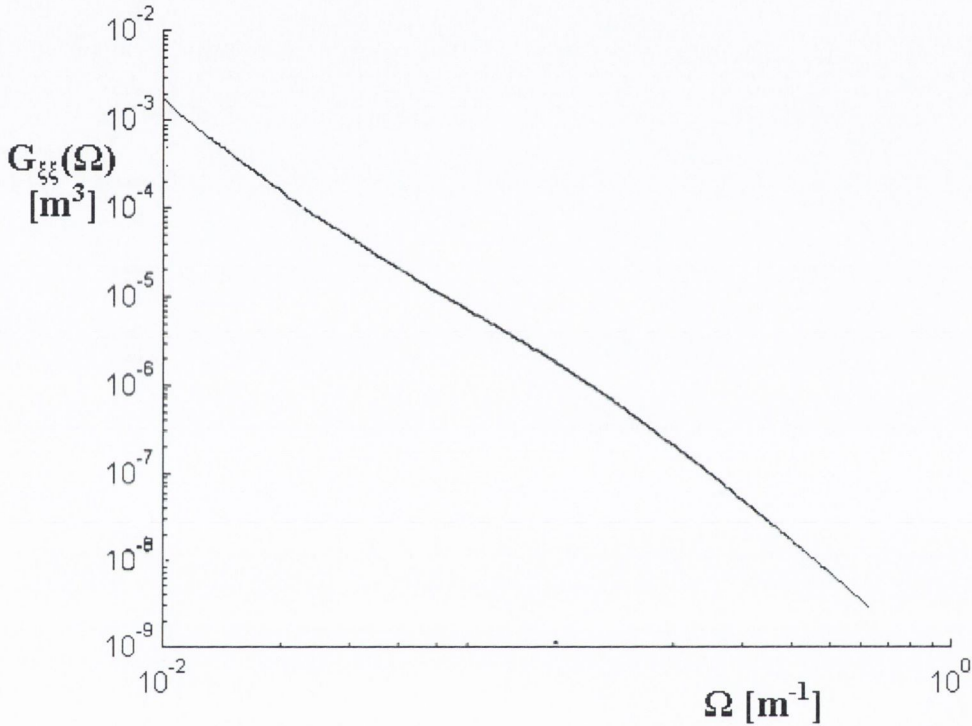


Fig. 3.2: PSD of random vertical track irregularities (FRA class 4)

The track irregularity PSD function is a very important quantity in the calculation of wheel-rail contact forces as it contains a large amount of information regarding the average track profile deviation from its mean. It should be noted once again, however, that this function does not represent discrete irregularities, such as a single dipped rail joint, or high frequency periodic roughness components such as corrugations, that may be present in the track profile. Only the response to a smoothed average of random irregularities from a population of track profiles is considered in this study.

One of the properties of a PSD function for a given process is that the mean square value (or variance) of the process is equal in magnitude to the integrated area beneath the PSD curve for that process. For example, the variance of the roughness about the mean for a Class 4 FRA PSD track roughness function is $7.35 \times 10^{-6} \text{m}^2$. A priori knowledge of the PSD function of the random input signal to the system, and of the dynamic system properties, allows for the PSD function (or functions, in the case of multiple output systems) of the resultant random vibration of the system to be calculated. Further mathematical techniques then allow the variance and other statistical properties of the random process to be determined (Iyengar & Jaiswal 1995). The calculation of some of these properties is detailed in Section 3.3.3 and Appendix A.

3.3 Mathematical Formulation

3.3.1 Frequency Response Functions

This study is focussed upon the calculation of the interactive wheel-rail contact force PSD functions. However, the method employed here also allows calculation of spectra for each of the bogie, wheelset and track displacements, velocities and accelerations. The initial step in the process of calculating the PSD function for the contact forces is to calculate the system frequency response functions (sometimes referred to as transfer functions). The derivation of the frequency response functions will be presented here under the assumption that the BEF track model is of infinite stiffness, ie. does not deform under loading. This assumption is applied so that the description of the mathematical formulation described here is more concise. The subsequent addition of a flexible beam modelling the track system to the mathematical model is trivial and was used to generate the results presented.

From Figure 3.1 it can be seen that the vehicle model motion is described in terms of the two translational coordinates $x_b(t)$ and $x_w(t)$. The track roughness is denoted

by $\xi(t)$. The new coordinate $z_w(t)$ is introduced at this point; this coordinate has been described previously before the previously explained assumption of zero beam deformation was applied (see Equation 3.1).

$$z_w(t) = \xi(t) - x_w(t) \quad (3.5)$$

This coordinate describes the relative displacement between the wheel and rail. Equation 3.5 is similar to Equation 3.1 but the beam deformation term is included in $\xi(t)$. The contact force is directly proportional to this relative displacement as a result of the linearisation of the Hertzian contact spring. The equation of motion of the vehicle model whose characteristics have been described previously (Section 3.2.1) is now given by:

$$\begin{aligned} \begin{bmatrix} m_b & 0 \\ 0 & m_w \end{bmatrix} \begin{Bmatrix} \ddot{x}_b(t) \\ \ddot{z}_w(t) \end{Bmatrix} + \begin{bmatrix} c_b & c_b \\ c_b & c_b + c_{kh} \end{bmatrix} \begin{Bmatrix} \dot{x}_b(t) \\ \dot{z}_w(t) \end{Bmatrix} + \begin{bmatrix} k_b & k_b \\ k_b & k_b + k_h \end{bmatrix} \begin{Bmatrix} x_b(t) \\ z_w(t) \end{Bmatrix} \\ = \begin{Bmatrix} c_b \dot{\xi}(t) + k_b \xi(t) \\ m_w \ddot{\xi}(t) + c_b \dot{\xi}(t) + k_b \xi(t) \end{Bmatrix} \quad (3.6) \end{aligned}$$

This system equation of motion can be manipulated to calculate the frequency response functions relating the absolute bogie displacement and relative wheel-rail displacement to the surface irregularity PSD function.

A Fourier transform (Newland 1993) is applied to both sides of Equation 3.6 to give Equation 3.7, which describes the system as a function of circular frequency (units rads^{-1}). This is in contrast to the original time domain Equation 3.6, which is expressed as a function of time, t . The transform of Equation 3.6 is relatively straightforward and is based on the mathematical property that the Fourier transform of the process $f(t)$, $\frac{d^n f(t)}{dt^n}$, is equal to $(i\omega)^n F(\omega)$ where $F(\omega)$ is the Fourier transform of $f(t)$.

$$\begin{aligned}
-\omega^2 \begin{bmatrix} m_b & 0 \\ 0 & m_w \end{bmatrix} \begin{Bmatrix} \hat{x}_b(\omega) \\ \hat{z}_w(\omega) \end{Bmatrix} + i\omega \begin{bmatrix} c_b & c_b \\ c_b & c_b + c_{kh} \end{bmatrix} \begin{Bmatrix} \hat{x}_b(\omega) \\ \hat{z}_w(\omega) \end{Bmatrix} \\
+ \begin{bmatrix} k_b & k_b \\ k_b & k_b + k_h \end{bmatrix} \begin{Bmatrix} \hat{x}_b(\omega) \\ \hat{z}_w(\omega) \end{Bmatrix} = \begin{Bmatrix} i\omega c_b + k_b \\ -\omega^2 m_w + i\omega c_b + k_b \end{Bmatrix} \hat{\xi}(\omega) \quad (3.7)
\end{aligned}$$

$\hat{x}_b(\omega)$, $\hat{z}_w(\omega)$ and $\hat{\xi}(\omega)$ denote the Fourier transforms of the translational processes $x_b(t)$, $z_w(t)$ and $\xi(t)$ respectively. The mass, damping and stiffness matrices are combined to give Equation 3.8.

$$\begin{aligned}
\begin{bmatrix} -\omega^2 m_b + i\omega c_b + k_b & i\omega c_b + k_b \\ i\omega c_b + k_b & -\omega^2 m_w + i\omega(c_b + c_{kh}) + (k_b + k_h) \end{bmatrix} \begin{Bmatrix} \hat{x}_b(\omega) \\ \hat{z}_w(\omega) \end{Bmatrix} \\
= \begin{Bmatrix} i\omega c_b + k_b \\ -\omega^2 m_w + i\omega c_b + k_b \end{Bmatrix} \hat{\xi}(\omega) \quad (3.8)
\end{aligned}$$

It is now possible to obtain the two system frequency response functions $H_{x_b}(\omega)$ and $H_{z_w}(\omega)$. These functions may be used to relate the vertical displacements of the bogie and wheelset to the roughness of the underlying track profile. The frequency response functions relate the two vehicle model displacements, ie. bogie and wheelset, to the profile irregularity and are equivalent to $\frac{\hat{x}_b}{\hat{\xi}}(\omega)$ and $\frac{\hat{z}_w}{\hat{\xi}}(\omega)$ respectively.

$$\begin{aligned}
\begin{Bmatrix} H_{x_b}(\omega) \\ H_{z_w}(\omega) \end{Bmatrix} = \begin{bmatrix} -\omega^2 m_b + i\omega c_b + k_b & i\omega c_b + k_b \\ i\omega c_b + k_b & -\omega^2 m_w + i\omega(c_b + c_{kh}) + (k_b + k_h) \end{bmatrix}^{-1} \\
\begin{Bmatrix} i\omega c_b + k_b \\ -\omega^2 m_w + i\omega c_b + k_b \end{Bmatrix} \quad (3.9)
\end{aligned}$$

Note again that $H_{z_w}(\omega)$ describes the relative, and not absolute, wheelset-track displacement. Both frequency response functions can now be evaluated over the

required frequency range, the extent of this range is dependent upon the input frequency characteristics.

3.3.2 Contact Force Power Spectral Density Function

The frequency response functions have now been formulated for displacements of the bogie model. These function describe the frequency domain response of the vehicle model masses to the random input to the model. Of particular interest to this study is the response function describing the relative wheelset-track displacement, $H_{z_w}(\omega)$. The contact force between the vehicle wheelset and the track is directly proportional to this relative displacement, and is quantified in the time domain by Equation 3.2.

The random track irregularity has been assumed to be a zero-mean process that is stationary and ergodic in space, an assumption validated by Iyengar & Jaiswal (1995) by means of an experimental study of Indian railway lines. All components of the vehicle system model possess linear force-displacement properties; therefore the system response is also stationary and ergodic with zero mean. The mean contact force is given by calculating the expectation of both sides of Equation 3.2.

$$m_{p(t)} = E[P(t)] = k_h E[z_w(t)] + c_{k_h} E[\dot{z}_w(t)] = 0 \quad (3.10)$$

The damping of the Hertzian contact spring is negligible and assumed to be zero; the velocity-proportional component of the righthand side of equation 3.10 is hence zero.

The autocorrelation contact force, referring to the definition of the autocorrelation function (Newland 1993), is given by

$$R_P(\tau) = E[P(t)P(t + \tau)] = k_h^2 R_{z_w}(\tau) \quad (3.11)$$

The Fourier transform of the autocorrelation function of a random process is, by definition (Newland 1993), the PSD function of the process. Applying the Fourier

transform to Equation 3.11, an expression for the PSD of the contact force process is obtained.

$$S_P(\omega) = k_h^2 S_{z_w}(\omega) \quad (3.12)$$

From stochastic process theory

$$S_{z_w}(\omega) = |H_{z_w}(\omega)|^2 S_\xi(\omega) \quad (3.13)$$

Combining the two previous equations an expression for the PSD function of the stochastic contact forces is obtained. This expression allows calculation of the PSD function for the contact force process over the range of frequencies for which the PSD function of the track roughness spectrum is defined.

$$S_P(\omega) = k_h^2 |H_{z_w}(\omega)|^2 S_{\xi\xi}(\omega) \quad (3.14)$$

3.3.3 Random Process Statistics

From statistical physics, it is known that the integral of the PSD function for a particular stationary random process is equal to the mean square value, or the variance, of that process (Yang 1986). For this reason the PSD function is sometimes referred to as the *Mean-Square Spectral Density* function. Therefore, the variance, σ_1^2 , of the stationary process $P(t)$, $E[P(t)^2]$, is expressed mathematically as

$$E[P(t)^2] = \sigma_1^2 = \int_0^\infty S_P(\Omega) d\Omega \quad (3.15)$$

As the FRA PSD functions of the vertical profile irregularities are defined over a finite range, it is possible to numerically integrate the output PSD function representing the contact force process over this range to obtain the variance of the process.

Classical level-crossing and peak-statistics theory (Nigam 1983) can now be exploited to relate the variance to the highest peak value (Iyengar & Jaiswal 1995). Before proceeding it is necessary to calculate the variance of the first and second derivatives, σ_2^2 and σ_4^2 , of the contact force process $P(t)$. These are given by the following equations as functions of the route frequency Ω .

$$\sigma_2^2 = \int_0^{\infty} \Omega^2 S_P(\Omega) d\Omega \quad (3.16)$$

$$\sigma_4^2 = \int_0^{\infty} \Omega^4 S_P(\Omega) d\Omega \quad (3.17)$$

The average number of zero crossings, N_0 , and process peaks, N_P , per unit distance travelled are functions of the process variances and are respectively given by

$$N_0 = \frac{\sigma_2}{\sigma_1} \quad (3.18)$$

$$N_P = \frac{\sigma_4}{\sigma_2} \quad (3.19)$$

Finally, the probability of a peak being greater than a level a_p where $\alpha = (a_p/\sigma_1)$ at any point is

$$P(\alpha) = 0.5\{1 - \text{erf}[\alpha/\sqrt{(2\beta)}]\} + 0.5(1 - \beta^2)^{0.5} \exp(-0.5\alpha^2) \{1 + \text{erf}[\alpha(1 - \beta^2)^{0.5}/(\sqrt{(2\beta)})]\} \quad (3.20)$$

where β is a bandwidth parameter defined by

$$\beta = [1 - \sigma_2^4(\sigma_1^2/\sigma_4^2)]^{0.5} \quad (3.21)$$

The peak level probability estimate is a particularly valuable tool in quantifying the effect of the fluctuating dynamic contact forces on the track structure. This

estimate allows for estimation of the probability of the wheel-rail force exceeding an arbitrary maximum value over a predefined distance of travel.

3.4 Parametric Study

3.4.1 Default System Parameters

Prior to proceeding with the parametric analysis a set of default values are assigned to the properties of both the vehicle and track models. The default vehicle properties are based upon the locomotive vehicle and passenger coach that were modelled by Xu, Zhang & Xia (2004) in a study of the dynamic effects of cross winds on a coupled vehicle-bridge system. These particular parameter values are chosen as their values are close to the average parameter values for a range of locomotive vehicles. Different studies do, however, apply different values to the vehicle parameters. For this reason, throughout the parametric study, the respective parametric values are varied both above and below their default values. The Rail Technology Unit of Manchester Metropolitan University have attempted to address the problem of parametric variation in simulations by publishing standard 'benchmark' values for railway vehicle and track parameters (Iwnicki 1998).

A railway track with Class 4 irregularity is assumed as the default track profile, along with default velocity of 40ms^{-1} (144kmhr^{-1} or 90mph), as outlined in Section 3.2.2. The default parameter values for both the locomotive and passenger coach models are given in Table 3.1. All suspension parameters have linear force-displacement characteristics. Modelling railway vehicle suspension systems is difficult due to their complexity and non-linearity. However, the spring and damper elements used to model the vehicle suspension may be linearised over certain ranges of suspension travel (Garg & Dukkipati 1984). Throughout the reviewed literature the suspension elements of railway vehicles are linearised as such (Dukkipati & Dong 1999, Lou 2005, Xu et al. 2004, Yoshimura, Nakaminami, Kurimoto &

Hino 1999). The parametric values for the BEF track model are based on values provided by Esveld (2001) specifically for the purpose of a BEF railway track model. These values are given in Table 3.2.

Parameter	Symbol	Unit	Locomotive	Passenger Coach
Bogie mass	m_b	kg	15,000	3,000
Wheelset mass	m_w	kg	2,700	1,700
Suspension stiffness	k_b	Nm^{-1}	3.0×10^7	1.5×10^7
Suspension damping	c_b	Nsm^{-1}	2.0×10^3	2.0×10^3

Table 3.1: Locomotive and passenger coach default parameters

Parameter	Symbol	Unit	Value
Mass per unit length	μ_t	kgm^{-1}	119
Young's Modulus	E_t	Nm^{-2}	2.07×10^9
Second Moment of Area	I_t	m^4	2.174×10^{-5}
Foundation Stiffness	κ_t	Nm^{-2}	4.0×10^7
Foundation Damping	γ_t	Nsm^{-2}	1.2×10^5

Table 3.2: BEF default model parameters

The linearised Hertzian spring constant is assigned a value of $1.96 \times 10^9 \text{Nm}^{-1}$ for the locomotive and $1.72 \times 10^9 \text{Nm}^{-1}$ for the passenger coach. These values are calculated by considering the static force, F_s , at each wheelset and applying the following approximation for the linearised Hertzian spring stiffness.

$$k_h = \frac{dF}{dy} = \frac{3}{2} c_h^{\frac{2}{3}} F^{\frac{1}{3}} \quad (3.22)$$

The value of c_h , the non-linear Hertzian spring constant is assumed throughout to be $1.0 \times 10^{11} \text{Nm}^{-3/2}$ (Sun & Dhanasekar 2002). These calculations of the linearised Hertzian spring stiffness are carried out under the assumption of static axle loads

of 22.8kN and 15.3kN for the locomotive and passenger vehicle respectively (Xu et al. 2004).

The variations in the parametric values that are considered throughout the study are given in Table 3.3. In general, the parametric changes are applied in equal increments. However, both the vehicle suspension and track stiffness and damping increments are scaled by an order of magnitude.

Frequency response functions were initially calculated for the vertical displacement of both the bogie and wheelset at the default parameter values. The absolute values of these respective frequency response functions, $|H_{x_b}(\omega)|$ and $|H_{z_w}(\omega)|$, for the bogie and wheel masses are illustrated on a log scale in Figure 3.3. These frequency response functions will subsequently be used to relate the stochastic contact forces to the underlying track profile irregularity.

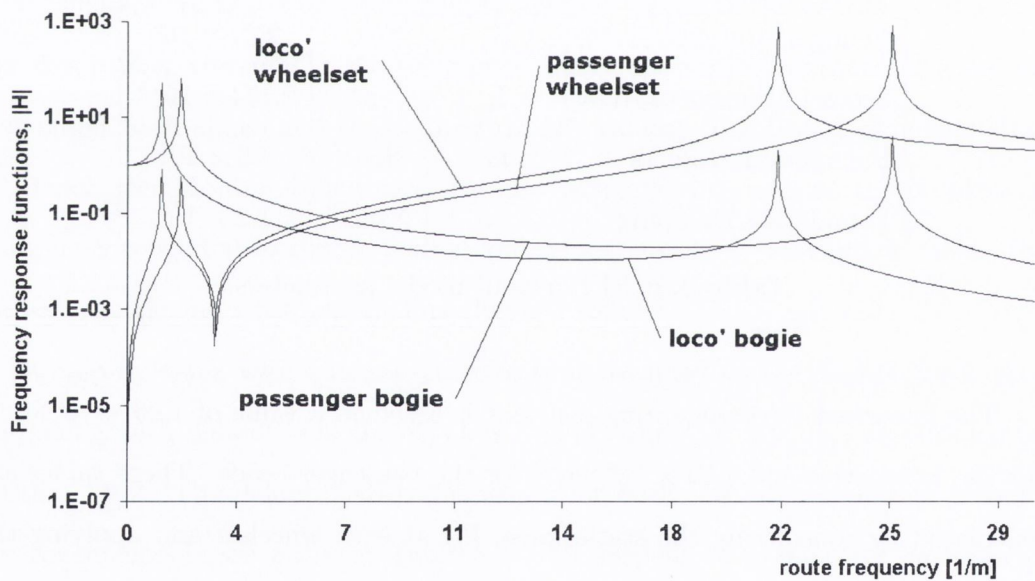


Fig. 3.3: Frequency response functions for vehicle model vertical displacements with default parameters

The frequency response functions show peaks at frequencies equal to the two natural frequencies of vibration of the vehicle model. The high frequency peaks

Parameter	Unit	Range	Increment
Track class	n/a	1 – 6	n/a
Vehicle velocity	ms ⁻¹	10 – 60	10
Locomotive			
Bogie mass	kg	10,000 – 20,000	2,500
Wheelset mass	kg	1,700 – 3,700	500
Suspension stiffness	Nm ⁻¹	3.0×10^5 – 3.0×10^9	$\times 10$
Suspension damping	Nsm ⁻¹	2.0×10^1 – 2.0×10^5	$\times 10$
Passenger Coach			
Bogie mass	kg	2,000 – 4,000	500
Wheelset mass	kg	1,200 – 2,200	250
Suspension stiffness	Nm ⁻¹	1.5×10^5 – 1.5×10^9	$\times 10$
Suspension damping	Nsm ⁻¹	2.0×10^1 – 2.0×10^5	$\times 10$
Track System			
Foundation stiffness	Nm ⁻²	4.0×10^5 – 4.0×10^9	$\times 10$
Foundation damping	Nsm ⁻²	1.2×10^3 – 1.2×10^7	$\times 10$

Table 3.3: Individual vehicle and track parameter ranges

occur at approximately 850Hz and 1005Hz, which correspond to the frequency of wheelset vibration upon the Hertzian spring. The large Hertzian spring stiffness results in the high frequency characteristic of this peak. The lower frequency peaks, at approximately 45Hz and 71Hz, are due to the bogie masses vibrating upon the suspension spring between the wheelset and bogie. It should be noted that these functions are illustrated here over a frequency range that greatly exceeds the range of the FRA roughness PSD functions. Even the location of the relatively low frequency bogie peaks is, at the default parameter values, above the upper limit of the smoothed FRA PSD irregularity function.

The frequency response functions give valuable visual information regarding the critical frequencies of vibration of the vehicle system. These functions display a similar shape for the locomotive and passenger vehicles. However, the function peaks occur at different frequencies due to the different physical vehicle parameters. For example, the initial peaks occur at lower frequency values for the locomotive vehicle than for the passenger vehicle model. This is due to the ratio of the bogie mass to the suspension spring being lower for the locomotive than for the passenger vehicle.

3.4.2 Parametric Variation

The results of the previously described mathematical calculations are presented in this section. The section comprises an overview of the effect of the parametric variation on the contact force PSD functions for both the locomotive and passenger vehicle models. The variation of each vehicle and track parameter is presented in turn. The individual contact force process PSD functions are illustrated graphically, compared and commented upon briefly. The parametric values are varied both above and below their default values so that the effects of both parametric value increase and decrease may be observed.

Track quality variation

The initial part of the parametric study focusses upon variation of the track profile PSD function between Classes 1 and 6. The resulting PSD functions for the wheel-rail contact forces are illustrated in Figure 3.4. One of the initial observations that is drawn, bearing in mind that the variance of the contact force process is equivalent to the integrated area under the PSD curve, is that the contact force variation about its mean value is clearly greater for the locomotive model than for the lighter passenger vehicle model. This characteristic can also be gleaned from the respective frequency response functions where the locomotive curve is more concentrated towards zero frequency. The input PSD function is also concentrated at low frequencies and this coincidence of higher function magnitudes results in higher contact force PSD magnitude for the locomotive model. This effect will be observed throughout each of the parametric variations. Additionally, this greater variation in the locomotive model contact forces is supplementary to a larger pre-imposed static axle load.

The Class 1 track, which is of the lowest quality, is seen, as one would intuitively expect, to generate higher contact force variances. The contact force PSD function variation between track classes is significant. For both models the contact force mean-square value is approximately sixteen times greater over Class 1 track than over Class 6 track. At 40ms^{-1} , the default velocity at which all of these particular tests were carried out, the frequency response peak corresponding to the bogie bouncing frequency occurs outside the FRA PSD function frequency band. The result is that no large peaks are observed in the resulting series of contact force PSD functions.

The cause of the increasing mean-square force with decreasing track quality is elementary. The frequency response function is constant throughout; it is the increasing value of the constant A (see Equation 3.3) that gives rise to the difference in mean-square contact force with track quality. The class 1 track results in a higher energy input to the bogie model. This energy is dissipated by the spring and

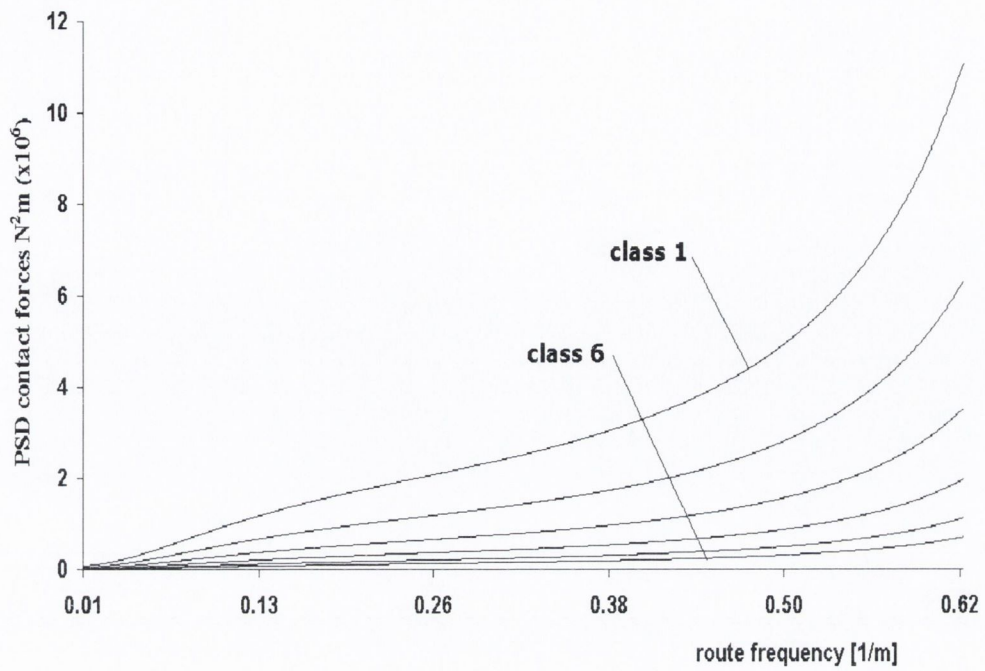
damper elements of the bogie suspension and the Hertzian contact spring through the vertical motions of both the bogie and wheelset masses. Greater energy input results in greater process energy in the contact force process and also in the bouncing motion of the wheelset.

Vehicle velocity variation

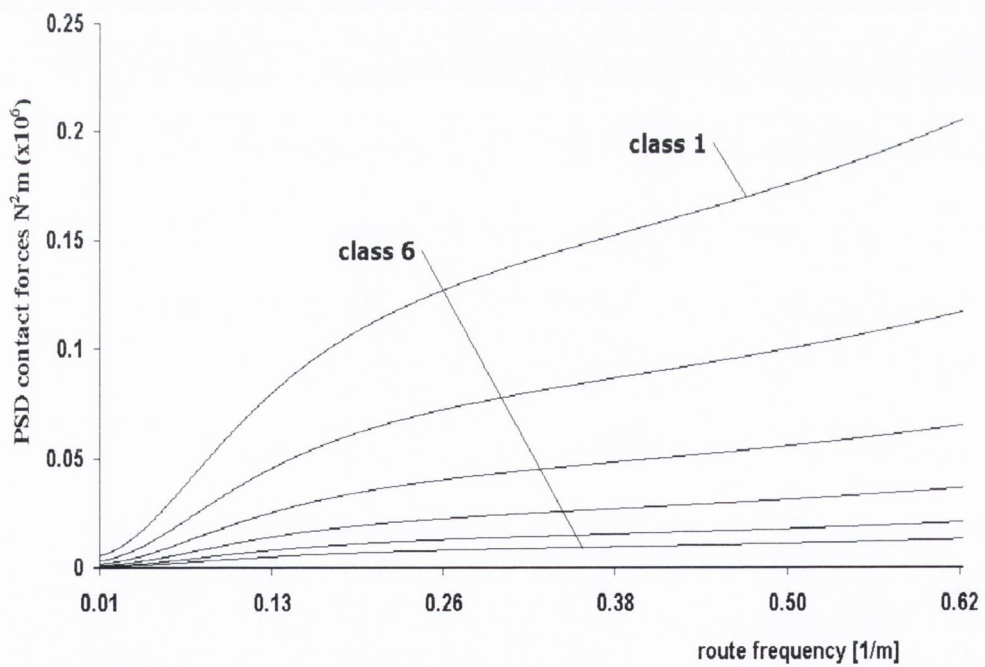
The vehicle velocity, c , is varied between 10ms^{-1} and 60ms^{-1} at 10ms^{-1} increments, for a constant track quality of Class 4 (the chosen default value). The resulting wheel-rail contact force PSD functions are illustrated in Figure 3.5.

The contact force variance increases with velocity. At 10ms^{-1} the contact force variance is close to negligible for the passenger vehicle and is also quite small for the locomotive model. Unlike the previous parametric variation of the track quality, the position of the PSD function peak at the bogie resonant route frequency is seen to change at different velocities. This occurs due to the fact that the route frequency is proportional to circular frequency, the constant of proportionality being the inverse of the vehicle velocity (see Equation 3.4). For this reason, increasing velocity causes the frequency response function peak to move in the direction of zero route frequency, where the input track roughness PSD function is of greatest magnitude. This effect increases the variance of the contact force process with increasing velocity.

The effect is especially significant for the locomotive model where, at 60ms^{-1} , the bogie resonant peak is encompassed by the FRA PSD function limits. This results in a greatly increased mean square force at this particular velocity. The large variation in the PSD function curves necessitated the use of a log scale in the case of the locomotive PSD function. The passenger vehicle model did not require the use of a log scale due to the fact that the peak in the frequency response function for this model was not encompassed by the FRA limits for any of the velocities tested.

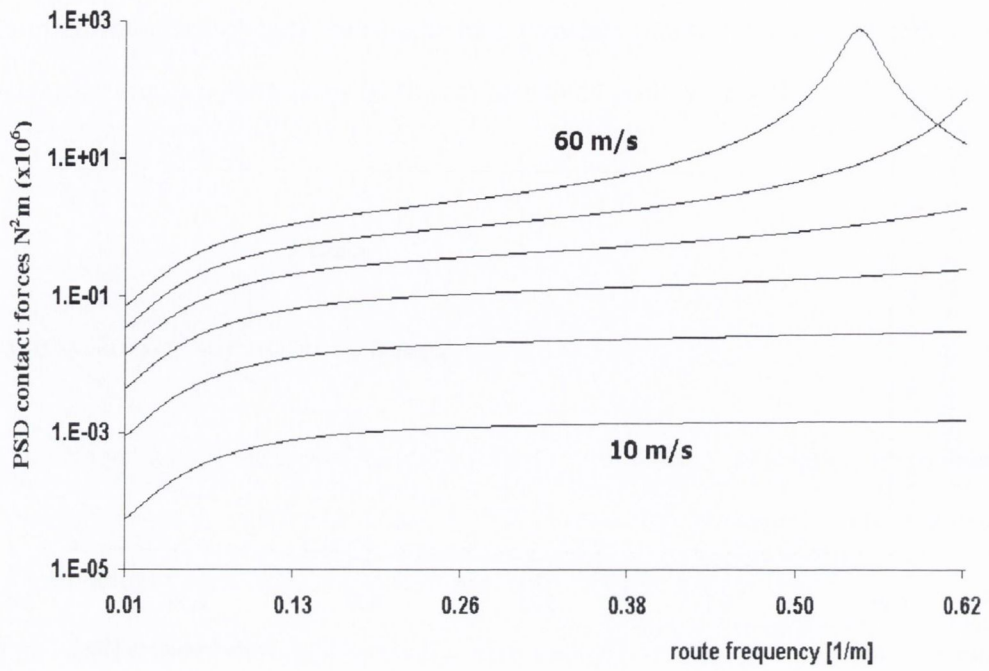


(a) Locomotive model

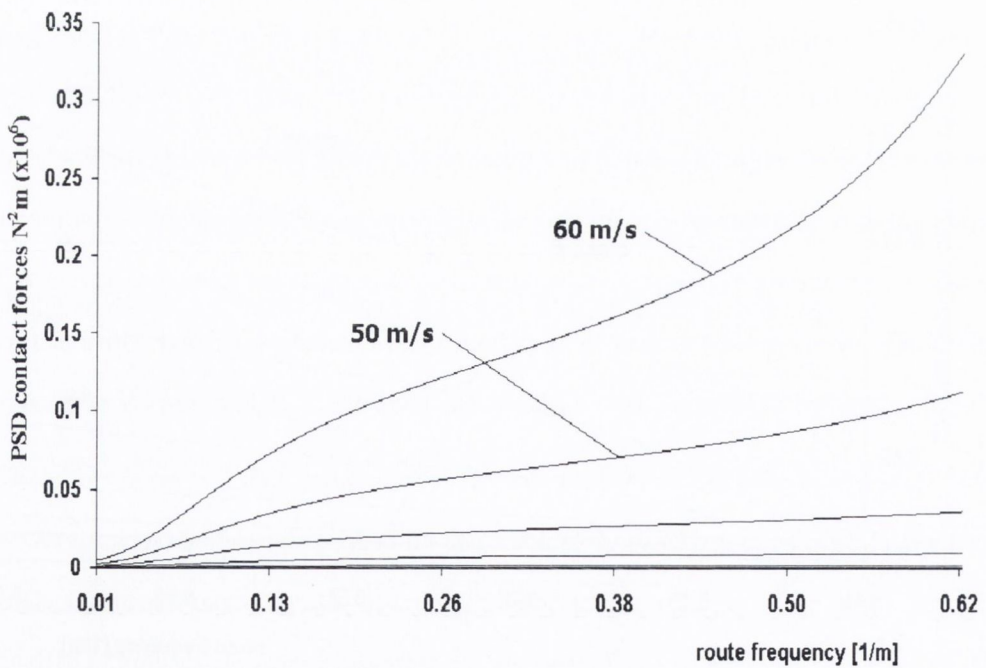


(b) Passenger vehicle model

Fig. 3.4: Contact force PSD variation with track class



(a) Locomotive model



(b) Passenger vehicle model

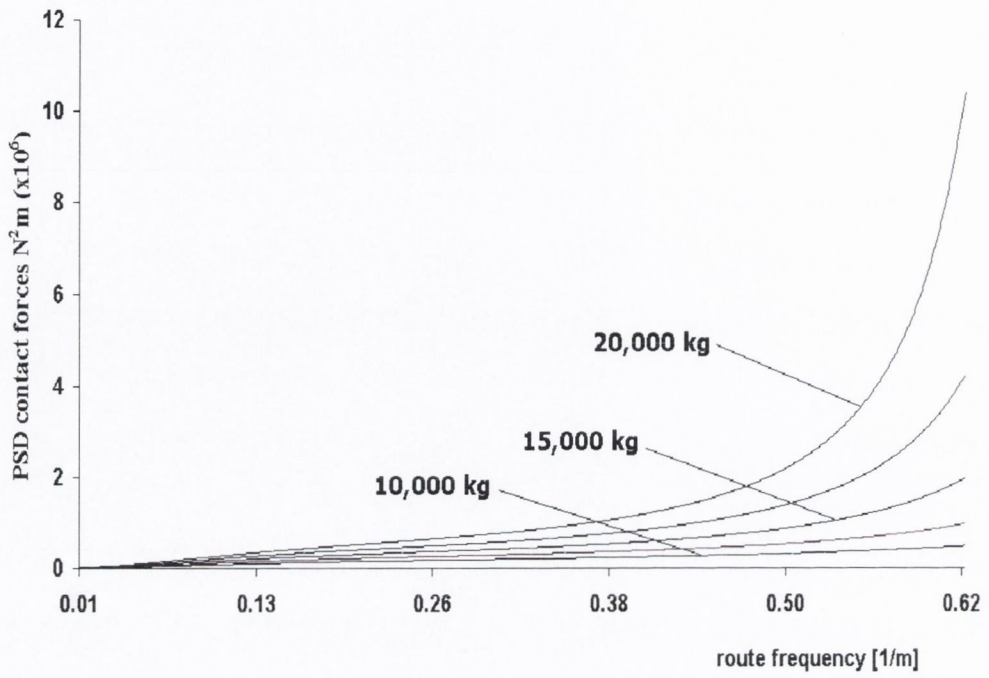
Fig. 3.5: Contact force PSD variation with velocity

Bogie mass variation

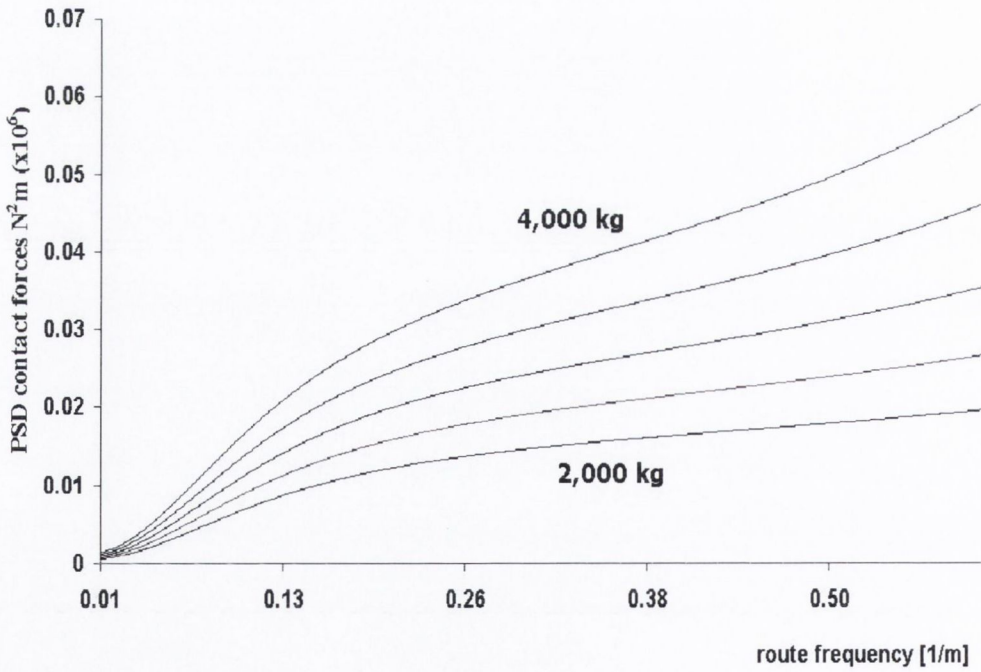
The first physical vehicle parameter variation is of the bogie mass, m_b , which is varied in two increments both above and below its default value. The magnitude of the increments used for the two vehicle models is not identical. Figure 3.6 illustrates the increase in contact force variance with bogie mass over the range of masses considered. As was the case for the track class variation, peak frequencies are not encompassed for any of the considered values. The peak contact force frequency response function value for varying bogie mass occurs at lower frequencies for greater masses. As before, decreasing the natural frequency increases the contact force process variance due to the low frequency dominance of the roughness PSD function. Though the frequency response function peaks remain outside the FRA PSD function limits the effect of the peak moving closer to the upper limit with increasing bogie mass is clear to see for both models.

Wheelset mass variation

The wheelset mass, m_w , is also varied about its default value. Figure 3.7 illustrates the small changes in the contact force variances over the range of values of m_w considered. This is due to the similarity of the respective frequency response functions over the range of the input track PSD function. The wheelset mass does not have a very significant effect on the frequency response function. The natural frequency of vibration of the wheelset mass, which is dependent upon the wheelset mass value, occurs at high values of route frequency. The roughness PSD magnitude is assumed to be zero at frequencies of these magnitudes. At the lower frequencies over which the FRA PSD functions are defined, the wheel-rail displacement frequency response function magnitude is not affected to a large extent by different wheelset masses. This results in similar contact force variances for all wheelset masses considered.

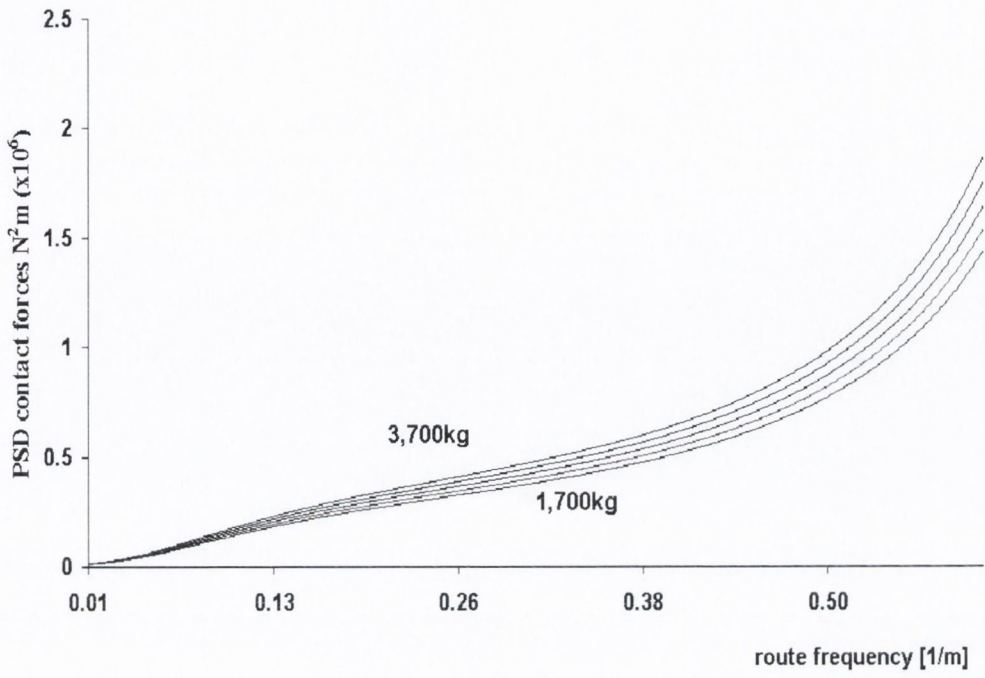


(a) Locomotive model

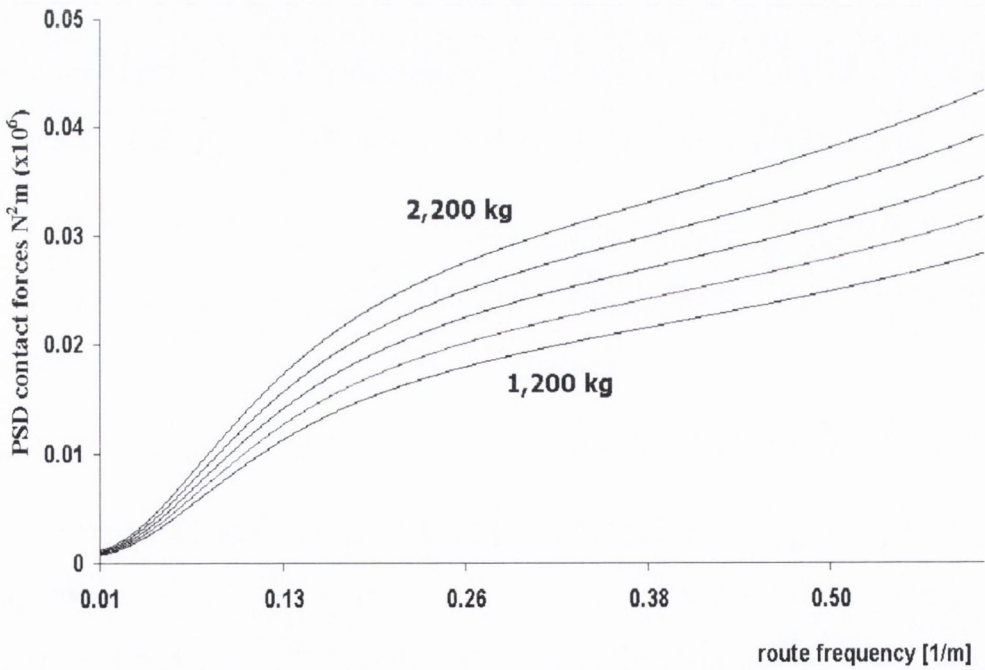


(b) Passenger vehicle model

Fig. 3.6: Contact force PSD variation with bogie mass



(a) Locomotive model



(b) Passenger vehicle model

Fig. 3.7: Contact force PSD variation with wheelset mass

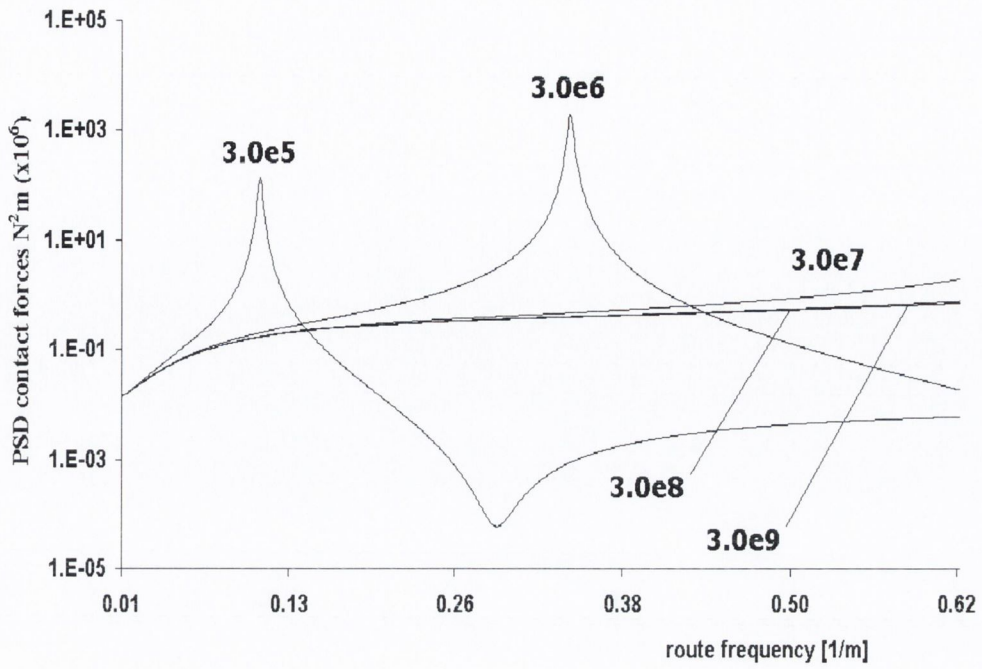
Suspension stiffness variation

A wide range of suspension stiffness values are considered. In addition, the increments are applied using a 'times ten' scaling factor in contrast to the previous variations where increments of equal magnitude were added. The variations in the suspension stiffness considered give rise to dramatic differences in the contact force PSD functions. Figure 3.8 illustrates the effect of these variations.

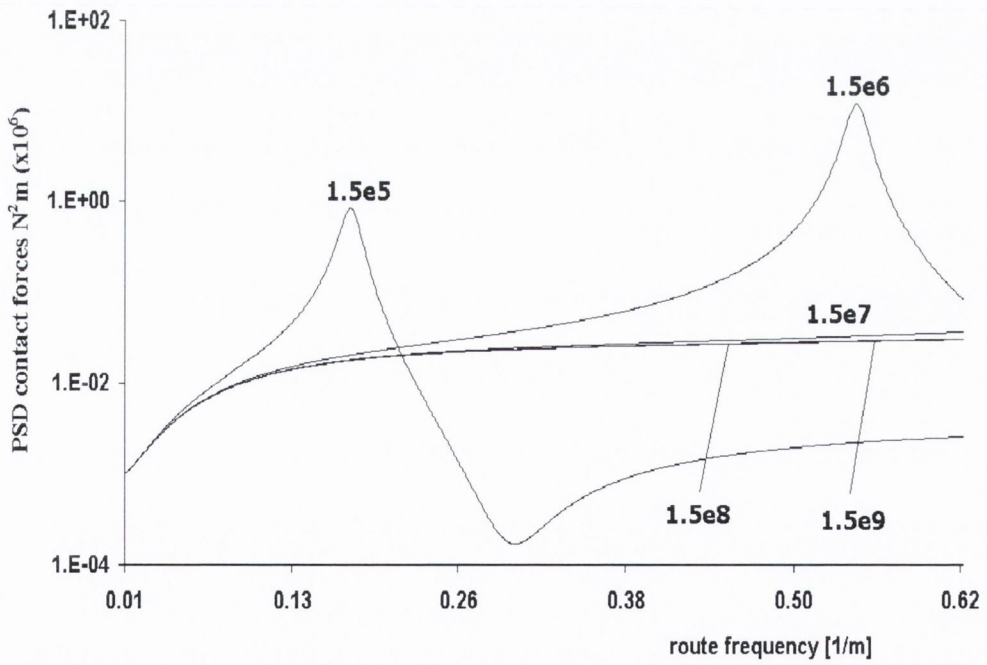
The two smaller values of spring stiffness considered, for both the locomotive and the passenger vehicle models, give rise to frequency response function peaks that occur within the input PSD range. Large contact force PSD function peaks result in these cases, with greater variance for the larger of these spring stiffness values. As the suspension stiffness value is increased above these two lower values the PSD functions tend to converge as the natural bogie frequency is pushed outside the range of the FRA PSD. The change in the position of bogie mass resonant frequency is more dramatic in this case than for the previous parameters considered, due to the larger differences between the stiffnesses considered. Once again, the low frequency content of the input frequency is coincident with only the two lower suspension stiffness frequency response peaks for the values tested. As a result, the contact force variances are higher for these two parametric values.

Suspension damping variation

The suspension damping is varied in a similar manner to the damping. However, the effect on the contact force PSD function of varying the vehicle suspension stiffness is found to be negligible. (see Figure 3.9). Increasing the suspension damping slightly decreases the variance of the contact forces over the range of damping values considered here. The four lower suspension damping values that were considered produced almost identical contact force PSD functions.

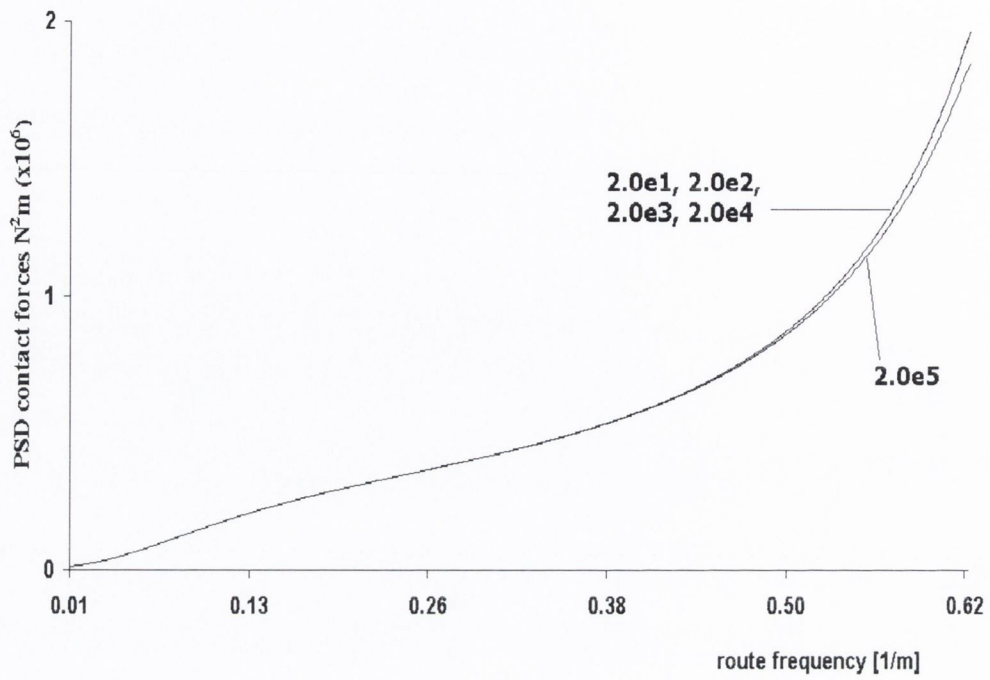


(a) Locomotive model

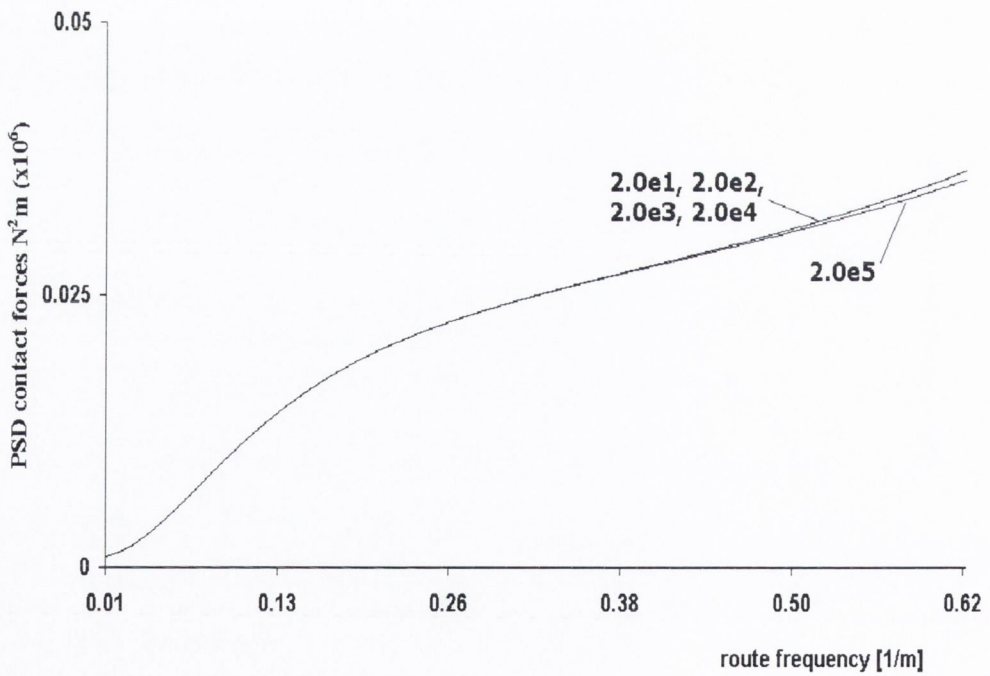


(b) Passenger vehicle model

Fig. 3.8: Contact force PSD variation with suspension stiffness



(a) Locomotive model



(b) Passenger vehicle model

Fig. 3.9: Contact force PSD variation with suspension damping

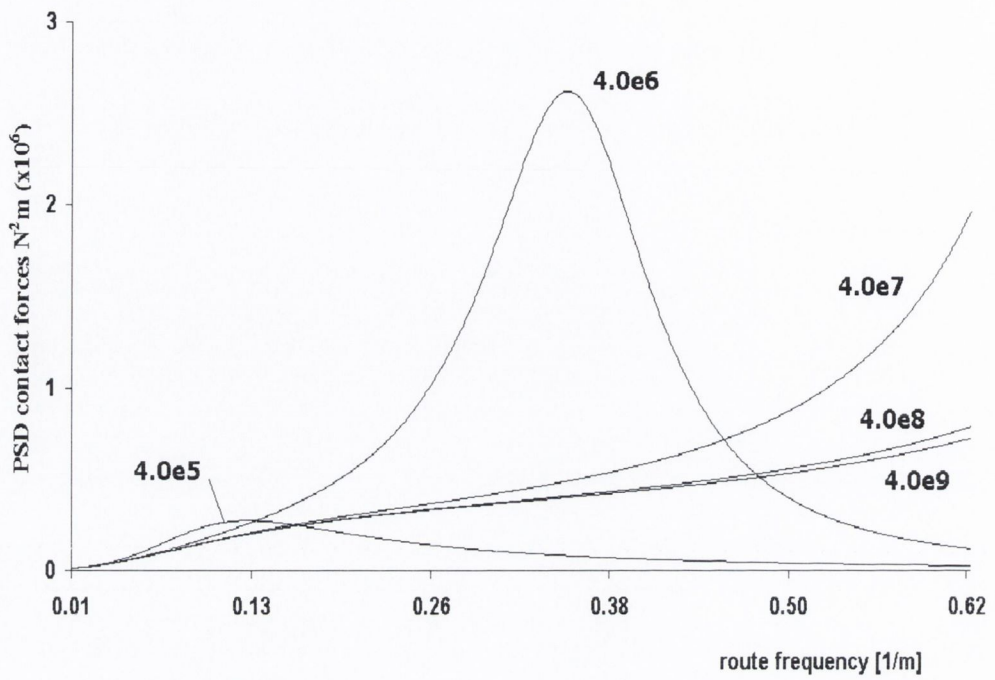
Track foundation stiffness

The PSD contact force functions for varying track foundation stiffness are illustrated in Figure 3.10. The track foundation stiffness value of $4.0 \times 10^6 \text{Nm}^{-2}$ is found to give rise to the greatest contact force variance for the locomotive model. The frequency response peak occurs outside the PSD limits for higher values of foundation stiffness and this results in almost constant variance for the three highest values tested. For the lowest foundation stiffness tested, $4.0 \times 10^5 \text{Nm}^{-2}$, the frequency response peak is within the PSD limits. However, the magnitude of the peak is very small in relation to the corresponding values for higher track foundation stiffness values.

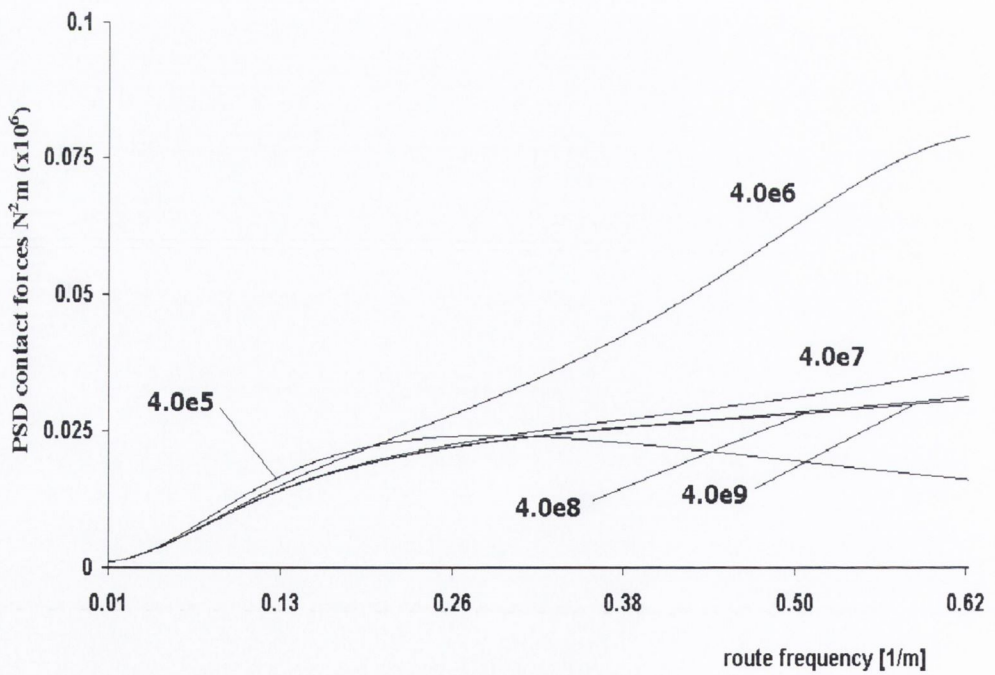
The PSD functions curves do not show such a dramatic effect for the passenger vehicle model. However, the same foundation stiffness as for the locomotive, $4.0 \times 10^6 \text{Nm}^{-2}$, is found once again to result in the highest contact force variance.

Track foundation damping

The PSD contact force functions for varying values of track foundation damping are illustrated in Figure 3.11. In general the effect of varying the damping within the range considered here is small. At the three lowest values the PSD functions are almost identical while, above these three values, the contact force variance decreases slightly with increasing track foundation damping.

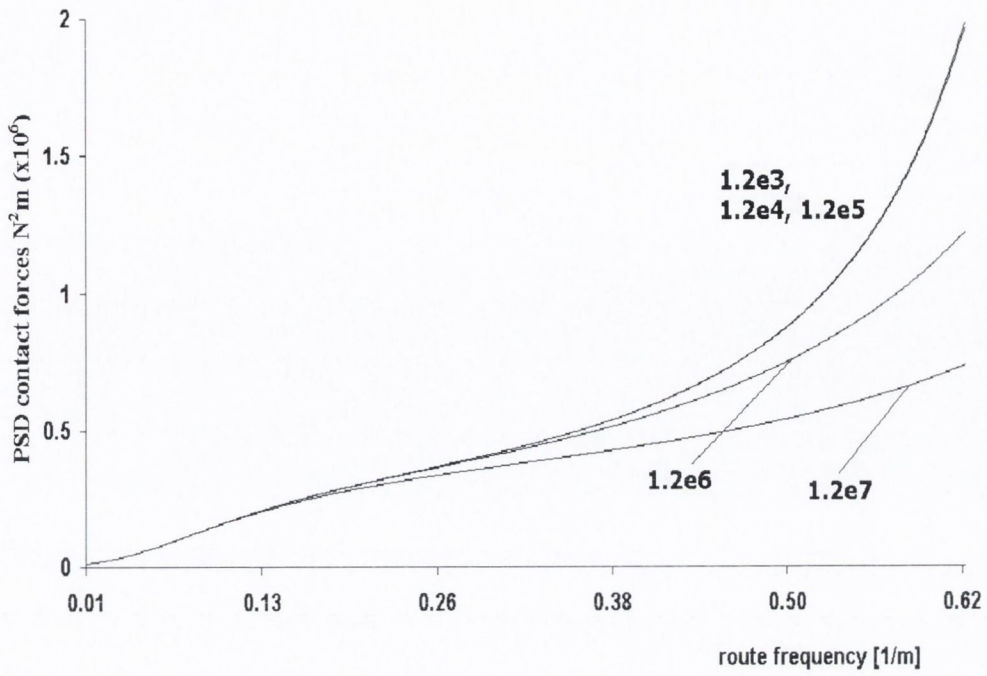


(a) Locomotive model

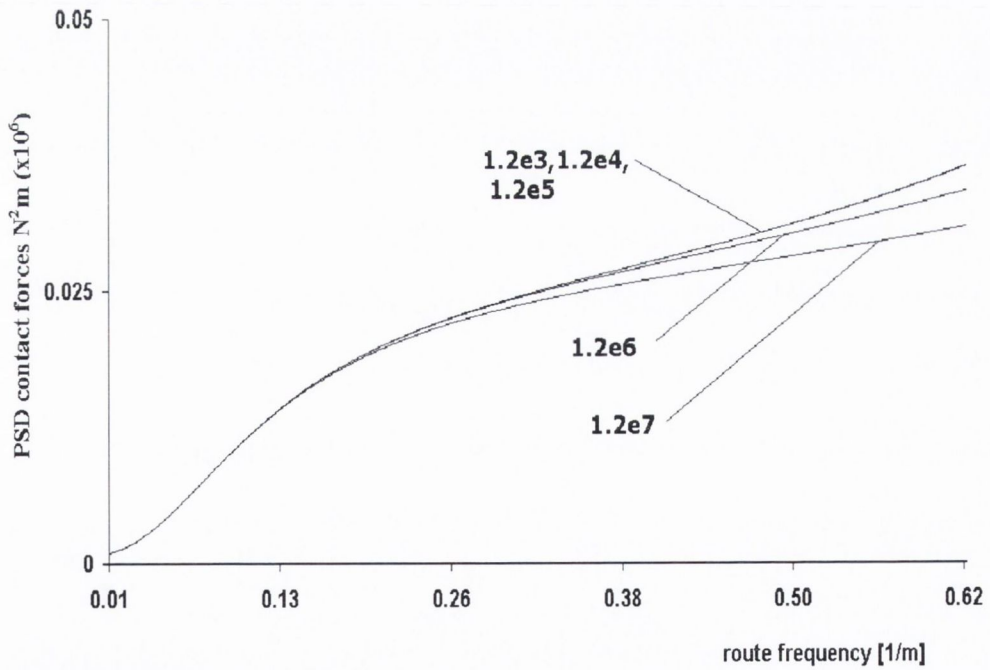


(b) Passenger vehicle model

Fig. 3.10: Contact force PSD variation with track foundation stiffness



(a) Locomotive model



(b) Passenger vehicle model

Fig. 3.11: Contact force PSD variation with track foundation damping

3.4.3 Contact Force Process RMS Variations

The mean value of the contact force process is the static axle load, about which the stochastic contact force processes vibrate randomly. The static axle load is greater for the locomotive model and, as been shown in the previous section, the contact force variance is also greater for this model. As a means of illustrating the physical results of this analysis, Figure 3.12 contains the random distribution of the contact force for both models under the default conditions. Both are distributed normally about the static axle load. The assumed profile roughness input is Gaussian random and so the contact force distribution shows the characteristic, bell-shaped, normal distribution curve. The wider distribution of the contact forces for the locomotive model is in evidence whilst the passenger vehicle contact forces are more concentrated around the static load. Despite the greater contact force variance for the locomotive model it is the passenger vehicle axle which has the greater probability of unloading.

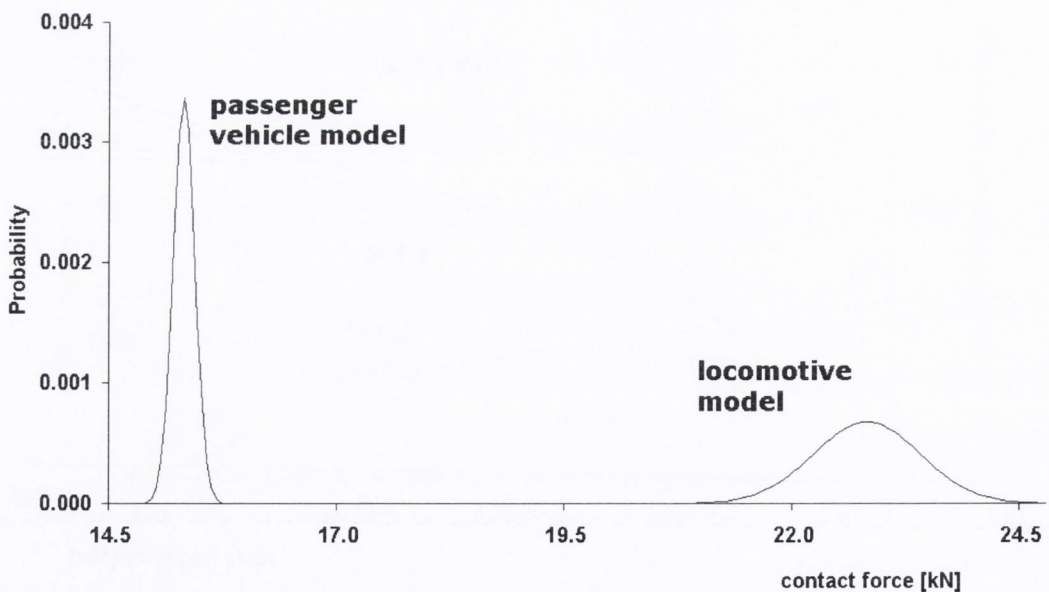


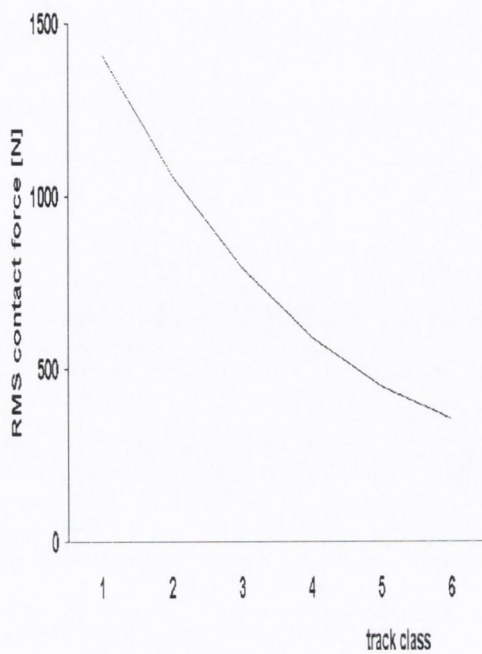
Fig. 3.12: Contact force probability density functions for vehicle models with default parametric values

The parametric variations in the root-mean-square (RMS) values for the contact force processes are illustrated in Figures 3.13 and 3.14 for the locomotive model and Figures 3.15 and 3.16 for the passenger vehicle model. While the PSD functions are useful in that critical frequency values and limits are easily observed, these RMS value plots give further information regarding the dependence of the variance of the contact force upon the particular parameter in question. The process RMS values are equivalent to the square root of the variance. The implications of these results are discussed in Section 3.5.1.

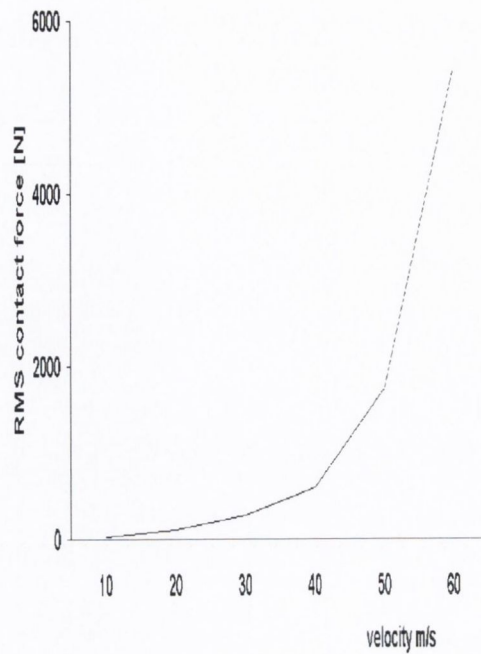
The purpose of the following two sections is to present a calculation of the probability of the wheel-rail contact force exceeding a particular, critical, value over a given distance of vehicle travel. The means by which the PSD functions for the contact forces, under the respective sets of parametric conditions, can be used to generate further statistical data regarding the contact forces is illustrated. The two individual sections are focussed upon the two individual bogie models for locomotive and passenger vehicles. The eight individual parametric values that have resulted in the highest contact force variances are considered.

3.4.4 Locomotive Peak Force Probabilities

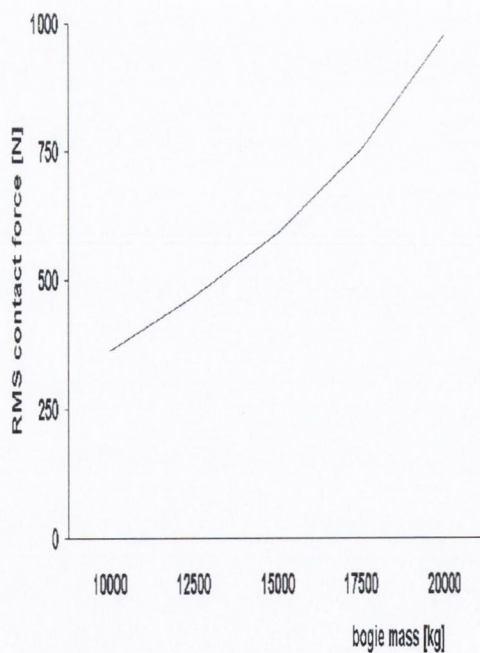
The static axle load for the locomotive vehicle specification is 22.8kN. The 'critical' force threshold that is considered here is selected as 120% of the static force, which is 27.36kN, while a vehicle running distance of 100m is chosen. The statistical method used is described in Appendix A and requires an initial solution of Equation 3.20. This technique facilitates the calculation of the probability that the j^{th} order peak among N_P peaks in a track length L will exceed a given level. The method is applied here whereby the respective probabilities that a single peak, ie. the first order peak, in the contact force process exceeds 27.36kN over a running distance of 100m, are calculated. It should also be noted that the probability of the contact force attaining a value of 80% of the static (18.24kN) is identical to the probability of occurrence



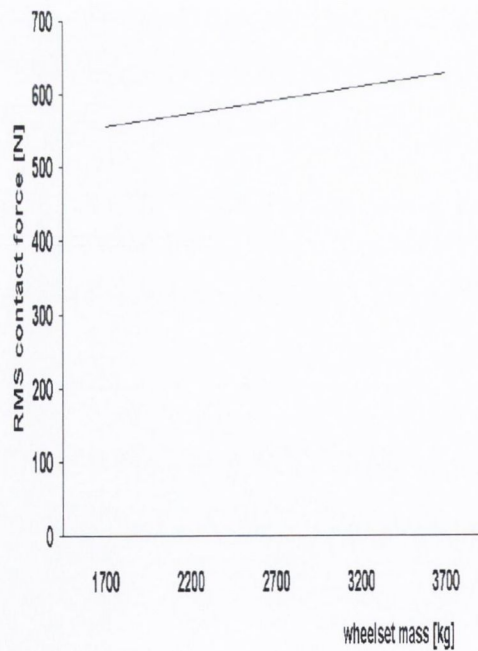
(a) Track class



(b) Velocity

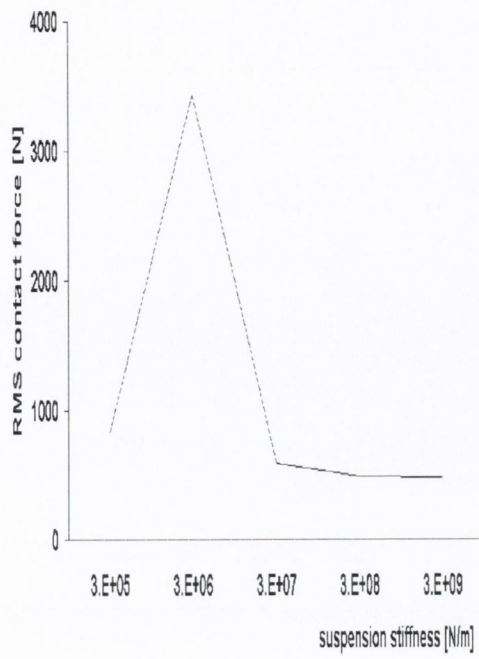


(c) Bogie mass

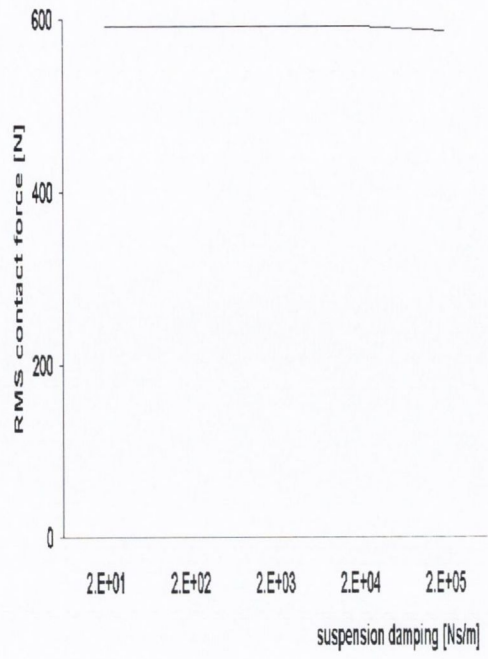


(d) Wheelset mass

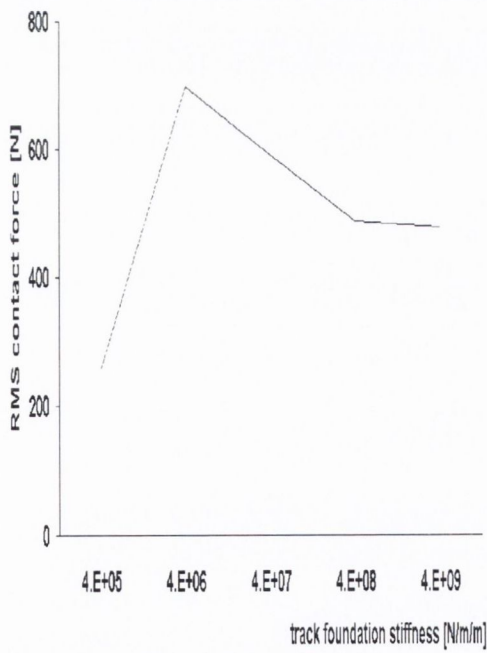
Fig. 3.13: Locomotive model contact force RMS parametric variations (A)



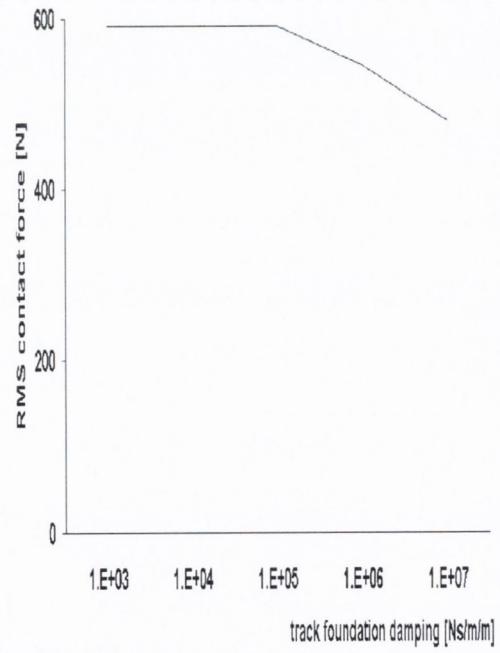
(a) Suspension stiffness



(b) Suspension damping

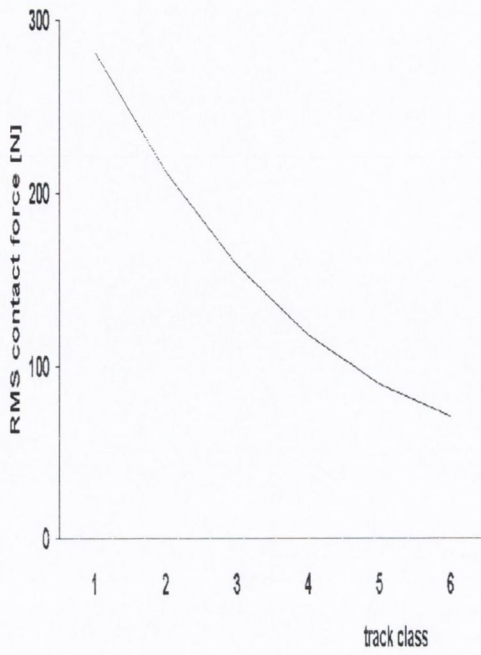


(c) Track foundation stiffness

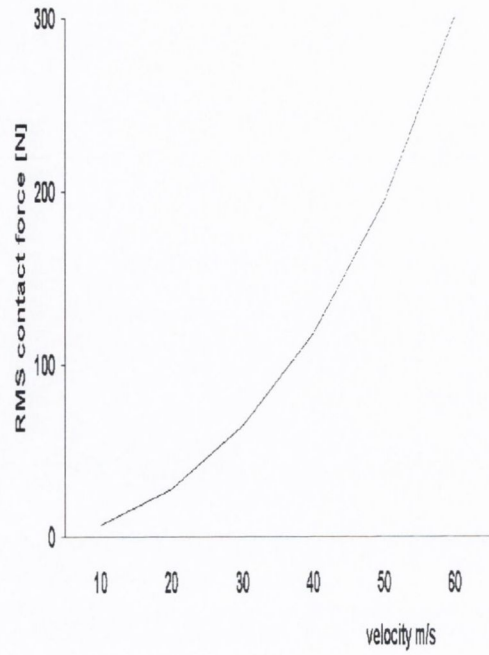


(d) Track foundation damping

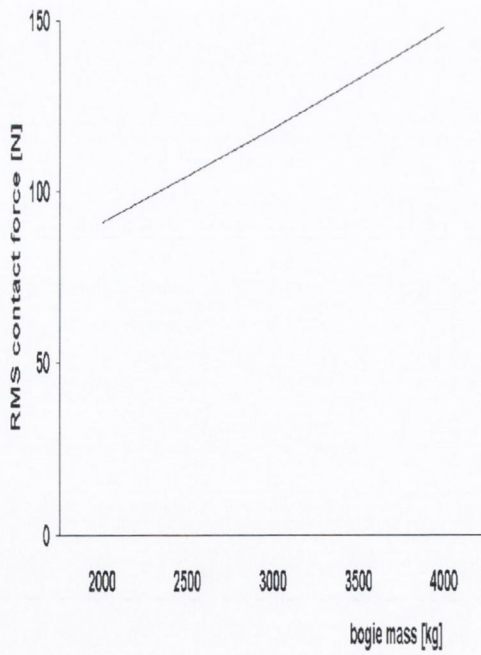
Fig. 3.14: Locomotive model contact force RMS parametric variations (B)



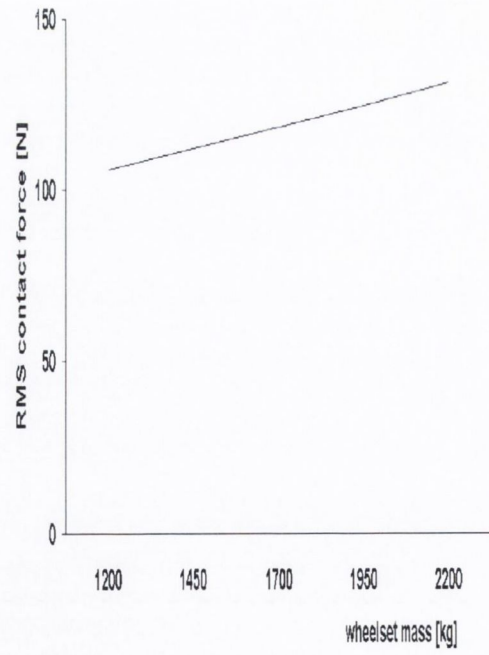
(a) Track class



(b) Velocity

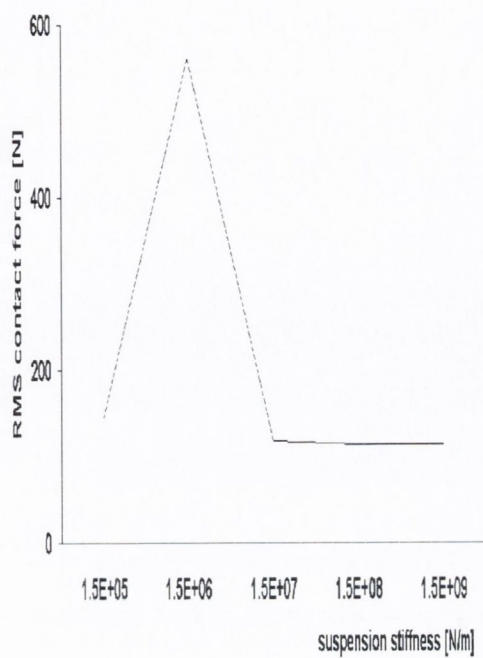


(c) Bogie mass

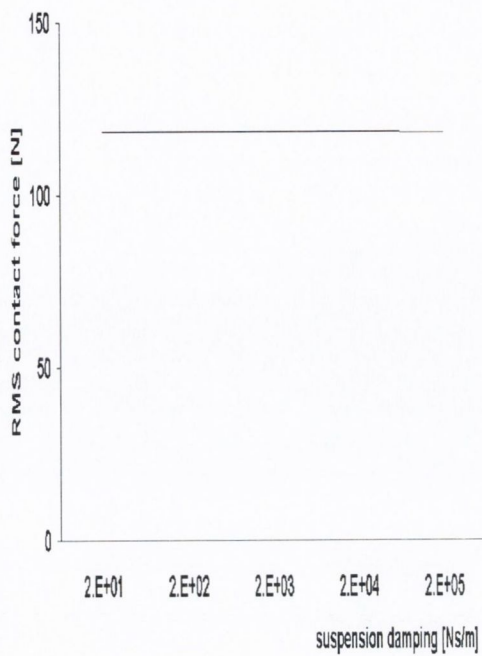


(d) Wheelset mass

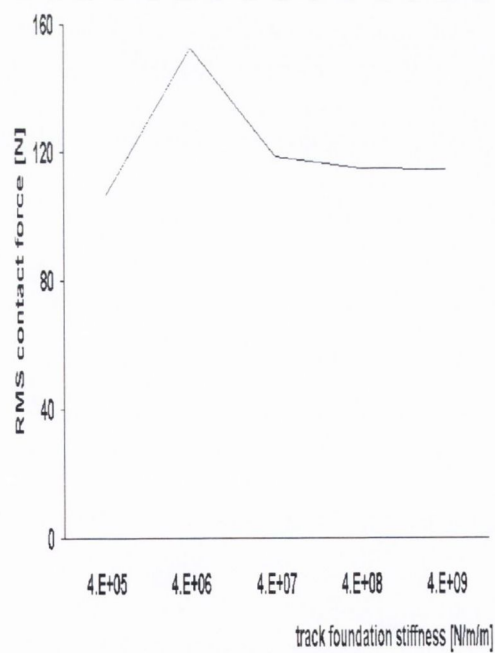
Fig. 3.15: Passenger vehicle model contact force RMS parametric variations (A)



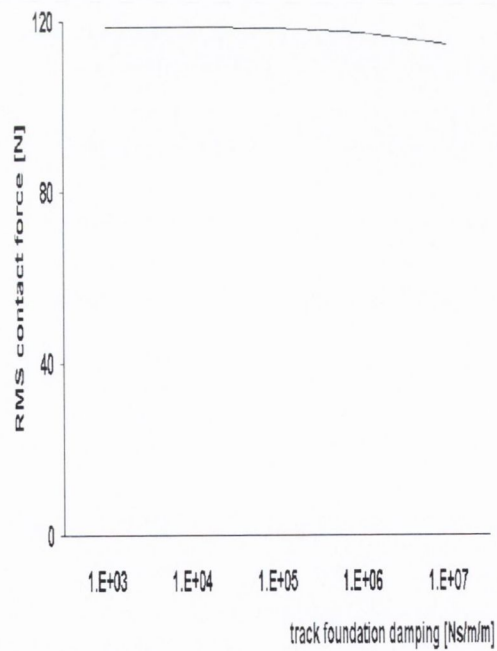
(a) Suspension stiffness



(b) Suspension damping



(c) Track foundation stiffness



(d) Track foundation damping

Fig. 3.16: Passenger vehicle model contact force RMS parametric variations (B)

of a force reaching 120% of the static. This is due to the normal distribution curve, which spreads symmetrically about the static axle load.

At the default parametric values the probability of a peak contact force exceeding 120% of the static is effectively zero (ie. less than 10^{-30}). However, parametric variation of the type investigated in this study results in far greater probabilities in some cases.

A number of the individual parameters that resulted in the highest variances over their respective ranges also resulted in negligible probabilities of exceeding 120% of the static force. These system parameters included wheelset mass, $O(10^{-11})^1$, suspension damping $O(10^{-12})$, track foundation stiffness $O(10^{-16})$ and track foundation damping $O(10^{-12})$. These results illustrate that, over the individual ranges of variation of these parameters, the wheel-rail contact forces are not affected to any significant extent. The equivalent bogie mass calculation also resulted in a relatively small probability value for its largest contact force variance. A bogie mass of 20,000kg gives a probability of exceeding 120% times the static of approximately 0.1%. The values of the three remaining parameters however, track class, vehicle velocity and suspension stiffness, that generated the highest process variances, had significant probabilities of exceeding the specified 120% 'cut-off' force over 100m of railway track.

The Class 1 vertical track irregularity profile resulted in a contact force variance of 1.97kN^2 . Under these track profile conditions and with a calculated expected number of process peaks per metre, N_p , of 0.53, the probability of a single peak exceeding the 'cut-off' over 100m is 22%. A 0.1% probability contact force value for this track class is 29.3kN over the same distance, 100m.

The vehicle velocity that gives greatest variance is 60ms^{-1} and at this velocity the probability of exceeding 120% is close to 100% over 100 metres distance. In essence, this means that typically, at least one peak will be greater than 27.36kN. In

¹The notation $O(x)$ is used to abbreviate "of the order of x "

addition, further manipulation of Equation A.5 showed that, for the same distance, there is an approximately 0.1% probability that an average of at least 49 peaks will exceed 27.36kN. This large number of peaks over the running distance generally results in a greater value for the highest single peak. For a 0.1% probability, the contact force for a single peak exceeding gives 48.15kN over the same 100m distance, more than twice the static axle load. Thus, it is obvious that the highest velocity value, 60ms^{-1} , results in contact forces that are significantly in excess of the static. The equivalent 0.1% probability for 50ms^{-1} is greatly reduced. This effect can be observed by inspection of Figure 3.13(b) where the 60ms^{-1} rms value is almost three times the 50ms^{-1} equivalent.

A suspension stiffness parametric value of $3.0 \times 10^4\text{Nsm}^{-1}$ results in a probability value close to 100% of a single peak exceeding 120% of the static force. The contact force that gives a 0.1% probability of occurrence of a single peak is 38.75kN, approximately 1.7 times the static. As was the case for the velocity, where one single tested value resulted in much more significant effects than for the other values, the remaining suspension stiffness values tested result in negligible probabilities of reaching this magnitude (see Figure 3.14(a)).

3.4.5 Passenger Vehicle Peak Force Probabilities

An identical mathematical analysis to that of Section 3.4.4 was performed on the data obtained from the passenger vehicle model. The static axle load for the passenger vehicle is 15.3kN. As for the locomotive model, a force threshold of 120%, or 80%, of the static force is considered. This equates to 18.36kN (or 12.24kN). Once again a vehicle travel distance of 100m is chosen.

The results of the parametric analysis of the passenger vehicle are in contrast to the locomotive vehicle results in that for all of the parametric variations considered, the probability of exceeding 120% of the static load is negligible.

3.5 Observations and Conclusions

3.5.1 Discussion of Results

This frequency domain analysis of a simple railway vehicle model has provided some statistical information about the wheel-rail contact force characteristics. The input to the system, random vertical track irregularity, is concentrated in the 0.01 to 0.628m^{-1} route frequency range. This equates to wavelengths of between 10 and 628m. Real vertical track irregularity is not constrained as such and is distributed over a much larger range of wavelengths. High frequency events, such as discrete irregularities or rail-head corrugations, are not considered here.

The analysis carried out is useful to both railway vehicle and track engineers. The effect of each of the systems' parameters upon the wheel-rail contact forces in the wavelength range considered is estimated. A number of the parameters are shown to have little or no effect on the resultant contact forces, but others generate markedly different contact force PSD functions dependent upon their magnitude. In addition to the parametric variation there are also significant differences between the PSD functions generated for the locomotive and the passenger vehicle models. The locomotive model, in general, resulted in higher contact force variances about the static load. It should also be noted that, in addition, this higher variation is centred about a greater static load.

Despite the lower static load generated by the passenger vehicle model, the probability of unloading of a wheel is negligible due to the relatively small variance of the contact forces under the influence of the random irregularities specified in this study. The probability of a locomotive vehicle wheel unloading is smaller, hence is it concluded that unloading of the wheels will not occur due to the sole effect of FRA specified random irregularities.

In all, eight parametric variations were considered. All variations affected the resultant contact force PSD functions to some extent. However, the parametric

variations considered in the case of wheelset mass, suspension damping and track foundation damping proved to be minimal, i.e. the contact forces were significantly independent of these parameters. Increasing the wheelset mass resulted in slightly greater contact force variances for both models. The larger masses cause the wheelset hop natural frequency to lower, pushing the corresponding resonant peak towards the low frequency input. This effect, however, is not especially significant and results in 12% and 24% RMS increases over the respective ranges considered for the locomotive and passenger vehicles. The effect of increasing damping of both vehicle suspension and track foundation was to slightly lower the contact force variance. In fact, the suspension damping did not affect the RMS values to any significant extent while track damping was significantly effective only at the two higher damping values considered for the locomotive model.

The variation of the bogie mass and the track foundation stiffness had a greater influence upon the contact forces than the three parameters discussed previously. Increasing the bogie mass increases the contact force variance. The effect is similar to that of the wheelset mass. However, in this case the bogie bounce natural frequencies are in close proximity to the input frequencies and the contact PSD function magnitude is more pronounced. The track foundation stiffness is of particular interest in the study of wheel-rail contact forces. The κ_t value of $4 \times 10^6 \text{Nm}^{-2}$ generates the highest contact force variance. Above and below this particular value the contact force RMS values decrease for both models.

While both the bogie mass and the track foundation stiffness affect the contact force PSD function significantly, their effect is not of the same magnitude as the final three parameters. The tested parametric variations of track class, vehicle velocity and vehicle suspension stiffness each had a relatively dramatic effect on the contact force PSD functions. One would expect the track quality parameter to affect the contact force characteristics. This proves to be the case. As the only variable in this case is the track quality parameter A, the variance of the contact force is proportional

to A throughout. The extreme values of A are 0.98 and 15.53; it follows that the contact force variance for track class 1 is approximately sixteen times that for class 6. The contact force RMS for class 1 track irregularity is approximately 1.4kN for the locomotive model. However, in practice, on such track vehicle velocities would be required to be restricted to a lower limit than the default velocity of 40ms^{-1} that is considered here.

The vehicle model velocity also has a very significant effect upon the wheel-rail contact forces. Increasing the velocity has the effect of decreasing the track irregularity wavelength relative to the moving vehicle. The contact force frequency response functions are also highly concentrated towards higher frequencies and this results in the higher variances. This effect is especially magnified at 50 and 60ms^{-1} , the highest velocities tested, where the frequency response peaks coincide with the irregularity PSD frequency band. The contact force RMS at 60ms^{-1} is approximately 6kN for the locomotive model, the highest RMS observed throughout any of the parametric variations carried out in this study. 60ms^{-1} (216km/hr) is a very high velocity for standard rolling stock, and these types of velocities are rarely achieved in practice. The exceptions to this are modern high speed trains that have advanced suspension characteristics and run on railway track of extremely high quality. However, for the models investigated here it should be noted that the default class 4 track profile was assumed. In general, a higher quality track would be necessary for all vehicles achieving speeds of this magnitude.

The suspension stiffness values considered also show large variation in contact force RMS values. However, unlike the track class or vehicle velocity, the contact force RMS values do not increase in line with the suspension stiffness. The variation in this case is similar to that of the track foundation stiffness, where a single intermediate value resulted in a significantly greater variance. A suspension stiffness of $3 \times 10^6\text{Nm}^{-1}$ for the locomotive and $1.5 \times 10^6\text{Nm}^{-1}$ for the passenger vehicle generate significantly higher contact force variances than for any other values considered.

Interestingly, it is stiffness values of this magnitude that are most frequently quoted for primary suspensions of railway vehicle. The reasons that these values are chosen in design is related to consideration of ride safety and comfort rather than the generation of lower wheel-rail contact forces. Examination of the RMS values for the locomotive bogie displacement reveals that $3.0 \times 10^6 \text{N}$ is the optimum value at which this displacement RMS approaches the RMS of the underlying railway track profile, ie. the minimum value at which the bouncing of the bogie approaches the underlying profile displacement.

3.5.2 Comment

Railway track geometry deteriorates under the influence of dynamic track loads (Esveld 2001). The frequency and magnitude characteristics of the dynamic track loads, as has been illustrated by the analysis contained in this chapter, are functions of the track geometry itself. The deterioration process, therefore, is iterative, with the rate of track deterioration increasing progressively over time. The annual deterioration of railway track is illustrated in Figure 3.17, which is taken from Nielsen (2003). The roughness variance is clearly seen to increase on average from year to year. This particular spectrum contains higher frequency irregularities than those that have been considered.

The investigation of the effects of the various vehicle parameters detailed in this chapter provides an overview of some of the basic relations between wheel-rail contact forces and vehicle, and track, parameters. These relations may facilitate optimising vehicle design from the point of view of minimising contact forces. It should be noted that the minimisation of the wheel-rail contact forces is not the sole objective in railway vehicle design, and other considerations such as ride quality and material property restrictions are of critical importance in vehicle design. In addition to the parametric observations, the characteristics of the stochastic dynamic track loading are determined, which is useful in studies concerned with the dynamic

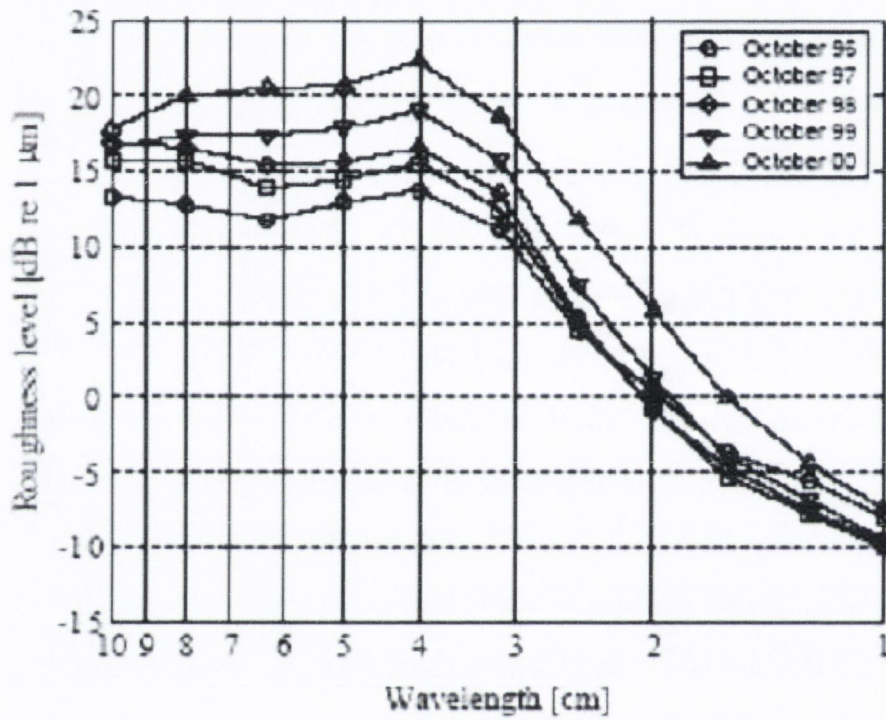


Fig. 3.17: Track roughness PSD illustrating deterioration over time
(Nielsen 2003)

response of the railway track system itself.

An further study was carried out whereby the optimum combinations of bogie mass, suspension stiffness and damping, and wheelset mass were determined. This optimum combination was calculated with a view to minimising the wheel-rail contact force energy. The optimal parameter values for both the locomotive and passenger vehicle models are given in Table 3.4. A Class 4 track and velocity of 40ms^{-1} was assumed for the purpose of this optimisation exercise.

Parameter	Symbol	Unit	Locomotive	Passenger Coach
Bogie mass	m_b	kg	10000	2000
Wheelset mass	m_w	kg	1700	1200
Suspension stiffness	k_b	Nm^{-1}	3.0×10^5	1.5×10^5
Suspension damping	c_b	Nsm^{-1}	2.0×10^4	2.0×10^4

Table 3.4: Locomotive and passenger coach optimal parameters

For each of the parameters, bogie mass, wheelset mass and suspension stiffness, the optimum parametric values were the lowest possible from the range of values included in the analysis. The optimum suspension damping was close to the maximum value in both cases. These findings agree with the parametric study carried out in this chapter, despite the fact that the previous parametric variation was performed with all other parameters held constant. While the calculated optimised parameters do minimise the wheel-rail contact forces it should be noted that vehicle design is concerned with other aspects of vehicular vibration such as wagon bounce, the vertical motion of the wagon body. The equivalent bogie bounce optimum parameters were also calculated and a different set of values was obtained. In particular, it was found that while minimisation of contact forces required as low a suspension stiffness value as possible, the minimisation of bogie bounce requires a suspension with maximum stiffness.

The vehicle model that is considered in this study is highly simplified. A full

representation of the vehicle system would obviously provide a more accurate response prediction. However, as both vehicle dimensions and loads vary greatly, it is often quite difficult to select suitable parameter values for a more complex vehicle model. This can increase the difficulty of comparing computer simulation results conducted by different research groups (Sun & Kennedy 2002).

Chapter 4

Wheelset Coupling Effects on Stochastic Contact Forces

4.1 Introduction

The coupling between two axles forming part of the same vehicle system, and the effect of this coupling upon the contact forces generated at each axle, is investigated in this chapter. The method by which the wheel-rail contact forces are calculated is similar to that applied in the previous chapter. Once again, the dynamic input to the model is random irregularity of the vertical track profile. The statistical characteristics of the random input are identical to the characteristics described previously in Chapter 3.

A vehicle model based upon a laden two-axle freight railway vehicle is considered. The model is necessarily more complex than that described in Chapter 3 because it is desired to observe the contact force processes at two wheelsets of the same vehicle. For this reason a vehicle model with two wheel-rail contact points is required. The previous two-degree of freedom model had a single wheel-rail contact point and considered only the vibration of a single wheelset and bogie. While the previous vehicle model is useful for the purpose of parametric investigation of both the vehicle

and track response to random irregularity, it is also extremely simplified in that it does not take into account the interaction between multiple wheelsets of the same vehicle. The multiple wheel-rail contact model provides a more complete description of the stochastic contact forces generated by a railway vehicle running along a random, irregular vertical track profile. Some of the two-degree of freedom model's shortcomings are identified immediately upon examination of the contact force data generated by the new model that will be introduced here.

This chapter introduces a simple model whereby this coupling effect may be observed. The new model is used to investigate the effect of axle-spacing upon the stochastic wheel-rail contact forces generated by random roughness in the vertical railway track profile. In particular, the difference between the statistical characteristics of the contact force processes at the two different wheelsets of the same vehicle model is investigated.

Section 4.2 describes the vehicle model physically and then details the development of the system equations of motion and frequency response functions. Upon determination of the frequency response functions the track irregularity PSD function is applied as before and contact force PSD functions are calculated.

Section 4.3 commences with an application of some default vehicular parameters to the system and observation of the contact force spectra under these parametric conditions. The effect of varying velocity upon the relationship between the contact force PSD functions at the front and rear wheelsets is then observed. This section concludes with an analytical comparison of the two frequency response functions.

4.2 Mathematical Formulation

4.2.1 Physical Model Description

As in the previous chapter, the railway vehicle model is planar and all degrees of freedom are in the vertical plane. However, the model is now more representative

of a complete vehicle system in that it possesses a rotational degree of freedom, as opposed to the previous two-degree of freedom (both vertical) simplification. The vehicle model is based upon a flatbed wagon railway vehicle chosen because of the relative simplicity of this type of vehicle and its widespread use. A flatbed wagon vehicle consists of a wagon supported directly upon two wheelsets, with no bogies or secondary suspension systems situated between the wagon and its wheelsets.

Unlike the single point surface contact model, the vehicle model that will be formulated here has two wheelset-rail contact points. Critically, these wheelsets are not independent of one another but are physically interconnected by means of the rigid body wagon mass. It will be seen, as this chapter progresses, that the wagon's physical parameters, such as its mass, rotational inertia and the wheelset spacing have an effect upon the contact force spectra that are generated at each of the wheelsets. The wagon itself can move in the vertical direction as did the bogie in the previous chapter, ie. bouncing motion, but it now has an additional rotational, or pitching, degree of freedom. The wagon is supported upon the two wheelset masses, each of which can bounce vertically. The vehicle model is illustrated in Figure 4.1.

The particular model used here is based upon the Manchester Benchmarks *Vehicle 2* specified by Iwnicki (1998). These particular prescribed parameters are based upon a simplification of a laden two-axle freight vehicle model. The vehicle is modelled as a two-axle mass-spring-damper system and consists of a car body and two axles. The car body is modelled as a rigid body with mass m_c and a mass moment of inertia I_c about the transverse horizontal axis through its centroid. Each axle and car body is connected by a spring of stiffness k_b and a dashpot of damping coefficient c_b . These linear elements are representative of the vehicle's suspension system. Further subscripts are used to denote their physical position within the system, front (f) or rear (r). The car body is assumed to be rigid, therefore its motion may be described by the translational displacement coordinate x_c , and the rotational coor-

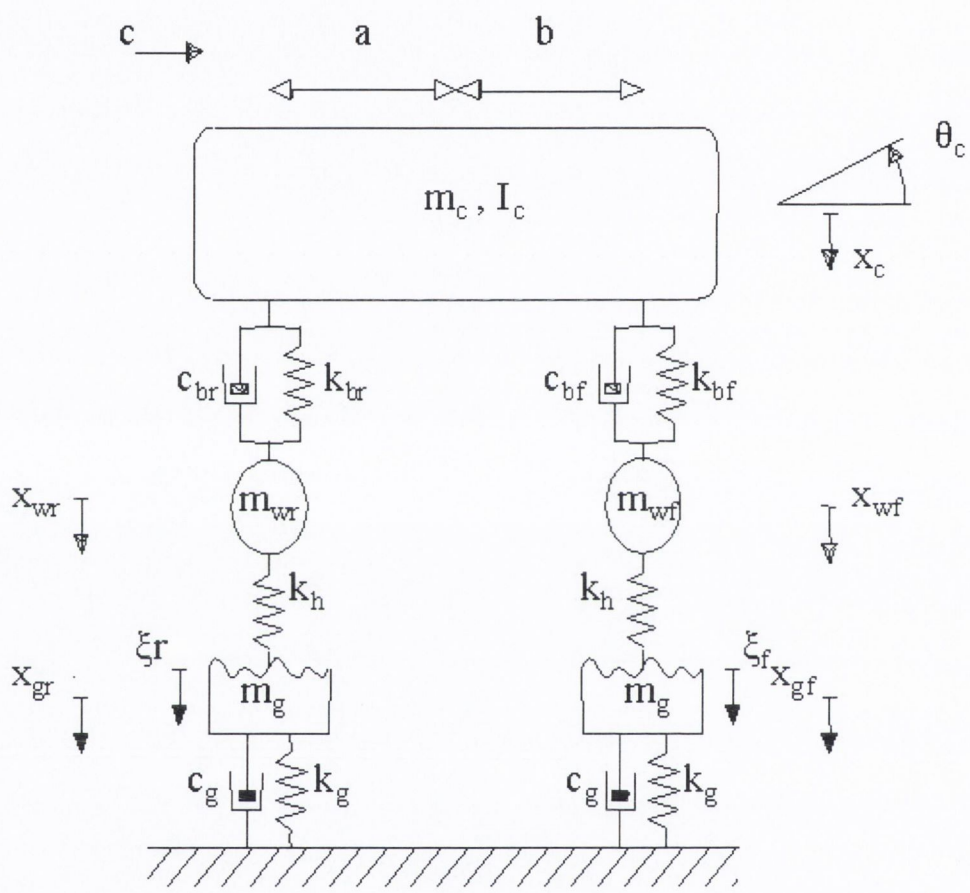


Fig. 4.1: Railway freight vehicle model with discretised mass track model

dinate θ_c about its centroid. The motions of the front and rear axles are described by the vertical displacement coordinates x_{wf} and x_{wr} respectively. Therefore, the total number of degrees of freedom for this vehicle model is four.

The vehicle axle-spacing distance is given by $a+b$ where a and b are the respective distances from the axles to the centre of rotation of the bogie mass. Finally, the linearised Hertzian contact springs are denoted k_h with the further subscripts, f or r , denoting position as for the suspension elements. The linearisation of the non-linear Hertzian spring is performed by applying Equation ?? where the non-linear Hertzian spring constant, c_h , is $1.0 \times 10^{11} \text{Nm}^{-3/2}$ as before.

The vehicle model is supported upon two discrete sprung masses representing the track system. In this case the track mass has been discretised into two point masses, in contrast to the finite element BEF that was applied in the previous chapter. The mass, damping and stiffness values, m_g , c_g and k_g , assigned to the discretised track model are also based on suggested Manchester Benchmark parameter values. The default parametric values for both the vehicle and the discretised track models are given in Table 4.1.

4.2.2 Equation of Motion

In the previous chapter a relative coordinate was introduced to describe the displacement of the wheel relative to the track profile. Two such coordinates, z_{wf} and z_{wr} , are introduced here to describe the motion of the two wheelset masses relative to the underlying track at the respective wheel-rail contact points. These coordinates are described, as follows, as functions of the wheelset displacement, the track displacement and the track irregularity function at the positions of the front and rear wheelsets respectively:

$$z_{wf}(t) = x_{gf}(t) + \xi_f(t) - x_{wf}(t) \quad (4.1a)$$

$$z_{wr}(t) = x_{gr}(t) + \xi_r(t) - x_{wr}(t) \quad (4.1b)$$

The equation of motion of the vehicle model is given by

$$[m_s]\{\ddot{x}_s(t)\} + [c_s]\{\dot{x}_s(t)\} + [k_s]\{x_s(t)\} = \{f_s(t)\} \quad (4.2)$$

where the system displacement vector, $x_s(t)$, is

$$\left\{ x_s(t) \right\} = \left\{ x_c(t) \quad \theta_c(t) \quad z_{wf}(t) \quad z_{wr}(t) \quad x_{gf}(t) \quad x_{gr}(t) \right\}^T \quad (4.3)$$

The details of the specific entries in the mass, damping and stiffness matrices are provided in Appendix B. Also included in Appendix B is the complete system forcing function vector.

4.2.3 Contact Force Spectra

The first step in calculating the PSD functions for the dynamic contact forces at both wheelsets of the bogie model is to generate frequency response functions for the relative displacements of each of the wheelsets. The methods applied here are identical to the analysis carried out in the previous chapter. A Fourier transform is applied to the system equation of motion. The transform of the left-hand side of Equation 4.2 is straightforward. The forcing function on the right-hand side of Equation 4.2, however, is a function of the two time dependent inputs, $\xi_f(t)$ and $\xi_r(t)$, and the Fourier transformation is more complex. Before the transform is applied the profile displacement from its mean at the rear wheel is expressed as a function of the equivalent displacement at the front wheel. This expression effectively reduces the problem from a dual input to a single input dynamic problem. The relationship between the two inputs is equivalent to a time delayed realisation of an identical

signal. As the vehicle is moving at constant velocity, c , and the two wheelsets are separated by the horizontal axle spacing distance $(a+b)$, the rigidity of the irregular profile ensures that this expression reduces to:

$$\xi_r(t) = \xi_f(t - \tau_0) \quad (4.4)$$

where τ_0 is the signal time-delay and is given by

$$\tau_0 = \frac{a + b}{c}. \quad (4.5)$$

The transformed forcing function is calculated based on the mathematical property that the Fourier transform of a time delayed signal is equal to the transform of the signal neglecting the time delay multiplied by an exponential function that is a function of the delay (Jordan & Smith 2002). The exponent is equivalent to the complex number $-i\omega\tau_0$. The transformed forcing function, $\{\hat{f}_s(\omega)\}$ is now expressed as

$$\left\{ \hat{f}_s(\omega) \right\} = \left\{ \begin{array}{l} k_{bf} + i\omega c_{bf} + (k_{br} + i\omega c_{br})e^{-i\omega\tau_0} \\ -bk_{bf} - i\omega bc_{bf} + (ak_{br} + i\omega ac_{br})e^{-i\omega\tau_0} \\ -\omega^2 m_{wf} + i\omega c_{bf} + k_{bf} \\ (-\omega^2 m_{wr} + i\omega c_{br} + k_{br})e^{-i\omega\tau_0} \\ k_{hf} \\ k_{hr}e^{-i\omega\tau_0} \end{array} \right\} \hat{\xi}_f(\omega) \quad (4.6)$$

and the transformed equation of motion for the system takes the form

$$(-\omega^2 [m_s] + i\omega [c_s] + [k_s]) \{\hat{x}_s(\omega)\} = \{\hat{f}_s(\omega)\} \quad (4.7)$$

where $\{\hat{x}_s(\omega)\}$ is the Fourier transform of the system displacement vector.

It is now possible to define a vector containing the complex frequency response functions for each of the degrees of freedom of the vehicle. This vector, $\{H_s(\omega)\}$, see

Equation 4.8, relates the transformed displacements of each of the vehicle components, and the two track masses, to the transform of the profile irregularity at the front wheel. The Fourier transform of ξ_f is now abbreviated to ξ and so,

$$\{H_s(\omega)\} = \begin{pmatrix} H_{x_c}(\omega) \\ H_{\theta_c}(\omega) \\ H_{z_{wf}}(\omega) \\ H_{z_{wr}}(\omega) \\ H_{x_{gf}}(\omega) \\ H_{z_{gr}}(\omega) \end{pmatrix} \equiv \frac{\{\hat{x}_s(\omega)\}}{\hat{\xi}(\omega)} \quad (4.8)$$

It has been shown (Newland 1993) that the various spectral densities of the model response $S_s(\omega)$ can be determined given that the spectral density of the profile irregularity $S_\xi(\omega)$ is known, where there is a single input, $\xi(t)$, to the system. The relationship between the spectra is dependent upon the system frequency response function, $\{H_s(\omega)\}$. As it is the contact force spectra that are required here it is the individual frequency response components $H_{z_{wf}}(\omega)$ and $H_{z_{wr}}(\omega)$ that are of interest in this case. The spectral densities for the displacements of each of the wheelsets relative to the profile are given by

$$S_{z_{wf}}(\omega) = |H_{z_{wf}}(\omega)|^2 S_\xi(\omega) \quad (4.9a)$$

$$S_{z_{wr}}(\omega) = |H_{z_{wr}}(\omega)|^2 S_\xi(\omega) \quad (4.9b)$$

The two equations (4.9a and 4.9b) give the expression for the spectra of the relative displacements of the wheelset masses. Sun & Kennedy (2002) implement a parameter known as a load transfer function (LTF), $A(\omega)$, which is used to describe the direct relationship between the spectra of the contact forces and track irregularity. LTFs are also used here and are functions of the respective wheel-rail contact element properties. The LTF expressions for the front and rear wheelsets are given by

$$A_{wf}(\omega) = |(k_{hf} + i\omega c_{hf})H_{z_{wf}}(\omega)|^2 \quad (4.10a)$$

$$A_{wr}(\omega) = |(k_{hr} + i\omega c_{hr})H_{z_{wr}}(\omega)|^2 \quad (4.10b)$$

In this particular case, ie. the idealised linear Hertzian contact model, the spring damping is assumed to be zero. The spectral densities for the contact forces are then calculated for each of the respective model wheelsets directly via these LTFs.

$$S_{P_{wf}}(\omega) = A_{wf}(\omega)S_{\xi}(\omega) \quad (4.11a)$$

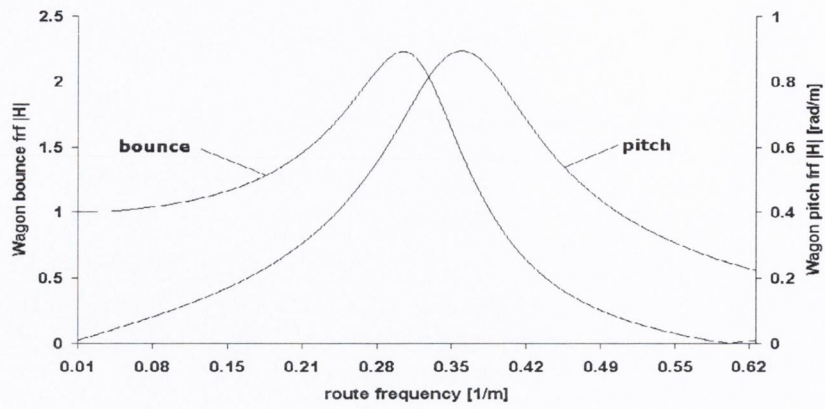
$$S_{P_{wr}}(\omega) = A_{wr}(\omega)S_{\xi}(\omega) \quad (4.11b)$$

4.3 Contact Force Spectra Analysis

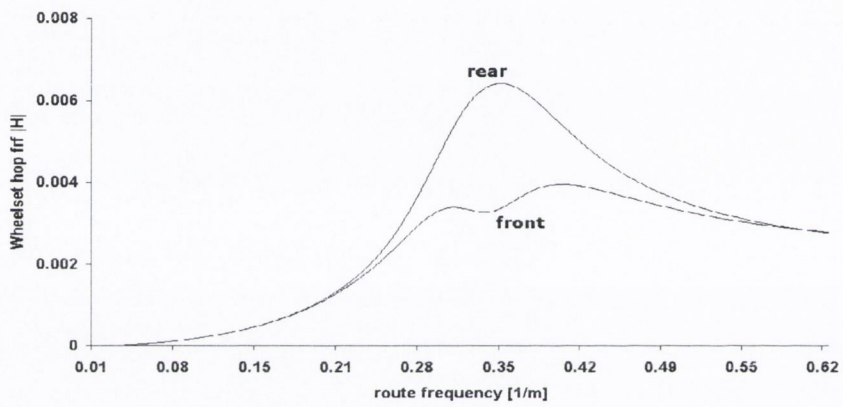
4.3.1 Default Parameter Spectra

The system frequency response functions for the default vehicle parameters (Table 4.1) are illustrated as a function of route frequency (units m^{-1}) in Figure 4.2. These particular illustrated functions were calculated for a vehicle velocity of $40ms^{-1}$. Figures 4.2(a), 4.2(b) and 4.2(c) show the functions for the wagon body bounce and pitch, the wheelsets' hop, and the track model displacement respectively. The frequency range considered here is identical to the range for the FRA irregularity PSD function.

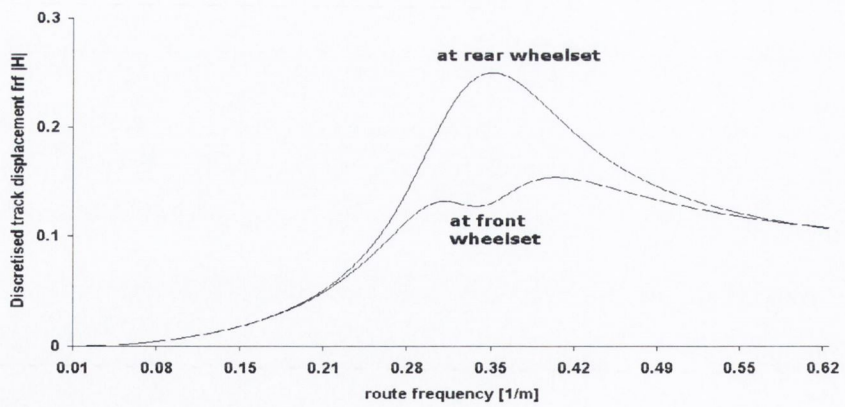
The freight wagon frequency response functions display peaks at the damped natural frequencies of vibration for wagon bounce and pitch. The wheelset and track mass natural frequencies occur at much higher frequency levels that are above the upper limit of the track roughness PSD function. The individual wheelset frequency response functions are not identical. This characteristic is a result of the coupling effect of the wheelsets.



(a) Wagon bounce and pitch



(b) Wheelset masses hop (relative)



(c) Discretised track masses

Fig. 4.2: Frequency response functions for freight vehicle on discretised track masses

Parameter	Symbol	Unit	Value
Wagon mass	m_c	kg	40.77×10^3
wagon rotary inertia	I_c	kgm^2	220.0×10^3
Wheelset mass	m_{wf}, m_{wr}	kg	1.925×10^3
Suspension stiffness	k_{bf}, k_{br}	Nm^{-1}	3.6×10^6
Suspension damping	c_{bf}, c_{br}	Nsm^{-1}	1.0×10^5
Contact spring stiffness	k_h	Nm^{-1}	1.95×10^9
Axle spacing	a,b	m	2.6
Discretised track mass	m_g	kg	119.0
Discretised track damping	k_g	Nsm^{-1}	2.0×10^5
Discretised track stiffness	c_g	Nm^{-1}	5.0×10^7

Table 4.1: Parametric values for vehicle and discretised track model

Further inspection of the wagon bounce and pitch frequency response functions, over a broader frequency interval on a log scale, reveal an undulating pattern between maxima and minima at constant intervals (see Figure 4.3). The wagon bounce response minima occur at wavelengths corresponding to $\frac{2(a+b)}{x}$ metres for $x=1,2,\dots,n$, while the corresponding maxima occur at $\frac{a+b}{x}$ metres for $x=1,2,\dots,n$. The maxima and minima for the bogie pitch correspond to the minima and maxima respectively, for bogie bounce, ie. maximum bounce corresponds to minimum pitch and vice-versa. The initial peaks in the bouncing and pitching responses do not comply with these formulae. The position of these peaks are distorted by the presence of the adjacent natural frequencies of vibration.

The PSD functions for the wheelset contact forces are illustrated in Figure 4.4 for a vehicle velocity, c , of 40ms^{-1} and a track profile with FRA Class 4 random vertical irregularity. The RMS values, equivalent to the square root of the variances, for the random contact force processes at the front and rear wheelsets are approximately 655.3N and 876.2N respectively. The variances are tabulated along

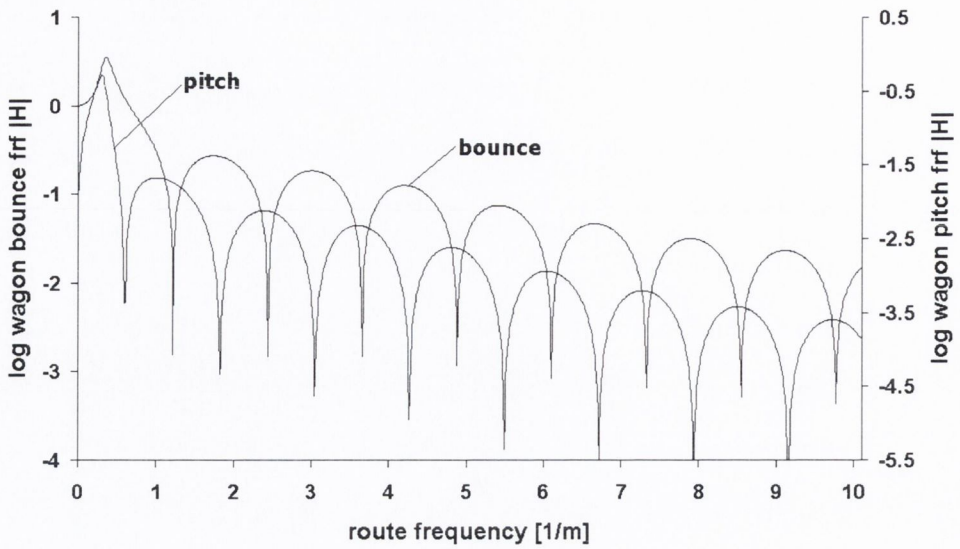


Fig. 4.3: Wagon frequency response functions over zero to 10m^{-1} route frequency range

with the derivative process variances in Table 4.2. Finally, the probability density functions of the individual contact force processes are illustrated in Figure 4.5. The distributions are centred about the static contact axle load which is 218.86kN for both wheelsets.

Wheelset	σ_1^2 [N^2]	σ_2^2 [N^2s^{-2}]	σ_4^2 [N^2s^{-4}]
front	429.442×10^3	45.355×10^3	6.934×10^3
rear	767.742×10^3	85.125×10^3	11.964×10^3

Table 4.2: Contact force process statistics

The existence of a difference in variance between the second wheelset contact force process and that of the front wheelset is obvious by means of visual inspection of their respective PSD, and frequency response, functions. This effect is a result of the dynamic coupling between the wheelsets via the rigid body wagon mass itself. In order to verify this discrepancy a number of numerical simulations of the freight vehicle model were undertaken. A fourth order Runge-Kutta approximation was

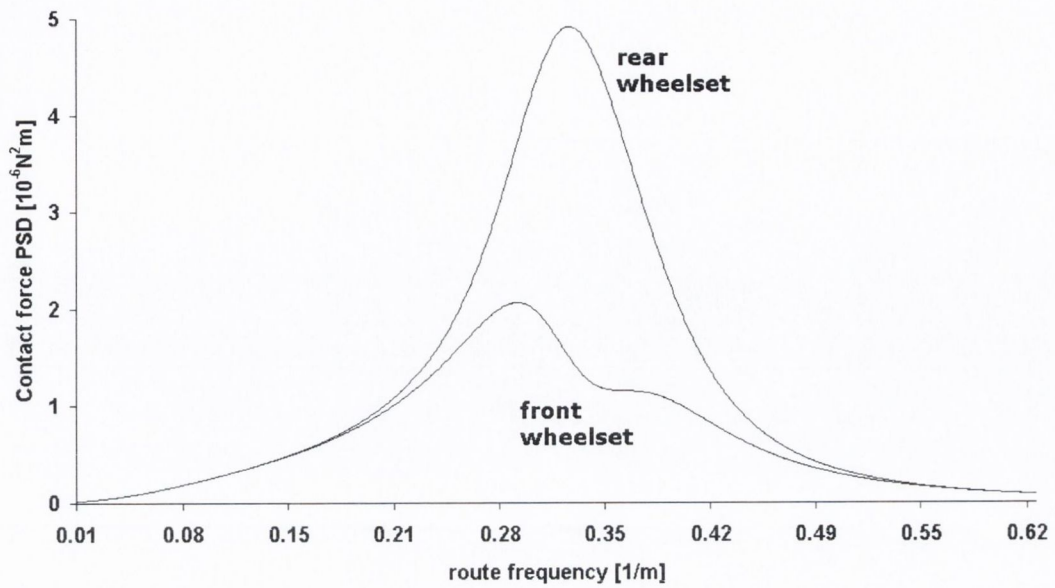


Fig. 4.4: Contact force spectra for front and rear wheelsets

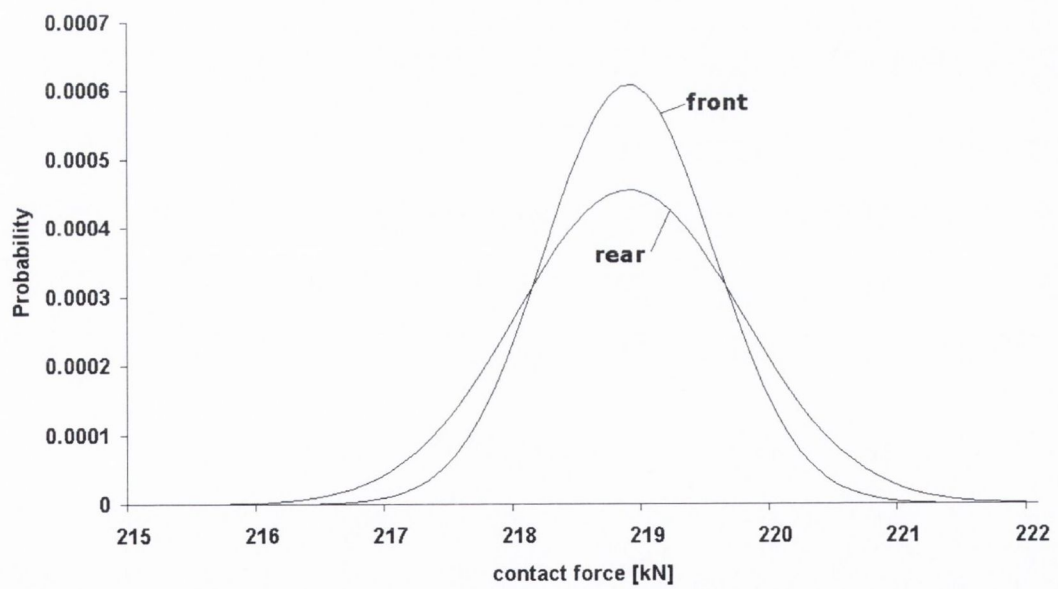


Fig. 4.5: Probability density functions for front and rear wheelset contact forces

applied to solve the differential equation of motion for the bogie model. A series of 1000m long random track profiles were generated using the following trigonometric series (Au et al. 2002):

$$\xi(x) = \sum_{k=1}^N a_k \cos(\Omega_k x + \phi_k) \quad (4.12)$$

where a_k is the amplitude of the cosine wave, Ω_k is a route frequency within the interval $[\Omega_l, \Omega_u]$ in which the PSD of the random irregularities is defined, ϕ_k is a random phase angle in the interval $[0, 2\pi]$, x is the global coordinate measured from the origin and N is the total number of terms used to build up the rail irregularities. The parameters a_k and Ω_k are computed respectively by

$$a_k = \sqrt{4G_{\xi\xi}(\Omega_k)\Delta\Omega} \quad k = 1, 2, \dots, N \quad (4.13)$$

$$\Omega_k = \Omega_l + (k - \frac{1}{2})\Delta\Omega \quad k = 1, 2, \dots, N \quad (4.14)$$

$$\Delta\Omega = \frac{\Omega_u - \Omega_l}{N} \quad (4.15)$$

The contact force variances were calculated for five different track profiles of 100m length. The results are presented in Table 4.3. In all cases the contact force variances at the second wheelset were found to be significantly greater than those at the first, thus verifying the results of the frequency domain analysis. The variances of the individual roughness profiles that were generated are also included.

The different random process characteristics for the two contact force processes also affects their respective peak value statistics. For the parameter values considered here the probability of a single peak force exceeding the static by 3kN over a distance of 100m is 0.000912 for the front wheel. The equivalent probability for the rear wheel is 0.089436, approximately two orders of magnitude greater. For a two

Test Profile	wheelset 1 [N]	wheelset 2 [N]	profile roughness variance [m ²]
1	670.2	924.4	1.85×10^{-5}
2	647.5	889.1	6.71×10^{-6}
3	673.6	937.7	7.64×10^{-6}
4	621.9	899.5	7.33×10^{-6}
5	669.1	928.3	1.23×10^{-5}
mean	656.5	915.8	

Table 4.3: Numerically calculated contact force RMS values

DOF model of the flatbed wagon model similar to the model applied in Chapter 3, the equivalent probability was 0.047675.

4.3.2 Velocity variation

The velocity chosen as the default is relatively high (at 40ms^{-1} , or 144km/hr) for a freight vehicle and was chosen so as to illustrate clearly the coupling effect between the two contact force processes. The effect is visible at lower velocities also but not to the extent of the 40ms^{-1} considered. Figure 4.6 illustrates the variation of the ratio of the two contact force RMS values as the vehicle model velocity increases. As velocity increases above 40ms^{-1} the two RMS values begin to converge.

This can be explained mathematically by considering the third and fourth forcing function components from Equation 4.6 which differ only by the multiplier exponential function $e^{-i\omega\tau_0}$. These components represent the dynamic excitation to the front and rear wheelsets of the vehicle model. As velocity increases the quantity τ_0 becomes smaller, hence the exponential function tends towards unity and the frequency response functions get closer in magnitude. By this reasoning, the respective RMS contact forces also converge as the axle spacing distance is minimised. It should be noted that, for this particular axle-spacing distance, the contact force

RMS is greater at all of the velocities considered (10ms^{-1} to 100ms^{-1}).

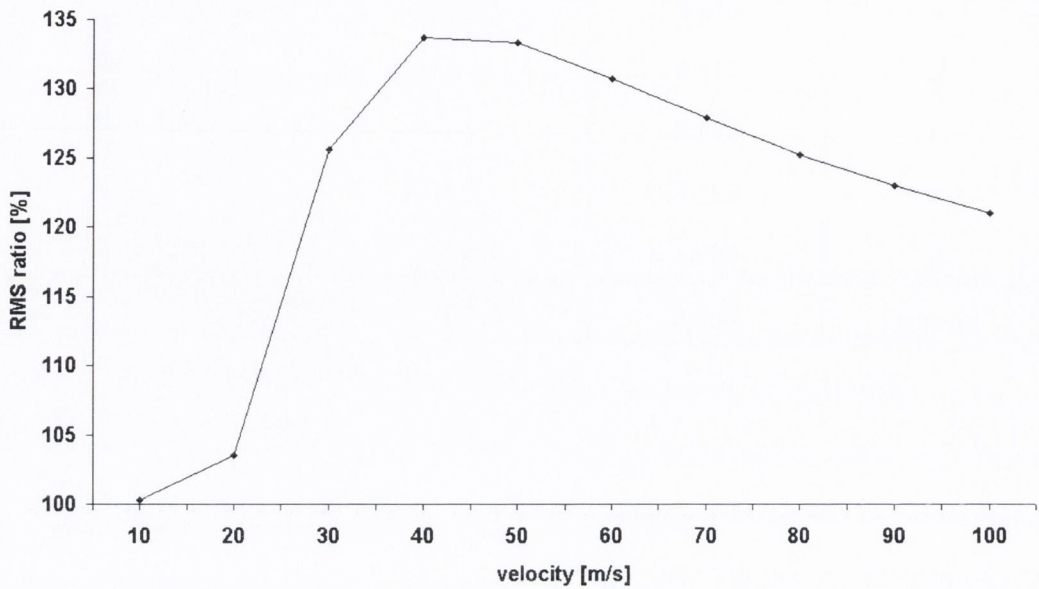


Fig. 4.6: Ratio of rear contact force process RMS to front equivalent, expressed as a percentage, as a function of vehicle model velocity

4.3.3 Comparison of Frequency Response Functions

The expressions for the frequency response functions in terms of the system parameters are extremely complex. Appendix B contains the expressions for these functions for the front and rear wheelsets respectively. It was assumed in the calculation of these functions that the vehicle model was perfectly symmetrical. This assumption was required in order to observe the functions because maintaining separate variables for the front and rear vehicle parameters generates unfeasibly long expressions for these functions.

The expressions, though simplified, remain highly complex. The input spectrum to each wheelset is identical, therefore the different responses calculated at the front and rear wheelsets are due entirely to the difference in the squared modulus of their frequency response functions. The frequency response functions may be expressed

more concisely as follows:

$$H_{z_{\text{wfr}}}(\omega) = \frac{1}{X(\omega)} (-A(\omega) - B(\omega) - C(\omega) - D(\omega)e^{-i\omega\tau_0}) \quad (4.16a)$$

$$H_{z_{\text{wrr}}}(\omega) = \frac{1}{X(\omega)} (-A(\omega) + B(\omega) - C(\omega)e^{-i\omega\tau_0} - D(\omega)) \quad (4.16b)$$

$$(4.16c)$$

The magnitude of the contact force process PSD at any given frequency is proportional to the square of the frequency response function moduli. It therefore follows that the difference in PSD magnitude between the front and rear wheelset processes can be expressed as a proportion of

$$\left| \frac{1}{X(\omega)} (-A(\omega) - B(\omega) - C(\omega) - D(\omega)e^{-i\omega\tau_0}) \right|^2 - \left| \frac{1}{X(\omega)} (-A(\omega) + B(\omega) - C(\omega)e^{-i\omega\tau_0} - D(\omega)) \right|^2 \quad (4.17)$$

which is equivalent to the difference between the squares of the frequency response functions. Despite the complexity of the difference expression it can be seen that the frequency response functions are identical when the following equality is satisfied.

$$-B(\omega) - C(\omega) - D(\omega)e^{-i\omega\tau_0} = B(\omega) - D(\omega) - C(\omega)e^{-i\omega\tau_0} \quad (4.18)$$

It can be seen from this expression that the condition of zero axle spacing is not the only condition whereby the the frequency response function moduli are identical.

4.4 Observations and Conclusions

The frequency content of the random dynamic input, specified by the FRA, to the vehicle and track systems is such that the peak excitation of the random contact forces are not significantly greater than the quasi-stationary forces. This was

previously observed by means of the analysis described in Chapter 3. The quasi-stationary vehicle-track interaction study of Dukkipati & Dong (1999) illustrates a variation, in the absence of irregularities, of between approximately 95% and 105% of the static load. This small dynamic increment is not surprising, given that the minimisation of both wheel hop and track vibration is a primary objective in the design of both systems.

This particular analysis is of more interest in that the difference between the contact force PSD functions at the front and rear wheelsets is illustrated. The relationship between the respective responses is complex and is dependent upon the properties of the wagon such as axle-spacing, body mass and moment of inertia, and suspension stiffness and damping.

Chapter 5

Numerical Track Model with Application to Random Track Irregularity

5.1 Introduction

The previous chapters (3 and 4) have been based upon analysis of wheel-rail contact forces resulting from random track irregularities using a frequency domain approach. A number of assumptions were applied in the mathematical formulation of the models. The track system was modelled as either a single sprung mass or as a finite length beam supported by a continuous elastic foundation. In addition, the non-linear Hertzian contact spring was linearised, as is required for simplified frequency domain analyses. This chapter details the formulation of a numerical track model that can be applied to a transient analysis of the vehicle-track system. Random irregularity profiles similar to those used in Chapters 3 and 4 are considered in this chapter. However, in this case the profiles are generated numerically from the PSD functions, then subsequently used to calculate the systems' time history outputs, whereas previously the spectra were applied directly to the frequency domain

equations and output spectra were calculated.

The new track model is formulated and subsequently validated using a number of different tests. These tests are carried out by comparing the numerically generated results with closed form analytical solutions. The model is then used, by means of applying a numerical time-domain technique to solve its dynamic equation of motion and obtain the time-history response, to generate the coupled response of a railway vehicle and track system. The effect of random track irregularities on the response of both the railway vehicle and track systems is observed and the nature of the resultant dynamic interaction between the two systems is investigated.

The railway track structure is modelled in this analysis as a single infinite beam founded upon a continuous elastic foundation. The model is abbreviated henceforth as BEF (beam on elastic foundation). The conceptual model is infinite in length, ie. of unlimited length in both the positive and negative directions. However, as the numerical Finite Difference Method (FDM) is used to model the beam mathematically, and an infinite system cannot be perfectly modelled numerically, a quasi-infinite beam model is derived here. The new quasi-infinite beam model, though an approximation, is based upon the mathematical assumptions of a theoretically infinite beam.

The static deflection under loading of a theoretically infinite beam has been well documented. The analytical Zimmermann equations (Hetényi 1946) detail the exact static response of such a beam to constant point loads as a function of the distance from the point of load application. The assumption of a uniform beam and continuous elastic foundation is advantageous because it allows the use of these static solutions in formulating the dynamic FDM equations of motion. However, the main advantage of the assumption of a BEF quasi-infinite model is that it allows for the differential equation of motion for the beam to be solved using a convected, or moving, coordinate formulation (Andersen et al. 2001). This formulation allows the response of the vehicle and beam system models to be solved over a theoretically

infinite time (and hence distance of travel). This is possible because, despite the fact that the track model is finite, it is formulated using a convected coordinated system as a quasi-infinite beam model.

Representing the railway track system as a BEF is a simplification. Conventional railway track consists of two parallel continuous beams, the rails, which are fixed at regular intervals onto sleepers supported from below and from the side by the ballast bed medium (Esveld 2001). The presence of the discretely placed sleepers means that the track support is not uniform along its length. Investigations have shown that an equivalent continuous elastic foundation can be substituted with good approximation for the combined sleeper and ballast support (Hetényi 1946). The track is modelled here as a single infinite Euler beam resting upon a continuous elastic foundation. The application of BEF models to railway dynamics problems is not uncommon in the literature (Chen & Huang 2003, Andersen & Nielsen 2003).

The derived quasi-infinite beam model is initially validated for a number of cases where a comparison with exact analytical solutions is possible. Once this validation is completed, random irregularity of the vertical track profile is included in the calculations of the wheel-rail contact forces which are a function of track profile irregularity and effectively determine the overall system response.

A frequency domain approach to the problem of discrete irregularities in the vertical profile, though useful, is not suitable in many cases. A frequency domain approach to the wheel-rail contact interaction involves a linearisation of the Hertzian contact spring about the nominal static wheel load. For low levels of surface roughness this linearisation gives satisfactory prediction. Larger defects may give rise to contact forces of sufficient magnitude that the linearisation deviates excessively from the real Hertzian spring behaviour. In the worst case, a loss of contact between wheel and rail cannot be modelled by the linearised spring. In general, for the larger discrete defects, such as wheel flats or rail joints, the non-linear effects are found to be significant (Thompson et al. 2003). This study concentrates upon

random irregularity, the effects of which do not in general cause the contact forces to vary greatly from the static case. However, a number of different random irregularity spectra were considered, some of which contain relatively high frequency and high magnitude displacements. For this reason a time domain approach was deemed appropriate.

It was found that this track model did not produce accurate results when discrete irregularities such as wheel flats were applied to the contact area geometry. This effect was also observed by Dong et al. (1994), whose elastic BEF model produced contact force results that were in excess of twice that obtained from experimental data. It is suggested that lumping the sleeper mass to the rail largely overestimates the impact load. At high frequencies only a small amount of sleeper mass takes part in the impact. It is concluded by Dong et al. that the equivalent track mass (sleeper and rail mass combined) for BEF models should be taken as a function of the response frequencies. Because the frequency content of the input irregularity considered in this study is spread over a range of values a compromise value is chosen. The response to the lower frequency random irregularities is not as dependent on the equivalent mass.

Section 5.2 details the mathematical formulation of the finite difference beam model. The beam equation of motion is converted from an expression in terms of a cartesian coordinate to one in terms of a convected coordinate. This equation is then used as the basis of the finite difference beam model, which comprises appropriate mass, damping and stiffness matrices, and system forcing vector.

Before the beam model is applied to the calculation of contact forces arising from random track irregularity, the model is validated in Section 5.3. A number of tests are carried out to test the numerical beam model response against previously derived analytical solutions.

Calculation of the wheel-rail contact forces generated by the beam model are presented in Section 5.4. The rms values of the contact force processes are calculated

for track profiles with various degrees of random irregularity.

Section 5.5 includes a comparison of the contact force values obtained using numerical analysis of the finite difference beam model with values obtained from the spectral approach using the model applied in Chapter 4.

5.2 Track Model Formulation

5.2.1 Equation of Motion in Convected Coordinates

The initial step in formulating the quasi-infinite beam model is to determine the equation of motion of an infinite beam. This equation is initially expressed in terms of a cartesian coordinate, and is then converted so that its expression is in terms of a moving coordinate.

The railway track system is modelled here as an infinite plane Euler beam with uniform Young's modulus E_b and constant second moment of area I_b . The mass per unit length of the beam, which is also constant, is denoted μ_b . The beam is supported by an elastic Kelvin foundation with constant spring stiffness κ_f and viscous damping γ_f per unit length. Axial deformation of the beam is assumed not to take place.

A fixed coordinate X is assigned to the system where X is measured along the length of the beam axis. For the purpose of this initial formulation the beam is considered to be free of external loading with the exception of a moving and time-varying point force with magnitude $P(t)$, which is located at the coordinate $X_P(t)$. The point force moves at constant velocity c along the beam in the positive direction of the coordinate X (see Figure 5.1).

The equation of motion of the beam in the fixed coordinate system is

$$EI \frac{\partial^4 u}{\partial X^4} + \kappa u + \gamma \dot{u} + \mu \ddot{u} = P(t) \delta(X_P(t) - ct) \quad (5.1)$$

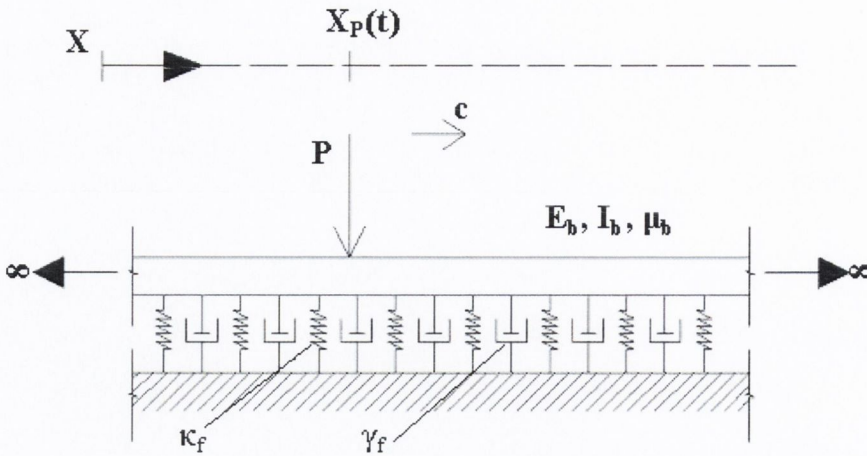


Fig. 5.1: Infinite Euler beam on Kelvin elastic foundation

where $u(X,t)$ is the displacement field. $\dot{u}(X,t)$ and $\ddot{u}(X,t)$ denote the beam velocity and acceleration. In terms of the fixed coordinate X , these are defined as

$$\dot{u}(X,t) = \frac{\partial u(X,t)}{\partial t}, \quad \ddot{u}(X,t) = \frac{\partial^2 u(X,t)}{\partial t^2} \quad (5.2)$$

In applied mechanics, the Dirac function $\delta(x)$ characterises the action of a unit force concentrated at the point $x=0$ (Ginsberg 2001). Referring to Equation 5.1, the moving force $P(t)$ acts only at the point where $X_P(t)$ is equal to the product of velocity and time, ct .

In the limiting case where the velocity is equal to zero, ie. a stationary load case, absorbing boundary conditions may be applied to a finite element or finite difference discretisation of Equation 5.1. However, in the general case the force is moving over an infinite continuum. Hence, this particular problem is better suited to analysis using a convected, or moving, coordinate system (Andersen et al. 2001). The equation of motion of the beam in convected coordinates is obtained by application of the Galilean transformation

$$x = X - ct \quad (5.3)$$

This equation relates the newly defined moving coordinate x to the previously defined fixed coordinate X in terms of both velocity and time. The partial derivatives of the respective coordinate systems are related as follows (Andersen et al. 2001):

$$\frac{\partial}{\partial X} = \frac{\partial}{\partial x} \quad (5.4a)$$

$$\left. \frac{\partial}{\partial t} \right|_x = \left. \frac{\partial}{\partial t} \right|_x - c \frac{\partial}{\partial x} \quad (5.4b)$$

$$\left. \frac{\partial^2}{\partial t^2} \right|_x = \left. \frac{\partial^2}{\partial t^2} \right|_x - 2c \left. \frac{\partial^2}{\partial x \partial t} \right|_x + c^2 \frac{\partial^2}{\partial x^2} \quad (5.4c)$$

The beam equation of motion in terms of the convected coordinate x is hence given by

$$E_b I_b \frac{\partial^4 u}{\partial x^4} + \kappa_f u + \gamma_f \left(\dot{u} - c \frac{\partial u}{\partial x} \right) + \mu_b \left(\ddot{u} - 2c \frac{\partial \dot{u}}{\partial x} + c^2 \frac{\partial^2 u}{\partial x^2} \right) = P \delta(x) \quad (5.5)$$

The Dirac function is now activated only at the point where the moving coordinate x is equal to zero. This is, at all times, the point of application of the moving point force. The displacement field is identical in fixed and moving coordinates as long as x and X describe the same material point, which is the case when the Galilean transformation, Equation 5.3, is applied.

5.2.2 Finite Difference Adaptation

The FDM is a numerical technique that is commonly applied in structural analysis. The theoretical basis of the method is described in detail by Ghali & Neville (1978). This technique allows the calculation of a numerical solution of the differential equation for the displacement or stress resultant for chosen points on a structure (Ghali & Neville 1978). These points are referred to as nodes, pivotal points or points of division. The numerical solution for the nodal displacements and stresses is obtained from differential equations which are applicable to the actual continuous structure.

The method of solution by finite differences generally requires replacing the derivatives of a function by difference expressions of the functions at the nodes. The individual nodal difference equations relate the displacement at that node and nodes in its vicinity to the external applied load.

Complex structures, such as the interactive railway vehicle and track systems, often require that numerical analysis techniques be applied. In this case the finite difference method was used to generate appropriate mass, damping and stiffness matrices for the track model. The order of these matrices is dependent on the chosen number of nodes. Upon calculation of these system matrices the vehicle model was applied to the track model and a time-stepping routine was used to calculate a time history of the dynamic response of both systems under the assumption that the interactive relationship between the systems is modelled by the non-linear Hertzian spring .

Any numerical approach to the solution of Equation 5.5 requires that only a finite part of the beam be considered. It is impossible to formulate an exact model of a structure that is infinite in space. The model that is formulated in this chapter is therefore a quasi-infinite representation of a theoretically infinite structure. For this particular purpose, this finite region will be defined by the moving interval $[x_b^-, x_b^+]$ where x characterises the convected coordinate system defined previously (see Equation 5.3). x_b^- and x_b^+ are the terminal points of the numerical quasi-infinite beam model. These beam extremes move at an identical velocity to that of the applied moving force.

In summary, it can be seen that, for the purpose of finite difference numerical modelling, the beam is separated into three distinct regions. These regions are $[-\infty, x_b^-]$, $[x_b^-, x_b^+]$, and $[x_b^+, +\infty]$ (see Figure 5.2).

In order for the model beam's dynamic behaviour to approach that of a theoretically infinite beam, suitable boundary conditions must be applied to the numerical beam model. These transmitting boundary conditions, at the extremes of the beam

model, x_b^- and x_b^+ , are calculated so that the contributions of the two infinite half beams $[-\infty, x_b^-]$ and $[x_b^+, +\infty]$ to the modelled beam, $[x_b^-, x_b^+]$, response are approximated as accurately as possible (see Figure 5.2).

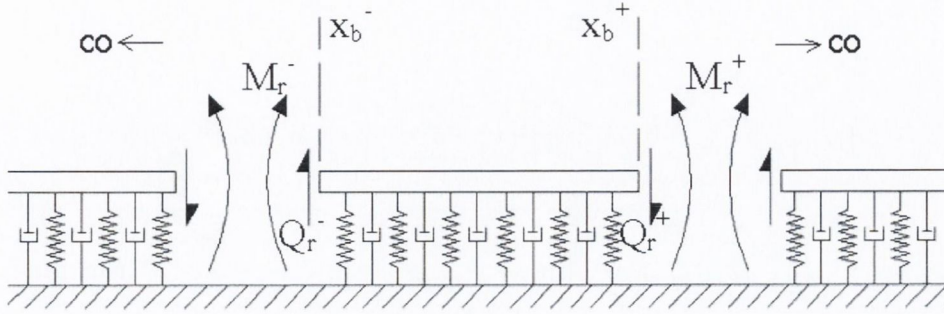


Fig. 5.2: Quasi-infinite beam reactions

The objective is to solve the differential equation of motion of the quasi-infinite beam (Equation 5.5) numerically. For the initial formulation of the numerical beam model, the loading is assumed to be a single time-varying moving point force (as in Figure 5.1). However, the complex dynamic loading induced by a moving railway vehicle requires that a model for the vehicle system be formulated also. In order for the governing differential equation of the beam model to be solved using the finite difference method it is necessary to adjust the beam stiffness matrix to allow for the influence of that part of the beam outside the modelled region. The overall system consists, not only of the beam which is to be modelled, but also the two infinite half beams outside the modelled region. Appropriate reactive forces must be applied at the interfaces between the respective regions.

The reaction forces, moment resisting M_r^- and M_r^+ , and shear resisting Q_r^- and Q_r^+ , are modelled at the interfaces. The calculations for the reaction expressions for the beam boundary at the left hand extreme of the modelled beam, ie. at x_b^- , are described in Section 5.2.3. The beam stiffness matrix terms for the right hand boundary will be symmetrical to those at the left hand side.

5.2.3 Finite Difference Beam Matrices

The finite difference stiffness matrix for a beam is based on the following static equation, where the deflection of a centrally located node, u_i , is related to the applied load at that node, F_i (Ghali & Neville 1978).

$$F_i = \frac{E_b I_b}{h^3} (u_{i-2} - 4u_{i-1} + 6u_i - 4u_{i+1} + u_{i+2}) \quad (5.6)$$

Consider the discretised beam depicted in Figure 5.3. The beam nodes are denoted n_1, n_2, \dots, n_n where n is the total number of nodes assigned to the numerically modelled part of the beam. The vertical displacement at the node n_i is denoted u_i . From the third node inwards the standard finite difference expressions are adequate (see Equation 5.6). This is due to the fact that the finite difference force-deflection relation for a centrally located beam node requires the terms for the deflection at the node in question and of the two immediately adjacent nodes at either side (Ghali & Neville 1978). However, the first two nodes, nodes n_1 and n_2 , not having pairs of two adjacent nodes, require that special force-deflection relations be derived. This also applies to the nodes n_{n-1} and n_n at the right hand extreme of the quasi-infinite beam.

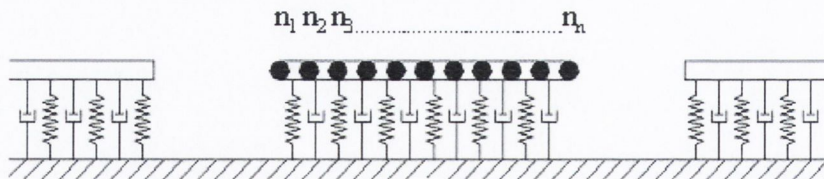


Fig. 5.3: Discretisation of infinite beam into nodal masses

The key observation here is that both M_r^- and Q_r^- , the moment and shear resistance applied by the external infinite half-beams, are functions of the slope, θ_1 , and deflection, u_1 , of the beam at the point x_b^- (see Equation 5.7). This discrete

end-point is common to both the modelled finite difference beam and the infinite half-beam $[-\infty, x_b^-]$. The quantities M_r^- and Q_r^- can be expressed approximately in terms of the vertical displacement of the first two nodes of the modelled section of the beam. This approximation is key to the modelling of the quasi-infinite beam.

$$Q_r^- = f(u_1, \theta_1) \quad (5.7a)$$

$$M_r^- = f(u_1, \theta_1) \quad (5.7b)$$

If h is the distance between the equally spaced nodes then θ_1 may be approximated by

$$\theta_1 = \frac{u_2 - u_1}{h} \quad (5.8)$$

The node at the left hand extreme of the beam model is considered in isolation initially (see Figure 5.4). We consider P_1 to be a hypothetical constant force, applied vertically, at the first node n_1 . The continuously sprung foundation has been discretised so that the node n_1 is supported by a single spring k_{f1} . The equilibrium equation at this node is given by

$$P_1 + Q_{1+\frac{1}{2}} = Q_r^- + R_{f1} \quad (5.9)$$

where R_{f1} is the force in the discretised foundation spring approximating to the continuous foundation stiffness, and is given by

$$R_{f1} = k_{f1} u_1 \quad (5.10)$$

$Q_{1+\frac{1}{2}}$ is the internal beam shear force between the nodes n_1 and n_2 . The finite difference formulation requires an expression for the nodal force in terms of the nodal displacement and so Equation 5.9 is rearranged to give

$$P_1 = Q_r^- + R_{f1} - Q_{1+\frac{1}{2}} \quad (5.11)$$

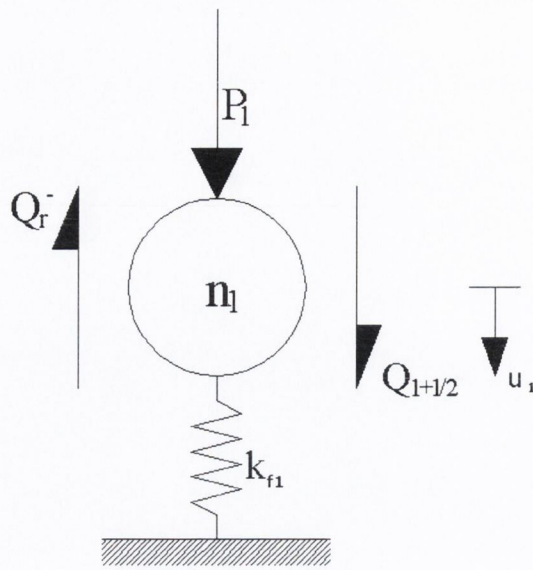


Fig. 5.4: Forces at first finite difference node at left-hand extreme

R_{f1} is a known function of u_1 (see Equation 5.10) and does not require further manipulation. The analytically derived expression for Q_r^- as function of the beam end displacement and rotation (Hetényi 1946) is modified by applying Equation 5.8 and now takes the following form

$$Q_r^- = \left(4\lambda^3 EI + 2\frac{\lambda^2 EI}{h} \right) u_1 - \left(2\frac{\lambda^2 EI}{h} \right) u_2 \quad (5.12)$$

λ is the inverse of the beam's characteristic length and is given by

$$\lambda = \left(\frac{k}{4EI} \right)^{1/4} \quad (5.13)$$

where k is the foundation stiffness per unit length. The final component of Equation 5.11 is the term containing the shear force between the first two nodes, $Q_{1+\frac{1}{2}}$. This force is approximated as a linear function of the bending moment at the first two nodes, M_1 and M_2 . The expression for the shear force between the nodes is given by

$$Q_{1+\frac{1}{2}} = \frac{M_2 - M_1}{h} \quad (5.14)$$

The bending moment at the first node is equal to the restraining moment at the beam end, M_r^- . Using the analytical formula derived by Hetényi and Equation 5.8 M_1 is given by

$$M_1 = M_r^- = \left(2\lambda^2 EI + 2\frac{\lambda EI}{h} \right) u_1 - \left(2\frac{\lambda EI}{h} \right) u_2 \quad (5.15)$$

It is possible to describe M_2 using the standard finite difference equation.

$$M_2 = -\frac{EI}{h^2} (u_1 - 2u_2 + u_3) \quad (5.16)$$

Substituting Equations 5.15 and 5.16 into Equation 5.14 the following finite difference expression for $Q_{1+\frac{1}{2}}$ is obtained

$$Q_{1+\frac{1}{2}} = \left(-2\frac{\lambda^2 EI}{h} - 2\frac{\lambda EI}{h^2} - \frac{EI}{h^3} \right) u_1 + \left(2\frac{\lambda EI}{h^2} + 2\frac{EI}{h^3} \right) u_2 + \left(-\frac{EI}{h^3} \right) u_3 \quad (5.17)$$

All of the terms on the righthand side of Equation 5.11 have now been expressed in terms of vertical nodal displacements. The final finite difference force-displacement equation for the first node is as follows:

$$P_1 = \left(k_{f1} + 4\lambda^3 EI + 4\frac{\lambda^2 EI}{h} + 2\frac{\lambda EI}{h^2} + \frac{EI}{h^3} \right) u_1 + \left(-2\frac{\lambda^2 EI}{h} - 2\frac{\lambda EI}{h^2} - 2\frac{EI}{h^3} \right) u_2 + \left(\frac{EI}{h^3} \right) u_3 \quad (5.18)$$

The nominal force has been described in terms of the first three beam displacements. A similar procedure based on the same approximations is followed for the second node, the resulting force-displacement relationship is a function of the first four beam node displacements and is given by

$$\begin{aligned}
P_2 = & \left(-2\frac{\lambda^2 EI}{h} - 2\frac{\lambda EI}{h^2} - 2\frac{EI}{h^3} \right) u_1 \\
& + \left(k_2 + 2\frac{\lambda EI}{h^2} + 5\frac{EI}{h^3} \right) u_2 \\
& + \left(-4\frac{EI}{h^3} \right) u_3 + \left(+\frac{EI}{h^3} \right) u_4 \quad (5.19)
\end{aligned}$$

The finite difference stiffness matrix for the quasi-infinite beam, $[k_b]$, is thus calculated using the standard finite difference expressions for the centrally located nodes and the derived expressions (Equations 5.18 and 5.19) for the two nodes at the extreme ends of the beam. The matrix is most clearly expressed as the sum of three component matrices (see Equation 5.20). The first matrix in the expression is the standard finite difference matrix for a beam structure. The second comprises the contribution of the foundation stiffness to the overall beam stiffness while the third matrix contains the contributions due to the effect of the two infinite half beams at each end of the modelled beam. This third matrix contains terms relating only to the first and last two beam nodes. It should be noted that the spring stiffnesses k_{f1} and k_{fn} are equivalent to $\frac{\kappa_f h}{2}$, while k_{f2} and k_{fn-1} are equivalent to $\kappa_f h$. These springs are simply spring elements calculated as a discretised approximation of the continuous foundation stiffness.

$$\begin{aligned}
\left[\kappa_b \right] &= \frac{E_b I_b}{h^3} \begin{bmatrix} 1 & -2 & 1 & 0 & \dots & \dots & \dots & \dots & 0 \\ -2 & 5 & -4 & 1 & 0 & & & & \vdots \\ 1 & -4 & 6 & -4 & 1 & 0 & & & \vdots \\ 0 & 1 & -4 & 6 & -4 & 1 & 0 & & \vdots \\ \vdots & \ddots & \ddots & \ddots & \ddots & \ddots & \ddots & \ddots & \vdots \\ \vdots & & 0 & 1 & -4 & 6 & -4 & 1 & 0 \\ \vdots & & & 0 & 1 & -4 & 6 & -4 & 1 \\ \vdots & & & & 0 & 1 & -4 & 5 & -2 \\ 0 & \dots & \dots & \dots & \dots & 0 & 1 & -2 & 1 \end{bmatrix} + \\
&\begin{bmatrix} \frac{\kappa_f h}{2} & 0 & \dots & \dots & \dots & \dots & \dots & \dots & 0 \\ 0 & \kappa_f h & 0 & & & & & & \vdots \\ \vdots & 0 & \kappa_f h & 0 & & & & & \vdots \\ \vdots & & 0 & \kappa_f h & 0 & & & & \vdots \\ \vdots & & & \ddots & \ddots & \ddots & & & \vdots \\ \vdots & & & & 0 & \kappa_f h & 0 & & \vdots \\ \vdots & & & & & 0 & \kappa_f h & 0 & \vdots \\ \vdots & & & & & & 0 & \kappa_f h & 0 \\ 0 & \dots & \dots & \dots & \dots & \dots & \dots & \dots & 0 \quad \frac{\kappa_f h}{2} \end{bmatrix} + \\
E_b I_b &\begin{bmatrix} 4\lambda^3 + 4\frac{\lambda^2}{h} + 2\frac{\lambda}{h^2} & -2\frac{\lambda^2}{h} - 2\frac{\lambda}{h^2} & 0 & \dots & \dots & \dots & \dots & \dots & 0 \\ -2\frac{\lambda^2}{h} - 2\frac{\lambda}{h^2} & 2\frac{\lambda}{h^2} & 0 & & & & & & \vdots \\ 0 & 0 & 0 & & & & & & \vdots \\ \vdots & & & \ddots & & & & & \vdots \\ \vdots & & & & \ddots & & & & \vdots \\ \vdots & & & & & \ddots & & & \vdots \\ \vdots & & & & & & 0 & 0 & 0 \\ \vdots & & & & & & 0 & 2\frac{\lambda}{h^2} & -2\frac{\lambda^2}{h} - 2\frac{\lambda}{h^2} \\ 0 & \dots & \dots & \dots & \dots & \dots & 0 & -2\frac{\lambda^2}{h} - 2\frac{\lambda}{h^2} & 4\lambda^3 + 4\frac{\lambda^2}{h} + 2\frac{\lambda}{h^2} \end{bmatrix}
\end{aligned}
\tag{5.20}$$

The finite difference mass matrix for the beam structure, $[m_b]$, is a diagonal matrix with each entry equal to the total mass of the beam divided by the number of nodes. If the nodal mass is denoted m_n then the mass matrix takes the form of Equation 5.21. The mass matrix is not adjusted but is a simple discretisation of the beam mass at the beam nodes.

$$[m_b] = \begin{bmatrix} m_n & 0 & \dots & 0 \\ 0 & m_n & \dots & 0 \\ \vdots & \vdots & \ddots & \vdots \\ 0 & 0 & \dots & m_n \end{bmatrix} \quad (5.21)$$

The formulation of the damping matrix $[c_b]$ beam system is dependent on the nature of the beam damping. Equation 5.5 can now be written in terms of the beam mass, damping and stiffness matrices, and the appropriate system vectors, as

$$[k_b] \{u\} + [c_b] \left(\{\dot{u}\} - c \left\{ \frac{\partial u}{\partial x} \right\} \right) + [m_b] \left(\{\ddot{u}\} - 2c \left\{ \frac{\partial \dot{u}}{\partial x} \right\} + c^2 \left\{ \frac{\partial^2 u}{\partial x^2} \right\} \right) = \{P\} \quad (5.22)$$

The vector $\{P\}$ has value zero at all nodes bar the node of application of the point force. As the equation of motion is formulated in terms of the moving coordinate x , the particular node of application of this force does not change over time. The partial derivatives are calculated as functions of the beam's nodal deflections and velocities and are given by the following relations:

$$\left. \frac{\partial u}{\partial x} \right|_i = \frac{1}{2h} (-u_{i-1} + u_{i+1}) \quad (5.23a)$$

$$\left. \frac{\partial u}{\partial x \partial t} \right|_i = \frac{1}{2h} (-\dot{u}_{i-1} + \dot{u}_{i+1}) \quad (5.23b)$$

$$\left. \frac{\partial^2 u}{\partial x^2} \right|_i = \frac{1}{h^2} (u_{i-1} - 2u_i + u_{i+1}) \quad (5.23c)$$

Equation 5.22 can be solved numerically if the initial conditions of the beam model are known.

5.3 Model Validation

The objective of the analysis was to calculate the wheel-rail contact forces that are generated by a railway vehicle as it moves along a length of randomly irregular railway track. The forces are a function of the relative wheel-rail non-linear Hertzian spring displacement. The results obtained are compared with the corresponding linear spring results that were calculated in Chapter 4. The effect of linearising the contact spring was thus observed.

A number of preliminary analyses were carried out as a means of validating the convected coordinate quasi-infinite numerical track model formulated in Section 5.2. Initially, the static beam response was considered. These static tests were followed by analysis of the beam response to a moving constant force. The dynamic system response was calculated throughout by implementing a numerical fourth order Runge-Kutta routine which generates a time-history of the dynamic response of the beam, and later the vehicle, models.

The beam model parameters used are based upon values for a single BEF railway track model used by Esveld (2001). The mass per unit length of the beam, μ_b , is 119kgm^{-1} which accounts in the model for both the mass of the rails and the discretely spaced sleepers. The product of the beam material Young's modulus and the section 2nd moment of area, $E_b I_b$, is $4.5 \times 10^6 \text{Nm}^2$. The foundation stiffness, κ_f , is $4.0 \times 10^7 \text{Nm}^{-2}$ and the foundation damping, γ_f , is $1.2 \times 10^5 \text{Nsm}^{-2}$.

The initial beam model validation tests were carried out under a static force load case. This type of test is relevant only to the stiffness matrix. The results of these tests are compared to the analytical solutions that have been detailed by Hetényi (1946). The total length of the finite difference part of the infinite beam that was modelled was 20m. The quasi-infinite beam mass was discretised into 201 equally spaced nodes equating to a nodal spacing of 0.1m.

The static response of quasi-infinite beam was found to match accurately the

theoretical deflection of an infinite beam to within 0.5%. Larger percentage discrepancies occurred only close to the theoretical points of zero deflection, rotation and bending moment. The comparison is illustrated graphically in Figure 5.5.

The initial dynamic test involved numerically solving the beam response for a single moving point force. The force is initially situated at the mid-span of the finite difference quasi-infinite beam. The force then commences its movement from 'at rest' initial conditions. The static deflection of the beam under the equivalent bogie mass is calculated and applied to the system prior to commencement of the numerical computation process. The nature of the convected coordinate solution ensures that, in effect, the force does not move from the central node throughout the numerical simulation. A detailed analytical solution for the problem of an infinite beam traversed by a moving point force is presented by Frýba (1999). For this type of problem there comes into existence a quasi-stationary state in which the beam is at rest relative to the moving coordinate system. In the quasi-stationary state the solution for the beam deflection is given by

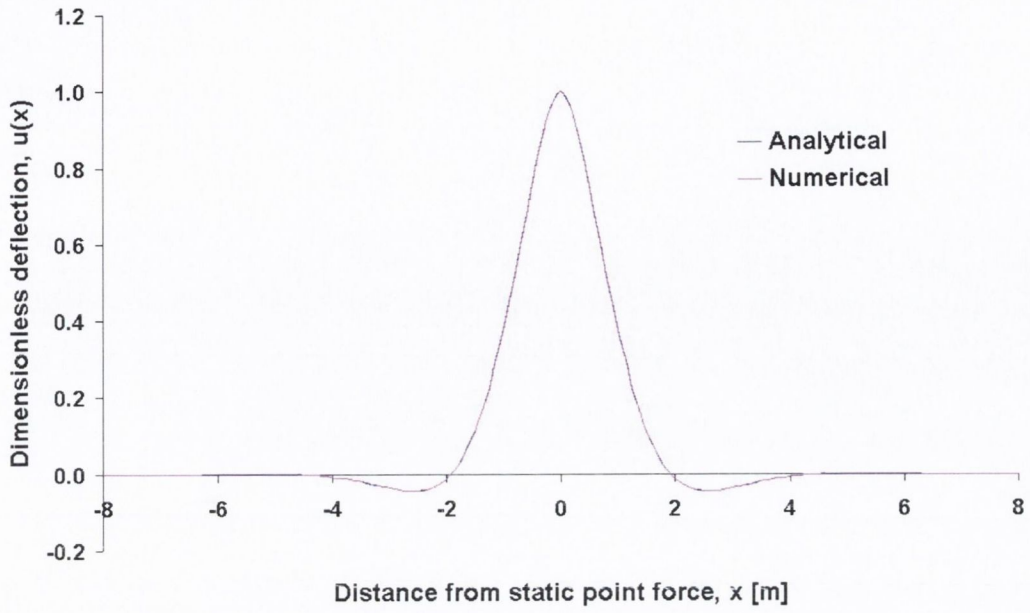
$$u(X, t) = u_0 u(x) \quad (5.24)$$

where x is the moving coordinate defined previously in Equation 5.3, u_0 is the static beam deflection, and $u(x)$ is the dimensionless deflection of the beam. Frýba also defined two additional dimensionless parameters, α and β , the dimensionless velocity and damping parameters respectively.

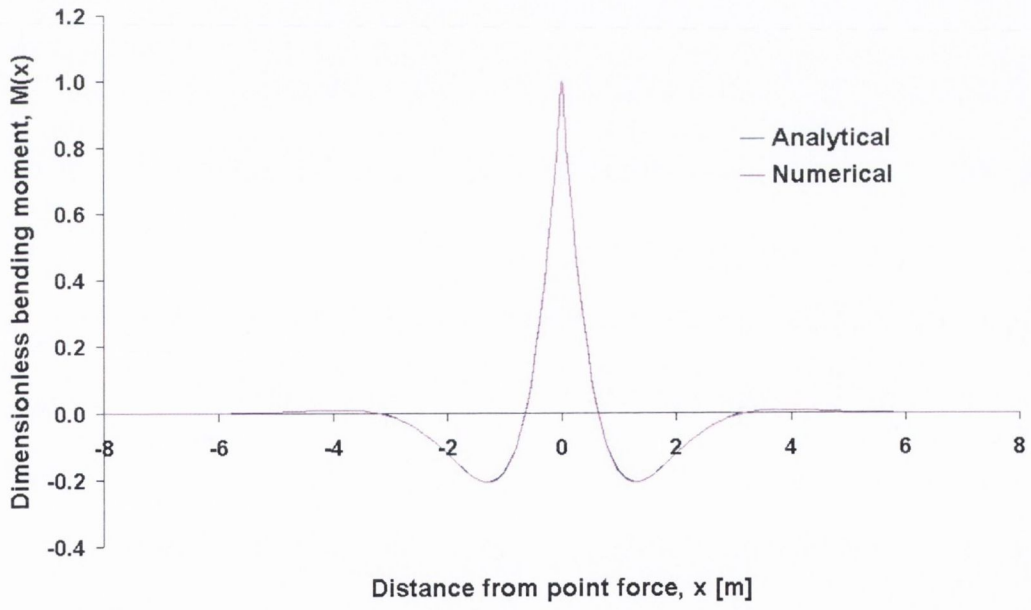
$$\alpha = \frac{c}{2\lambda} \sqrt{\frac{\mu_b}{E_b I_b}} \quad (5.25)$$

$$\beta = \frac{\gamma}{2\mu} \sqrt{\frac{\mu_b}{k_f}} \quad (5.26)$$

The dimensionless beam deflection, $u(x)$, was calculated numerically over a practical range of velocities using the quasi-infinite beam model formulated previously.



(a) Deflection



(b) Bending moment

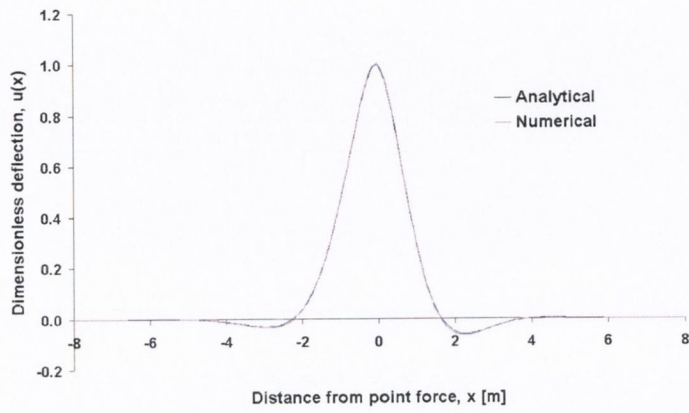
Fig. 5.5: Static beam response to single point force

These deflections were then compared with their analytical equivalents. For the track model parameters specified the value of the constant β is 0.8697. One initial observation is that this particular damping value generates dimensionless deflections at the force contact point, ie. where $x = 0$, that are smaller than unity. This implies that the quasi-stationary deflection of the beam at the contact point is smaller than the static deflection. This characteristic applies to all force velocities for these particular beam model parameters. However, it should be noted that the maximum track deflection does not necessarily occur at the contact point. Over the range of velocities considered here the maximum deflection takes place just behind the point of contact.

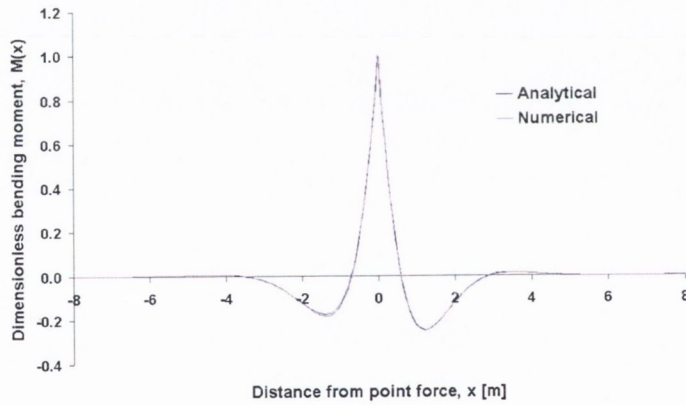
The point force was initially at a stationary initial condition. and was accelerated instantly to the velocity required. The initial beam deflection was its static position under the point force. The instantaneous acceleration of the force to a non-zero velocity gives rise to a starting transient which takes some time to be dissipated. Once the transient has been damped out the beam attains its quasi-stationary state. The dynamic quasi-stationary state response of the finite difference numerical model was found to approximate to the analytically predicted response. This comparison is illustrated in Figure 5.6 for a point force velocity of 60ms^{-1} . Both the dimensionless deflection and velocity are considered.

It should be noted that the agreement between the analytical and numerical solutions was validated for the 201 noded model only at realistic railway vehicle velocities. At higher velocities the numerical quasi-stationary beam response diverges from the analytical solution. Figure 5.7 illustrates this divergence for a point force moving at 250ms^{-1} . Further expansion of the beam model to 40m length and 401 nodes resulted in convergence of the respective solutions. This indicates that at higher velocities sufficient wave reflection occurs at the beam extremes to distort the numerical analysis results.

The next step in checking the validity of the convected coordinate model was the

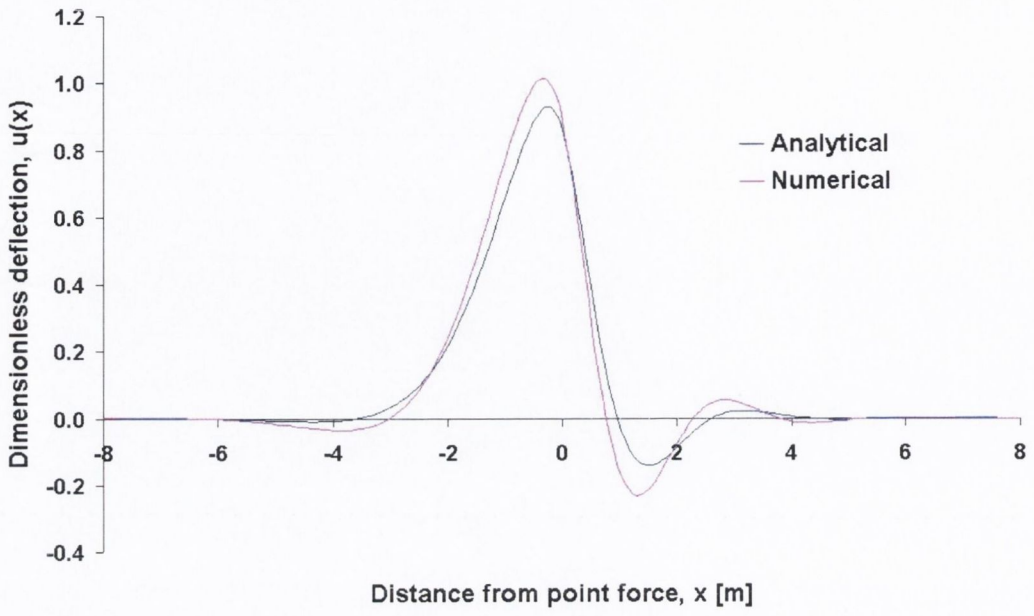


(a) Deflection

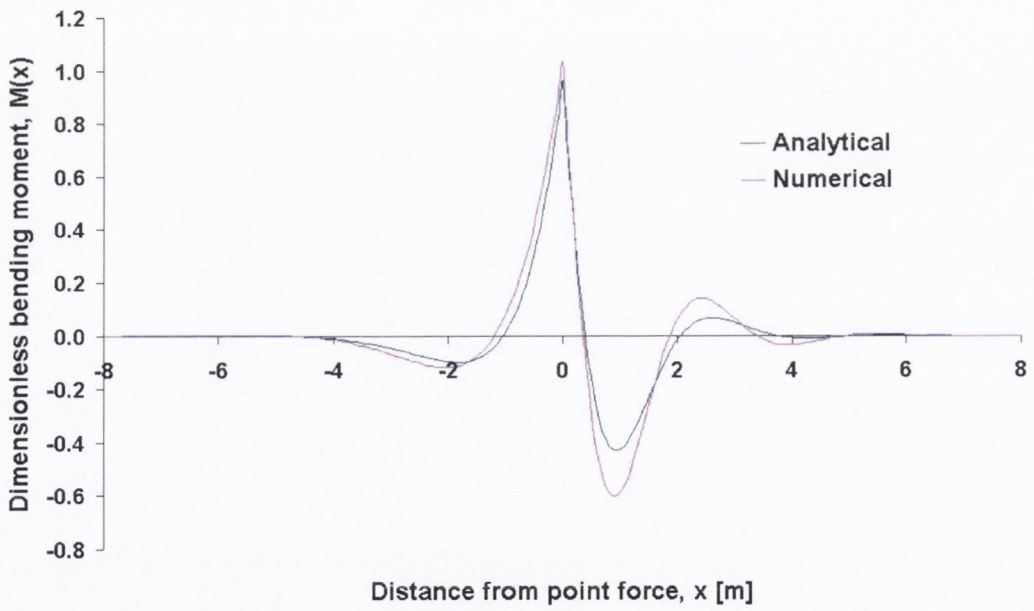


(b) Bending moment

Fig. 5.6: Quasi-stationary infinite beam response at 60ms^{-1}



(a) Deflection



(b) Bending moment

Fig. 5.7: Quasi-stationary infinite beam response at 250ms^{-1}

application of a moving sprung load model to the beam system. The application of a moving vehicle model adds complexity to the dynamic solution because the equations of motion of both coupled systems must be solved interactively. In effect the vehicle model is subjected to vertical forces at each of its wheelsets while the beam model is subjected to equal and opposite time-varying vertical point forces. Frýba (1999) draws the important conclusion that, for the infinite BEF in the quasi-stationary state, the load exerts no inertia effects on the system response.

A railway vehicle possesses multiple wheels as opposed to the single point contact models that have been tested thus far. If we consider a single two-axle bogie model and model the individual axle loads as point forces the beam deflection will not, according to the analytical solution, be identical at each contact point in the quasi-stationary state. This is due to non-symmetry of the beam deflection about the point of action of the load at non-zero velocities. Two individual point forces, 3m apart and each of magnitude 100kN, were applied to the numerical beam model. The 20m, 201 node beam was used for this purpose. The response was calculated over the same range of realistic railway vehicles as previously (0 to 60ms⁻¹). The results were found to be in good agreement with the analytical predicted response. The comparison is illustrated for a force velocity of 60ms⁻¹ in Figure 5.8. As before, when the vehicle velocity was increased significantly the analytical and numerical sets of results were found to diverge for the 201 node model.

For the purpose of the final beam model verification, a four degree-of-freedom bogie model was applied to the numerical beam model (see Figure 5.9). The bogie properties are based upon those of a locomotive railway vehicle. The bogie mass is 15,260kg and its moment of inertia is 13,665kgm². The two wheelsets each have a mass of 2670kg. A pre-load of 250kN, representing the gravitational weight of the locomotive body, is also applied vertically to the bogie mass. The mathematical model of the contact mechanism between wheel and rail is characterised by the non-linear relationship of equation 5.27 (Nielsen & Igeland 1995). The relationship between

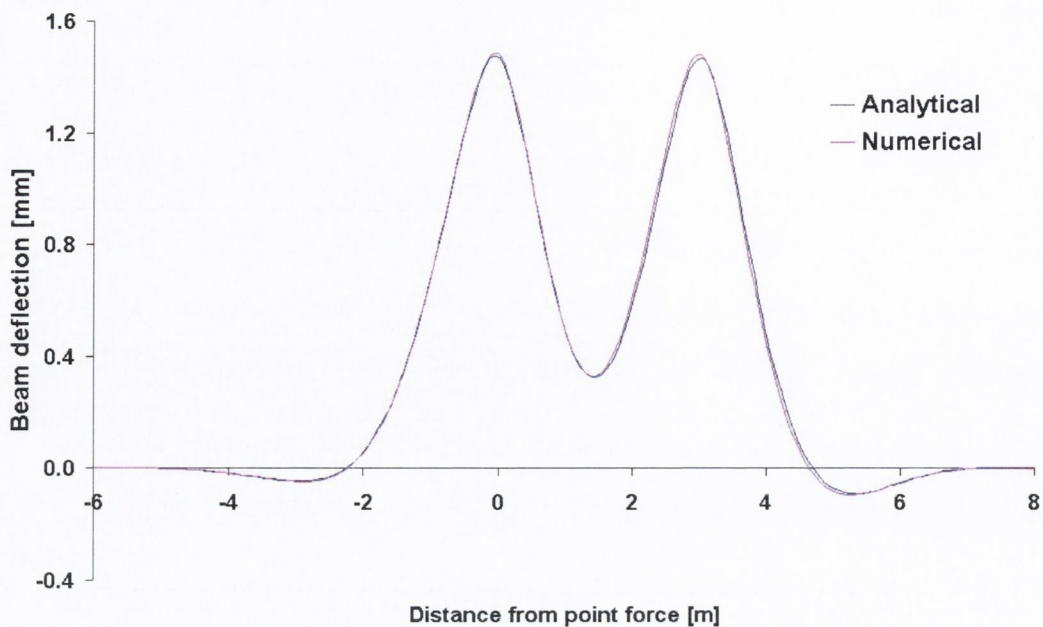


Fig. 5.8: Beam quasi-stationary response to two point forces moving at 60ms^{-1}

the linearised Hertzian spring stiffness k_H , and the relative wheel-rail displacement is given by

$$k_H = \begin{cases} c_H(x_w - x_r)^{\frac{1}{2}}, & \text{for } x_w - x_r > 0; \\ 0, & \text{else.} \end{cases} \quad (5.27)$$

where c_H is the non-linear Hertzian spring stiffness with units $[\text{Nm}^{-3/2}]$, x_w and x_r are the respective wheel and rail displacements. The value of $93 \times 10^9 \text{Nm}^{-3/2}$ is assigned to the non-linear stiffness, c_H , in this case. This model for the spring contact is easily interpreted physically. The spring stores zero energy in the event of loss of contact between wheel and rail. However, compressive energy may be stored in the spring due to the indentation of the wheel into the rail surface when the relative displacement is positive.

As expected, the beam model's quasi-stationary response (once all of the starting transients had been damped out) to the moving bogie model was identical to the equivalent response to two moving point forces in the zero to 60ms^{-1} velocity range.

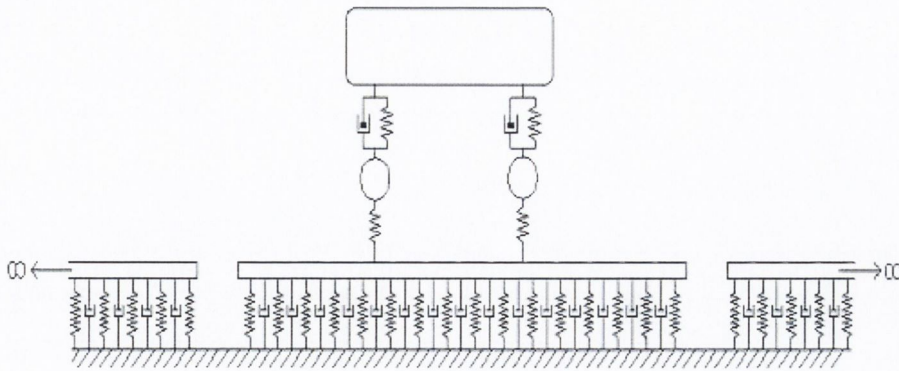


Fig. 5.9: Beam on elastic foundation traversed by four-degree of freedom vehicle model

This quasi-stationary simulation dynamic response provides validation of the finite difference beam model formulation prior to further use of the model in the investigation of random vertical track profile irregularities.

5.4 Effect of Random Vertical Profile Irregularity

5.4.1 Introduction

The coupling between the vehicle and track systems has been accomplished through the calculation at each time-stepping iteration of the interactive forces between the wheelsets of the vehicle model and nodal contact points of the the beam model. Gaussian random irregularity of the vertical profile of the railway track system is now considered. Random profiles are generated numerically from smoothed PSD functions using trigonometric series. An identical vehicle model to that considered previously in Section 5.3 is applied.

The trigonometric series used to generate the random profiles is expressed in Equation 5.28, where $\xi(x)$ is the profile deviation from its mean value at the coor-

dinate x and $S_{xx}(\Omega)$ is the one-sided PSD function characterising the irregularities.

$$\xi(x) = \sum_{i=1}^N \sqrt{2S_{xx}(\Omega_i)\Delta\Omega_i} \cos(\Omega_i x - \beta) \quad (5.28)$$

where β_i is a phase angle randomly distributed between zero and 2π and Ω is the route frequency. An value of N of 2000 was chosen based on a previous study by Au et al. (2002).

The profiles generated were 1500m in length. This particular distance was chosen because profile variances of 1000m were found to match, within less than 5%, the variances of the parent PSD functions. Shorter profile lengths resulted in variances that deviated excessively from the PSD function variances. While 1000m was satisfactory to obtain an acceptable profile variance, 50% extra distance was considered for the simulations to allow starting simulation transients time to damp out sufficiently. The initial parts (20 metres for every ms^{-1} velocity) of the time-histories were not considered in the calculation of the contact force rms values for the same purpose.

5.4.2 Comparison of Empirical PSD Functions

Initially, railway track profiles with FRA Class 4 and Class 1 random vertical irregularity were considered. The vehicle model velocity was 40ms^{-1} . The time-histories of the Hertzian spring contact forces at the front and rear wheelsets are recorded. The contact forces are illustrated in Figure 5.10 in their quasi-stationary state, ie. after the initial starting transient in the numerical simulation has been damped out. The static contact force per wheelset for this vehicle model is approximately 226kN.

Different PSD functions representing random railway track irregularity have been applied in the various analyses of railway vehicle-track interaction in the literature. The FRA PSD functions are the most prevalent (Au et al. 2002, Wu & Yang 2003). Lei & Noda (2002), in their study of the vehicle-track coupling system, took their PSD function from America Railway Standard (ARS) where line grades from one

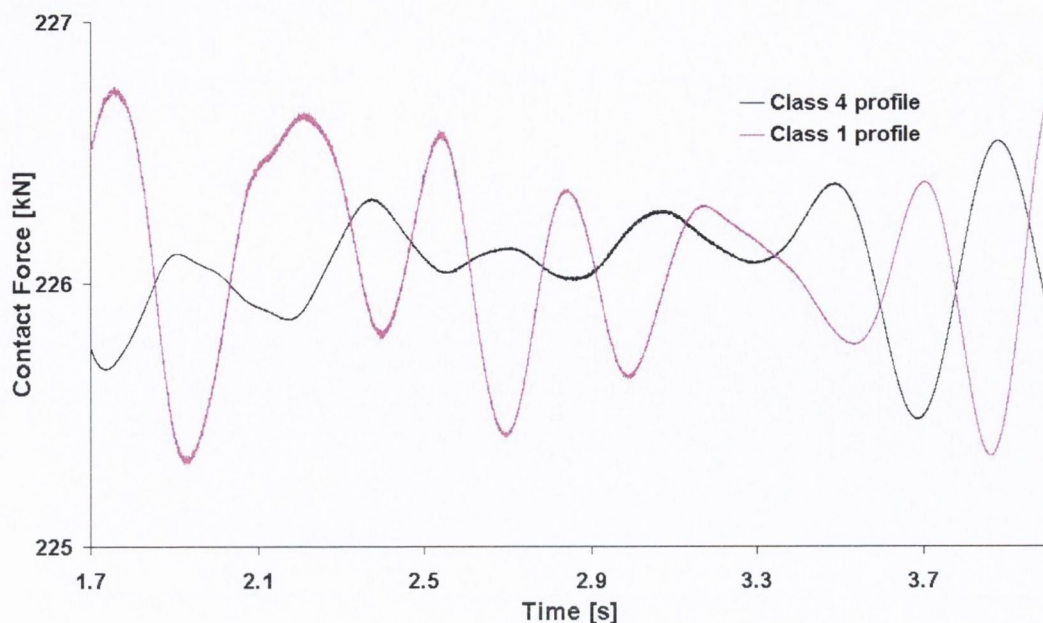


Fig. 5.10: Contact force variation at velocity of 40ms^{-1} for FRA PSD functions to six are specified. Once again, like the FRA functions, Grade 1 is the worst line and 6 the best. The ARS PSD function is given by

$$S_{xx}(\Omega) = \frac{kA_v\Omega_c^2}{(\Omega^2 + \Omega_c^2)\Omega^2} \quad (5.29)$$

where k and Ω_c are constants equal to 0.25 and 0.131m^{-1} respectively. The upper and lower frequency bounds over which the PSD is defined are 0.02 and 2m^{-1} . It is the variation A_v that controls the line standard. The two irregularity PSD functions, FRA and ARS, are illustrated in Figure 5.11.

A sample of the contact force variation resulting from this particular PSD function (Grades 1 and 4 once again) is illustrated in Figure 5.12. The ARS PSD functions give rise to much greater contact force magnitudes and higher frequency content than the FRA functions. This result is expected due to the greater rms value obtained through integration of the ARS curve. However, it does illustrate the discrepancies that exist between different track roughness PSD functions.

The ARS Grade 1 profile results in a contact force rms of 12.36kN while the

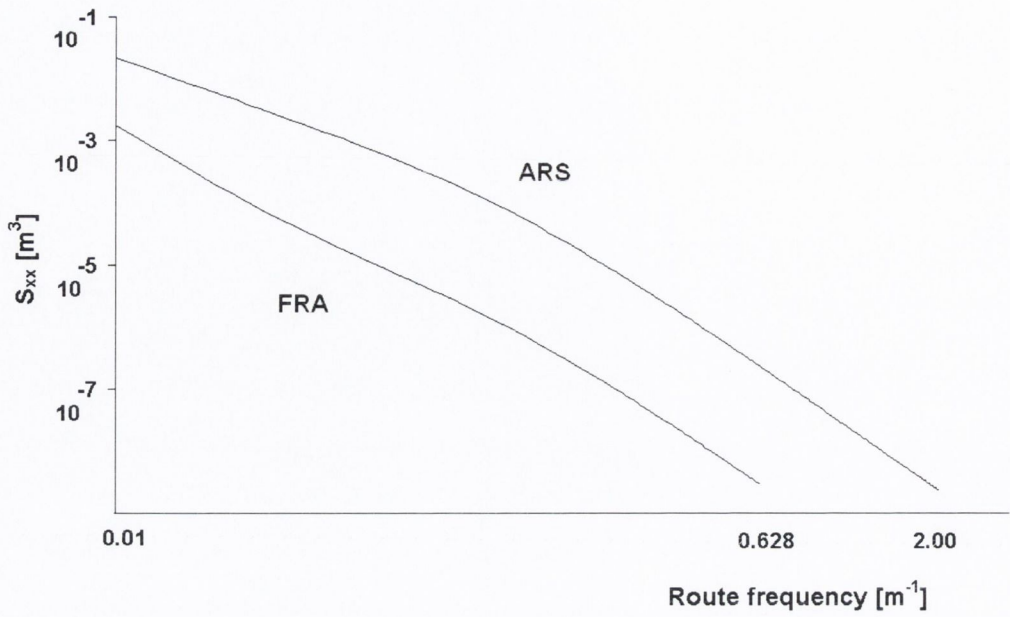


Fig. 5.11: Comparison of FRA and ARS Class 4 PSD functions

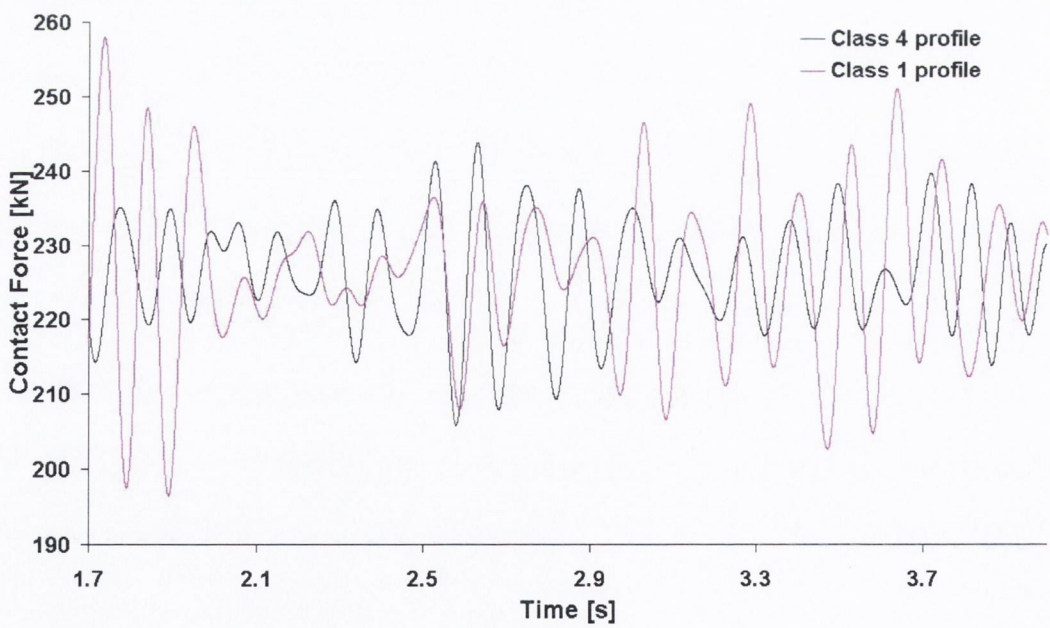


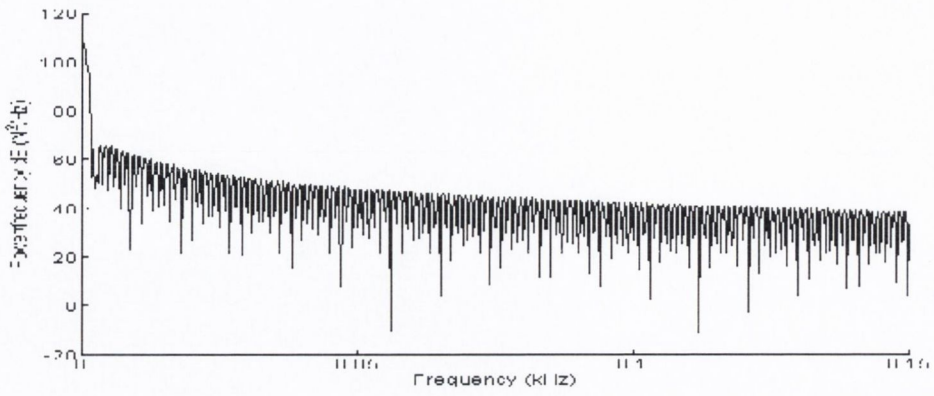
Fig. 5.12: Contact force variation at velocity of 40ms^{-1} for ARS PSD functions

Grade 4 profile equivalent is 7.88kN. The values for the FRA Class 1 and 4 profiles are 0.459kN and 0.218kN respectively, significantly smaller than the ARS irregularities. In addition to the higher variance the frequency characteristics of the contact force waveforms differ greatly. Figures 5.13, 5.14, 5.15 and 5.16 illustrate the PSD functions for the wheel-rail contact forces for the four characteristic profiles considered.

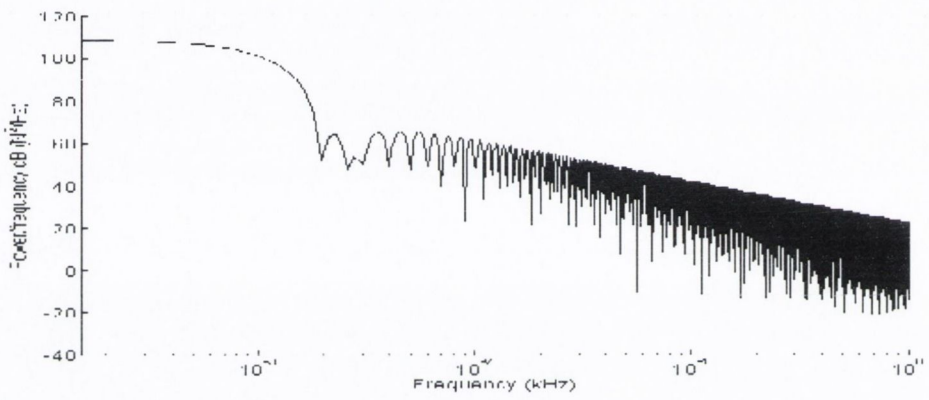
The contact force PSD frequency distributions are all concentrated in a low frequency range. This concentration is due to the track irregularity input frequency characteristics which are low frequency. Note once again that the continuous BEF model does not include the effect of discretely supported sleepers which would generate harmonic impulses at higher frequency levels (Lei & Noda 2002).

In the case of the ARS profiles it is noticeable that there is a visible peak in the contact force PSD at approximately 10Hz. This equates approximately to the natural frequency of vibration of the bogie mass itself. There is also a lesser peak at a slightly higher frequency corresponding to the natural frequency of bogie rotation about its centre of mass.

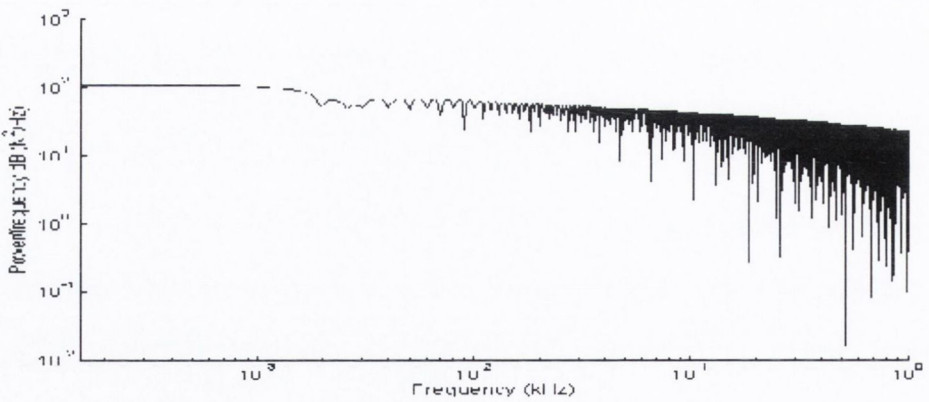
The effect of velocity is significant upon considerations of contact force process response. A similar series of analyses was carried out for a vehicle velocity of 70ms^{-1} . The contact force rms values for the Class 1 and 4 FRA profiles increased to 2.43kN and 1.18kN respectively. The maximum contact force observed for the 40ms^{-1} velocity analysis was approximately 227kN while this value increased to over 230kN for the case of 70ms^{-1} velocity. This effect is more pronounced for ARS PSD generated profiles. The maximum observed contact force exceeded 300kN for the Class 1 track while the maximum for the Class 4 track was approximately 286kN. All variance in contact forces takes place relative to a static force of 226kN.



(a) Cartesian

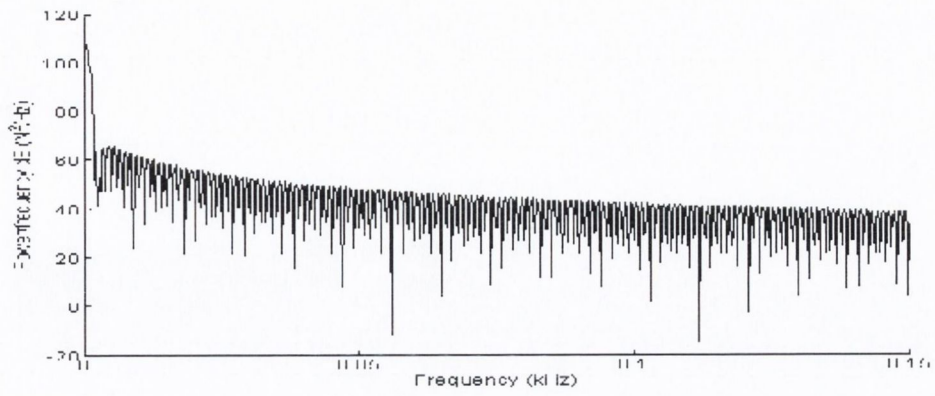


(b) Semi-log

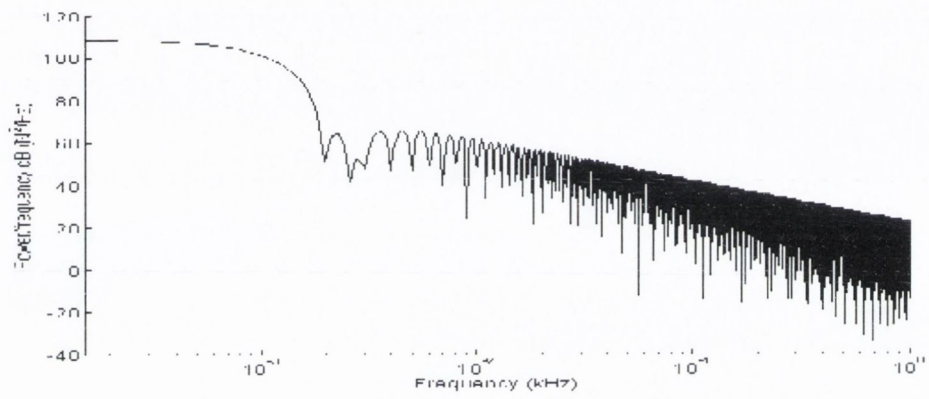


(c) Log-log

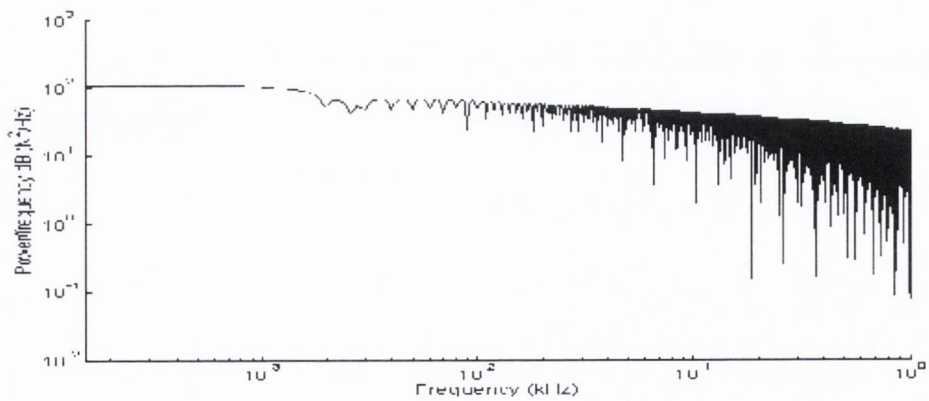
Fig. 5.13: Contact force PSD for FRA Class 1 profile irregularity at 40ms^{-1}



(a) Cartesian

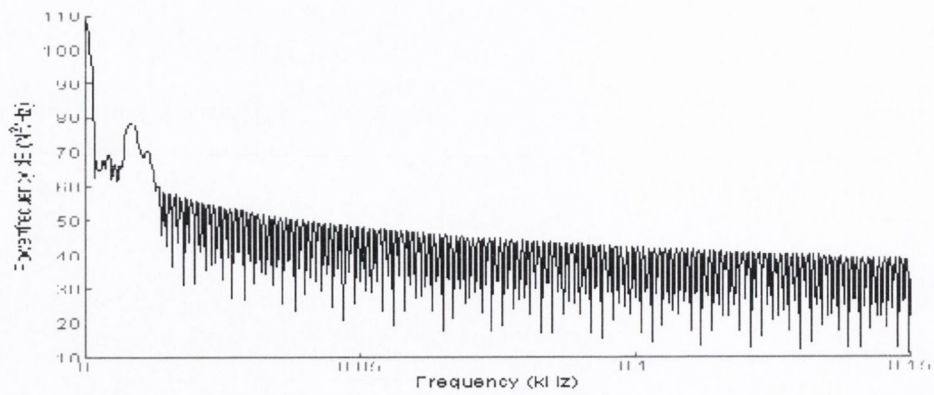


(b) Semi-log

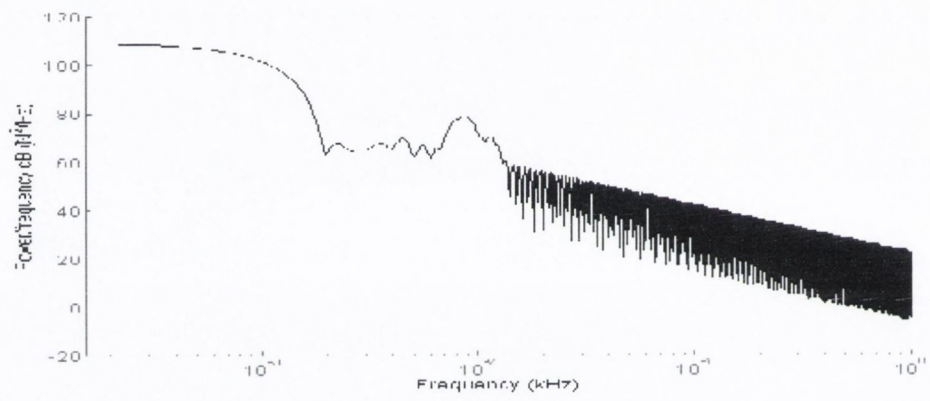


(c) Log-log

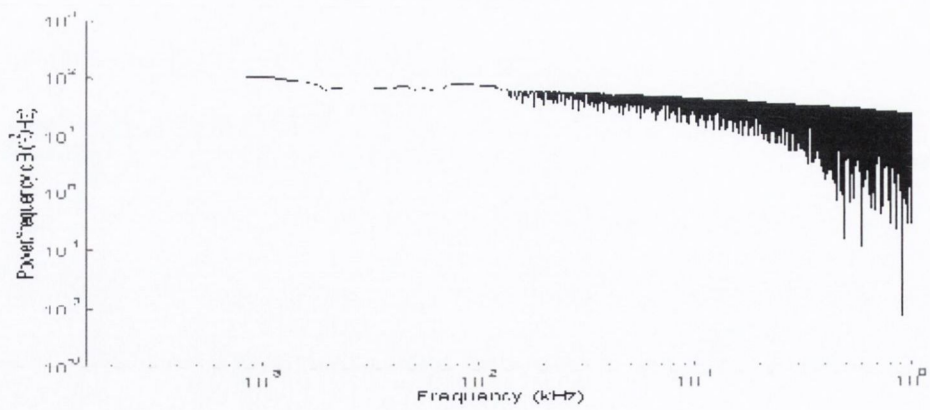
Fig. 5.14: Contact force PSD for FRA Class 4 profile irregularity at 40ms^{-1}



(a) Cartesian

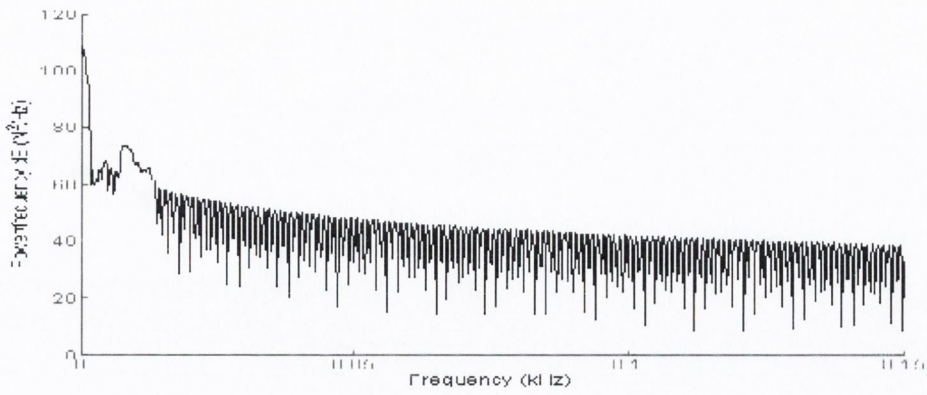


(b) Semi-log

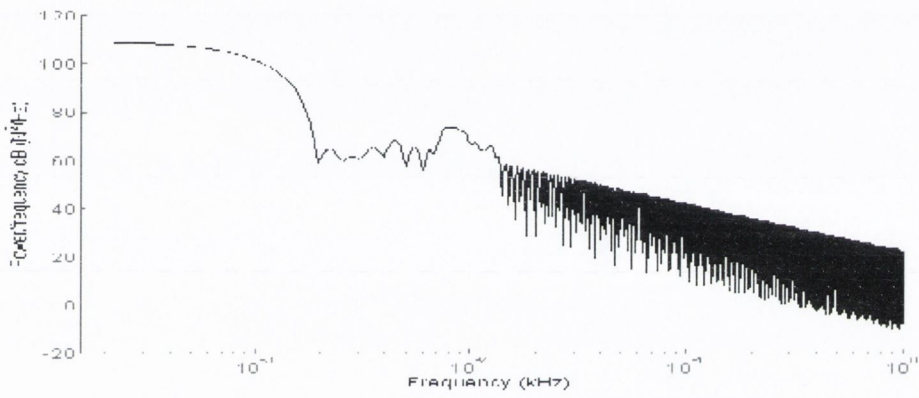


(c) Log-log

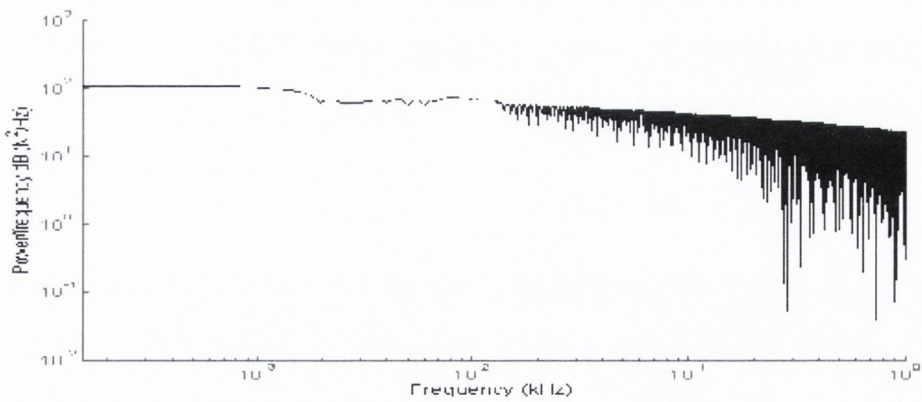
Fig. 5.15: Contact force PSD for ARS Grade 1 profile irregularity at 40ms^{-1}



(a) Cartesian



(b) Semi-log



(c) Log-log

Fig. 5.16: Contact force PSD for ARS Grade 4 profile irregularity at 40ms^{-1}

5.5 Effect of Non-linear Hertzian Spring

A comparison is made here between the mean square contact forces calculated using the finite difference beam model and the equivalent forces calculated by applying the frequency domain approach of Chapter 4. The obvious difference between the two model formulations is in the modelling of the wheel-rail Hertzian contact. The purpose of this is to determine the validity of the Hertzian contact spring linearisation for applications involving random rail irregularity.

The frequency domain model is linear. However, the linearisation of the Hertzian contact spring is dependent upon the static contact force F_{stat} . The linear spring constant, k_H is calculated from the equation ((Esveld 2001):

$$k_H = \frac{dF}{dy} = \frac{3}{2} c_H^{2/3} F_{\text{stat}}^{1/3} \quad (5.30)$$

It follows from Equation 5.30 that the application of the 250kN preload that was applied to the bogie model in this Section 5.4 results in a different k_H value. The frequency domain analysis was therefore carried out for two different k_H values, $1.43 \times 10^9 \text{Nm}^{-1}$ and $1.88 \times 10^9 \text{Nm}^{-1}$, corresponding to models without and with the preload applied respectively (F_{stat} values of 101.043kN and 226.043kN, ie. tare and fully laden). The transient analysis of the quasi-infinite beam model was also carried out with and without the application of the preload.

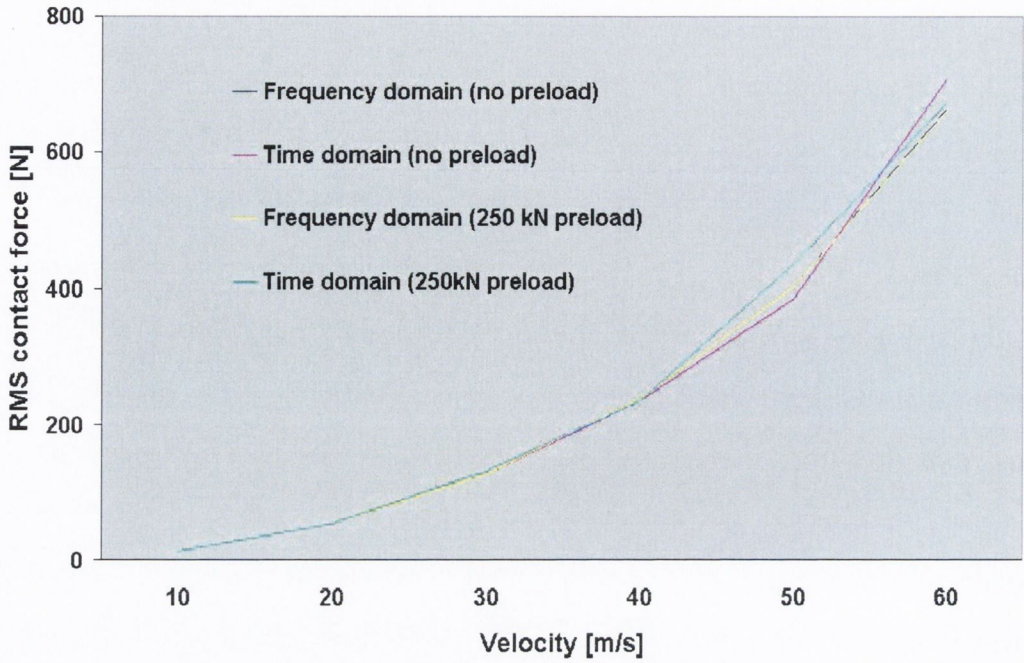
While the analyses described in Chapter 4 were based on a similar mathematical model, the model parameters were based on a flatbed wagon vehicle. In this case, the model parameters are those of a single bogie. The difference between the contact force process variances at the front and rear wheelset is negligible at the velocities tested for these bogie model parameters. This is in contrast to the contact forces for the flatbed wagon model, which showed significant differences between contact forces at the respective wheelsets.

The comparison was carried out using FRA and ARS Class 4 profiles and bogie

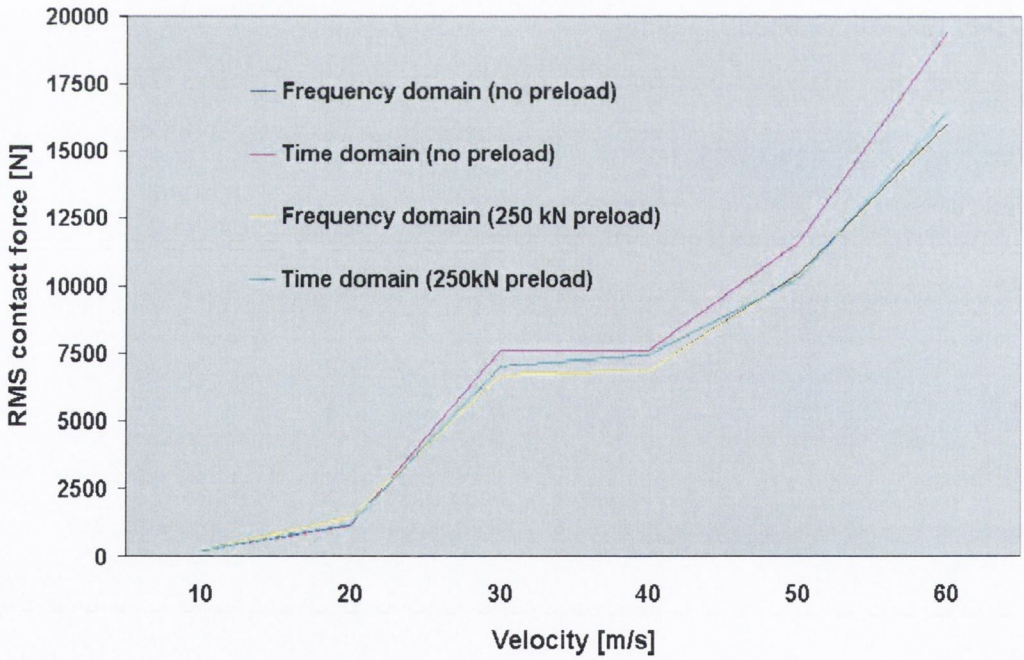
models with and without the 250kN preload. The FRA data showed good agreement both between the frequency and time domain analyses and regardless of the imposition or otherwise of the 250kN preload (Figure 5.17(a)). This is especially true at the lower velocities while at higher velocities there is small deviation. Note that the frequency domain results are, as expected, identical, due to the linearity of the system.

From Figure 5.17(b) however, it is observed that there is a more significant effect for the ARS profile. The numerically calculated rms values deviate from the equivalent frequency domain results. This deviation is greater when the 250kN preload is not included in the numerical analysis. Comparison of the numerical results as a percentage of the equivalent frequency domain results shows that the error in the assumption of a linearised Hertzian contact spring is more significant for the higher frequency ARS profile.

It is thus concluded that the linearisation of the Hertzian spring is less valid for higher frequency random excitation. The greater deviations of the numerical analysis results from the frequency domain results in the case of the higher frequency FRA profiles demonstrates this, as does the general trend of greater deviation at higher velocities.



(a) FRA Class 4 irregularity



(b) ARS Class 4 irregularity

Fig. 5.17: Comparison of frequency and time domain analysis results

5.6 Observations and Conclusions

The track profiles tested throughout this chapter have been numerically generated based on smoothed PSD functions described by empirical formulae. The resultant contact force time-histories varied greatly depending upon the profile PSD that was applied in a particular instance. Figure 5.18 illustrates the significant differences between the Class 4 profiles generated using the FRA and ARS PSD functions over a 100m track length. The rms displacements for the two functions vary between 2.764mm (FRA) and 9.164mm (ARS), which is significant. However, also significant is the different frequency content of the PSD functions which is readily observed by inspection of the numerically generated profiles. The ARS profile contains a significantly greater higher frequency content. The interaction between wheel and rail, being of high frequency characteristic, is more susceptible to the ARS PSD function excitation, hence there is greater variance of the contact force process for the ARS function.

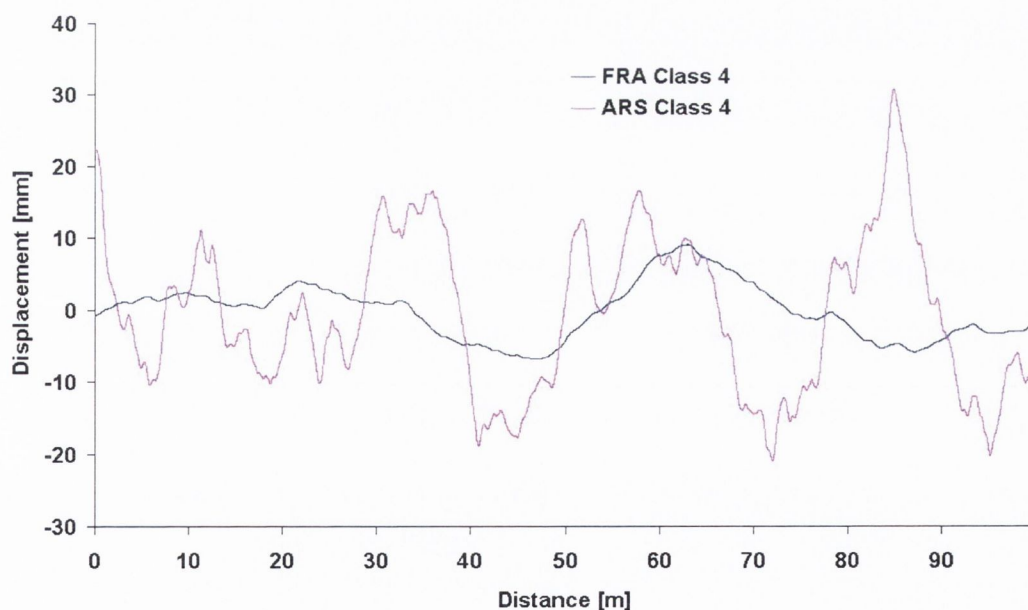


Fig. 5.18: Sample vertical track profiles 100m in length

The study has shown that random irregularities can generate contact forces that

are significantly in excess of the static forces. This was not the case for the FRA spectra. However, there are a great number of PSD functions that have been used in analysis of the wheel-rail interaction. Frýba (1996) cites a number of these empirical functions including those used by the Czechoslovak State Railways (CSD) and French National Railways (SNCF). When the ARS PSD function was applied to the finite difference quasi-infinite beam model the contact force variation was significantly greater than for the FRA PSD function.

It has been shown that the assumption of a linearised Hertzian spring for the frequency domain analysis of Chapter 4 is valid for low frequency random profile irregularity. However, the assumption is not valid for higher frequency irregularity. This is especially true for lower static wheel-rail contact forces where the Hertzian linearisation of the Hertzian contact spring is more sensitive to varying force (see Figure 5.19).

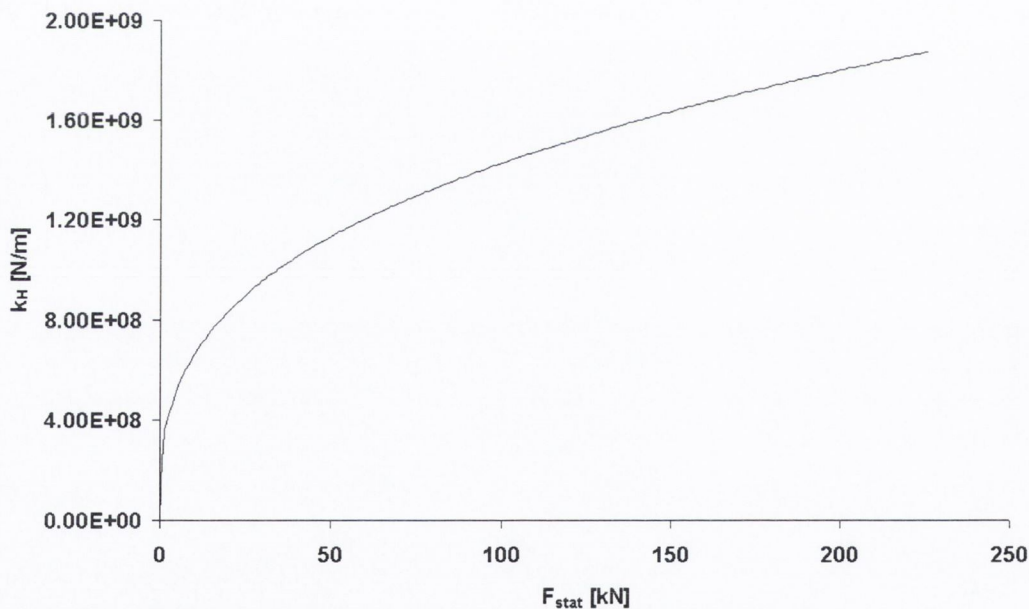


Fig. 5.19: Variation of linearised k_H value with static load

The primary drawback of the quasi-infinite beam model is that it does not include the effect of discrete sleeper spacing. The assumption of a continuous elastic

foundation, though sufficient for the investigation of the system response to random irregularities of relatively low frequency, is not suitable for application to high frequency input at the wheel-rail interface. However, the model is advantageous in that the non-linearity of the Hertzian spring can be easily incorporated and the system response calculated over any desired length of railway track.

Chapter 6

Finite Element Track Model with Applications to Discrete Defects

6.1 Introduction

The analyses detailed in the previous three chapters (3, 4 and 5) have considered only the specific effects of random railway track irregularity on the dynamic vehicle-track interaction. This chapter moves on from the investigation of these random track defects to consider discrete irregularities in the wheel-rail contact geometry. The effect of a number of different types of geometric imperfections on the interactive wheel-rail contact process are considered in this study. The particular irregularities considered are vehicle wheel flats, unsupported sleepers, and dipped joints. These imperfections considered may both be categorised as discrete, or isolated, irregularities. One of the defects considered, the wheel flat, may be further categorised as periodic. This periodicity occurs due to the constant repeated rolling of the flat part of the wheel over the track surface, the frequency of excitation is dependent upon the wheel radius and the vehicle velocity. However, when the effect of a single impact is considered the defect may be classified as isolated. The effect of soft and stiff ballast beds on the system response is also investigated.

The FDM quasi-infinite beam track model developed in Chapter 5 has proved adequate for the purpose of modelling the wheel-rail contact forces that occur as a result of low frequency track irregularity. The empirical PSD functions that have been specified by the FRA and ARS for random irregularity can be categorised as such. For higher frequency events, however, it is found that the resultant modelled contact forces deviate substantially from previously published results (Dong et al. 1994). In the specific case of wheel flats the impact factors numerically calculated were found to be far in excess of previously published estimates (Dong et al. 1994, Thompson et al. 2003). This deviation may be due to a number of reasons, but is primarily a resultant of the simplification of the multi-layer track-sleeper system as a single beam. Dong et al. (1994) suggest that only a small part of the sleeper mass can take part during impact at these types of high frequency events. As a result, the lumping of the sleeper mass with the rail largely overestimates the impact loads. Hence, a new track model, incorporating separate rail and sleeper components, is developed here for the purpose of investigating the effect of high frequency discrete type irregularities.

The finite element method (FEM) is used as the mathematical basis for modelling the railway track system. The track is modelled as a continuous beam using Timoshenko beam elements supported at discrete intervals. According to a review completed by Knothe & Grassie (1993) such a model is appropriate for a frequency range up to about 2.5kHz, a range that is adequate for modelling the dynamic effects of wheel flats. Positioned at the aforementioned discrete intervals are lumped point masses representative of track sleepers. The track is supported above the sleepers by means of railpads; these components are modelled as discrete spring-damper elements. The track ballast bed is assumed to lie upon an underlying rigid foundation. The ballast itself is discretised by a series of spring-dampers, with characteristics similar to the pad elements, situated directly below the sleepers (see Figure 6.1).

All results generated throughout the chapter are derived using time domain

analyses. Numerical solutions of the governing differential equations of motion of both vehicle and track systems are obtained by means of a time-stepping technique. The fourth order Runge Kutta method is applied for this purpose throughout.

6.2 Track System Model Formulation

6.2.1 Model Assumptions

Prior to proceeding with the formulation of the computational models of the railway track a number of assumptions are made regarding the dynamic system models of both the track and vehicle.

1. The entire system model is planar and the dynamic responses of both the track and vehicle models are calculated solely in the vertical plane, ie. only one half of the vehicle and track structures are modelled. Hence, an initial assumption of symmetry of the system is made and the respective mass, damping and stiffness parameters from both sides of a three-dimensional vehicle are added appropriately;
2. The dynamic responses of both the track and vehicle models are calculated as unique functions of the wheel-rail contact forces that occur at the wheel-rail coupling interface. As a result the dynamic load input to both systems takes place in the vertical direction only, ie. only vertical dynamic loads are considered in the model;
3. The standard Hertz expression for two elastic cylinders in perpendicular contact is applied to calculate the magnitude of the interactive contact forces. A non-linear Hertzian spring stiffness, c_H , of $100 \times 10^9 \text{N/m}^{3/2}$ is assumed throughout;
4. The track rail is considered as a finite series of individual beams of finite length. The rail is supported at regular intervals by massless spring damper elements

modelling the rail pads. These elements are, in turn, supported upon discrete sleepers. The railway track ballast is represented by discrete, massless springs at each of the sleepers. The model is formulated such that the positions of the sleepers coincide with the Timoshenko beam element nodes. The sleepers are therefore placed at appropriate nodes of these beam elements;

6.2.2 Finite Element Matrices

Unlike the previous chapter's quasi-infinite beam model this structure is finite in space. This conceptual track model is illustrated in Figure 6.1. The rail model boundary conditions are such that the nodes at both beam model extremities are free in both translation and rotation. It is ensured throughout the analyses that the dynamic response is considered at a sufficient distance from the beam extremes. This is achieved by keeping the track model boundaries at a sufficient distance from the load application points.

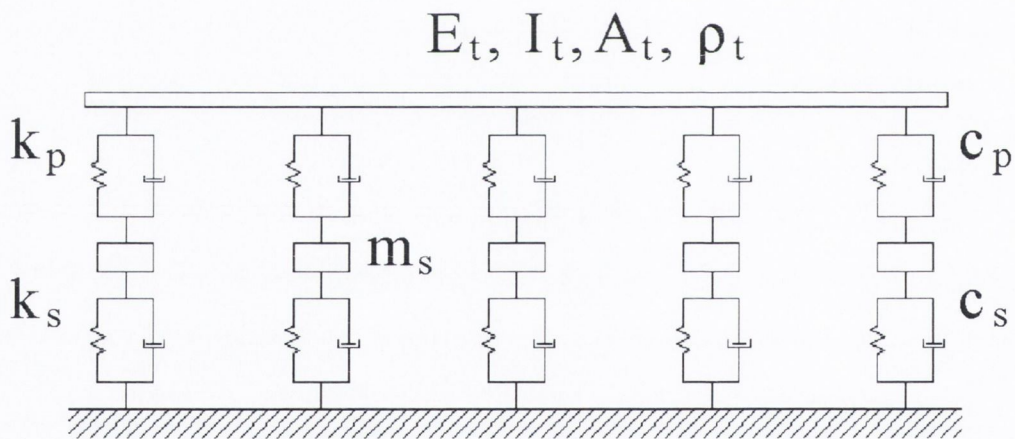


Fig. 6.1: Railway track model

The track model is made up of plane Timoshenko beam elements with bending stiffness $E_r I_r$ and shear stiffness $T_r G_r A_r$. Bending and shear strains are continuous at all points within this beam model. The Timoshenko beam element differs from the

Bernoulli-Euler element in that, while both have identical degrees of freedom, the Timoshenko model includes a first order correction for transverse shear flexibility. The extent of this flexibility is dependent upon the rail steel shear modulus G_r and the shear area of the rail section, $T_r A_r$ (T_r is the shear coefficient). The Timoshenko beam element is a four degree of freedom element with nodal coordinates described as follows:

$$\{\eta^e\} = \{u_n^e \theta_n^e u_{n+1}^e \theta_{n+1}^e\}^T \quad (6.1)$$

where u_n^e and θ_n^e are the elemental vertical displacement and rotation of the beam at node n .

The elemental stiffness matrix for the Timoshenko beam element, $[k]_e$, is given by

$$[k]_e = \frac{E_r I_r}{L_e^3 (1 + \Phi)} \begin{bmatrix} 12 & 6L_e & -12 & 6L_e \\ 6L_e & L_e^2(4 + \Phi) & -6L_e & L_e^2(2 - \Phi) \\ -12 & -6L_e & 12 & -6L_e \\ 6L_e & L_e^2(2 - \Phi) & -6L_e & L_e^2(4 + \Phi) \end{bmatrix} \quad (6.2)$$

where L_e is the elemental length and Φ is a constant given by

$$\Phi = \frac{12EI}{T_r G_r A_r L_e^2} \quad (6.3)$$

The Timoshenko mass matrix, $[m]_e$, is composed of the standard Bernoulli-Euler beam mass matrix and an additional component that allows for the rotary inertia under the Timoshenko beam assumptions regarding shear.

$$\begin{aligned}
[m]_e = & \frac{\rho_r A_r L_e}{420} \begin{bmatrix} 156 & 22L_e & 54 & -13L_e \\ 22L_e & 4L_e^2 & 13L_e & -3L_e^2 \\ 54 & 13L_e & 156 & -22L_e \\ -13L_e & -3L_e^2 & -22L_e & 4L_e^2 \end{bmatrix} \\
& + \frac{\rho_r I_r}{30L_e} \begin{bmatrix} 36 & 3L_e & -12 & 3L_e \\ 3L_e & 4L_e^2 & -3L_e & -L_e^2 \\ -12 & -3L_e & 36 & -3L_e \\ 3L_e & -L_e^2 & -3L_e & 4L_e^2 \end{bmatrix} \quad (6.4)
\end{aligned}$$

An equivalent Bernoulli-Euler beam model stiffness matrix may be derived from this matrix by taking a very large value for the shear modulus. Similarly, the Bernoulli-Euler mass matrix is obtained by dropping the rail rotational inertia, I_r in the mass matrix.

The spring-damper elements of the track model behave linearly in compression. However, provision is required to be made in the model, in some cases, for rail lift-off from the sleeper and sleeper lift-off from the ballast (Dong et al. 1994). When either of these situations occur the track system matrices are adjusted accordingly so that the appropriate damping and stiffness values are set to zero. The track and sleeper displacements are checked and the appropriate values of the spring and damping constants applied at every time-step for this purpose.

For reference purposes, the values for the track system parameters are similar to those applied by Lei & Noda (2002). The properties of the rail section and other applicable parameters are listed in Table 6.1. These properties are based on the CEN design rail section 56 E 1 (previously RT113A).

6.2.3 Steady State Response

The so-called steady state interaction is an idealised situation in which the rails are perfectly smooth, the wheels have no defects, the track structure is uniform and the

Parameter	Symbol	Unit	Value
Rail cross-section area	A_r	m^2	7.17×10^{-3}
Rail second moment of area	I_r	m^4	2.35×10^{-5}
Young's modulus	E_r	Nm^{-2}	2.07×10^{11}
Shear modulus	G_r	Nm^{-2}	81.0×10^9
Shear coefficient	T_r	—	0.34
Rail mass per length	μ_r	kgm^{-1}	56.0
Rail material density	ρ_r	kgm^{-3}	7.810×10^3
Rail pad stiffness	k_p	Nm^{-1}	2.8×10^8
Ballast spring stiffness	k_b	Nm^{-1}	4.66×10^7
Rail pad damping	c_p	Nsm^{-1}	3.0×10^4
Ballast spring damping	c_b	Nsm^{-1}	4.0×10^4
Sleeper mass	m_s	kg	250

Table 6.1: Track model parameter values

vehicle structure is perfectly symmetric (Hou et al. 2003). The latter condition does not apply to this analysis due to the planar nature of both the track and vehicle models. The steady state system reaction provides information on the minimum variation in the dynamic forces generated as a railway vehicle moves along a track. The steady state response of the railway-track vehicle system is analysed here initially as a means of validating the system model prior to incorporating geometric contact area defects. It is also important to observe the steady state response as the steady state dynamics can influence the effect of these defects.

The total length of the railway track model is 42m (or 70 sleeper spacings). However, in order to minimise boundary effects within the track system model, the track and vehicle responses are recorded only over the central section of the beam, at a minimum of 15m (25 sleeper spacings at 0.6m each) from the track model extremes. Dukkupati & Dong (1999) suggest that the steady state interaction is usually obtained after the vehicle has travelled about 4 to 5 sleeper spacings in the conventional train speed range. At higher speeds it requires a longer distance to reach the steady state. Further, Lei & Noda (2002) state that previous computation experience has shown that a 20m distance from the rail ends is required for the boundary effects of the finite track model to be considered negligible. As this 42m long track model is not of sufficient length to fulfill this criterion a number of comparative preliminary tests were carried out using progressively shorter track models. Although 20m was suggested by Lei & Noda (2002), these tests showed that 15m was adequate for this purpose. At this distance, significantly different results were not observed in comparison to longer track models. This reduction in size of the track model matrices enabled the simulations to be carried out in a significantly shorter length of time. It is assumed throughout this study that all starting transients that may have been induced by initialising the vehicle motion have been sufficiently damped out, and that boundary effects are negligible, by the time the vehicle has travelled to the 15m point along the track model.

The FE Timoshenko beam elements are, for this purpose, formulated such that their length is equal to one half of the sleeper spacing, 0.3m. This is the minimum number of elements that can accurately describe the track deflection at intermediate points between sleepers as a function of the nodal deflections and rotations. When a model with a single element between each sleeper, similar to the model of Lei & Noda (2002), was tested, it is found that the correct displacements at intermediate points in the element cannot not be determined from the shape functions.

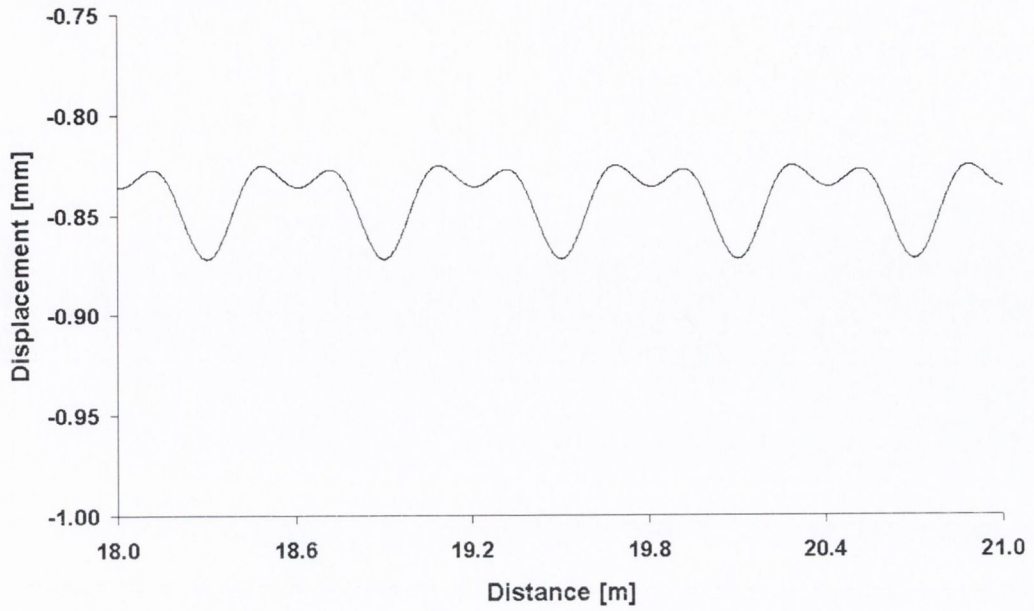
The track model response is initially calculated under the action of a single moving constant force equivalent to a 15,192kg mass. This is the simplest possible moving load case. Figure 6.2(a) illustrates the track displacement response at the point of application of the force. Rail lift-off from sleepers and sleeper lift-off from the ballast are not considered here, ie. the spring damper elements of the track system model behave perfectly linearly in both tension and compression. The dominant periodic wave (ie. that of largest magnitude) in the response is equal in wavelength to the sleeper spacing. This characteristic is in agreement with previous studies in the literature (Dong et al. 1994, Dukkipati & Dong 1999, Hou et al. 2003, Lei & Noda 2002, Nielsen & Igeland 1995, Wu & Thompson 2004). Further frequency characteristics of the response vary throughout the literature due mainly to different applied loading conditions, but also due to varying track model formulations.

Figure 6.2(b) shows the respective variations in the rail-pad and the idealised ballast spring forces at the central sleeper as the moving force passes above it. The peak forces created by the passage of the moving force are approximately 65kN for both the pad and the ballast spring, the ballast force being slightly greater due to the additional sleeper weight. This figure is approximately 2.3 times smaller than that of the static wheel-rail contact force. Hou et al. (2003) calculated corresponding values of approximately 3.0 times smaller than the static force. However, the vehicle modelled by Hou et al. was a double wheel-rail Hertzian contact model where the interaction between two wheelsets was taken into consideration, which has not been

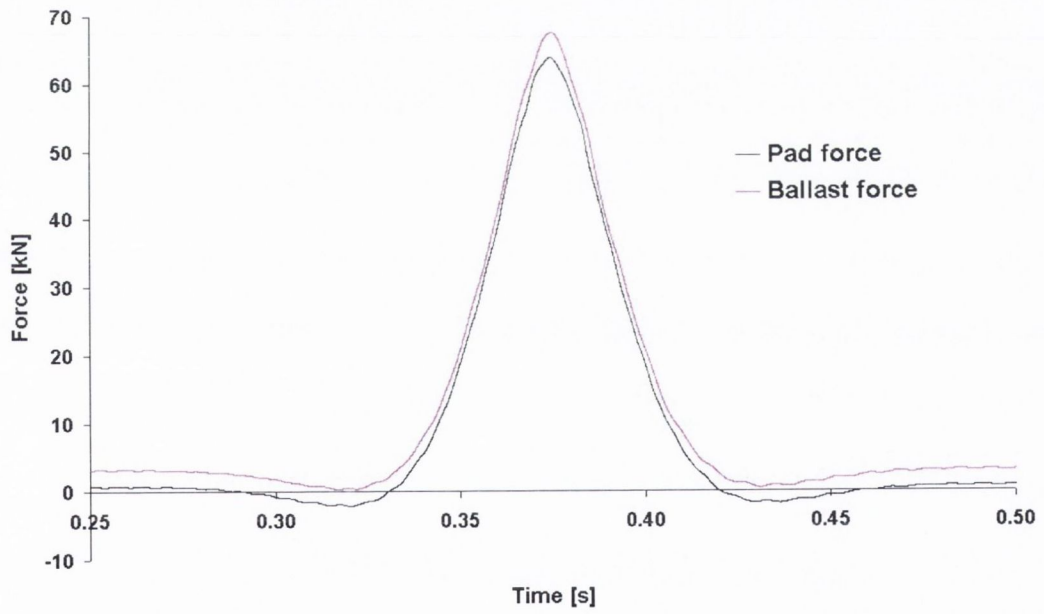
the case here. Effectively, the load was shared between two sleepers.

The loading function is now developed further from a constant force to a system of sprung masses representing a vehicle bogie. The vehicle model is developed so that it has two track contact points (wheelsets) and possesses four degrees of freedom in the vertical plane. Three point masses are representative of a vehicle bogie and two wheelsets. The total mass of the bogie itself is 3,000kg, to which a further static force of 250kN is applied vertically. The wheelset masses are each 950kg. The combination of these masses and forces results in static wheel loads of 149.0345kN, which was the equivalent magnitude of the single point force considered previously. The bogie model suspension spring elements each have stiffness values of $1.5 \times 10^7 \text{Nm}^{-1}$ and damping values of $3.2 \times 10^3 \text{Nsm}^{-1}$. The rotary inertia of the bogie itself about its centre of mass is 2,900kgm². These parameter values are based on the vehicle parameters applied by Nielsen & Igeland (1995). The wheel-rail contact force, a function of the relative displacement between wheel and rail, is based on the non-linear Hertzian contact theory with a c_H value of $100 \times 10^9 \text{N/m}^{3/2}$.

At this point in the analysis of the steady state response the effect of applying rail lift-off from the sleepers and sleeper lift-off from the ballast are also considered. This non-linearity incorporated into the track model allows for the fact that the sleepers are not heavy enough to remain in contact with the ballast throughout and that the pads do not always hold the rail to the sleepers. This particular part of the steady state analysis was carried out in a similar manner to the study of Dong et al. (1994). The wheel-rail contact force variations in the steady state are illustrated for both track models in Figure 6.3. The responses are quite similar but the non-linear track model does generate slightly higher maximum and lower minimum peak forces, the difference being less than 1% in both cases. There are two distinct periodic waves in both of the contact force histories. The major wave is caused by the sleeper spacing effect. The dynamic peak force occurs at approximately two thirds distance along the sleeper spacing.



(a) Rail displacement at point of application of force



(b) Rail-pad and ballast spring forces at central sleeper

Fig. 6.2: Steady state response of track system model to constant force moving at 40ms^{-1}

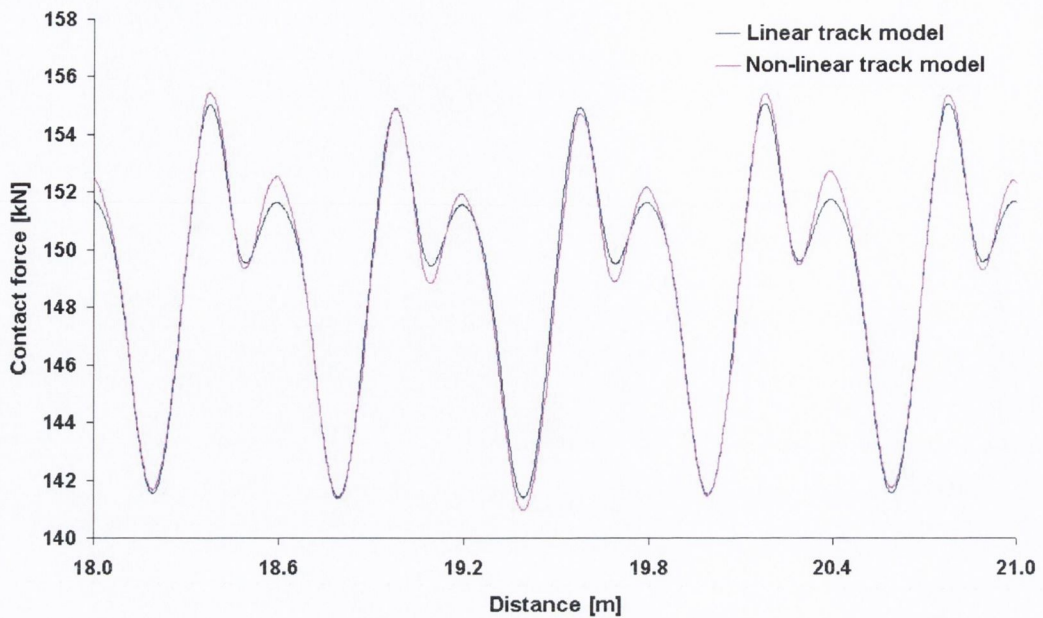
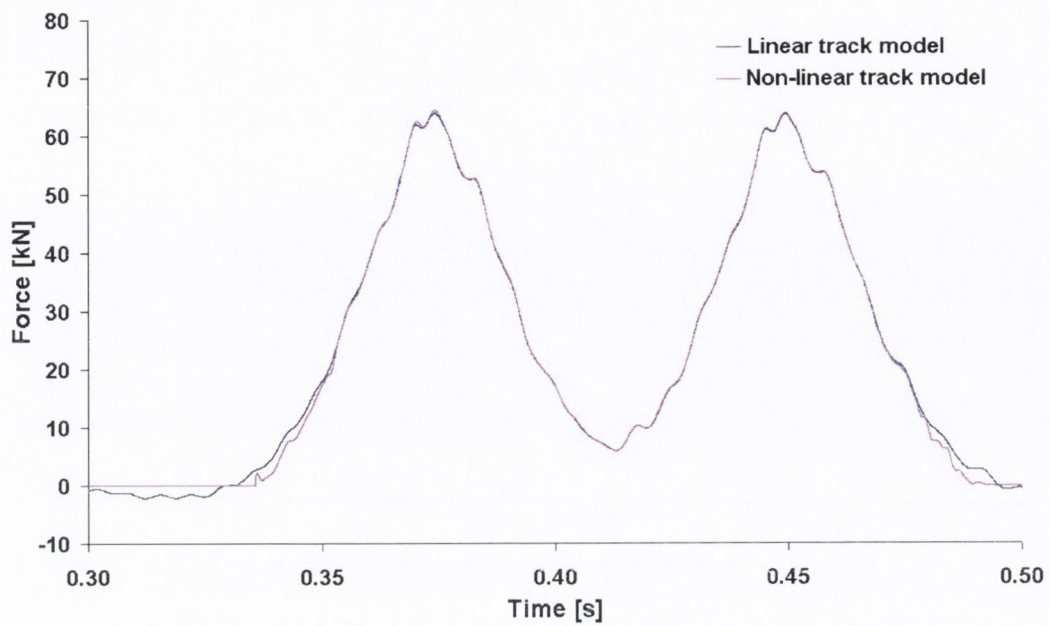


Fig. 6.3: Wheel-rail contact forces comparison

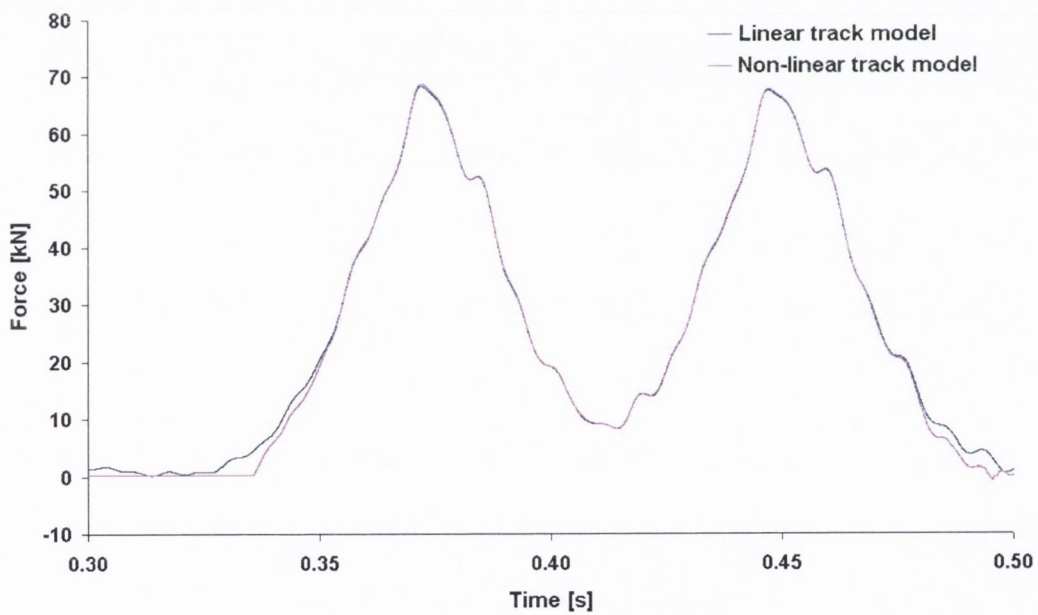
Figure 6.4 illustrates the pad and ballast force variations for both track models. The peak forces are once again similar with very slightly higher magnitudes for the non-linear model, although the difference is negligible. The two peaks in the force histories are due to the two bogie wheels (passing at a $\frac{3\text{m}}{\text{velocity}}$ time interval).

Because the comparison of the linear and non-linear track system model yielded information that showed that the wheel-rail contact, rail pad and ballast forces obtained were similar for both, it was decided to proceed with the linear track model, which has been the more prevalent model in the literature (? , Lei & Noda 2002, Nielsen & Igeland 1995). The wheel and rail displacements at the point of wheel-rail contact are illustrated in Figure 6.5. The rail displacement, as previously identified for the constant force load case, displays a predominant wavelength equal to the sleeper spacing. The wheel displacement also displays the sleeper spacing characteristic wavelength.

The time histories of these displacements appear identical but this is not the case and there are fluctuations in the wheel-rail contact force histories. The peaks



(a) Rail pad force variation



(b) Ballast force variation

Fig. 6.4: Rail pad and ballast forces model comparison at central sleeper

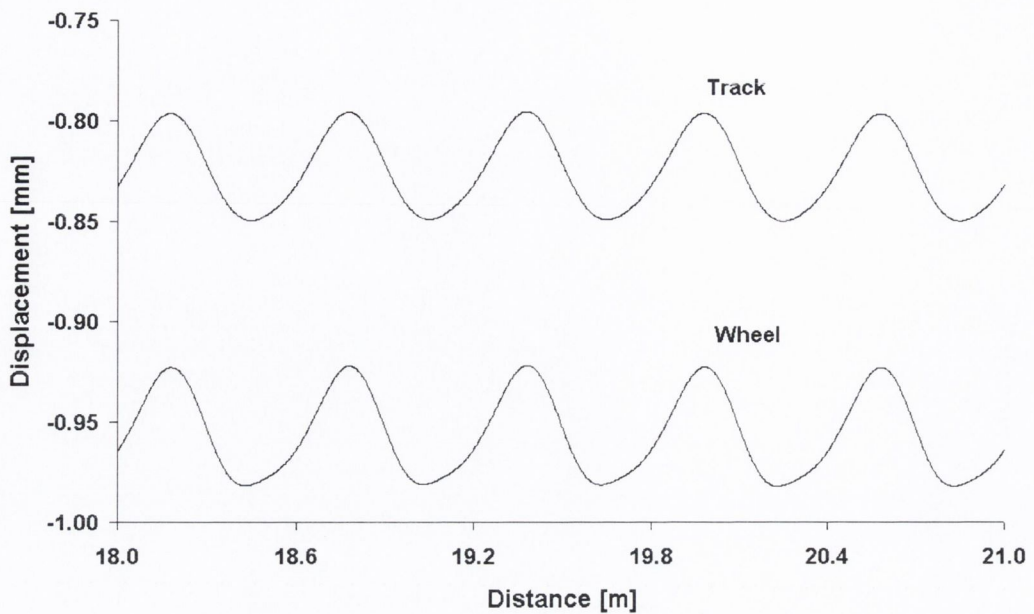


Fig. 6.5: Wheel and rail displacements in steady state

obtained in the steady state contact force variation compares well with the study of Dukkupati & Dong (1999), from whose model the parameter values applied in this analysis were obtained. The contact force varies between approximately 5% above and 5% below the static value. Other studies have shown greater amplitudes in the extent of this variation. Sun & Dhanasekar (2002) and Dong et al. (1994) have obtained steady state contact force factor values of approximately 5% and 7% respectively. The different model parameters, and indeed physical characteristics, applied throughout the literature give rise to large variations in the reported steady state contact force factors.

6.3 Wheel Flat

6.3.1 Wheel Flat Model

The first type of geometric defect in the wheel-rail contact area considered is a wheel flat. A railway vehicle wheel flat is a flat part of the wheel circumference caused

by unintentional sliding of the wheel under braking. Wheel flats generally result in a severe out-of-roundness of the wheel profile and give rise to potentially large dynamic vehicular effects. In addition, the influence of out-of-roundness of a railway vehicle wheel on the dynamic train-track interaction is often considerable (Nielsen & Igeland 1995). Wheels with flats produce high levels of impact loading to the track, which can lead to extensive damage of the various track components. Typical wheel flats are around 50mm in length but in extreme cases may measure up to 150mm (Thompson et al. 2003).

Figure 6.6 depicts a schematic representation of this type of wheel deformation. L represents the length of the wheel flat, while d is its depth (alternatively described as the maximum decrease in wheel radius). The radius of the wheel is referred to as r throughout and ϕ is the angle subtended at the centre of the wheel by two radial lines extending to the extremes of the wheel flat length.

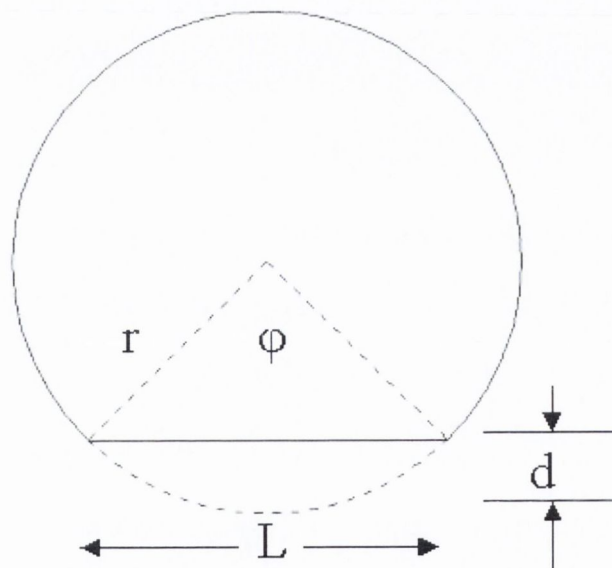


Fig. 6.6: Idealised wheel flat

The flats considered in this particular study are based upon idealised representations of the geometrical profile of a wheel with a flat (as in Figure 6.6). In reality,

flats do not have definite extents, but following their initial formation become worn at their corners due to the high load concentrations at these points. While the illustrated idealised geometric shape could be modelled by implementing a straightforward dip in the vertical track profile, the effect of a worn flat requires a more complex irregularity function.

Figure 6.7 illustrates the movement of the wheel during rotation through the flat point on the circumference. The shape of the flat wheel can be seen to correspond to a circular arc dip in the railhead. An expression for the profile irregularity function for a wheel flat is given by Dong et al. (1994) (see Equation 6.5). This cosine function has been found to provide a good approximation (Tunna 1988) and will be applied in this study.

$$f(x) = \frac{d}{2} \left(1 - \cos \left(\frac{2\pi x}{L} \right) \right) \tag{6.5}$$

This particular irregularity as a function of distance is illustrated in Figure 6.8.

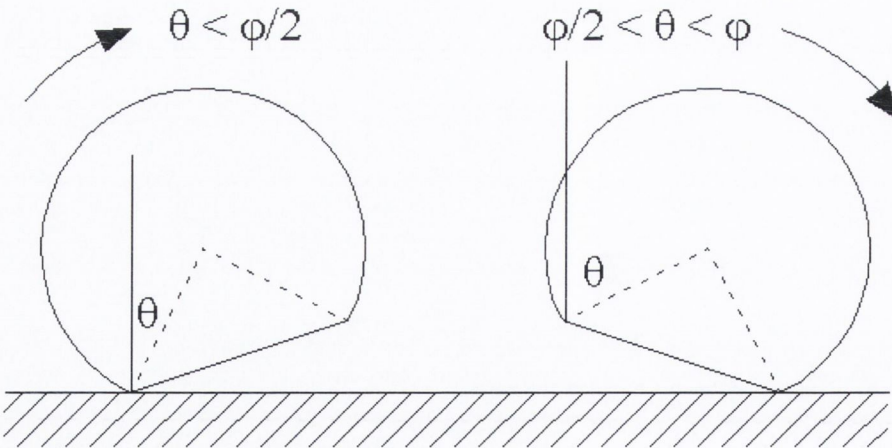


Fig. 6.7: Rolling of wheel with idealised flat

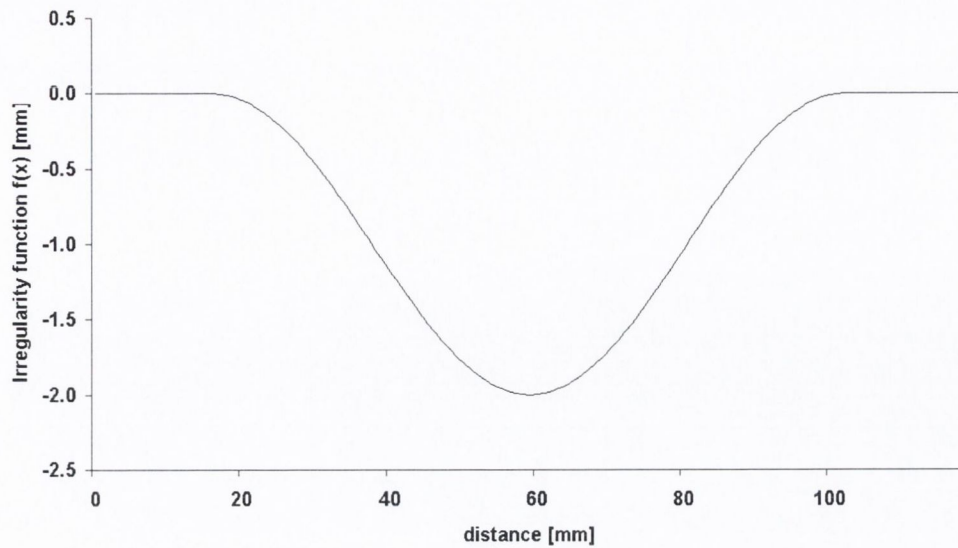


Fig. 6.8: Typical profile irregularity function for a wheel flat

6.3.2 Dynamic Response to Wheel Flat

The wheel flat that is considered here is 90mm in length and 0.93mm depth. These values are applied in the following numerical analyses to Equation 6.5 as the variables L and d respectively. The wheel flat is applied only to the front wheel of the bogie model, the rear wheel geometry is assumed to be perfect. Assuming a wheel radius of 400mm, the wheel passes through the flat part of its circumference approximately every 2.5m of travel. If it is initially assumed that the first wheel flat impact occurs directly above a sleeper then it follows that the five subsequent impacts will occur at 0.1m, 0.2m, 0.3m, 0.4m and 0.5m distance along the sleeper bays (the sleeper spacing is assumed to be 0.6m). In this way the effect of the wheel flat impact occurring at various distances along the sleeper spacings may be observed.

A previous study (Nielsen & Igeland 1995) has demonstrated that a dynamic impact factor of approximately four times the static contact force is observed at 40ms^{-1} for a wheel flat of these particular characteristics. A similar value was obtained in this study (see Figure 6.9). The damaged wheel is seen to lose contact with the rail on encountering the wheel flat at this particular velocity as the contact

force attains a zero value. This results in the rail accelerating upwards (see Figure 6.10), free from vehicle loading. The large impact factor is generated when the wheel and rail recover contact.

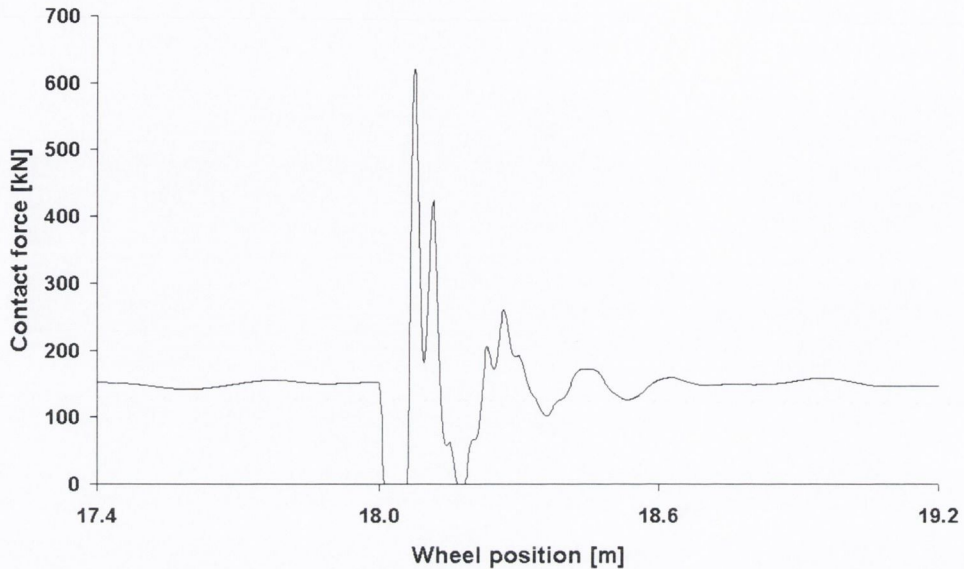


Fig. 6.9: Contact force resulting from wheel flat at velocity 40ms^{-1}

The effect of the wheel flat impact was observed over a range of different vehicle velocities. The time histories of the individual contact forces at the leading wheel are illustrated in Figure 6.11. It should be noted that this particular figure features the contact forces due to the flat occurring directly over a sleeper. At the lower velocity, 10ms^{-1} , loss of contact between wheel and rail does not occur. However, at all higher velocities loss of contact does occur. As expected, the maximum observed contact force increases with velocity.

The contact forces were calculated for six consecutive wheel flat impacts, each impact occurring at a different distance along the sleeper spacings. The maximum contact forces for each wheel flat impact are illustrated in Figure 6.12. At the two lower velocities tested the difference in impact factors was relatively small regardless of distance from sleepers. However, at the three higher velocities a pattern emerges. In all cases, the impact factors are greater when the wheel flat impacts at a sleeper

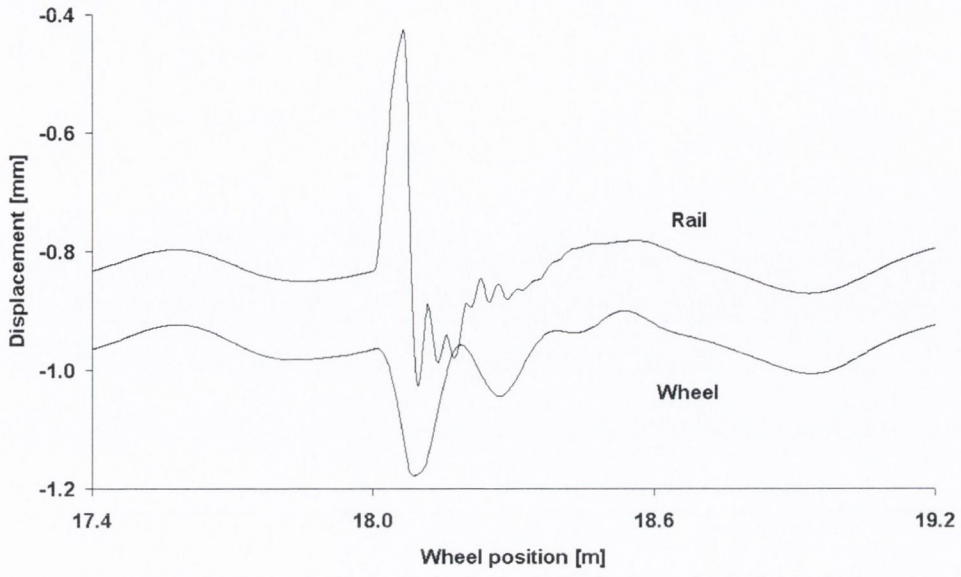


Fig. 6.10: Wheel and rail displacements at 40ms^{-1}

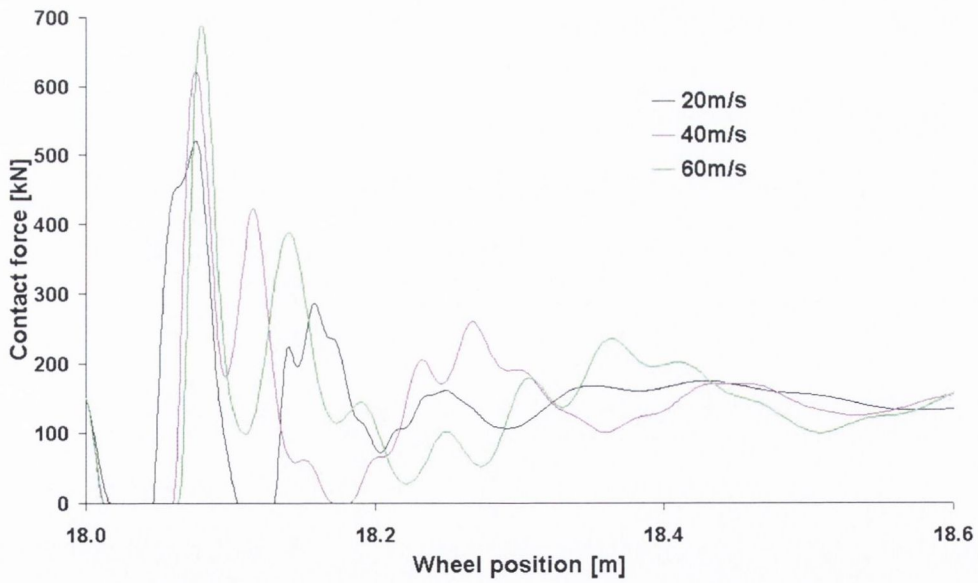


Fig. 6.11: Contact forces due to wheel flat impacting over sleeper

than when impact occurs at the midpoint between two sleepers, which is in agreement with the previous study of Nielsen & Igeland (1995). However, at each velocity the maximum impact occurs when the flat impacts at a distance of 0.2m before a sleeper while the minimum impacts occur 0.2m beyond the sleepers.

This observed dependence of the impact factor upon the position of impact of the wheel flat may be explained by observing the quasi-steady state contact force time history between two sleepers (see Figure 6.3). There are two contact force minima and maxima that occur within each sleeper spacing. The minima are observed at distances of approximately 0.2m and 0.5m beyond the initial sleeper while the maxima are at distances of 0.05 and 0.4 respectively (see Figure 6.3). These points correspond closely to the positions of minima and maxima in Figure 6.12.

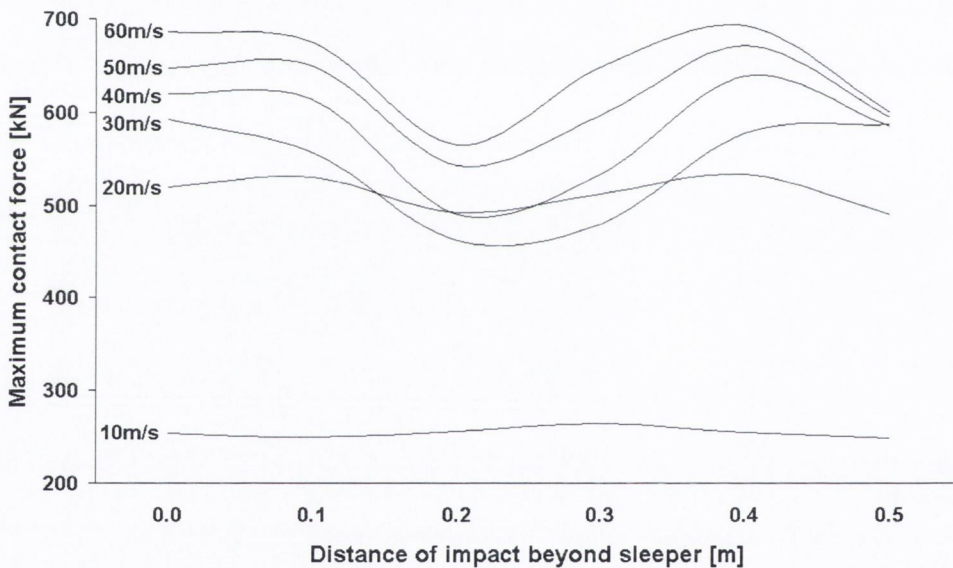


Fig. 6.12: Contact force variation with distance beyond sleeper

The ballast and pad forces at the point of impact of a wheel flat are illustrated in Figure 6.13. It is observed that the dynamic impact factor is significant only for the pad. The effect of a wheel flat upon the ballast spring force is quite small in comparison to the pad effect though the impact factor is greater than 1.5. The impact factor for the pad is approximately 5.2. The illustrated pad and ballast

impact forces were generated for the case of a flat hitting directly over the sleeper located at 18m from the model's leftmost extremity.

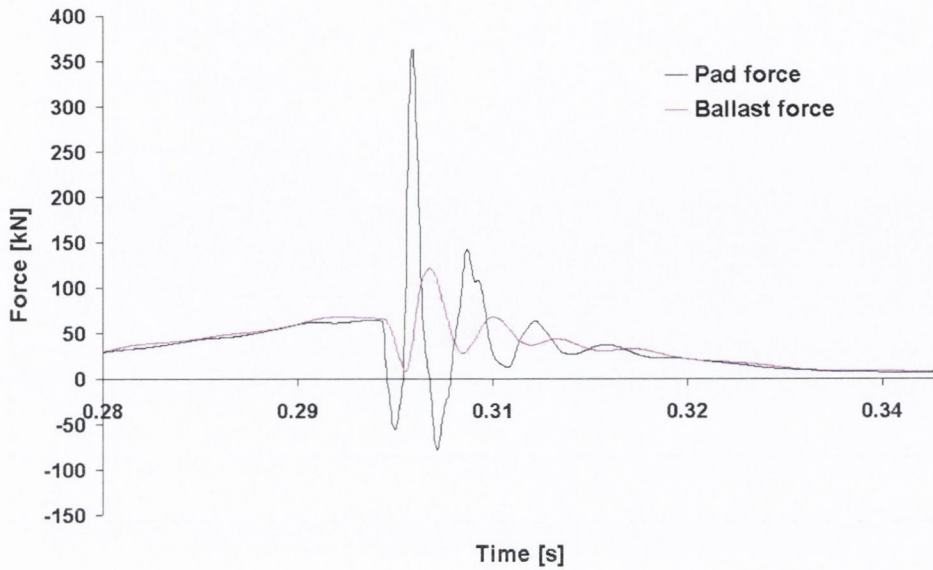
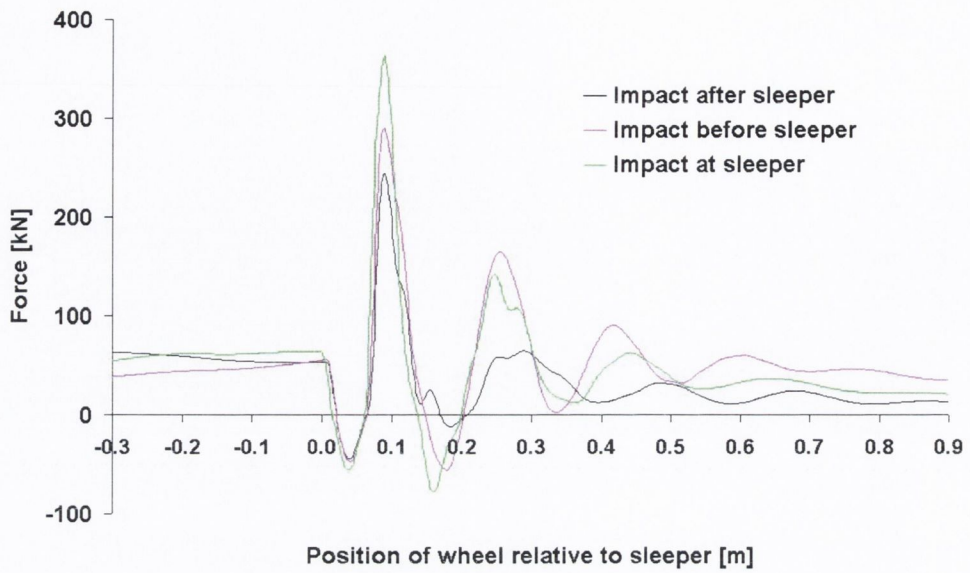
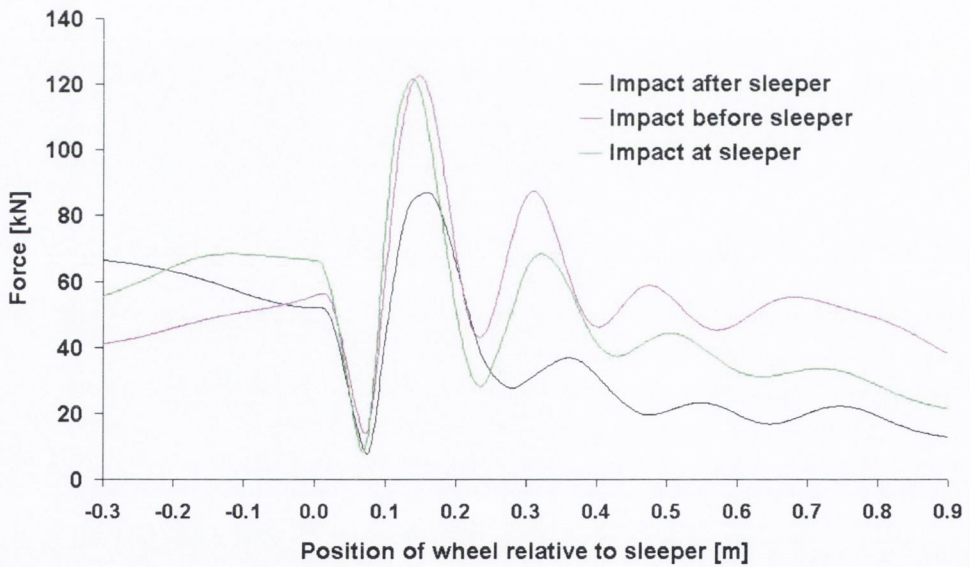


Fig. 6.13: Pad and ballast forces due to wheel flat impact over sleeper for 40ms^{-1} velocity

The pad and ballast forces generated by a wheel flat are maximised for the case shown in Figure 6.13. For wheel flats hitting halfway across a sleeper spacing the dynamic effects on these components of the model are not as severe, mainly due to the energy of the impact force being absorbed by the two adjacent pad and ballast springs. Figure 6.14 illustrates the pad and ballast forces at a centrally located (18m) sleeper as a vehicle passes over. The three cases considered are a flat impacting 0.3m before, 0.3m after, and exactly above, this sleeper. The pad impact that occurs before the sleeper results in the higher pad force (290kN compared to 240kN for 0.3m after). Neither of these figures is as high as the impact force (361kN) generated when the impact occurs directly over the sleeper. Similarly, a higher peak ballast spring force is generated when impact occurs before the sleeper. However, in the case of the ballast, the impact force for a wheel flat hitting directly over the sleeper is approximately identical to the case of impact before the sleeper.



(a) Pad forces



(b) Ballast forces

Fig. 6.14: Pad and ballast forces at 18m located sleeper due to wheel flat impacts 0.3m before and after sleeper at 40 ms^{-1}

6.4 Unsupported Sleeper

6.4.1 Unsupported Sleeper Model

The second defect that is considered is not strictly a track geometrical defect but a defect of the track structure. A non-uniformity of the track support given to the vehicle where a single track sleeper is unsupported upon the ballast bed is applied to the FE track model. This particular structural irregularity can occur due to excessive degradation of the ballast medium. Poor ballast drainage, and the resulting erosion, is the general source of this problem (Nielsen & Igeland 1995). In order to implement and observe the effect of this type of structural track defect, the centrally located sleeper ballast spring in the track model is assigned zero numerical values of stiffness and damping. In effect the sleeper is modelled as hanging from the track with its pad spring in tension under the gravitational weight of the sleeper, hence the term 'hung' sleeper which is sometimes used to describe this situation.

6.4.2 Dynamic Response to Unsupported Sleeper

The ballast support spring is removed from the sleeper located at the midpoint of the track model, ie. at 21m. Figure 6.15 illustrates the variation in the displacement at the point of contact between wheel and rail as the wheel encounters this lack of track support. The results of the unsupported sleeper are track maximum displacements equal to almost twice the steady state displacements at the highest velocity tested of 60ms^{-1} . The maximum deflections were lower at the lower velocities, however at 10ms^{-1} the maximum deflection is still 1.8 times greater than the steady state equivalent. Over these velocities therefore, the effect of the hung sleeper on the maximum track deflection is found not to vary greatly with velocity. The absence of the ballast support does, however, cause a substantial increase in track deflection of the order of twice the steady state maximum deflection, ie. when no hung sleepers are considered.

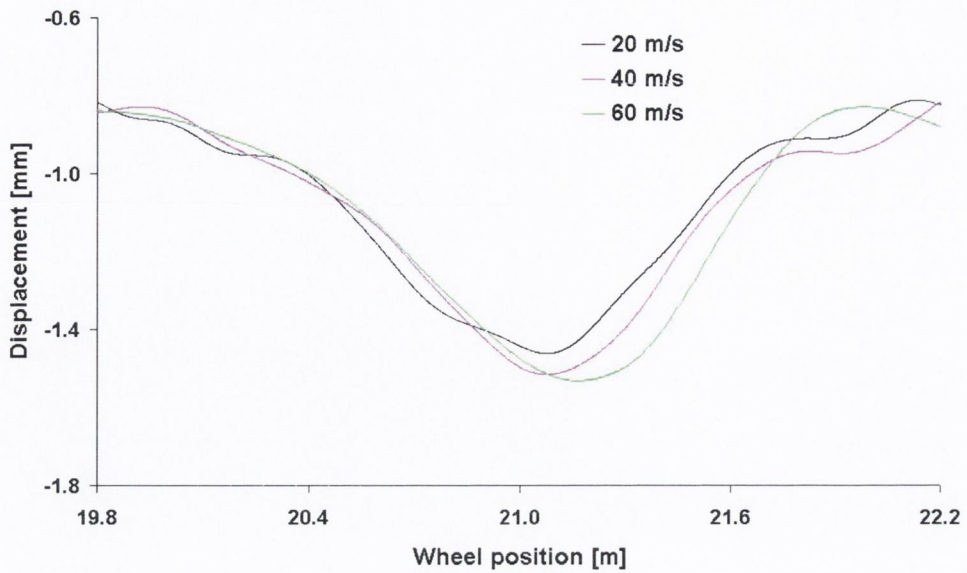


Fig. 6.15: Track model displacement at wheel-rail contact point due to hung sleeper at 21m

The resulting wheel-rail contact force process is significantly different from the steady state response as the hung sleeper is encountered. Figure 6.16 illustrates the contact force responses at 20, 40 and 60ms^{-1} . At 60ms^{-1} the peak contact force is close to 190kN , 25% greater than the static contact force. The peak forces are less at the lower velocities at 9% greater than the static at 40ms^{-1} and only 3% greater at 20ms^{-1} .

The excessive deflections that have been observed result in higher track bending moments. In the steady state the maximum track sagging bending moment observed at the wheel rail contact points is approximately 29kNm . For the CEN design rail section 56 E 1 this equates to a tensile stress at the the extreme fibre of the rail foot of approximately 92MPa . As was the case for the displacements these steady state stress maxima do not vary significantly with velocity over the range considered. The unsupported sleeper generates larger bending moments which result in maximum rail foot tensile stresses of 134MPa , which occur at the midspan of the run-on and run-off sleepers. As was the case for the steady state, velocity does not greatly affect

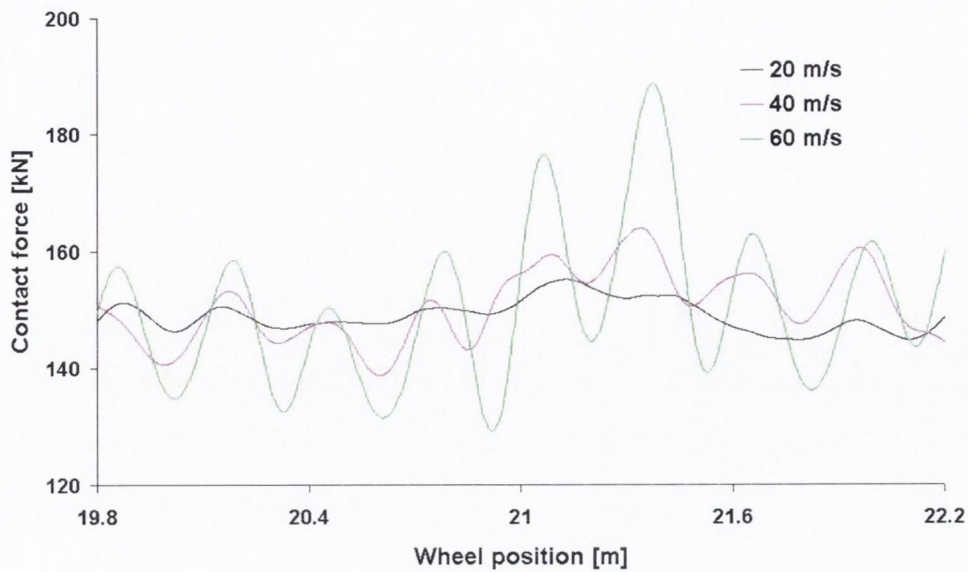


Fig. 6.16: Wheel-rail contact forces due to hung sleeper at 21m

the magnitude of these stresses.

The bending moments in the rail at the run-on and run-off sleepers were also recorded, i.e. the sleepers located at 20.4m and 21.6m. Unlike the bending moment histories at the wheel-rail contact points, the bending moment histories at these sleepers show tensile stresses at the top fibre of the rail. Maximum hogging moments of approximately 12kNm were observed, equating to 43MPa tensile stresses at the top of the rail. These maxima occurred, in the case of the both the run-on and run-off sleepers, when the wheel is just beyond the sleeper bay midspan. In the steady state the maximum tensile stress at the top of the rail is 36MPa, the maximum for the hung sleeper situation is more than 11% greater.

The effect of two consecutive unsupported sleepers is now considered. For this purpose the sleepers at locations 21m and 21.6m are given zero ballast support in the mathematical track model. While the dynamic effects generated by a single isolated sleeper were relatively small, the absence of two consecutive sleeper supports is found to be more dramatic. As one might expect the track displacements are greater again in this situation. As before, while the deflections do become slightly larger with

increasing velocity, this effect is small. However, the maximum track displacement at 60ms^{-1} is now 2.7mm, more than three times the steady state maximum. The maximum contact forces also increase, once again this effect is more pronounced at the higher velocities (see Figure 6.17).

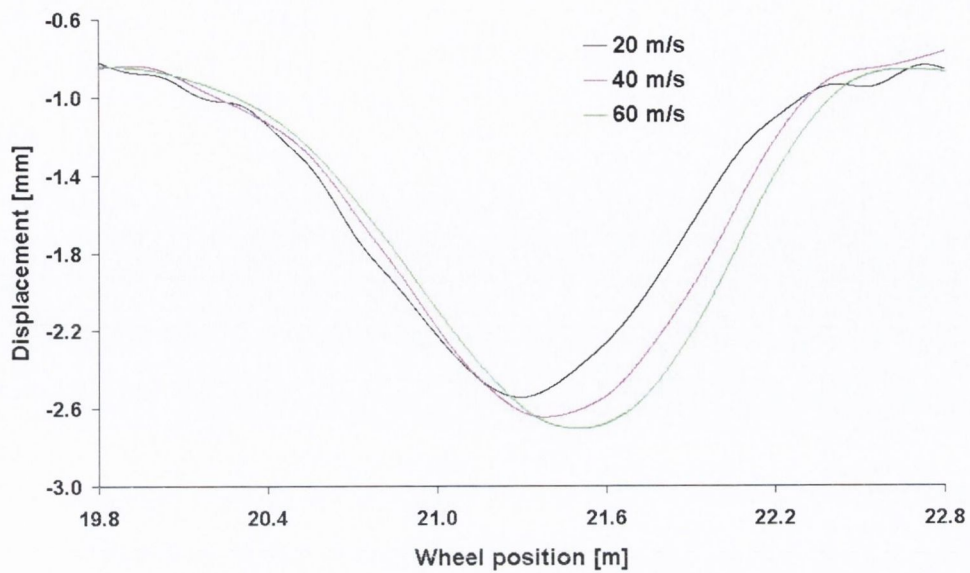
The maximum tensile stresses in the rail foot are significantly higher than for the case of a single hung sleeper. At 40ms^{-1} a maximum of 177MPa is observed, 30% greater than the maximum for the previous case. The maximum tensile stresses at the top of the rail are approximately 77MPa at the run-on sleeper and 53MPa at the run-off sleeper. These values are 114% and 47% greater respectively than the maximum tensile stress observed at the top of the rail in the steady state. Once again, the maximum stresses observed are approximately constant over the range of velocities considered.

6.5 Dipped Joint

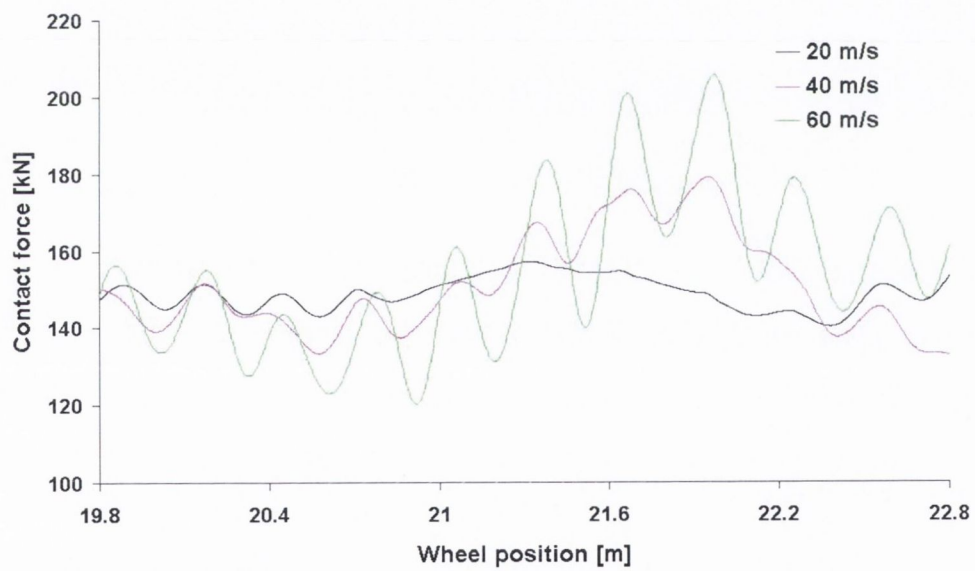
6.5.1 Dipped Joint Model

The next discrete irregularity considered is a rail joint, a relatively common discrete discontinuity in the track profile that causes an impact force to occur. Indeed, rail joints are the most severe of all track discontinuities (Wu & Thompson 2003). The rail commonly dips in the vicinity of a joint, even in the case of welded rail.

A dipped joint gives rise to two readily distinguishable dynamic increments (Harvey et al. 1993). The first, high-frequency, increment acts over a very short time span and is denoted the P_1 force. The second force, which is known as the P_2 force, acts at medium frequency. The P_1 force is generated as a result of track mass oscillation upon the Hertzian wheel-rail contact spring. The peak of this force occurs a few centimetres beyond the joint. The P_2 force occurs due to the wheel mass oscillating on the track spring. This force reaches its peak value later than the P_1 force, typically over the running on sleeper.



(a) Track displacement



(b) Contact forces

Fig. 6.17: Dynamic response to two hung sleepers located at 21m and 21.6m respectively

Both force increments can cause deterioration of the track structure. The P_1 force contributes to rail-end and fishplate damage, and also to bolt hole fatigue cracks. The P_2 force causes rail-end batter and star cracks. This force increment also damages sleepers in the vicinity of the joint.

A dipped rail joint with a gap and height difference can be described using quadratic functions (Wu & Thompson 2003), similar to the wheel flat model; the technique that is applied here to calculate the effect of a joint on the dynamic system response is based on this type of quadratic representation. In this case a sinusoidal downward ramp of 1:100 over a distance of 0.3m was considered and is followed by a symmetric upward ramp. The joint apex is assumed to occur at the midpoint between two railway sleepers.

6.5.2 Dynamic Response to Dipped Joint

The system response to the bogie model was observed over the same velocity range as in Sections 6.3 and 6.4. The wheel-rail contact force history at the leading wheelset is illustrated in Figure 6.18 for a vehicle velocity of 40ms^{-1} . The wheel initially loses contact with the rail as the profile dips before the apex of the joint. When the wheel regains contact at the apex a large contact force is generated. The initial peak is due to the P_1 force while a second peak, the P_2 increment, is seen to occur just before the following sleeper. It should be noted that 40ms^{-1} was the lowest velocity at which the wheel loses contact with the rail. At lower velocities the wheel remained in contact throughout. Other studies have shown loss of contact at these lower velocities (Dong et al. 1994, Hou et al. 2003). The results calculated here may be due to the sinusoidal shape of the dip, which results in a more gradual fall away from the mean track profile level.

The track bending moment history at the sleepers before and following the dipped joint are illustrated in Figure 6.19. When the wheel encounters the joint apex the track shows large hogging moments at both sleepers. At 40ms^{-1} , the moment

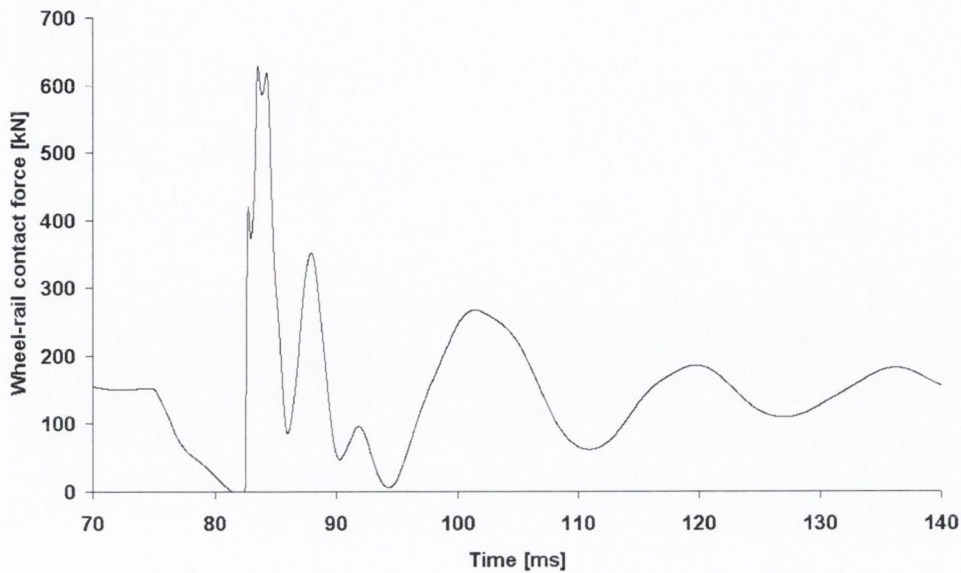


Fig. 6.18: Wheel-rail contact forces due to 3mm dipped joint in track at vehicle velocity of 40ms^{-1}

at the sleeper before the joint is greater at approximately 15kNm compared to a maximum quasi-steady state hogging rail moment of approximately 6kNm . The dynamic impact factor for hogging moment is therefore not as great as that for the wheel-rail contact force, but is significant nonetheless. The rail at the sleeper beyond the dipped joint shows a very high sagging moment as the wheel moves beyond the joint apex. At 40ms^{-1} a 61kNm maximum value is observed. This compares to a steady state maximum of 29kNm , an equivalent impact factor of 2.1. Once again, the P_1 and P_2 increments are visible in the rail response.

The analytical formulae for these force increments are given in Section 2.3.2 (Equation 2.7). The results obtained by substitution into these formulae are now compared with the numerically calculated response (see Figure 6.20). There is significant variation between the two sets of data. One explanation for this is that the analytical P_1 and P_2 contact forces calculation is carried out on the assumption that the track profile is a linear ramp rather than the sinusoidal hollow dip that is modelled here. In addition, the analytical calculation does not consider the effect of

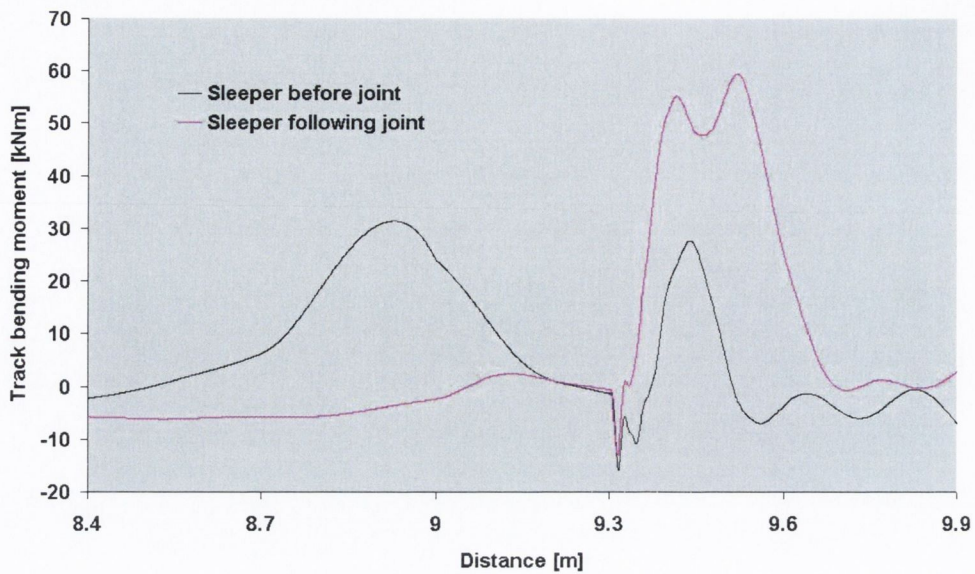


Fig. 6.19: Track bending moments at vehicle velocity of 40ms^{-1}

the sprung mass inertia or bogie rotary inertia as in the numerical bogie model.

6.6 Ballast Stiffness Effects

The effect of different degrees of ballast spring stiffness in the track model is now considered. The ballast is modelled as a series of discrete springs, with each spring located at one of the sleepers. The default linear spring constants for these ballast springs is $4.66 \times 10^7 \text{Nm}^{-1}$. The values observed here are varied above and below with this as the mean value. Values of 0.25, 0.5, 2.0 and 4.0 times this mean value are considered. A bogie model velocity of 40ms^{-1} is assumed throughout this particular analysis.

The recorded model track displacement, contact forces and track bending moments at the front wheel of the bogie model are illustrated in Figure 6.21. These time histories are shown over two complete sleeper spacings from 21m to 21.2m and, as such, are representative of the steady state. As one would expect, the lower ballast spring stiffness values result in greater track deflections. However, higher

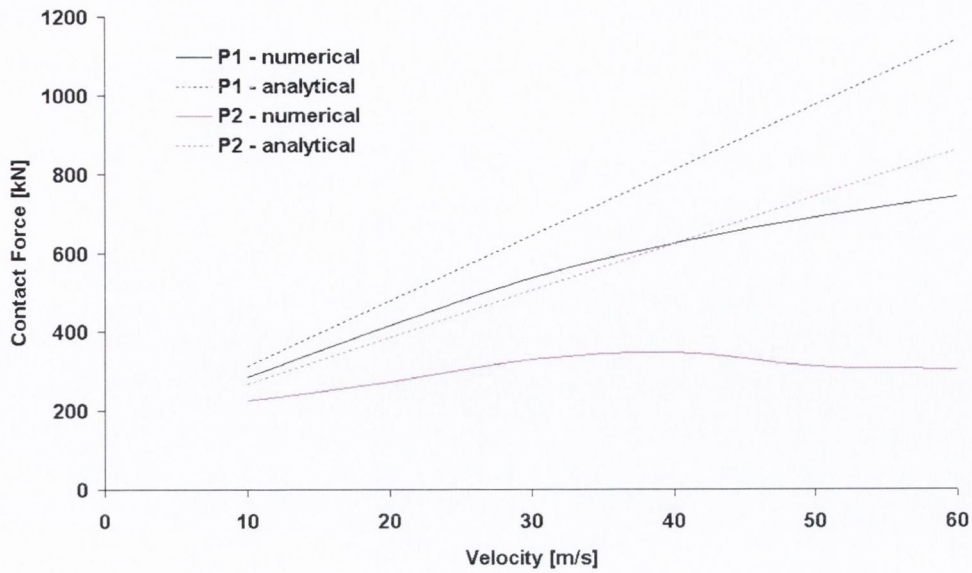
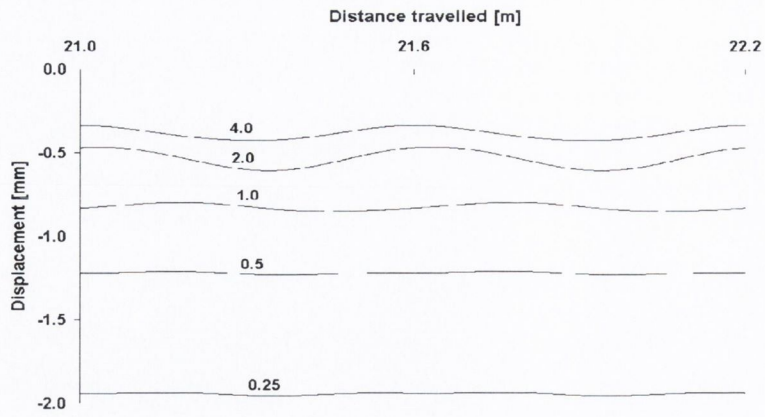


Fig. 6.20: Comparison of numerically calculated P_1 and P_2 contact forces with their analytical equivalents

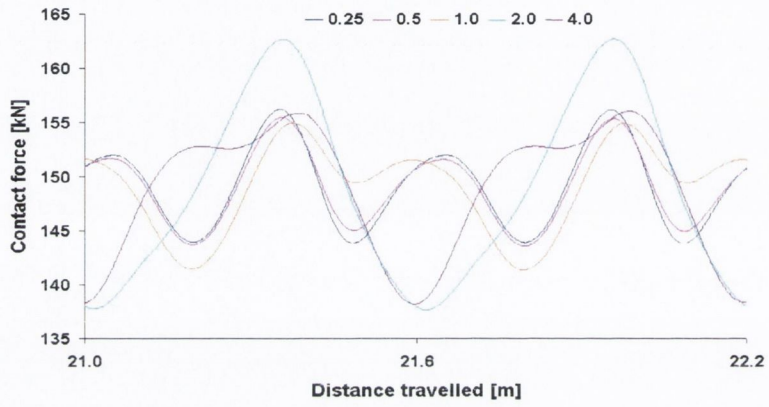
ballast stiffness values result in greater variation in the deflections at and between the sleepers because greater resistance is given to the vertical sleeper movement as the wheelset passes above (see Figure 6.21(a)).

Unlike the displacement histories the contact force histories vary dramatically with varying ballast stiffness (Figure 6.21(b)). It is observed that the characteristic shape of the contact force time history is greatly dependent on the ballast stiffness. This may account for some of the differences in the steady state contact force time histories that have been observed in the literature. The two lower spring stiffness values produce similar results while the default value and four times the default generate maximum forces of similar magnitude (approximately 155kN). However, at twice the default ballast stiffness value the maximum steady state contact forces are in excess of 162kN. The smallest minimum steady state contact forces are observed at the two higher ballast stiffness values tested (these are approximately 138kN).

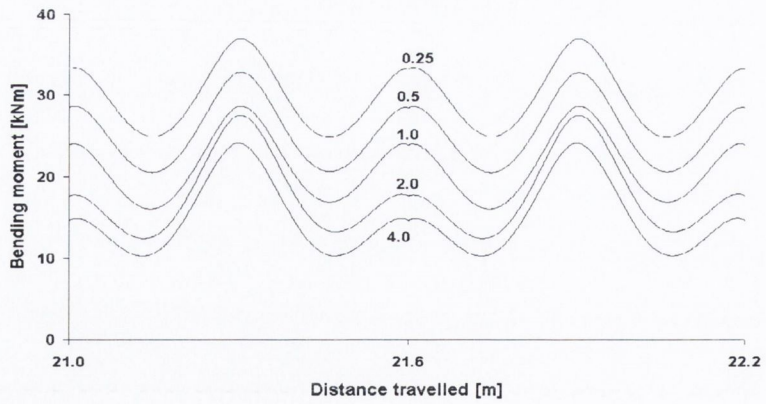
Greater track bending moments at the wheel-rail contact point are observed when the ballast stiffness is at its minimum value. This pattern is consistent over



(a) Track displacement



(b) Contact forces



(c) Track bending moments

Fig. 6.21: Steady state response variation with ballast stiffness (Ballast stiffness expressed as a fraction of the default value)

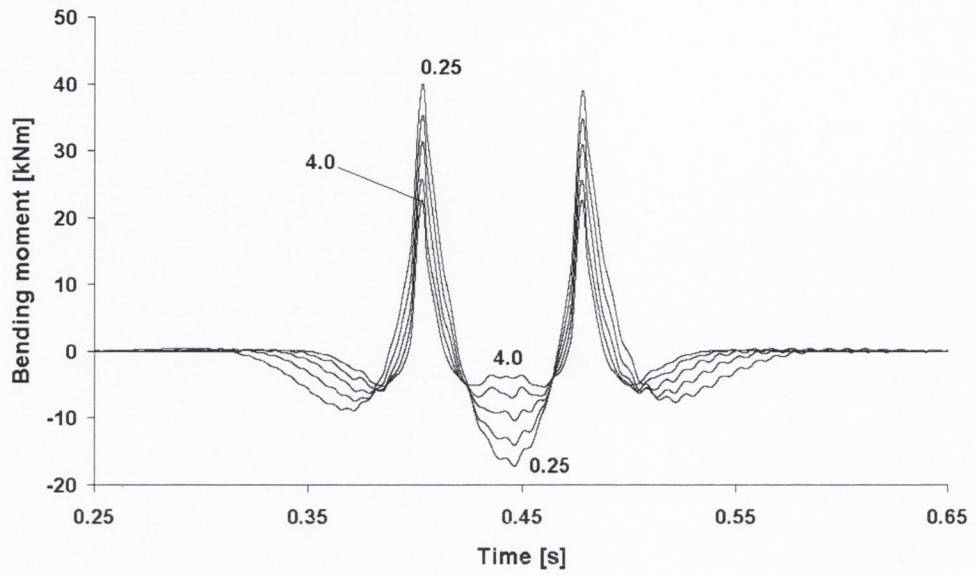
the values tested (see Figure 6.21(c)). However, unlike the track displacement and wheel-rail contact force processes, the point of wheel-rail contact is not the point at which maximum bending moment is observed. For this reason the bending moments are also observed at two stationary points on the track, one directly over a sleeper and one at the midspan of two sleepers (see Figure 6.22).

A maximum track bending moment of 37kNm was observed at the wheel-rail contact point in the steady state. This was maximised for the minimum ballast stiffness value. When the time history of the bending moment at a single point over a sleeper is considered a maximum of 40kNm is observed. Once again this value is a maximum for minimum ballast stiffness. A similar situation is observed at the midspan of two sleepers, the maximum in this case, however, is increased to in excess of 42kNm. These peaks occur just prior to the wheel passing the particular point in question.

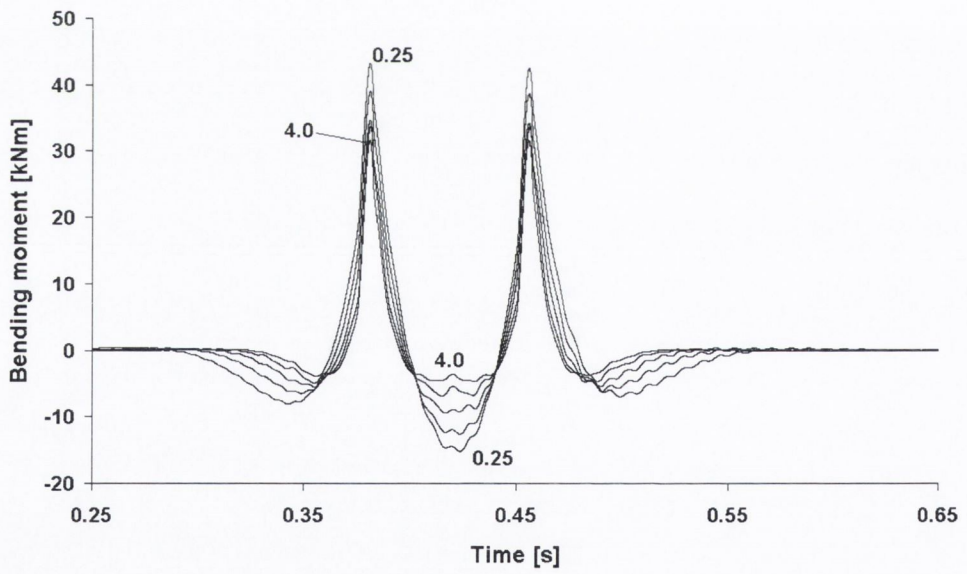
Only peak sagging rail bending moments have been considered up to this point. Hogging moments also occur, although not at the wheel-rail contact point. The largest hogging moments observed are 16.5kNm and 14.5kNm for the sleeper and midspan points respectively. Were only a single vehicle wheel considered the maximum hogging moment would be approximately half of these values. However, the two-wheel bogie model, with wheels in close proximity, induces a significantly larger rail hogging moment at the midpoint between the wheels.

6.7 Observations and Conclusions

The FE track model was found to be suitable for the purpose of monitoring the effect of the discrete irregularities that were applied. The beam was modelled using Timoshenko beam elements because a previous study (Dong et al. 1994) had shown that this beam element was better suited to high frequency analysis than the Euler beam element. While the track was modelled using Timoshenko beam elements the



(a) Track bending moment at sleeper



(b) Track bending moments at sleeper midspan

Fig. 6.22: Track bending moments at fixed points (variation with ballast stiffness)

model can easily be adapted as an Euler beam by adjusting the shear modulus and rotary inertia. The FE model was formulated because the FD model of Chapter 5 was found to be ineffective when modelling these types of defects due to the modelling assumption of a continuous elastic foundation.

The first application of the FE track model was to the dynamic effect of a wheel flat. The model was initially validated by means of comparison with another study (Nielsen & Igeland 1995). The position of impact of the wheel flat in relation to the two adjacent sleepers was shown to influence the magnitude of the maximum resultant contact force. When the wheel flat impacted at the midpoint between two sleepers the maximum contact force was found to be smaller than when impact occurred close to the sleepers themselves.

The effect of a wheel flat impact on the rail pad and ballast forces was also considered. As one would expect, these forces are smaller when the impact occurs between two sleepers. This is due to the fact that the impact force is distributed between two pads, two sleepers and two ballast springs, and also the resulting smaller inertial effect of the sleeper mass. When the impact occurs directly between two sleepers the rail pad in front of the wheel shows a higher force impact factor than the rail pad that the wheel has just passed. When the impact occurs directly over a sleeper, a considerable peak is observed in the rail pad contact force history. The ballast force impact factors are small by comparison with those of the pad.

The second application of the model was to the case of an unsupported, or 'hung' sleeper. The track displacement directly above the position of the hung sleeper increases to approximately double its previous value due to vehicle loading. There is also an increment in the wheel-rail contact force of approximately 1.3 times the static. The dynamic effect of two consecutive unsupported sleepers was to more than treble the maximum track displacement at the wheel-rail contact point. The maximum contact force was also increased in this instance to approximately 1.4 times the static force.

The presence of a dipped joint causes a large dynamic impact factor to be observed in the wheel-rail contact force time history. In addition, an excessive rail hogging bending moment is observed at the adjacent sleeper as the wheel encounters the joint. The rail sagging moment generated at the sleeper before the joint does not rise above its steady-state value due to the impact. However, a large rail sagging moment is observed at the sleeper beyond the joint. The analytical solutions for calculation of the peak contact forces caused by a dipped joint (Harvey et al. 1993) do not correspond to the numerically calculated values observed in this study. A number of factors may be responsible for this, but primarily the sinusoidal shape of the joint considered here is unlike the linear ramp assumed for the analytical derivation.

Finally, the effect of the ballast medium stiffness was observed. The maximum ballast spring stiffness is shown to cause the minimum track deflection under vehicle loading, but also minimises the track bending moment. The maximum wheel-rail contact force is observed for a ballast stiffness of twice the mean value, which is equivalent to $9.32 \times 10^7 \text{Nm}^{-1}$. At all other values, including the maximum ballast spring stiffness, the maximum contact forces observed were similar in magnitude.

Chapter 7

Effect of Random Track

Irregularities upon Bridge Impact

Factors

7.1 Introduction

Analyses based upon the dynamic response of railway bridges to moving loads have been extremely prevalent in the literature. Less common, however, are studies that focus specifically upon the bridge system response when the additional dynamic input of random vertical track irregularity is considered. The paper of Au et al. (2002) is an example of such an investigation. In that particular case the dynamic bridge impact factors generated by a railway vehicle moving across a cable-stayed bridge with vertical track profiles of varying quality were calculated numerically. The study (Au et al. 2002) was specific to the case of a particular cable-stayed bridge with a main span of 430m. The particular study presented here is based upon the analysis of the response of simplified plate girder bridge models to vehicles running over randomly irregular vertical track profiles. The objective of the study is to determine whether the effect of random track irregularity is significant in the

calculation of bridge impact factors and, if so, what is the degree to which these factors are influenced.

The study of the wheel-rail dynamic interaction due to random irregularities lends itself to a spectral approach (see Chapters 3 and 4). However, while the vertical track irregularity profiles considered in this study may be characterised by one-sided PSD functions, the objective of the study is to calculate bridge impact factors. A deterministic approach is more suitable for this purpose. Random profiles associated with the FRA PSD functions are generated using trigonometric series and applied to the bridge and vehicle models in numerical analyses.

This study, as a parametric analysis, is focussed upon the effect of random track irregularities upon the dynamic impact factors for three different plate girder bridges. The three bridges considered in Section 7.2 are of short (10m), medium (35m) and long (70m) span. The bridge parameters chosen do not relate to any specific structures but are given typical values based on a study of 113 railway bridges undertaken by Frýba (1996). The bridges are idealised throughout as simply-supported beams. The vehicle model considered here is a single locomotive model with two bogies and four axles, comprising ten degrees of freedom in all. Two different characteristic random profiles are considered, one of medium quality (Class 4) and one of poor quality (Class 1).

Section 7.3 involves an analysis of the impact factors generated due to the passage of a more complete vehicle model with a number of coaches following the same locomotive model as before. The effect of varying track quality on the wheel-bridge contact forces is also considered in this section. Finally, in Section 7.4, the influence of the railway track structure on the dynamic bridge response is investigated. Prior to this section the vehicle models are considered to be directly in contact with the beam model with no track structure included in the system model.

7.2 Random Profile Irregularity Effect on Dynamic Impact Factors

7.2.1 Finite Element Model Validation

The response of a typical short span bridge is considered initially for the purpose of model validation. The steel plate-girder bridge is modelled as a simply-supported beam. Railway bridges are often idealised as beams, the dynamic stiffness of which is a function of the bridge stiffness and mass per unit length. This dynamic stiffness B is calculated by means of regression coefficients calculated by Frýba (1996) on the basis of an experimental study of a large number of railway bridges. B is calculated directly from the equation

$$B = \sqrt{\frac{EI}{\mu}} \quad (7.1)$$

The dynamic stiffness constant B for the type of bridge considered here with a span of 10m, as defined by Frýba (1996), is approximately equal to $500\text{m}^2\text{s}^{-1}$. It should be noted that the bridge is, for the purpose of this investigation, considered to be ballasted. The distinction between ballasted and non-ballasted bridges is required in this case due to the differing regressive coefficients suggested by Frýba for the two specific cases. As the bridge models used in this section are not based on existing or proposed bridge data, B was used to calculate a suitable second moment of area on assuming a suitable mass per unit length and Young's modulus. The bridge model Young's modulus (E), second moment of area (I) and mass per unit length (μ) are equal to $210 \times 10^9\text{Nm}^{-2}$, 0.014m^4 and $1.2 \times 10^4\text{kgm}^{-1}$ respectively. These parametric values give a fundamental beam period, T_f , of 0.1286s, ie. ω_f is 48.86rads^{-1} (7.78Hz).

Initially, for the purpose of validating the finite element beam model, the moving vehicle load is simplified as a single point force. Exact solutions have been

determined for problems of this nature, ie. a simply-supported beam traversed by a constant force moving at constant velocity along the beam surface. Such a solution is detailed by Warburton (1976), where it is assumed that the beam displacement is dominated by the contribution from the first mode of vibration. A more rigorous exact solution has been developed by Frýba (1999) where the beam response is calculated as the sum of an infinite series of modal responses. In effect, the solution of Warburton is equivalent to that of Frýba with only the first term in the same infinite series considered.

At practical railway vehicle velocities the maximum mid-span deflection of a simply-supported beam occurs during the load traverse. A critical velocity exists at which the dynamic maximum is not attained until the load departs the beam. Frýba (1999) defines this critical velocity as a function of the beam's material, section properties, and its length. For the plate girder beam model considered in this case the critical velocity is approximately 155ms^{-1} (660km/hr), while the maximum vehicle model velocity considered in this study is 60ms^{-1} . The calculation of dynamic impact factors is therefore confined to consideration of the beam response prior to departure of the vehicle. For this reason the beam's free response following departure of the railway vehicle is not required to be considered for the case of a single moving force or single moving mass.

The dynamic impact factors generated using three different analysis methods are presented graphically in Figure 7.1. The first series of factors is based on the fundamental modal solution of Warburton, the second on the multi-modal solution of Frýba with the initial 100 response modes considered, and the third series results from a numerical finite element method (FEM) analysis. The 10m beam consists, in the case of the FE model, of 24 identical Euler beam elements. Sufficient simulation convergence was obtained at this level of elemental discretisation. The dynamic impact factors are defined as the ratio of peak dynamic mid-span deflection of the beam to the static mid-span deflection with the force placed at mid-span. These

factors are calculated at 5ms^{-1} intervals over the $5 - 60\text{ms}^{-1}$ range. The Warburton series shows the smallest impact factor values for all velocities. As expected, the Frýba impact factors are higher due to the consideration of the contributions from higher order modes. The FEM analysis generates values that are consistently in the interval between the two analytical values over the velocity range considered. One of the fundamental constraints of the FE technique is the fact that finite nodal spacing is such that higher order frequencies, whose contribution is added using the Frýba solution, cannot be incorporated into the FE numerical model at the levels of elemental discretisation considered. However, it should be noted that the analytical solution is an infinite series itself and, as such, is an estimation also.

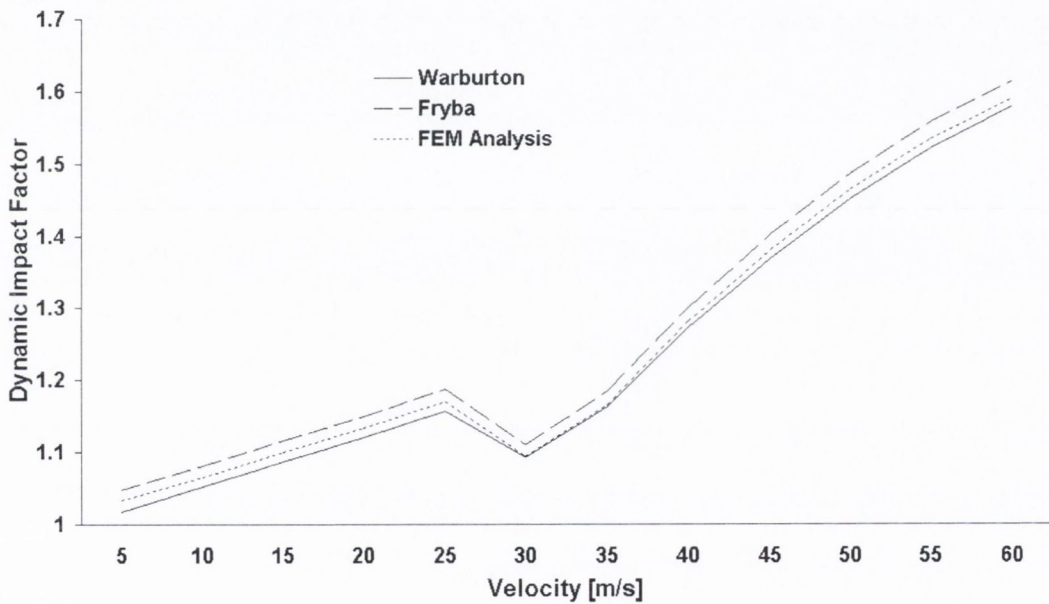


Fig. 7.1: Impact factors variation with velocity for moving point force (Short span bridge model)

It should be noted that the exact analytical solutions of Warburton and Frýba do not consider the initial static deflection of the beam under its own gravitational self-weight. For this reason and due to the comparative nature of this particular exercise the beam's initial displacement due to its own self-weight was not considered

in the FEM solution. Inclusion of this factor would distort the results obtained as the relative dynamic displacement of the beam would be smaller due to its additional initial gravitational displacement. Physically, the exclusion of the self-weight gravitational displacement may be valid, especially in the case of ballasted track, due to the probable levelling during placement of the ballast medium upon the gravitationally displaced bridge deck.

While the illustrated data has been presented here for the case of the short-span beam only, a similar model validation procedure was followed for both the medium-span and long-span span bridges. A Bernoulli-Euler FE beam model with 24 elements was found to give adequate convergence in all three cases. This constant number of elements applied to the three bridge models results in longer beam FE elements for the longer-span models.

The vehicle that is being considered for the purpose of this initial testing is a single 181 locomotive. This locomotive is a four axle 'BoBo' vehicle possessing individual static axle loads of 159.3kN. These four axle loads were previously combined into a 637.2kN point force for the purpose of validating the numerical FE bridge model. Henceforth, however, the four individual vehicle contact points are considered. A bridge model identical to that validated for a single moving constant force is subjected to four moving constant forces which modelled a 181 locomotive travelling at a constant velocity. This particular analysis does not consider the bridge-vehicle interaction.

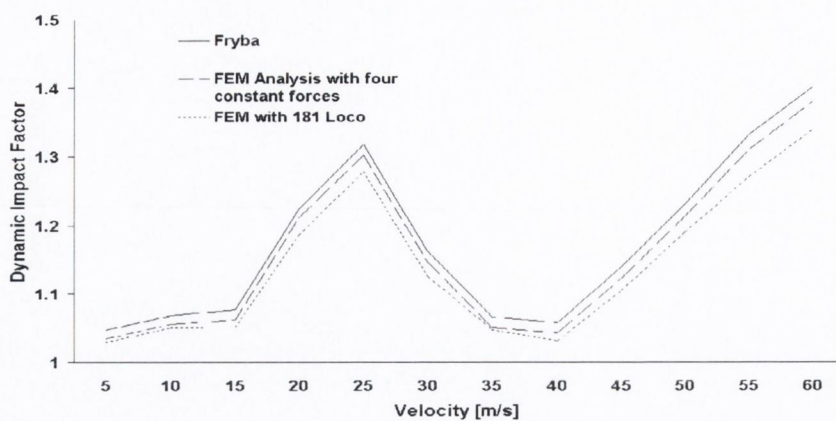
The maximum static mid-span deflection is smaller in this case than for the single moving force model due to the dispersion of the load along the bridge length, the dispersion resulting from the axle spacing. This maximum static deflection is calculated as the maximum mid-span deflection considering all locations of the vehicle along the span. This is not identical to the static mid-span deflection with the locomotive positioned symmetrically over the mid-span point. This clarification is required as the maximum static deflection for all spans considered does not occur

with the vehicle placed symmetrically about the mid-span. The dynamic impact factors are calculated with respect to the maximum mid-span static deflection for all vehicle positions along the beam.

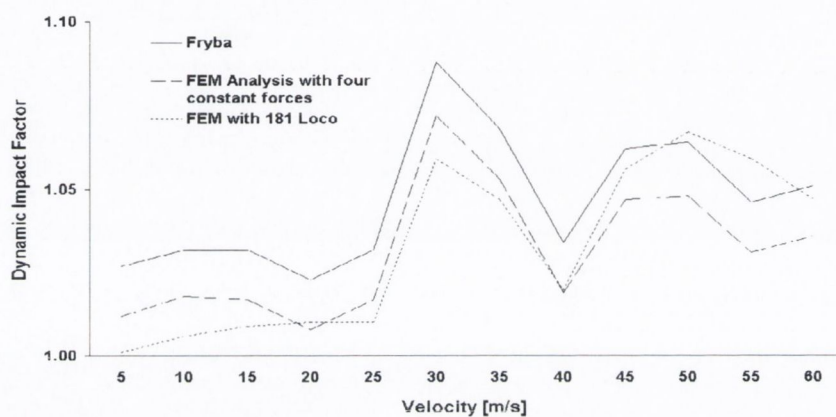
The linearity of the simply supported beam system allows the system response, calculated using the analytical Frýba solution, for four individual forces to be superimposed. However, unlike the previous analysis, where free vibration was not considered, the free vibration response of the beam is required to be calculated until the point when all four forces have completely traversed the beam. This solution is then compared to a numerical FE analysis with an identical loadcase, ie. four constant moving point forces. A 181 locomotive vehicle system model was then incorporated into the FE beam numerical analysis. The vehicle model possesses the same static properties as the four forces (ie. its static wheel loads are identical) but, in the dynamic case, allows for fluctuation of the contact forces as the vehicle wheelsets oscillate on the Hertzian contact spring and the other vehicle masses vibrate on the primary and secondary suspension springs. Track irregularity is initially not included in the case of the vehicle model and so this particular response is henceforth referred to as the quasi-steady state response. The dynamic impact factors are illustrated in Figure 7.2 for the three bridge models (short, medium and long spans) and for the three different vehicle model formulations (analytical-moving forces, numerical-moving forces and numerical-moving vehicle). The properties of the three individual bridge models are given in Table 7.1.

The constant force models, ie. the Frýba formulation and the FEM analysis with constant forces, display results that have very similar characteristics. This is to be expected as the FEM analysis is a numerical solution for the beam response to loading that is identical to that for the analytical Frýba solution. However, the Frýba solution gives consistently higher impact factors. This effect was previously observed in the bridge model validation under the loading of a single force.

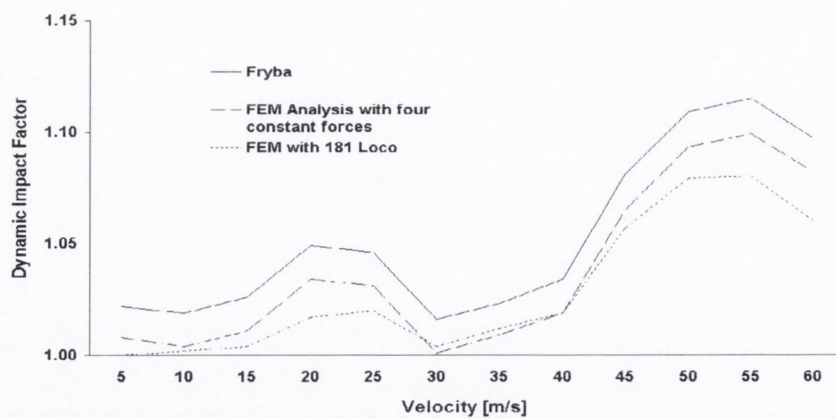
The factors obtained for the locomotive vehicle model on the FEM beam model



(a) Short span



(b) Medium span



(c) Long span

Fig. 7.2: Variation of impact factors with velocity for various beam and vehicle models

Parameter	Short span	Medium span	Long span
Span , L	10m	35m	70m
Dynamic Impact Factor, B	$500\text{m}^2\text{s}_{-1}$	$3000\text{m}^2\text{s}_{-1}$	$7500\text{m}^2\text{s}_{-1}$
Mass per unit length, μ	$1.2 \times 10^4\text{kgm}^{-1}$	$1.2 \times 10^4\text{kgm}^{-1}$	$1.2 \times 10^4\text{kgm}^{-1}$
Second Moment of Area, I	0.014m^4	0.514m^4	3.214m^4
Young's Modulus, E	$210 \times 10^9\text{Nm}^{-2}$	$210 \times 10^9\text{Nm}^{-2}$	$210 \times 10^9\text{Nm}^{-2}$

Table 7.1: Plate girder bridge models parameters

do not display the same pattern of variation with velocity. In the case of the short span bridge model the impact factors for the locomotive model are consistently lower than for four equivalent constant forces. For the medium-span and long-span bridge models the locomotive impact factors fluctuate above and below the constant force model. It has been shown (Delgado & dos Santos 1997) that the extent of this effect is dependent upon the suspension stiffness and mass ratio values. For higher suspension stiffness values greater impact factors would generally be observed.

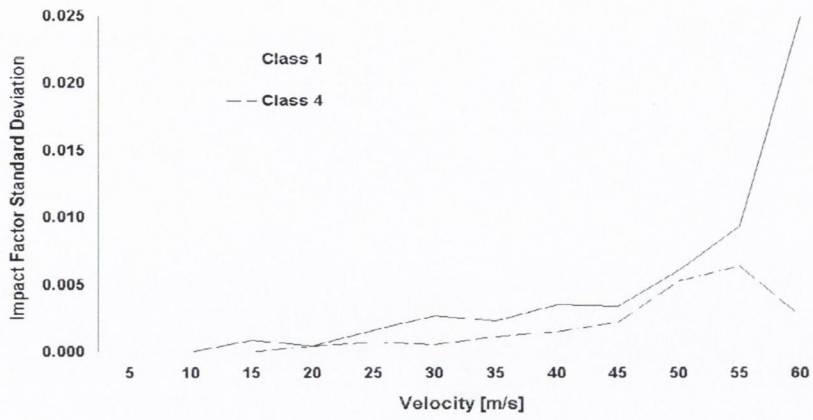
The impact factors are significantly higher for the locomotive vehicle over the short-span bridge model than for the medium-span and long-span. The maximum factor for the locomotive and short-span model is 1.340 while the equivalent maxima for the medium-span and long-span models are 1.067 and 1.080 respectively. While the maximum impact factor for the short span model occurs at the highest velocity (60ms^{-1}), the largest factors for the medium-span and long-span models occur at 50 and 55ms^{-1} respectively, while the impact factors at 60ms^{-1} actually drop off. Lin & Trethewey (1990) showed that the maximum mid-span deflection response to a moving force occurs when the ratio of the bridge's fundamental period to the force's crossing time is 1.234. When a vehicle model such as this is applied the response is more complex due to the interaction effects between the multiple axle loads. However, as for the single force, threshold velocities are found to exist, beyond which the mid-span response decreases.

7.2.2 Effect of Random Irregularities

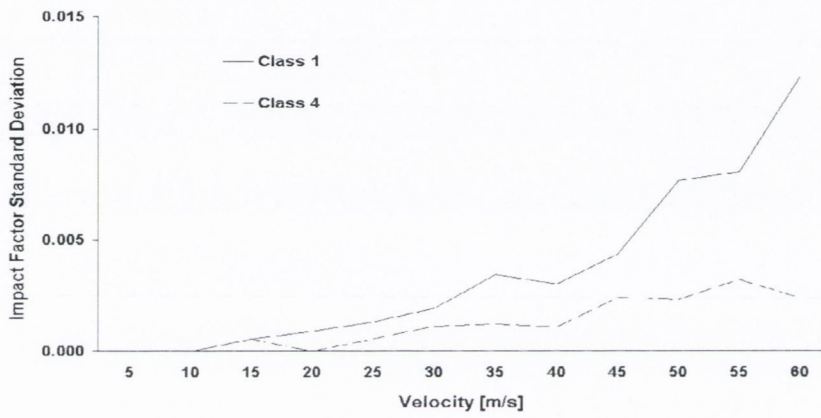
The next step in the analysis is the incorporation of random irregularity in the vertical track profile into the FE model so that the effect of such irregularity upon the impact factors may be observed. Random profiles with statistical properties equivalent to the Federal Railroad Administration (FRA) power spectral density (PSD) functions are generated numerically. The vertical profiles are then applied to the contact force calculations at the wheel-bridge contact interface. The FRA specifies six track classes. A Class 4 track, of intermediate quality, is initially applied to the model. Five different Class 4 sample track profiles are generated numerically and impact factors are calculated for each of these samples. The same procedure is then followed for the case of a Class 1 track, which is of the poorest quality specified. The track irregularity has the effect of shifting the wheel-bridge contact forces from their quasi-steady state and hence altering the bridge impact factors from their steady state values. The PSD functions are defined over the route frequency band 0.01m^{-1} to 0.628m^{-1} . The vast majority of the PSD energy is concentrated towards the lower end of the spectrum at route frequency 0.01m^{-1} . In the velocity range considered in this study (5 to 60ms^{-1}) this equates to a random profile periodic range of approximately 10s to 125s .

Five random profiles are generated and tested at the same vehicle velocity increments previously described. It is found that the mean of all the impact factors for each model equate to the the factors generated for a perfectly smooth contact area, ie. the quasi-steady state. The individual impact factor values, however, varied about the mean with varying standard deviations for each velocity. Figure 7.3 illustrates the variation in these standard deviations with increasing velocity.

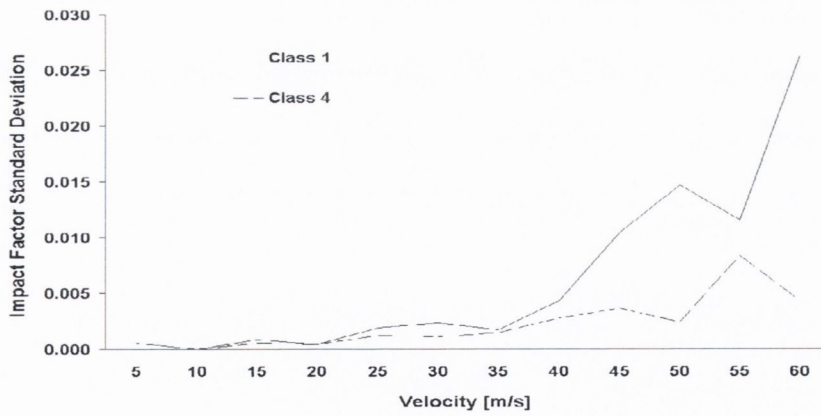
The standard deviations do not vary greatly between the short, medium and long span bridge models, especially at the lower velocities, but do increase with increasing vehicle velocity. The largest impact factor standard deviation value, 0.026 , is obtained for both the short and long span bridges at 60ms^{-1} . The largest standard



(a) Short span



(b) Medium span



(c) Long span

Fig. 7.3: Impact factor standard deviations

deviation for the medium span bridge model is 0.012. Upon calculating the standard deviations it is important to bear in mind that the quasi-steady state impact factors are very low for both the medium and long span models. The fluctuation of the impact factors about the mean for different profiles does not generate excessively large impact factors.

The quasi-steady state factors are higher for the short span bridge model. It has been illustrated that, for this particular model, the dynamic impact factor, as defined above, is not independent of the track quality. At 60ms^{-1} the impact factor, neglecting any track profile irregularity, was equal to 1.340. The incorporation of random track irregularity in to the model causes the impact factors to fluctuate about this mean value. In the worst case, and assuming that the impact factors are normally distributed, it may be concluded that, while the mean impact factor is 1.340 for Class 1 track and vehicle velocity 60ms^{-1} , for 1% of profiles the factor will exceed 1.400.

7.3 Case Study

7.3.1 Background

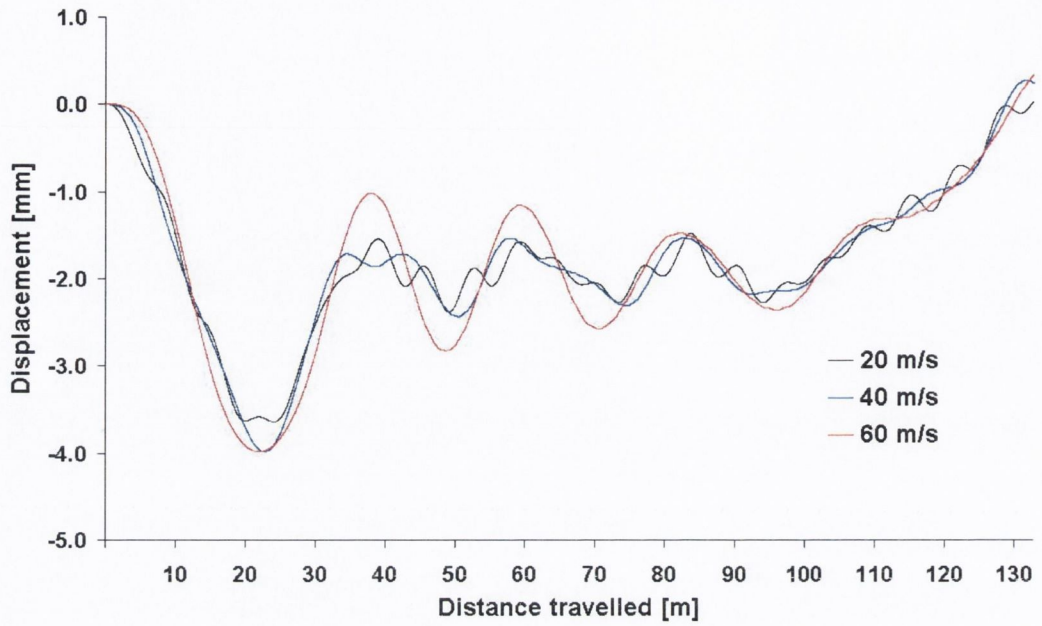
Previously, the impact factor variances for a simply supported beam bridge model traversed by a single moving vehicle model have been considered. The dynamic impact factors resulting from varying quality track profiles were calculated for short-span, medium-span and long-span bridge models. The results obtained have shown that the low frequency content of the FRA PSD functions for vertical random track irregularity do not greatly affect the dynamic impact factors for the bridges considered. The sole impact factor that was considered previously was the ratio of dynamic to static deflections at mid-span. The equivalent mid-span bending moment ratio is also considered here. In addition to the dynamic impact factors, the varying wheel-bridge contact forces are also considered in this section.

The vehicle model consists of a 181 locomotive as before but now being followed by four Mark 3 coaches. These five individual components of the vehicle are assumed to move completely independently of one another. A concrete bridge is modelled as a simply supported beam of 30m span with the two approaches supported upon rigid embankments. For preliminary comparative purposes an identical bridge to a bridge modelled by Lou (2005) is modelled here. The beam Young's modulus is $2.943 \times 10^{10} \text{Nm}^{-2}$ and its second moment of area is 3.81m^4 . The mass per unit length of the bridge is $3.4088 \times 10^4 \text{kgm}^{-1}$. Bridge damping is not considered which means that the numerical analysis gives a conservative result for the calculated impact factors. During the FE analysis the bridge is divided into 26 elements of equal length (approximately 1.154m).

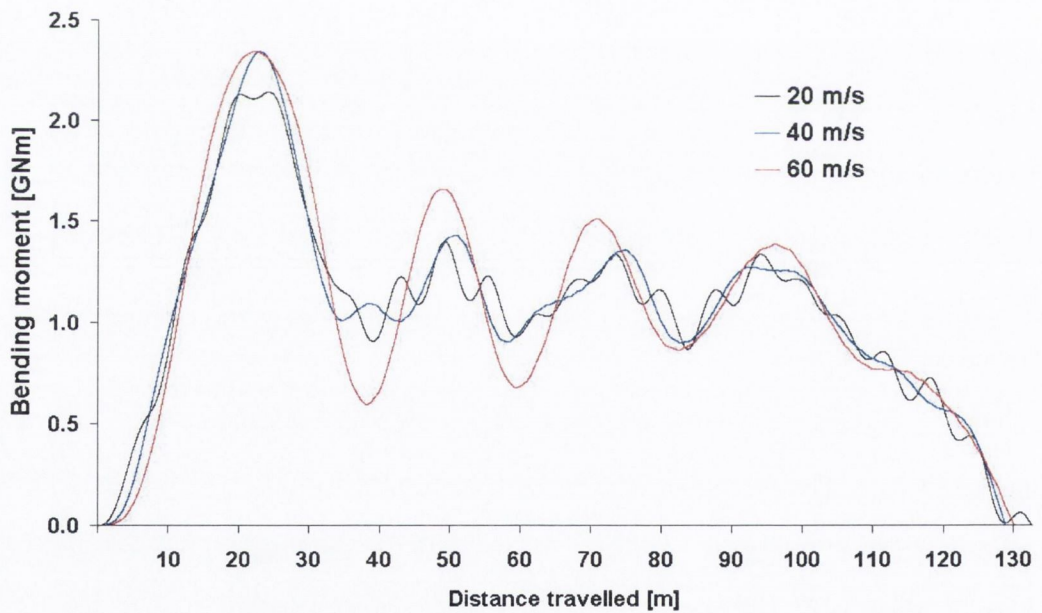
The FE bridge model was initially tested in the quasi-steady state. The mid-span response is illustrated in Figure 7.4. Both the deflection and bending moment at the beam mid-span are shown. The impact factors for the deflection and moment are found to be in agreement with one another to within less than 1% at all of the velocities considered. The maximum mid-span response occurs when the centre of gravity of the locomotive is situated approximately at mid-span. Peak responses do occur, but to a lesser degree, during the passage of each of the trailing coaches. Indeed, the magnitude of the successive peaks decreases significantly as the vehicle traverses the bridge.

The contact force variation at each of the four locomotive axles is illustrated in Figure 7.5. The forces are illustrated during and beyond the passage of these axles over the bridge model. No profile irregularity has been assumed here and, as a result, there is little variation in the observed contact forces.

As the axles initially encounter and leave the beam model there is excitation of the axle as the axles move from the rigid approach to the flexible beam and vice-versa. However, these transients quickly damp out. It should be noted once again that the vehicle axles are in direct contact with the upper surface of the FE beam,



(a) Displacement



(b) Bending moments

Fig. 7.4: Quasi-steady response at bridge mid-span

ie. no track model is included in this analysis. Were a track model included the approach-beam transition would be smooth. Neglecting these transitional transients the contact forces whilst the axles are in contact with the beam vary between approximately 157.5kN and 161.5kN. This is equivalent to a variation above and below the static contact force of 1.2%.

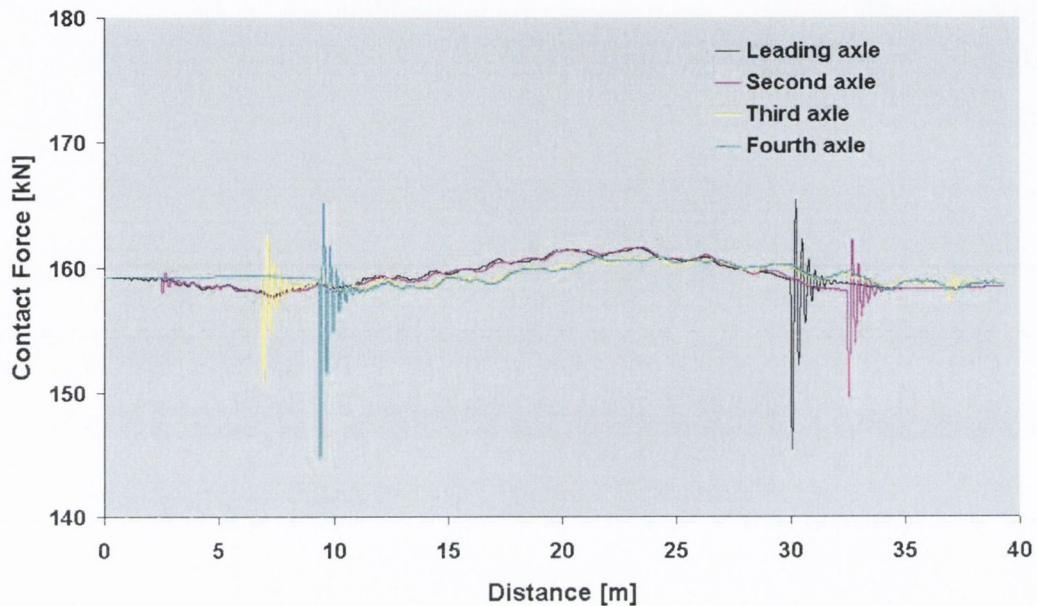


Fig. 7.5: Wheel-bridge contact force variation at leading locomotive axle in quasi-steady state at 40ms^{-1}

The minimum axle contact forces occur when the axle is located at approximately one quarter the beam span while the maximum is observed at three quarters of the span. This fluctuation can be linked to the pitching motion of the locomotive body and the two bogies. The time history of the leading bogie rotation (or pitch) is illustrated in Figure 7.6. The contact force drops off initially as the beam moves downwards under the action of the first moving axle. The bogie itself rotates in a clockwise direction but its lower natural frequency dictates that this process lags behind the beam and axle displacements resulting in a contact force reduction. The beam begins to move upwards as the bogie moves beyond the mid-span point. This

motion, in addition to the clockwise position of rotation of the bogie, generates a large contact force that pushes the bogie into anticlockwise rotation.

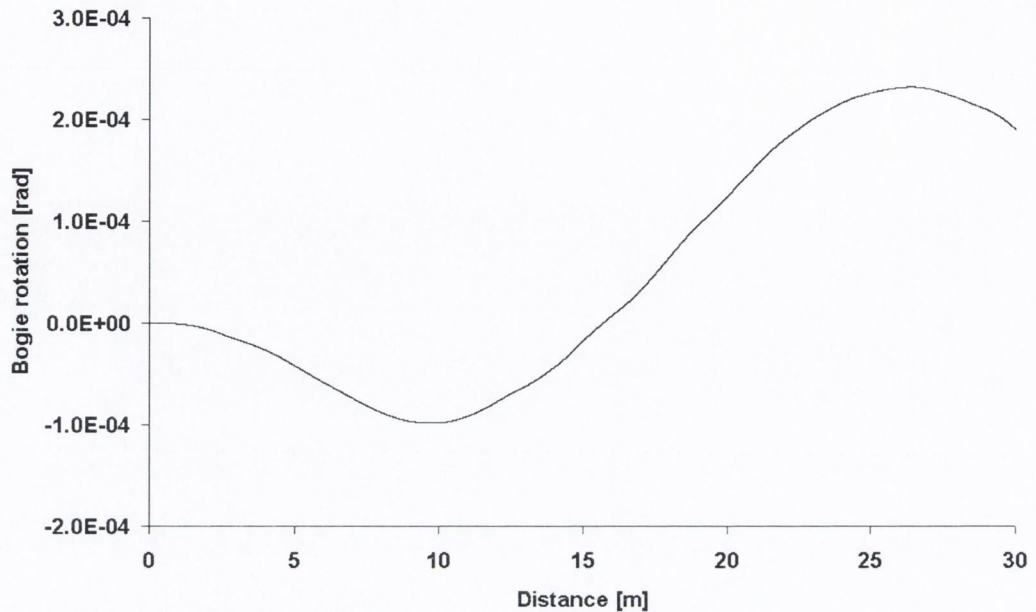


Fig. 7.6: Leading bogie rotation in quasi-steady state at 40ms^{-1}

The contact forces are illustrated for the case where the vehicle velocity was 40ms^{-1} . The bridge model dynamic impact factors at this velocity were 1.078 for deflection and 1.079 for bending moment.

7.3.2 Profile Irregularity Analysis

Having observed the quasi-steady state response of this bridge model the Class 4 track vertical profile is now applied to the upper surface of the beam. The same vehicle system (181 locomotive with four trailing Mark 3 coaches) is considered, moving at 40ms^{-1} across the bridge span. A sample of ten random profiles is numerically generated in this case, and the resulting bridge model dynamic impact factors resulting from each profile are calculated. The total running time for each individual simulation is 3.3856s, which is the time required for the entire vehicle to traverse the bridge. The wheel-bridge contact forces are also recorded, in addition

to mid-span deflection and bending moment. As before, the dynamic impact factors vary about a mean value which is found to approximate to the quasi-steady state dynamic impact factor. The standard deviation of this variation is extremely small at 0.003.

Class 1 irregularity profiles were then generated and applied to the model. In contrast to the Class 4 results, the dynamic impact factors generated by the Class 1 random irregularity profiles differed in that the mean impact factor was greater than that observed in the quasi-steady state. The variance was also greater with a standard deviation of 0.005. The normal distribution functions for the impact factors for Class 4 and Class 1 track profiles are illustrated in Figure 7.7. The quasi-steady state impact factor is 1.078. A Class 1 track will, on average, generate a dynamic impact factor greater than 1.093 for approximately 1.5% of crossings while the Class 4 equivalent probability of this occurring is negligible at approximately $10^{-6}\%$ of crossings.

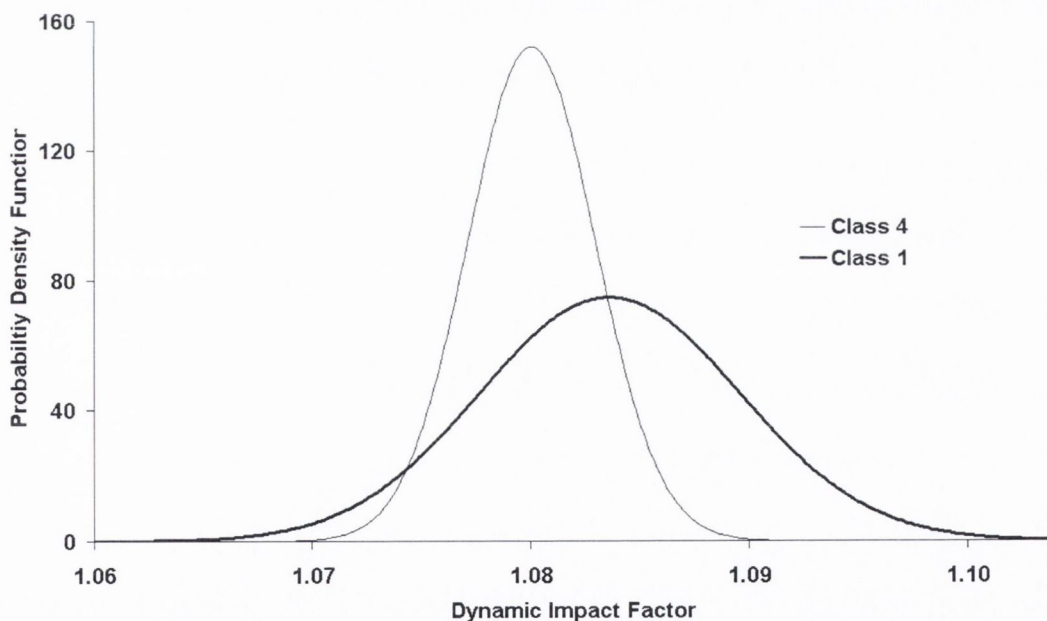


Fig. 7.7: Estimate of distribution of dynamic impact factors (assuming normal distribution)

The maximum contact forces observed at each axle, though varying individually for each random profile, also converge to a mean value approaching the quasi-steady state maximum value to within 1% in the case of the Class 4 track profile. As was the case for the impact factors however, the mean maximum contact force exceeds the quasi-steady state maximum force for the Class 1 profile (see Figure 7.8).

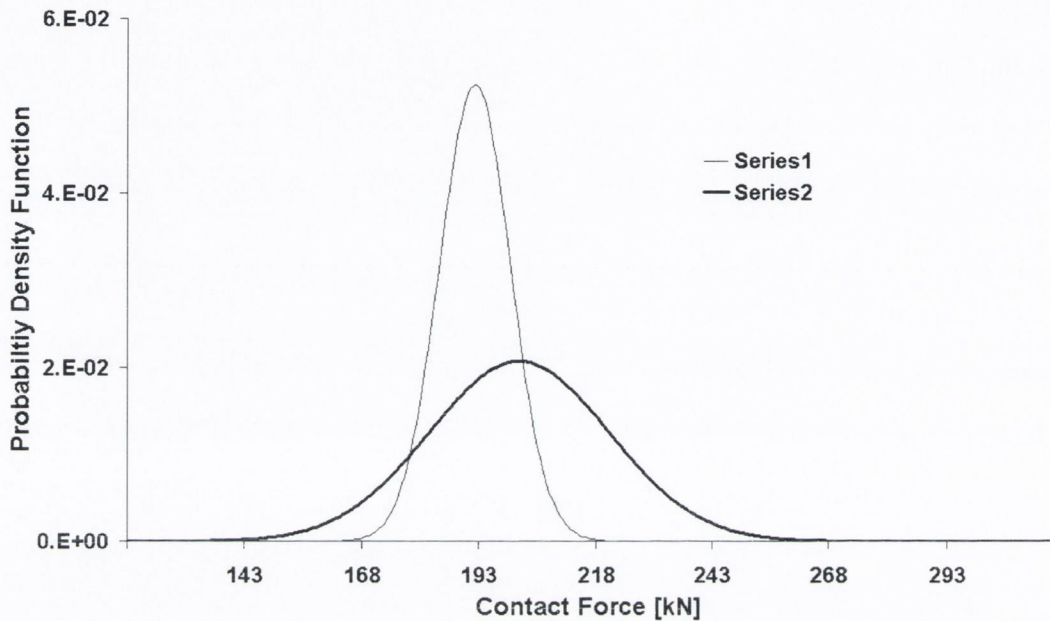


Fig. 7.8: Distribution of maximum front axle contact forces (assuming normal distribution)

7.4 Influence of Track Structure

7.4.1 Background

The effect of incorporating a track structure into the finite element model is examined in this section. The previous models assumed that the vehicle models ran directly along the upper surface of a simply supported beam. The track structure, which is in effect a second beam lying upon the bridge deck, was not included in the analytical nor the FE models.

The railway track is now modelled as a Bernoulli-Euler beam of finite length and extends beyond the simply supported beam bridge model in both directions. The track sleepers are spaced at intervals of 0.6m and are each 250kg in mass. The track is supported above the sleepers by discrete spring elements with linear spring constant values of $4.0 \times 10^8 \text{Nm}^{-1}$. These elements model the effect of the rail pads. The ballast medium below the sleeper layer is also modelled by discrete linear springs. These springs are situated below the sleepers and their spring constant value is $6.32 \times 10^7 \text{Nm}^{-1}$. The track parameter values are taken from Dong et al. (1994). Both springs are once again conservatively assumed to be undamped. The FEM model for the track structure is 49.2m in length and extends beyond the extents of the bridge model a distance of 9.2m in both directions. The vehicle system considered here is again a single 181 locomotive vehicle model.

7.4.2 Analysis Results

The quasi-steady state system response is considered for a vehicle velocity of 40ms^{-1} . The dynamic impact factor for the original simply supported beam bridge model is 1.078. The calculated equivalent factor for the beam with track model is identical to three decimal places of precision. Note that the impact factor for the track-bridge is defined in terms of the bridge, and not the track, deflection. This finding is in agreement with the study of Lou (2005), where it is stated that the track structure effect on the bridge deflection is insignificant in the quasi-steady state. However, random rail irregularity was not considered by Lou. Figure 7.9 illustrates the central response of both beam models. The maximum central displacements are almost identical though their peaks are slightly out of phase with one another. The mid-span displacement of the model inclusive of the track peaks fractionally earlier. It is assumed that this is due to the additional dispersion of the vehicle load along the track structure. The vehicle load is applied to the beam via the 0.6m spaced ballast springs rather than directly from the Hertzian contact springs. The dynamic

impact factors over the same range of velocities (5 to 60ms^{-1}) are in agreement with the previous analyses where the track structure was not modelled.

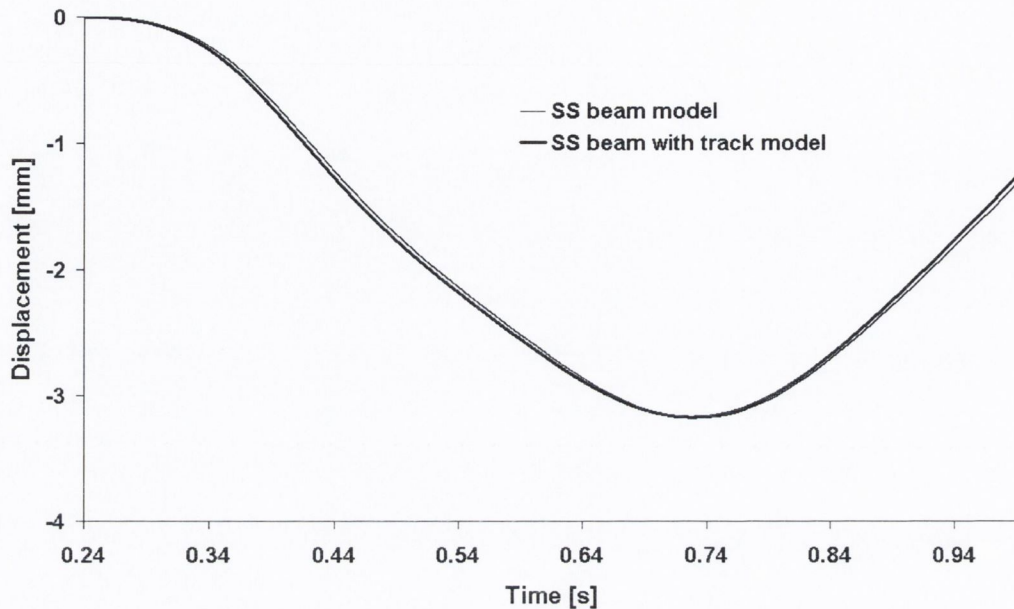


Fig. 7.9: Mid-span response of beam models

While the dynamic impact factors are not affected by the integration of the track model into the analysis, the contact forces characteristics are influenced. Figure 7.10 illustrates both the contact force history for the leading wheelset with and without the track model. There is greater high frequency oscillation (approximately 188Hz) of the Hertzian contact spring when the track model is present. The bogie pitching effect on the wheel-rail contact forces is once again prominent. Another observation is the contact force variation as the wheelset leaves the bridge structure. For the simple beam model the effect of leaving the beam is an initial decrease in the contact force followed by damped oscillation of the contact force until the quasi-steady state force is attained. For the beam and track model, a force increase is observed as the wheelset approaches the end of the bridge span followed by a significant force drop off of almost 30kN . The force then gradually returns to its steady state.

The track also has the effect of slightly increasing the maximum contact force

and decreasing the minimum (neglecting the effects as the vehicle leaves the bridge). The maximum and minimum observed contact forces are approximately 165kN and 156kN. The equivalent values for the simple beam model were 161kN and 158kN respectively.

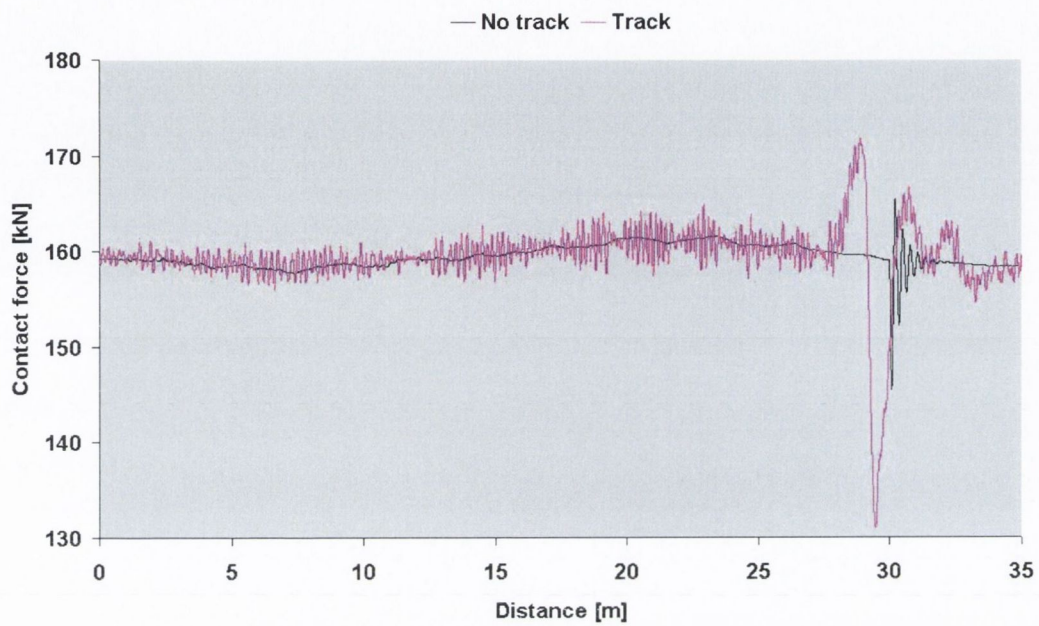


Fig. 7.10: Contact force variations at leading axle

Class 4 and Class 1 vertical irregularity profiles were then applied to the track surface profile of the track-bridge model. Ten random profiles of each class were generated. The calculated dynamic impact factors for the Class 4 profiles were very similar to the quasi-steady state factors which resulted in a mean impact factor of 1.078. The mean for Class 1 profiles was marginally higher at 1.080. This indicates that the presence of the track model at the interface between the vehicle and bridge negates to some extent the effect that was observed previously when the track model was not included.

The contact force histories for Class 4 and Class 1 irregularities were almost identical (see Figure 7.11). The forces display identical frequency characteristics with some minor differences in magnitude.

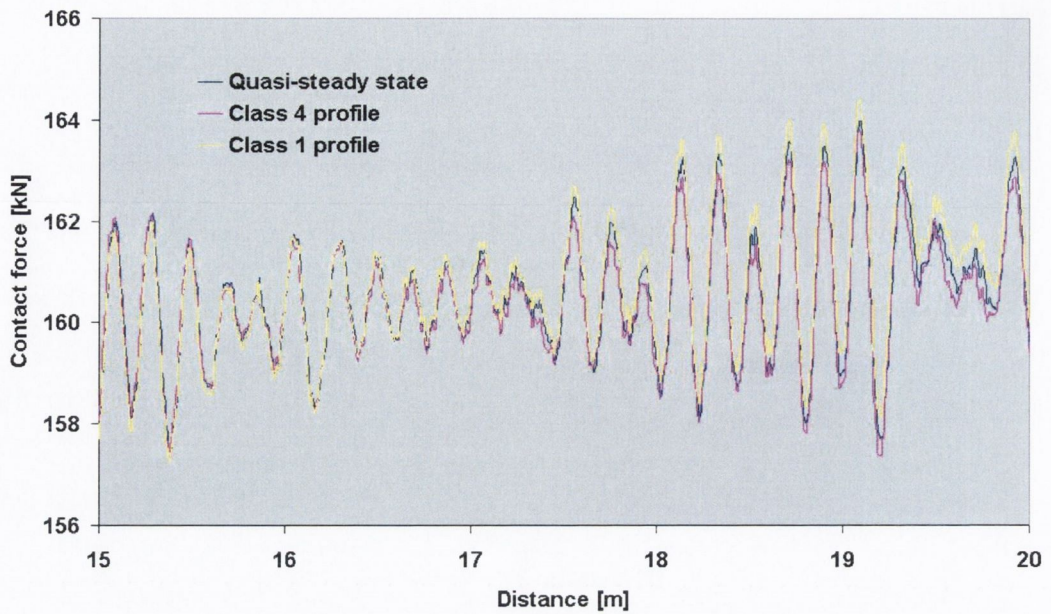


Fig. 7.11: Sample of contact force histories at leading axle for perfectly smooth, Class 4 and Class 1 track profiles

7.5 Conclusions

While profile irregularity has been shown to influence the magnitude of the bridge dynamic impact factors, the extent of this influence is relatively small. The most general observation that can be made is that the influence of random track irregularities causes the impact factors to fluctuate above and below the quasi-steady state impact factors, the degree of this fluctuation being proportional to both the vehicle velocity and the classification of irregularity. The short span bridge impact factors however, showed fluctuation about a value in excess of the quasi-steady state impact factor.

As a means of investigating the relationship between the random impact factor variance and the quasi-steady state impact factor a new variable is defined here. This variable, N_r , is equal to the ratio of the variance, σ , to the quasi-steady state impact factor, IF_{ss} (see Equation 7.2). This factor is introduced for the reason that the quasi-steady state impact factors do not increase with velocity over the velocity

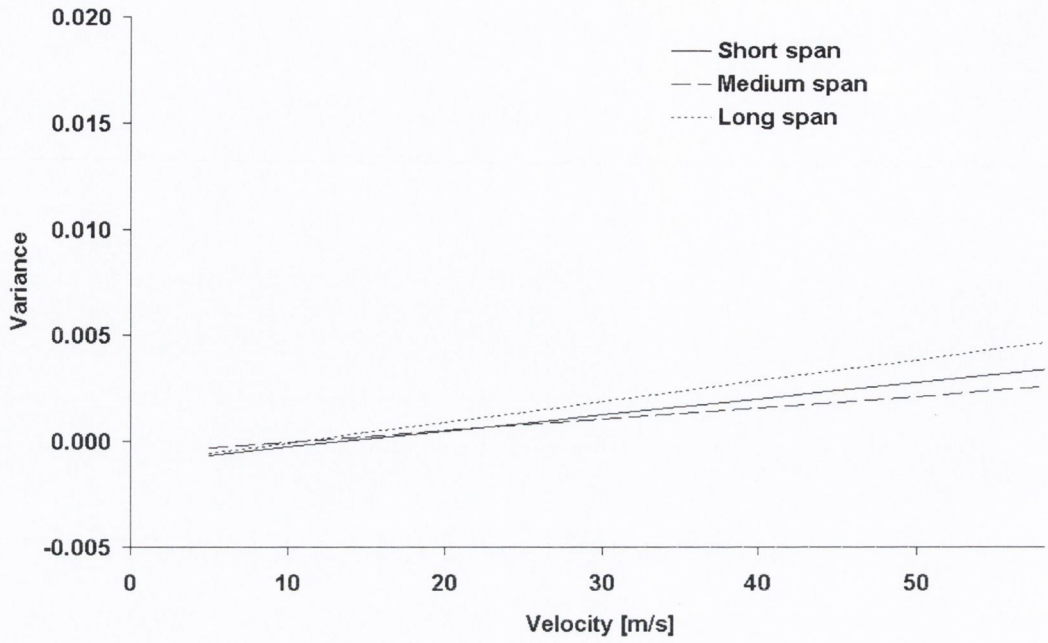
range considered in this study. It is hoped that by calculating the quasi-steady state impact factor, the variance might be calculated for a given class of vertical track profile.

$$N_r = \frac{\sigma}{IF_{ss}} \quad (7.2)$$

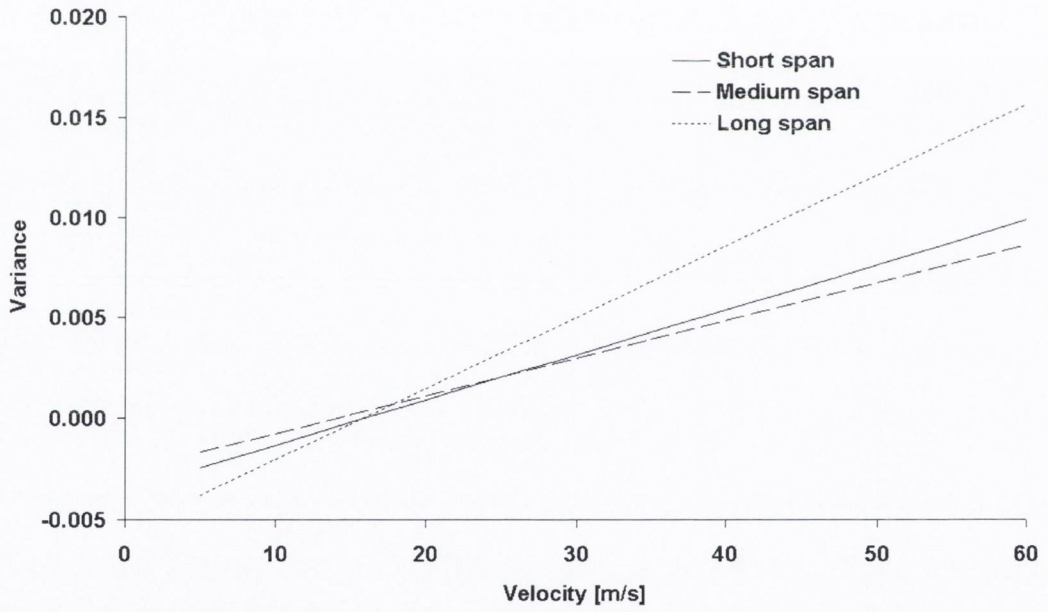
The values of N_r are calculated for each of the three bridge spans and two track classes. The results of a linear regression analysis using *Microsoft Excel* of N_r are illustrated in Figure 7.12 where the lines of best fit for each data set are plotted. The plots display very similar characteristics despite the fact that the variance scale is much greater for the Class 4 profiles. The ranges of the respective x-axes are identical so that this difference in the individual variance ranges may be more readily observed.

The long span bridge models are more susceptible to large N_r values at higher velocities while the medium span bridge values are least affected by velocity. The N_r increase with velocity in all cases. The significance 'F' value calculated by *Excel* was in all six cases smaller than 0.003. When this value, which serves the same function as a P-value, is less than 0.1, it may be said that the model is statistically significant.

Only the FRA PSD functions have been considered in this particular analysis. There are other empirical PSD functions available to describe random irregularities, each with different statistical characteristics. The poorest quality of track described by the FRA PSD functions was used here so that the worst case could be observed. One further observation that should be made is that bridges will generally have better aligned track than a random selected section of track. While the effects of Class 1 irregularities were observed here it is unlikely that a section of track on a railway bridge will be of such poor quality.



(a) Class 4 irregularity



(b) Class 1 irregularity

Fig. 7.12: Lines of best fit for N_r , the ratio of the variance to the quasi-steady state impact factor

Chapter 8

Summary and Conclusions

8.1 Summary

The research undertaken in this thesis was concerned with the development of computational models for the purpose of estimating the vertical dynamic response of both railway vehicles and track. The individual vehicle and track responses govern the characteristics of the contact forces generated between the two systems; the calculation of these forces is the main focus of this research. For a system with perfect geometry the system response attains a quasi-steady state. The effect of different types of geometrical defects on the response was considered. The types of irregularities that were considered were categorised as random and discrete.

Frequency domain techniques were applied to determine the characteristics of the vertical contact forces generated when a railway vehicle travels along a railway track with a vertical profile that is randomly irregular. Two different types of vehicle models were analysed: a locomotive and a passenger vehicle. The vehicles were modelled as two-DOF systems. The linearisation of the non-linear Hertzian contact spring between wheel and rail was required prior to the frequency domain analysis.

The contact forces generated by a flatbed wagon model travelling on a similar

random profile were also calculated using frequency domain techniques. The model in this case possesses four DOFs, which allowed the differences in the contact force process characteristics at two different wheelsets to be observed.

The validity of the linearisation of the Hertzian contact spring was investigated using numerical analysis. A track model was formulated using the Finite Difference Method. Random profiles of similar characteristics to those applied in the frequency domain analyses were generated and implemented at the wheel-rail interface. A comparison of the contact forces generated by track profiles with characteristics specified by two empirical PSD functions, FRA and ARS, was also carried out. The ARS contact forces were found to be of greater variance with peaks of higher magnitude than those generated by FRA profiles.

In addition to the frequency domain analyses of random track irregularity, the effect of a number of discrete irregularities on the system response were investigated using numerical techniques. In this case however, the track model was formulated using the Finite Element Method. The specific cases of a wheel-flat, an unsupported sleeper (and two consecutive unsupported sleepers), and a dipped joint have been considered. The position of impact of the wheel flat was found to be a factor in the impact magnitude. The results of numerical analyses were compared with the standard analytical formulae for the P_1 and P_2 , and divergence between the two was observed.

The effect of random vertical track irregularities on the bridge impact factors caused by a moving railway vehicle was investigated. The response of three different bridge models was calculated numerically for different vehicle velocities and track profile qualities. The effect of the inclusion or omission of the track structure from the model was also investigated.

8.2 Conclusions

The work carried out in this research has led to the following conclusions:

1. The suspension stiffness parametric variation showed the most dramatic increases in contact force rms values for both vehicle models. At values of $3.0 \times 10^6 \text{Nm}^{-1}$ for the locomotive model and $1.5 \times 10^6 \text{Nm}^{-1}$ for the passenger vehicle model, larger contact force rms values are observed. These larger rms values occur as a result of the natural frequency of bogie bounce being encompassed by the frequency band of the FRA irregularity PSD function. These suspension stiffness values are similar to many of those quoted in the literature (Au et al. 2002, Hou et al. 2003, Nielsen & Igeland 1995, Sun & Dhanasekar 2002, Wu & Yang 2003). The apparent neglect of possible excessive contact forces in the design of vehicle suspensions is due to the fact that the stiffness properties are designed for the primary purpose of minimising carriage bounce and pitch. The stiffness values that minimise carriage bounce are coincident with those that maximise contact force rms values. However, the extent of the contact forces increase is seen as an acceptable 'trade-off'; this is shown in this research to be valid for the case of randomly irregular track as specified by the FRA.
2. The analytical formulae for the P_1 and P_2 contact force increments were shown to have limitations when compared with the results obtained from dynamic FE analysis of the vehicle and track systems. There are a number of reasons for this divergence of analytical and numerical results. The analytical formulae do not account for the curvature of the railway track in the vertical plane. An angular ramp is assumed. The effect of loss of contact between wheel and rail is not accounted for accurately in the analytical solution. In addition, the formulae are derived based on a single wheel while the FE analysis was carried out using a vehicle model with multiple wheels. The inertial effect of

the vehicle bogies and body has an effect on the response at the wheel-rail interface that is not accounted for by the analytical formulae.

3. When the dynamic excitation to a railway vehicle is random vertical profile irregularity, the contact force process characteristics at the individual wheelsets are not generally identical. The extent of the difference between the various process characteristics is dependent upon a complex combination of the vehicle velocity and parametric properties. For the flatbed wagon vehicle model tested, it was found that resonant effects do not occur due to the low frequency content of the track irregularities considered.
4. The wheel-rail contact force processes generated by the two random track irregularity PSD functions, FRA and ARS, vary greatly. The application of the ARS PSD function, it being of higher frequency content and greater variance, resulted in significantly greater contact force variance. The ARS function also resulted in higher peak forces. It was also observed that the linearisation of the Hertzian spring is a more valid assumption for the FRA random track profile irregularities; the assumption is more valid with irregularity functions of lower frequency content.
5. The position of occurrence of a wheel flat, relative to the adjacent sleepers, is an important factor in the resulting impact force magnitude. The maximum impact occurs when the impact takes place 0.4m beyond a sleeper. The minimum occurs when the flat impacts 0.2m beyond a sleeper. Rail pad and ballast force magnitudes due to wheel flat impacts are also a function of the position of occurrence of the impact and are maximised for impacts directly above a sleeper.
6. The influence of the random irregularities as specified by the FRA on dynamic bridge impact factors is small. The mean of the impact factor values generated by considering a large number of profiles is equal to the steady state impact

factor. However, the variance of the impact factors when track irregularities are considered causes some larger impact factors to be observed, especially in the cases of high velocities on the short-span and long-span bridge models that were considered. While the short span model steady state impact factor is approximately 1.34 at 60ms^{-1} , for 1% of Class 1 profiles the factor will exceed 1.40.

7. The contact force variations that are caused by random vertical track irregularities as specified by the FRA empirical PSD functions is of little significance for both of the vehicles modelled. The contact force variance increases with both vehicle velocity and track quality deterioration. However, the extent of these increases is relatively small (ie. maximum rms of approximately 5.5kN about a static locomotive axle load of 22.4kN for 60ms^{-1}) and the probability of wheel unloading, or of contact forces exceeding twice their static values, due to random track irregularity is negligible. The parametric variation of the various vehicle parameters, with the exception of the suspension stiffness variation, did not yield excessive contact force variance values.

8.3 Recommendations for Further Research

Based on the research detailed in this thesis it is considered that the following topics be considered as areas of further study of wheel-rail contact forces caused by railway track and wheel defects:

1. The formulation of alternative formulae for the P_1 and P_2 contact force increment that takes account of sleeper spacing and the interaction between multiple wheelsets of the same vehicle.
2. Extend the two-dimensional models that have been presented in this thesis to three dimensions to allow for lateral effects. The combination of vertical

and lateral random track irregularity may, in some instances, be a source of excessive wheel-rail contact force variance. Only vertical loads were considered in this thesis. Derailment involves a combination of excessive lateral loading and vertical unloading. A three-dimensional model is required to observe the interaction between vertical and lateral axle loads.

3. Apply the three-dimensional model to investigate the effects of random irregularity on ride quality in addition to contact forces.
4. Investigate the effects of discrete track irregularities on three-dimensional vehicle models. The occurrence of such irregularities at a single side of the vehicle may result in large forces and stresses. The two-dimensional models presented in this thesis do not allow for the imposition of irregularity on a single side of a vehicle.
5. Investigate the effect of discrete track and wheel defects on railway bridge impact factors. Lateral bridge and vehicle response could also be included.

Bibliography

- Andersen, L., Nielsen, S. & Kirkegaard, P. (2001), 'Finite element modelling of infinite euler beams on kelvin foundations exposed to moving loads in convected co-ordinates', *Journal of Sound and Vibration* **241**(4), 587–604.
- Andersen, L. & Nielsen, S. R. (2003), 'Vibrations of a track caused by variation of the foundation stiffness', *Probabilistic Engineering Mechanics* **18**, 171–184.
- Andersen, L., Nielsen, S. R. & Iwankiewicz, R. (2002), 'Vehicle moving along an infinite beam with random surface irregularities on a kelvin foundation', *Journal of Applied Mechanics* **69**, 69–75.
- Au, F., Wang, J. & Cheung, Y. (2002), 'Impact study of cable-stayed railway bridges with random rail irregularities', *Engineering Structures* **24**, 529–541.
- Bartels, M. N., Jelic, S., Ngai, P., Gates, G., Newandee, D., Reisman, S. S., Basner, R. C. & Meersman, R. E. D. (2004), 'The effect of ventilation on spectral analysis of heart rate and blood pressure variability during exercise', *Respiratory Physiology & Neurobiology* **144**(1), 91–98.
- Bhattacharyya, B. & Chakraborty, S. (2002), 'Stochastic dynamic sensitivity of uncertain structures subjected to random earthquake loading', *Journal of Sound and Vibration* **249**(3), 543–556.
- Biondi, B., Muscolino, G. & Sofi, A. (2005), 'A substructure approach for the

dynamic analysis of train-track-bridge system', *Computers and Structures* **83**, 2271–2281.

Blader, F., Elkins, J., Wilson, N. & Klauser, P. (1989), Development and validation of a general railroad vehicle dynamics simulation (NUCARS), in 'IEEE/ASME Joint Railroad Conference', Philadelphia, Pennsylvania, pp. 39–46.

Cai, C., Cheung, Y. & Chan, H. (1988), 'Dynamic response of infinite continuous beams subjected to a moving force - an exact method', *Journal of Sound and Vibration* **123**(3), 461–472.

Chen, Y.-H. & Huang, Y.-H. (2003), 'Dynamic characteristics of infinite and finite railways to moving loads', *Journal of Engineering Mechanics* **129**(9), 987–995.

Cheng, Y., Au, F. & Cheung, Y. (2001), 'Vibration of railway bridges under a moving train by using bridge-track-vehicle element', *Engineering Structures* **23**, 1597–1606.

Crandall, S. H. & Mark, W. D. (1963), *Random Vibration in Mechanical Systems*, Academic Press, London.

Delgado, R. & dos Santos, S. (1997), 'Modelling of railway bridge-vehicle interaction on high speed tracks', *Computers and Structures* **63**(3), 511–523.

Demic, M., Lukic, J. & Milic, Z. (2002), 'Some aspects of the investigation of random vibration influence on ride comfort', *Journal of Sound and Vibration* **253**(1), 109–128.

Dong, R., Sankar, S. & Dukkipati, R. (1994), 'A finite element model of a railway track and its application to the wheel flat problem', *Journal of Rail and Rapid Transit* **208**(F1), 61–72.

Dukkipati, R. & Dong, R. (1999), 'Idealized steady state interaction between railway

vehicle and track', *Proceedings of the I MECH E Vol 213 Part F, Journal of Rail and Rapid Transit* pp. 15–28.

Eisenmann, J. (1981), *Railroad Track*, Frederick Ungar Publishing Co., New York, chapter 2, pp. 10–82.

Ertz, M. & Knothe, K. (2002), 'A comparison of analytical and numerical methods for the calculation of temperatures in wheel/rail contact', *Wear* **253**(3-4), 498–508.

Esveld, C. (1989), *Modern Railway Track*, 1st edn, MRT-Productions.

Esveld, C. (2001), *Modern Railway Track*, 2nd edn, MRT-Productions.

Fermér, M. & Nielsen, J. (1995), 'Vertical interaction between train and track with soft and stiff railpads - full scale experiments and theory', *Proceedings of the I MECH E Part F, Journal of Rail and Rapid Transit* **209**(F1), 39–47.

Fřyba, L. (1996), *Dynamics of Railway Bridges*, 1st edn, Thomas Telford.

Fřyba, L. (1999), *Vibrations of Solids and Structures under Moving Loads*, 3rd edn, Thomas Telford.

Fřyba, L. (2001), 'A rough assessment of railway bridges for high speed trains', *Engineering Structures* (23), 548–556.

Garg, V. K. & Dukkipati, R. V. (1984), *Dynamics of Railway Vehicle Systems*, Academic Press Canada.

Ghali, A. & Neville, A. (1978), *Structural Analysis; A Unifed Classical and Matrix Approach*, Chapman and Hall.

Gilbert, B. (2001), *VAMPIRE - Opportunities for fast, optimised, railway simulations*, AEA Technology Rail, Derby, UK.

- Ginsberg, J. H. (2001), *Mechanical and Structural Vibrations*, 1st edn, John Wiley & Sons, Inc.
- Guagliano, M. & Vergani, L. (2005), 'Experimental and numerical analysis of sub-surface cracks in railway wheels', *Engineering Fracture Mechanics* **72**(2), 255–269.
- Hart, G. C. & Wong, K. (1999), *Structural Engineering for Structural Engineers*, John Wiley and Sons, Inc.
- Hartnett, M. (2000a), 'The application of a spectral response model to fixed offshore structures', *Computers and Structures* **78**, 355–364.
- Hartnett, M. (2000b), Linear and Non-Linear Spectral Analysis of Offshore Lattice Structures, PhD thesis, Department of Civil, Structural and Environmental Engineering, Trinity College Dublin, Éire.
- Harvey, R., Gosling, R. & Cope, G. (1993), *British Railway Track; Design, Construction and Maintenance*, 6th edn, The Permanent Way Institution, chapter 26, pp. 507–526.
- Hetényi, M. (1946), *Beams on Elastic Foundation*, University of Michigan Press.
- Hou, K., Kalousek, J. & Dong, R. (2003), 'A dynamic model for an asymmetrical vehicle/track system', *Journal of Sound and Vibration* **267**, 591–604.
- Iwnicki, S. (1998), 'The manchester benchmarks for railway vehicle simulation', Manchester Metropolitan University.
- Iyengar, R. & Jaiswal, O. (1995), 'Random field modeling of railway track irregularities', *Journal of Transportation Engineering* **121**(4), 303–308.
- Jenkins, H., Stephenson, J., Clayton, G., Morland, G. & Lyon, D. (1974), 'The effect of track and vehicle parameters on wheel/rail vertical dynamic forces', *Railway Engineering Journal* pp. 2–16.

- Jergéus, J. (1997), Martensite formation and damage around railway wheel flats, in '6th International Heavy Haul Conference', Cape Town, South Africa, pp. 889–904.
- Jergéus, J. (1999), 'Full-scale railway wheel flat experiments', *Proceedings of the IMECH E, Part F, Journal of Rail and Rapid Transit* **213**(1), 1–13.
- Jezequel, L. (1981), 'Response of periodic systems to a moving load', *Journal of Applied Mechanics* **48**, 613–618.
- Jin, X., Wen, Z. & Wang, K. (2005), 'Effect of track irregularities on initiation and evolution of rail corrugation', *Journal of Sound and Vibration* **285**(1-2), 121–148.
- Johnson, D. (2000), Maximizing the vehicle/infrastructure interface, in 'Railway Infrastructure', The Railway Division of the Institution of Mechanical Engineers (IMechE), Professional Engineering Publishing Limited, Railtex 2000, National Exhibition Centre, Birmingham, UK., pp. 39–45.
- Johnson, K. (1985), *Contact Mechanics*, Cambridge University Press, Cambridge, MA.
- Jones, C., Sheng, X. & Petyt, M. (2000), 'Simulations of ground vibration from a moving harmonic load on a railway track', *Journal of Sound and Vibration* **231**(3), 739–751.
- Jordan, D. & Smith, P. (2002), *Mathematical techniques : an introduction for the engineering, physical, and mathematical sciences*, 3rd edn, Oxford University Press.
- Kalker, J. & Périard, F. (1996), 'Wheel-rail noise: impact, random, corrugation and tonal noise', *Wear* **191**, 184–187.

- Karakasis, K., Skarlatos, D. & Zakinthinos, T. (2005), 'A factorial analysis for the determination of an optimal train speed with a desired ride comfort', *Applied Acoustics* **66**(10), 1121–1134.
- Kawano, K. & Venkataramana, K. (1999), 'Dynamic response and reliability analysis of large offshore structures', *Computer Methods in Applied Mechanics and Engineering* **168**(1-4), 255–272.
- Knothe, K. & Grassie, S. (1993), 'Modelling of railway track and vehicle/track interaction at high frequencies', *Vehicle System Dynamics* **22**, 209–262.
- Koh, J. & Sarkar, T. K. (2005), 'Spectral analysis of nonuniformly spaced data using least square method', *Digital Signal Processing* **15**(1), 44–55.
- Kurek, E. (1981), *Railroad Track*, Frederick Ungar Publishing Co., New York, chapter 2, pp. 10–82.
- Lee, H. (1998), 'Dynamic response of a timoshenko beam on a winkler foundation subjected to a moving mass', *Applied Acoustics* **55**(3), 203–215.
- Lei, X. & Noda, N.-A. (2002), 'Analysis of dynamic response of vehicle and track coupling system with random irregularity of track vertical profile', *Journal of Sound and Vibration* **258**(1), 147–165.
- Lin, Y.-H. & Trethewey, M. (1990), 'Finite element analysis of elastic beams subjected to moving dynamic loads', *Journal of Sound and Vibration* **136**(2), 323–342.
- Lou, P. (2005), 'A vehicle-track-bridge interaction element considering vehicle's pitching effect', *Finite Elements in Analysis and Design* **41**, 397–427.
- Mastinu, G., Gobbi, M. & Pace, G. (2001), 'Analytical formulae for the design of a railway vehicle suspension system', *Proceedings of the Institution of Mechanical Engineers, Journal of Mechanical Engineering Science* **215**(C), 683–698.

- Mead, D. (1970), 'Free wave propagation in periodically supported infinite beams', *Journal of Sound and Vibration* **6**(12), 187–197.
- Mead, D. (1986), 'A new method of analyzing wave propagation periodically structures: application to periodic timoshenko beams and stiffened plates', *Journal of Sound and Vibration* **104**, 9–27.
- Moreau, A. (1992), 'Characteristics of wheel/rail contact', *Rail Engineering International Edition* (3), 15–22.
- Murakami, Y. (2002), *Metal Fatigue: Effects of Small Defects and Nonmetallic Inclusions*, Elsevier, London.
- Newland, D. (1993), *An Introduction to Random Vibrations, Spectral and Wavelet Analysis*, 3rd edn, Longman Scientific & Technical.
- Nielsen, J. (2003), 'Numerical prediction of rail roughness growth on tangent railway tracks', *Journal of Sound and Vibration* **267**(3), 537–548.
- Nielsen, J. & Abrahamsson, T. (1992), 'Coupling of physical and model components for analysis of moving nonlinear dynamic systems on general beam structures', *International Journal of Numerical Methods in Engineering* **33**, 1843–8159.
- Nielsen, J. & Igeland, A. (1995), 'Vertical dynamic interaction between train and track - influence of wheel and track imperfections', *Journal of Sound and Vibration* **187**(5), 825–839.
- Nielsen, J. & Oscarsson, J. (2004), 'Simulation of dynamic train-track interaction with state-dependent track properties', *Journal of Sound and Vibration* **275**, 515–532.
- Nigam, N. (1983), *Introduction to Random Vibrations*, 1st edn, MIT Press, Cambridge, Massachusetts.

- Nishimura, K., Perkins, N. & Zhang, W. (2004), Suspension optimization and design optimization of a high speed railway vehicle, *in* 'Proceedings of the 2004 ASME/IEEE Joint Rail Conference', ASME/IEEE, Baltimore, Maryland, USA, pp. 129–139.
- O'Dwyer, D., Hegarty, D. & Basu, B. (2002), Modelling the vertical response of railway freight wagons due to track irregularities, *in* B. Topping & Z. Bittnar, eds, 'Sixth International Conference on Computational Structures Technology, Prague, Czech Republic'.
- O'Dwyer, D. W., Hegarty, D. P. & Basu, B. (2004), Numerical modelling of railway vehicle-track interaction with infinite beam track model, *in* 'Railway Engineering'.
- ORE (1978), Permissible maximum values for the y and q forces as well as the ratio y/q , Technical Report C 138 (2), Office for Research and Experiments of the International Union of Railways, Utrecht.
- Pakko, M. R. (2003), 'A spectral analysis of the cross-country consumption correlation puzzle', *Economics Letters* **84**(3), 341–347.
- Piszczyk, K. & Nizioł, J. (1986), *Random Vibration of Mechanical Systems*, Ellis Horwood, Chichester.
- Profillidis, V. (2000), *Railway Engineering*, 2nd edn, Ashgate Publishing Limited, Aldershot, England.
- Robson, J. (1963), *An introduction to random vibration*, Edinburgh U.P.
- Sheng, X., Jones, C. & Petyt, M. (1999), 'Ground vibration generated by a load moving along a railway track', *Journal of Sound and Vibration* **228**(1), 129–156.

- Song, M.-K., Noh, H.-C. & Choi, C.-K. (2003), 'A new three-dimensional finite element analysis model of high-speed train bridge interactions', *Engineering Structures* **25**, 1611–1626.
- Stichel, S. (1999), 'On freight wagon dynamics and track deterioration', *Proceedings of the Institution of Mechanical Engineers* **213**(F), 243–254.
- Sun, L. (2001a), 'Closed-form representation of beam response to moving line loads', *ASME Journal of Applied Mechanics* **68**, 348–350.
- Sun, L. (2001b), 'Computer simulation and field measurement of dynamic pavement loading', *Mathematics and computers in simulation* **56**, 297–313.
- Sun, L. (2001c), 'Dynamic displacement response of beam-type structures to moving line loads', *International Journal of Solids and Structures* **38**, 8869–8878.
- Sun, L. (2002), 'A closed-form solution of beam on viscoelastic subgrade subjected to moving loads', *Computers and Structures* **80**.
- Sun, L. & Kennedy, T. W. (2002), 'Spectral analysis and parametric study of stochastic pavement loads', *Journal of Engineering Mechanics* **128**(3), 318–327.
- Sun, Y. & Dhanasekar, M. (2002), 'A dynamic model for the vertical interaction of the rail track and wagon system', *International Journal of Solids and Structures* **39**, 1337–1359.
- Takewaki, I. (2005a), 'Bound of earthquake input energy to soilstructure interaction systems', *Soil Dynamics and Earthquake Engineering* **25**, 741–752.
- Takewaki, I. (2005b), 'Frequency-domain analysis of earthquake input energy to structurepile systems', *Engineering Structures* **27**(4), 549–563.

- Tan, G., Brameld, G. & Thambiratnam, D. (1998), 'Development of an analytical model for treating bridge-vehicle interaction', *Engineering Structures* **20**(1-2), 54-61.
- Tanabe, M., Wakui, H., Matsumoto, N., Okuda, H., Sogabe, M. & Komiya, S. (2003), 'Computational model of a shinkansen train running on the railway structure and the industrial applications', *Journal of materials Processing Technology* **140**, 705-710.
- Thambiratnam, D. & Zhuge, Y. (1996), 'Dynamic analysis of beams on an elastic foundation subjected to moving loads', *Journal of Sound and Vibration* **198**(2), 149-169.
- Thompson, D., Wu, T. & Armstrong, T. (2003), Wheel/rail rolling noise - the effects of non-linearities in the contact zone, in 'Tenth International Congress on Sound and Vibration', Stockholm, Sweden.
- Timoshenko, S. (1921), 'On the correction for shear of the differential equation for transverse vibrations of static bars', *Philosophical Magazine Series* **6**(41), 744-746.
- Timoshenko, S. (1926), Statical and dynamical stresses in rails, in 'Proceedings of the International Congress on Applied Mechanics', Zurich, pp. 407-418.
- Tunna, J. (1988), Wheel/rail forces due to wheel irregularities, in 'Proceedings of the 9th International Wheelset Congress', number 6-2, Montreal, Canada.
- Warburton, G. (1976), *The Dynamic Behaviour of Structures*, Oxford: Pergamon Press.
- Wickens, A. (2003), *Fundamentals of Rail Vehicle Dynamics*, Swets & Zeitlinger.
- Wiriychai, A., Chu, K.-H. & Garg, V. K. (1982), 'Bridge impact due to wheel and track irregularities', *ASCE Journal of Engineering Mechanics* **108**(4), 648-666.

- Wirsching, P. H., Paez, T. L. & Ortiz, K. (1995), *Random Vibrations: Theory and Practice*, Wiley, Chichester.
- Wu, T. & Thompson, D. (2001a), 'The effects on railway rolling noise of wave reflections in the rail and support stiffening due to the presence of multiple wheels', *Applied Acoustics* **62**, 1249–1266.
- Wu, T. & Thompson, D. (2001b), 'Vibration analysis of railway track with multiple wheels on the rail', *Journal of Sound and Vibration* **239**(1), 69–97.
- Wu, T. & Thompson, D. (2003), 'On the impact noise generation due to a wheel passing over rail joints', *Journal of Sound and Vibration* **267**(3), 485–496.
- Wu, T. & Thompson, D. (2004), 'On the parametric excitation of the wheel/track system', *Journal of Sound and Vibration* **278**, 725–747.
- Wu, Y.-S. & Yang, Y.-B. (2003), 'Steady-state response and riding comfort of trains moving over a series of simply supported bridges', *Engineering Structures* **25**(2), 251–265.
- Xia, H. & Zhang, N. (2005), 'Dynamic analysis of railway bridge under high-speed trains', *Computers and Structures* **83**(23-24), 1891–1901.
- Xu, Y., Zhang, N. & Xia, H. (2004), 'Vibration of coupled train and cable-stayed bridge systems in cross winds', *Engineering Structures* **26**, 1389–1406.
- Yang, C. (1986), *Random Vibration of Structures*, John Wiley & Sons, Inc.
- Yang, Y.-B., Yau, J.-D. & Hsu, L.-C. (1997), 'Vibration of simple beams due to trains moving at high speeds', *Engineering Structures* **19**(11), 936–944.
- Yoshimura, T., Nakaminami, K., Kurimoto, M. & Hino, J. (1999), 'Active suspension of passenger cars using linear and fuzzy logic controls', *Control Engineering Practice* (7), 41–47.

Zhai, W. & Cai, Z. (1997), 'Dynamic interaction between a lumped mass vehicle and a discretely supported continuous rail track', *Computers and Structures* **63**(5), 987–997.

Zhang, Q.-L., Vrouwenvelder, A. & Wardenier, J. (2001), 'Numerical simulation of train-bridge interactive dynamics', *Computers and Structures* **79**, 1059–1075.

Appendix A

Order Statistics of Random Process Peaks

Consider that there are N peaks in the contact force random process over a track stretch of length L (Iyengar & Jaiswal 1995). The peaks are denoted as a_1, a_2, \dots, a_N and are arranged in descending order, ie.

$$a_1 > a_2 > a_3 > \dots > a_N \quad (\text{A.1})$$

The probability that the j^{th} order peak will exceed the level $\alpha = \frac{a}{\sigma_1}$ is

$$F_j(\alpha) = \text{Prob}(a_j > \alpha) = \text{Prob}(\text{at least } j \text{ number of } a_i \text{ are greater than } \alpha) \quad (\text{A.2})$$

Now, assuming that the peaks are statistically independent equation A.2 is equivalent to

$$\begin{aligned}
F_j(\alpha) &= P(\text{only } j \text{ peaks } > \alpha) + P(\text{only } (j + 1) \text{ peaks } > \alpha) \\
&\quad + P(\text{only } (j + 2) \text{ peaks } > \alpha) \\
&\quad + \dots + P(\text{only } N \text{ peaks } > \alpha) \\
&= \sum_{i=j}^N P(\text{only } i \text{ out of } N \text{ peaks } > \alpha) \quad (\text{A.3})
\end{aligned}$$

From probability theory

$$P(\text{only } i \text{ out of } N \text{ peaks } > \alpha) = C_{i,N} P^i(\alpha) [1 - P(\alpha)]^{N-i} \quad (\text{A.4})$$

where $C_{i,N} = \frac{N!}{i!(N-i)!}$ and $P(\alpha)$ is given by equation 3.20. Thus, finally

$$F_j(\alpha) = \sum_{i=j}^N C_{i,N} P^i(\alpha) [1 - P(\alpha)]^{N-i} \quad (\text{A.5})$$

is the probability that the j^{th} order peak among the N number of peaks over a track length L will exceed a given level $\alpha = \frac{a}{\sigma_1}$.

Appendix B

Four Degree of Freedom Model

The equation of motion for the four degree of freedom vehicle model upon two discretised track masses (see Figure 4.1), with relative wheelset displacements, is as follows:

$$[m_s]\{\ddot{x}_s(t)\} + [c_s]\{\dot{x}_s(t)\} + [k_s]\{x_s(t)\} = \{f_s(t)\} \quad (\text{B.1})$$

The mass, damping and stiffness matrices, $[m_s]$, $[c_s]$ and $[k_s]$ are given by the following three equations:

$$[m_s] = \begin{bmatrix} m_c & 0 & 0 & 0 & 0 & 0 \\ 0 & I_c & 0 & 0 & 0 & 0 \\ 0 & 0 & m_{wf} & 0 & -m_{wf} & 0 \\ 0 & 0 & 0 & m_{wr} & 0 & -m_{wr} \\ 0 & 0 & 0 & 0 & m_{gf} & 0 \\ 0 & 0 & 0 & 0 & 0 & m_{gr} \end{bmatrix} \quad (\text{B.2})$$

$$[c_s] = \begin{bmatrix} c_{bf} + c_{br} & ac_{br} - bc_{bf} & c_{bf} & c_{br} & -c_{bf} & -c_{br} \\ ac_{br} - bc_{bf} & a^2c_{br} + b^2c_{bf} & -bc_{bf} & ac_{br} & bc_{bf} & -ac_{br} \\ c_{bf} & -bc_{bf} & c_{bf} + & 0 & -c_{bf} & 0 \\ c_{br} & ac_{br} & 0 & c_{br} & 0 & -c_{br} \\ 0 & 0 & 0 & 0 & c_{gf} & 0 \\ 0 & 0 & 0 & 0 & 0 & c_{gr} \end{bmatrix} \quad (B.3)$$

$$[k_s] = \begin{bmatrix} k_{bf} + k_{br} & ak_{br} - bk_{bf} & k_{bf} & k_{br} & -k_{bf} & -k_{br} \\ ak_{br} - bk_{bf} & a^2k_{br} + b^2k_{bf} & -bk_{bf} & ak_{br} & bk_{bf} & -ak_{br} \\ k_{sf} & -bk_{bf} & k_{bf} + k_{hf} & 0 & -k_{bf} & 0 \\ k_{bf} & ak_{br} & 0 & k_{br} + k_{hr} & 0 & -k_{br} \\ 0 & 0 & k_{hf} & 0 & k_{gf} & 0 \\ 0 & 0 & 0 & k_{hr} & 0 & k_{gr} \end{bmatrix} \quad (B.4)$$

The system forcing function, $f_s(t)$, is as follows:

$$\left\{ f_s(t) \right\} = \left\{ \begin{array}{l} c_{bf}\dot{\xi}_f(t) + c_{br}\dot{\xi}_r(t) + k_{bf}\xi_f(t) + k_{br}\xi_r(t) \\ -bc_{bf}\dot{\xi}_f(t) + ac_{br}\dot{\xi}_r(t) - bk_{bf}\xi_f(t) + ak_{br}\xi_r(t) \\ m_{wf}\ddot{\xi}_f(t) + c_{bf}\dot{\xi}_f(t) + k_{bf}\xi_f(t) \\ m_{wr}\ddot{\xi}_r(t) + c_{br}\dot{\xi}_r(t) + k_{br}\xi_r(t) \\ k_{hf}\xi_f(t) \\ k_{hr}\xi_r(t) \end{array} \right\} \quad (B.5)$$

ξ_f and ξ_r are the track roughness coordinates at the points beneath the wheelsets m_{wf} and m_{wr} respectively. The vector describing the system displacement, $\{x_s(t)\}$ is given by

$$\left\{ x_s(t) \right\} = \left\{ x_c(t) \quad \theta_c(t) \quad z_{wf}(t) \quad z_{wr}(t) \quad x_{gf}(t) \quad x_{gr}(t) \right\}^T \quad (B.6)$$

where z_{wf} and z_{wr} are the relative wheelset-rail displacements.

The wheel hop frequency response functions for the front and rear wheelsets of the freight vehicle model are given in Equations B.7 and B.8 as function of circular frequency ω . These particular functions have been formulated on the assumption that track deformation does not occur, ie. the track mass springs are assume to be infinitely stiff. Inclusion of these springs would serve only to increase the complexity of the response.

$$\begin{aligned}
H_{z_{wf}}(\omega) = & \frac{1}{X(\omega)} \times \left(\right. \\
& - \\
& \{ -i\omega^5 I_c m_w c_b - \omega^4 I_c c_b^2 + i\omega^3 I_c c_b k_h + 2i\omega^3 I_c c_b k_b - \omega^4 I_c m_w k_b + \omega^2 I_c k_h k_b \\
& + \omega^2 I_c k_b^2 - 2\omega^4 a^2 c_b^2 m_w + 2\omega^2 a^2 c_b^2 k_h + 4i\omega^3 a^2 c_b m_w k_b - 4i\omega a^2 c_b k_h k_b \\
& + 2a^2 k_b^2 \omega^2 m_w - 2a^2 k_b^2 k_h \} \\
& \times [i\omega c_b + k_b + (i\omega c_b + k_b)e^{-i\omega\tau_0}] \\
& - \\
& \{ a(ak_h k_b^2 + 2\omega^4 c_b^2 m_w - 4i\omega^3 c_b m_w k_b - 2\omega^2 c_b^2 k_h + 4i\omega c_b k_h k_b - i\omega^3 m_c c_b k_h \\
& - 2i\omega^3 m_c c_b k_b - \omega^2 m_c k_h k_b + i\omega^5 m_c m_w c_b + \omega^4 m_c c_b^2 + \omega^4 m_c m_w k_b \\
& - \omega^2 m_c k_b^2 - 2\omega^2 m_w k_b^2) \} \\
& \times [-ak_b - i\omega a c_b + (ak_b + i\omega a c_b)e^{-i\omega\tau_0}] \\
& - \\
& \{ -2\omega^2 m_c a^2 k_b k_h + 2\omega^4 m_c a^2 k_b m_w + i\omega^5 m_c I_c c_b + \omega^4 m_c I_c k_b + \omega^4 m_c I_c k_h \\
& - 2i\omega^3 m_c a^2 c_b k_h - \omega^6 m_c I_c m_w - 2i\omega^3 m_c a^2 c_b k_b + 2i\omega^5 m_c a^2 c_b m_w - \omega^2 m_c a^2 k_b^2 \\
& + \omega^4 m_c a^2 c_b^2 + 4a^2 k_b^2 k_h + 2\omega^4 I_c m_w k_b - 2\omega^2 I_c k_h k_b - 4a^2 k_b^2 \omega^2 m_w \\
& + 4\omega^4 a^2 c_b^2 m_w - 4\omega^2 a^2 c_b^2 k_h - 8i\omega^3 a^2 c_b m_w k_b + 8i\omega a^2 c_b k_h k_b + 2i\omega^5 I_c m_w c_b \\
& - 2i\omega^3 I_c c_b k_h - 2i\omega^3 I_c c_b k_b + \omega^4 I_c c_b^2 - \omega^2 I_c k_b^2 \} \\
& \times [-\omega^2 m_w + i\omega c_b + k_b] \\
& - \\
& \{ \omega^2 (-\omega^2 m_c a^2 c_b^2 + 2i\omega m_c a^2 c_b k_b + m_c a^2 k_b^2 + \omega^2 I_c c_b^2 - 2i\omega I_c c_b k_b - I_c k_b^2) \} \\
& \times [(-\omega^2 m_w + i\omega c_b + k_b)e^{-i\omega\tau_0}] \\
& \left. \right) \quad (B.7)
\end{aligned}$$

$$\begin{aligned}
& X(\omega) \\
& = \\
& - 4a^2k_b^2k_h^2 + 16i\omega^3c_b a^2k_b m_w k_h + 2i\omega^3c_b I_c k_h^2 + 2i\omega^7c_b I_c m_w^2 + 4\omega^2c_b^2 a^2k_h^2 \\
& + 2i\omega^7m_c I_c m_w c_b - 2i\omega^5m_c I_c c_b k_h - 8i\omega c_b a^2k_b k_h^2 - 4i\omega^5c_b I_c m_w k_h \\
& - 4i\omega^5c_b I_c m_w k_b + 4i\omega^3c_b I_c k_h k_b - 8i\omega^5c_b a^2k_b m_w^2 - 2i\omega^5m_c I_c c_b k_b \\
& + 2i\omega^7m_c a^2c_b m_w^2 - 4i\omega^5m_c a^2c_b m_w k_h - 4i\omega^5m_c a^2c_b m_w k_b + 2i\omega^3m_c a^2c_b k_h^2 \\
& + 4i\omega^3m_c a^2c_b k_h k_b - 8\omega^4c_b^2 a^2 m_w k_h + 8a^2k_b^2\omega^2 m_w k_h - 4k_b\omega^4 I_c m_w k_h \\
& + 2\omega^2m_c a^2k_b k_h^2 + 2\omega^2m_c a^2k_b^2 k_h + 2\omega^6m_c I_c m_w k_h + 2\omega^6m_c I_c m_w k_b \\
& - 2\omega^4m_c I_c k_h k_b + 2\omega^6m_c a^2k_b m_w^2 - 2\omega^4m_c a^2k_b^2 m_w + 2\omega^6m_c a^2c_b^2 m_w \\
& - 2\omega^4m_c a^2c_b^2 k_h + \omega^6m_c I_c c_b^2 - \omega^4m_c I_c k_b^2 - \omega^4m_c I_c k_h^2 - \omega^8m_c I_c m_w^2 \\
& - 2\omega^4 I_c m_w k_b^2 + 2\omega^2 I_c k_h k_b^2 - 4a^2k_b^2\omega^4 m_w^2 + 2k_b\omega^2 I_c k_h^2 + 2k_b\omega^6 I_c m_w^2 \\
& \quad + 2\omega^6c_b^2 I_c m_w - 2\omega^4c_b^2 I_c k_h + 4\omega^6c_b^2 a^2 m_w^2 - 4\omega^4m_c a^2k_b m_w k_h \quad (B.9)
\end{aligned}$$

Appendix C

Railway Vehicle Parameters

C.1 181 Locomotive Parameters

Parameter	Unit	Value
Vehicle body mass	t	40.0
Bogie frame mass	t	8.477
Wheelset mass	t	2.0
Body moment of inertia	tm^2	1255.159
Bogie moment of inertia	tm^2	13.665
Secondary suspension spring stiffness	kNm^{-1}	500.0
Primary suspension spring stiffness	kNm^{-1}	1600.0
Secondary suspension spring damping	kNsm^{-1}	100.0
Primary suspension spring damping	kNsm^{-1}	200.0
Distance between two bogie frame centres	m	3.429
Distance between axle centres	m	1.235
Overall length of vehicle	m	13.424

Table C.1: 181 Locomotive model parameters

C.2 Mark 3 Coach Parameters

Parameter	Unit	Value
Vehicle body mass	t	33.992
Bogie frame mass	t	3.0
Wheelset mass	t	2.0
Body moment of inertia	tm^2	2086.0
Bogie moment of inertia	tm^2	3.47
Secondary suspension spring stiffness	kNm^{-1}	1000.0
Primary suspension spring stiffness	kNm^{-1}	550.0
Secondary suspension spring damping	kNsm^{-1}	100.0
Primary suspension spring damping	kNsm^{-1}	200.0
Distance between two bogie frame centres	m	13.4
Distance between axle centres	m	1.3
Overall length of vehicle	m	23.0

Table C.2: Mark 3 coach model parameters

Vita

David Hegarty was born in Dublin, Ireland, on the 20th of August, 1977. After completing the Leaving Certificate examination at St. Michaels Diocesan School, Trim, Co. Meath, he went on to Trinity College Dublin where he studied Civil, Structural and Environmental Engineering and received a first class honours degree in July 2001. He worked as a site engineer for Ascon/Rohcon Ltd., a civil and structural engineering contractor prior to reentering Trinity College as a postgraduate student. Here he worked as a teaching assistant while researching in the field of computational mechanics in the specific area of railway dynamics.

Permanent Address: Department of Civil, Structural and Environmental Engineering
Museum Building
Trinity College
Dublin 2
Éire

This dissertation was typeset with L^AT_EX 2_ε¹ by the author.

¹L^AT_EX 2_ε is an extension of L^AT_EX. L^AT_EX is a collection of macros for T_EX. T_EX is a trademark of the American Mathematical Society. The macros used in formatting this dissertation were written by Dinesh Das, Department of Computer Sciences, The University of Texas at Austin.